Università degli Studi di Ferrara

DOTTORATO DI RICERCA IN
"SCIENZE CHIMICHE"

CICLO XXIV°

COORDINATORE Prof. CARLO ALBERTO BIGNOZZI

REACTIVE TRANSPORT OF POLLUTANTS IN POROUS MEDIA

Settore Scientifico Disciplinare CHIM/01

Dottorando
Dott. NASSI MARIANNA

Tutore
Prof. PASTI LUISA

Anni 2009/2011

Ai miei genitori

e a Nicolò, il mio primo nipote

CONTENTS

Chapter 1

INTRODUCTION

Water quality is one of the fundamental determinants of public health and it greatly enhances or complements economic progress and sustainable development of a country. Water is an essential substance for living systems as it allows the transport of nutrients and waste products in living systems. Research shows a clear correlation between diseases and the amount and types of pollutants found in water [5].

There are many types of pollutants in groundwater, but complex mixtures of hazardous chemicals such as volatile organic chemicals (VOCs) and emerging contaminants like endocrine disrupting compounds (ECDs) and pharmaceuticals and personal care products (PPCPs) can have severe effects on animal and human health as well as environmental quality [6].

Organic compounds in water derive from three major sources: the breakdown of naturally occurring organic materials, domestic and economic activities, and reactions that occur during water treatment and distribution. Most of the organic contaminants are called VOCs (volatile organic chemicals). Volatile organic compounds (VOCs) are defined by the US EPA (the United States Environmental Protection Agency) as stable products exhibiting a vapour pressure above 0.1 mmHg at ambient conditions. VOCs can be toxic, carcinogenic, irritating, and/or flammable, and thus may pose serious health problems if allowed to enter the human environment. Three broad groups of VOCs have been found in water. One group includes compounds found in petroleum products, especially aromatics like benzene, toluene and xylenes. Major sources of these compounds are leaks in fuel and gasoline tanks and piping due to deficient installation or corrosion especially in old underground storage tanks. Another group is the halogenated VOCs, which are used as solvents and degreasers. Their former use as septic tank cleaners also accounts for many instances of private well contamination. The third group includes some of the chlorinated volatile organic compounds (CVOCs) which contain some chlorine in the compounds, and most, if not all, are made by humans. Among the least desired CVOCs are the trihalomethanes, since they are known as suspected carcinogens [7-8].

EDCs and PPCPs have been continuously disc0harged into the aquatic environment for more than a century without any restrictions. Some compounds such as ibuprofen and salicylic acid are generally removed with high efficiency by conventional wastewater treatment plants, but others, such as carbamazepine and clofibric acid, are not efficiently removed. Many studies have indicated trace level (ng/L to µg/L) occurrence of EDCs and PPCPs causing adverse impacts on human and ecosystem. Therefore the occurrence of detection of EDCs and PPCPs in the aquatic environment has been receiving increasing attention in recent times, notably in industrialised countries. EDCs are a diverse group of natural or synthetic chemicals that interfere with the functioning of hormone systems resulting in unnatural responses in the receiving organism. The US EPA defines endocrine disrupting compounds like exogenous agents that interfere with the synthesis, secretion, transport, binding, action or elimination of natural hormones in the body that are responsible for the maintenance of homeostasis, reproduction, development and/or behaviour [9]. EDCs are certain natural and synthetic hormones, alkilphenols, pesticides, herbicides, organochlorines, polyaromatic hydrocarbons (PAHs), dioxins. Pharmaceuticals and personal care products (PPCPs) such as cosmetics, sunscreens, detergents, shampoos can also act as ECDs. EDCs and PPCPs found in the aquatic environment are structurally diverse [10-11].

It has been proven that most of these compounds undergo both incomplete removal in wastewater treatment plants and slow natural degradation, consequently they are found in surface waters receiving effluent from treated plants.

Since many pollutants resist to conventional treatments, other strategies are needed. Several methods have been reported for degrading emerging organic contaminants. In addition to nanofiltration and reverse osmosis, other techniques, including ozonation and chemical oxidation, have been identified in successfully treatments of organic contaminants in water. The latter processes can lead to the formation of oxidation intermediates which are, to date, mostly unknown. In adsorption technology, inorganic adsorbents are often employed since they offer advantages due to their stability towards the radioactive and thermal treatments which are necessary to induce the complete degradation of adsorbates and, therefore, the regeneration of exhausted adsorbents. Among inorganic adsorbents, it has been proven that zeolites are efficient in removing small organic compounds from the environmental matrix, as has surfactant-modified zeolite (SMZ) in removing volatile organic compounds like benzene, toluene, ethylbenzene, and xylenes (BTEX) [3-4]. Likewise, mesoporous silica materials, and their surface modifications were also studied as adsorbents/supports in contaminant removal

processes. To date, studies and applications on organic pollutant adsorption in microporous zeolitic materials from aqueous media have been relatively scarce. Zeolites are environmentally compatible crystalline alumino-silicates, which have well defined micropore dimensions and composition in a rigid crystal lattice. Zeolite frameworks consist in tetrahedral units of SiO_4 and AlO_4, and their silica alumina ratio (SAR) determines zeolite polarity. Their three-dimensional framework, generating nanometre-sized channels and cages, imparts high porosity and a large surface area onto these materials. One of their defining features is that the shape of their internal pore structure can strongly affect their adsorption selectivity toward host molecules. It has been shown that zeolites are more effective in removing certain organic molecules from water than activated carbon and are less sensitive than GAC to the presence of dissolved natural organic matter in the water stream being treated.

We focused on the volatile organic chemicals (VOCs) and in particular three different substances (toluene, tert-butyl methyl ether, 1,2-diclhoroethane) belonging to four class of compounds found in the wastewater were considered. This study, therefore, has a dual purpose: i) to measure the sorption capacity of hydrophobic commercial zeolite materials weighed against contaminants dissolved in water and to quantify aspects of their removal efficiency for potential use in wastewater and groundwater remediation, and ii) to understand zeolite structural features for the adsorption of contaminants from aqueous solutions. Coupling the information gathered from these approaches can help in selecting adsorbent materials for water treatment. In the present work, three organophilic synthetic zeolites (ZSM-5, MOR and Y), which are cheap and available on the market, differing in topology, channel systems and free window apertures, and various organic contaminants differing in chemical properties and molecular dimensions, were tested. These zeolites are hydrophobic, they have a high Si/Al ratio and therefore they are able to remove pollutants from aqueous solution and widely used in adsorption-related applications.

1.1 POROUS MATERIALS

Porous materials can be classified on the basis of pore dimensions in: microporous (pore diameter, $d_{pore} \leq 20Å$), mesoporous ($d_{pore} \sim 20\text{-}500Å$) and macroporous ($d_{pore}>500Å$) materials. The aluminosilicate materials employed in the present work belong to the first two categories. In particular, microporous materials belonging to various member of the large family of aluminosilicates known as zeolites, and mesoporous silica or aluminosilicate materials, with a regular structure, such as Mobil Composite of Matter (MCM) and Hexagonal Mesoporous Silica (HMS), were studied.
In the following these materials are described in detail.

1.1.1 MICROPOROUS MATERIALS

The history of zeolites began in 1756 when the Swedish mineralogist Cronstedt discovered the first zeolite mineral, stilbite. He recognized zeolites as a new class of minerals consisting of hydrated aluminosilicates of the alkali and alkaline earths. Since the crystals exhibited intumescence when heated in a blowpipe flame, Cronstedt called the mineral a “zeolite” derived from two Greek words, “zeo” and “lithos” meaning “to boil” and “stone”. Only in 1930 the first structure of zeolites were determined by Taylor and Pauling and in 1932 McBain established the term “molecular sieve” to define porous materials that act as sieves on a molecular scale. In 1948, Barrer reported the first definite synthesis of zeolites including the synthetic analogue of the zeolite mineral mordenite and then many progresses have been done in the synthesis of zeolites. A large number of zeolites with new framework topologies, compositions, and properties have been successfully prepared through continued synthetic efforts. Nowadays, zeolites are available on a large scale and in a variety of applications, since they have a lot of properties: ion-exchange properties, good sorption capacity, shape selectivity, high catalytic activity, very high thermal stability and can be used at high temperatures [12-13].

Zeolites are crystalline aluminosilicate from group IA and group IIA elements such as sodium, potassium, magnesium, and calcium. Chemically, they are represented by the empirical formula:

$$M_{2/n}O * Al_2O_3 * ySiO_2 * wH_2O$$

Where y is 2 to 10, n is the cation valence, and w represents the number of water molecules contained in the voids of the zeolite. Structurally, zeolites are crystalline, based on an infinity extending three-dimensionally, four-connected framework of AlO_4 and SiO_4 tetrahedra linked to each other by the sharing of oxygen ions. Each AlO_4 tetrahedron in the framework bears a net negative charge which is balanced by an extra-framework cation. The framework structure contains channels or interconnected voids that are occupied by the cations and water molecules. The cations are mobile and ordinarily undergo ion exchange. Water may be removed reversibly, generally by heating.

The structural formula of a zeolite is based on the crystallographic unit cell, the smallest unit of structure, represented by:

$$M_{x/n}[(AlO_2)_x(SiO_2)_y] * wH_2O$$

Where n is the valence of cation M, w is the number of water molecules per unit cell, x and y are the total number of the tetrahedra per unit cell, and y/x usually has a value of 1-5. In the case of high zeolites, y/x is 10 to 100. There are two types of structures: one provides a system of uniform channels which, in some instances, are one-dimensional channel system. The preferred type has two- or three-dimensional channels to provide rapid intracrystalline diffusion in adsorption and catalytic applications. In most structures the primary structural units, the AlO_4 or SiO_4 tetrahedra, are assembled into secondary building units which may be simple polyhedral such as cubes, hexagonal prism, or cubi-octahedra (see Figure 1.1). The final framework structure consists of assemblages of secondary units. Some of the more important zeolite types, most of which have been used in commercial applications, include the zeolite minerals mordenite, chabazite, erionite and clinoptilolite, and the synthetic zeolites type A, X, Y, L, “Zeolon” mordenite, ZSM-5, beta and zeolites F and W [14].

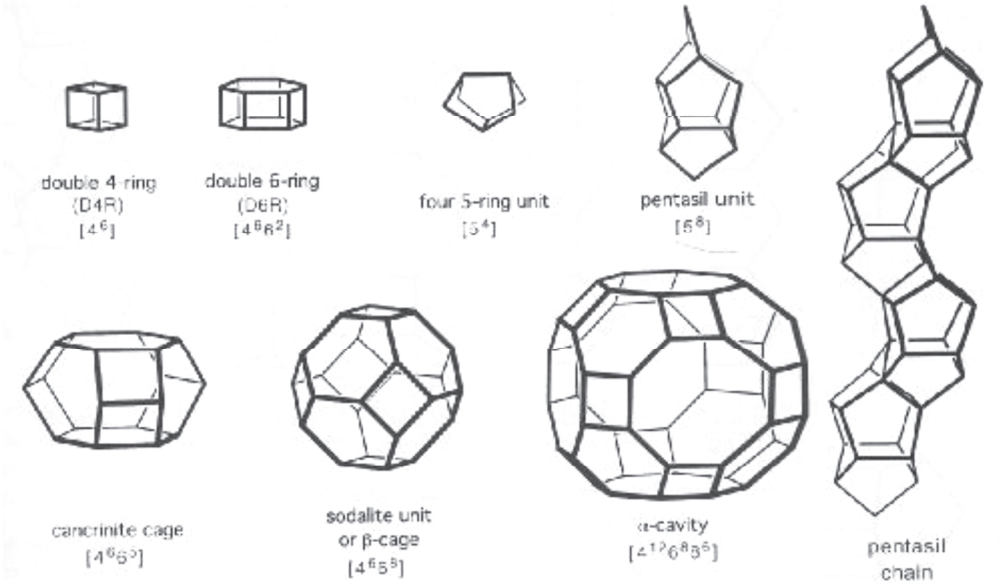

Figure 1.1: Some subunits and cage/cavities and one example of chains which recur in several framework types.

1.1.1a Aluminosilicate zeolites and silica molecular sieves

The evolution of aluminosilicate zeolites is based on an increasing framework Si/Al composition. This class is divided into four categories: low Si/Al zeolites (1 to 1.5), intermediate Si/Al zeolites (2 to 5), high Si/Al zeolites (10 to 100) and silica molecular sieves (silicalite).

The thermal stability increases from about 700°C in the low silica zeolites to 1300°C in the silica molecular sieves. The surface selectivity, which is highly hydrophilic in the low silica zeolites, is hydrophobic in the high silica zeolites and the silica molecular sieves. The acidity tends to increase in strength with an increasing Si/Al ratio. As the Si/Al ratio increases, the cation concentration and ion exchange capacity (proportional to the aluminum content) decreases. The structures of the low silica zeolites are predominantly formed with 4-, 6-, and 8-rings of tetrahedra. In the intermediate silica zeolites, the onset of 5-rings in mordenite and omega zeolite can be seen. In the high silica zeolite structures and the silica molecular sieves, a predominance of 5-rings of tetrahedral can be found.

The low silica zeolites represented by zeolites A and X are aluminum-saturated, have the highest cation concentration, and give optimum properties in terms of capacity, pore size and three-dimensional channel systems. They represent highly heterogeneous surfaces with a strongly hydrophilic surface selectivity. The intermediate Si/Al zeolites (Si/Al of 2-5) consist

of the natural zeolites erionite, chabazite, clinoptilolite and mordenite, and the synthetic zeolites Y, mordenite, omega and L. These materials are still hydrophilic in this Si/Al range.
The high silica zeolites with a Si/Al of 10-100 can be generated by either thermochemical framework modification of hydrophilic zeolites or by direct synthesis. These materials are reported to be hydrophobic and organophilic and represent a range of pore sizes from 0.4-0.8 nm. A very large number of high silica zeolites, prepared by direct synthesis, have now been reported, including beta, ZSM-5, ferrisilicate and borosilicate analogs of the aluminosilicate structures. Silicalite and fluorite silicalite are typical of the reported silica molecular sieves.
In summary, if we compare the properties of the low and intermediate zeolites with those of the high silica zeolites and silica molecular sieves, we find that their resulting properties allow the low and intermediate zeolites to remove water from organics and to carry out separations and catalysis on dry streams. In contrast, the hydrophobic high silica zeolites and silica molecular sieves can remove and recover organics from water streams and carry out separations and catalysis in the presence of water [14].

1.1.1b Characterisation techniques

The basic characterisation techniques for zeolites and molecular sieves developed in the 1950, particularly by the Union Carbide workers, were X-ray powder diffraction (XRD), gravimetric adsorption measurements on multi-tube McBain-Bakr balances different molecular-sized adsorbates, and various tests to screen applications.

The X-ray powder diffraction pattern is a method which is still used and is a typical "fingerprint" which allows one to determine sample impurity, degree of crystallinity, or the size of a unit cell of a zeolite. Furthermore, by sampling synthesis mixtures at regular time intervals, it is possible to monitor the progress of a reaction very closely. The determination of the degree of crystallinity is only possible by sample comparison with a standard material. Adsorption measurements give pore size and pore volume, in earlier times McBain-Bakr balances were used, now modern and automated volumetric methods are used and produce isotherms. The gas is introduced into the sample in incremental steps, and the pressure difference is measured and the isotherm can be calculated. Thermal gravimetric analyses can provide useful information regarding the thermal treatment of zeolites. Graphs of weight loss vs. temperature often give clear indications as to the temperature required to burn off organic templates or the temperature required for a complete or optimum regeneration in TSA processes. Nowadays, to better understand the structure and chemistry of molecular sieves

other techniques are used, for instance computer modelling, the application of solid state nuclear magnetic resonance (NMR), infrared (IR) and Raman spectroscopies and scanning electron microscopy (SEM) techniques. This latter technique has become a versatile technique in product development and quality control during zeolite production. With a resolution of a few nanometres, SEM produces high quality images of single zeolite crystals and of agglomerates and may show extra-zeolite phases or amorphous compounds. The morphology is influenced by conditions used during synthesis. Infrared and Raman spectroscopies provide information on bonds between atoms. These may be atoms constituting the zeolite or molecules sorbed into the pores or the outer surface. NMR can help facilitate structure solution, for example, in good cases the number of crystallographically independent atoms of a particular type in the structure can be ascertained from the number of resonance in an NMR spectrum. Theoretical calculations and modelling can also play an important part in structure solution and there is a great deal to be said for using chemical experience and intuition in building possible model structures which may match the size of a measured unit cell or the structure as seen in electron micrographs [12-13-14].

1.1.1c Applications

Applications of zeolite and molecular sieves in the 80's and 90's showed a growth in petroleum refining applications with an emphasis on resid cracking and octane enhancement, this is due to the zeolites surface acidity. ZSM-5 was commercialized as an octane enhancement additive in fluid catalytic cracking (FCC) where Si-enriched Y zeolites serve as the major catalytic component in high-octane FCC catalysts. The use of zeolite catalysts in the production of organic (fine) chemicals appeared as a major new direction, because if zeolite has high silica content in the framework, it resists at the high temperature that occur during catalytic and regeneration cycles.

Zeolites have maximum cation exchange properties when the framework contains an equal number of aluminium and silicon atoms, each oxygen atom is linked to one aluminium and to one silicon atom. Zeolites with maximum cation exchange capacity are of interest as detergents in removing calcium and magnesium water that hinders washing efficiency. This function has been performed mainly by phosphates which are now discouraged by environmental pressures. Zeolite ion exchange products, both synthetic and natural (especially clinoptilolite), were used extensively to purify waters and to remove toxic metal cations, such as Fe, Mn, Cu, Co, Pb and Ni. This property also allowed Sr, Cs and other radioisotopes to be scavenged from nuclear waste [3-4-13].

Zeolites and related nanoporous materials are widely used in adsorption applications due to their properties, which are reported in the following:

Stability. Zeolite is expected to remain active for long periods of time. Operational life is expected to be 10 to 20 years. However, experience over such period is not yet available. Therefore, its replacement or regeneration is easily achieved. After adsorption, the exhausted zeolites are normally subjected to a regeneration process by operating at temperatures ranging from 250° to 350°C, for a time ranging from 30 minutes to 1.5 hours, and in the presence of an air flow (ranging from 1.5 to 2.5 m^3/hr). Under these particularly mild conditions zeolite materials maintain their structural integrity, so that they can be regenerated several times without substantially modifying their adsorbing properties

Availability and cost. Remediation costs using PRB systems are reported to be up to 50% lower than those of the pump-and-treat method used so far. Considerable quantities of both natural or synthetic zeolites can be purchased at low prices.

Environmental compatibility. It is important that the reactive media does not form any by products when reacting with contaminants and that it is not a source of contamination itself by solubilisation or other mobilization mechanisms.

High Efficiency. Zeolites have recently been used to irreversibly remove high amounts of drugs from water, such as sulfonamide antibiotics, erythromycine (ERY), carbamazepine (CBZ) and levofloxacin (FLX). The adsorption kinetics of the isolated drugs in zeolite Y were very favourable, and their removal from water was complete in less than 1min. Therefore, it has been proved that *the adsorption efficiency of zeolite is not modified* in the presence of dissolved natural organic matter in the water stream being treated. In all cases the embedding of drugs into zeolite cages was revealed by unit cell parameter variation and structural deformation of the framework obtained by X-ray structure analysis. The efficiency of other zeolites with different framework topologies such as mordenite, ZSM-5 and beta zeolites, respectively, was also tested. These excellent results suggest the development of this type of investigation on other pollutants classes.

Shape selectivity. One of the most important features of zeolite is their ability to adsorb selectively and separate organic molecules. The shape of their internal pore structure can strongly affect their adsorption selectivity towards host molecules. In particular, zeolites are versatile adsorbents for VOC monitoring; in fact they can adsorb a wide array of VOCs even at low concentrations in indoor environment. Recently Vignola et al. [3-4] have demonstrated that hydrophobic zeolites are able to effectively adsorb molecules against which ZVI or GAC are totally ineffective. In particular, ZSM-5 zeolite turned out to be suitable for mono-

aromatic molecules, such as BTEX (Benzene, Toluene, Ethyl benzene and Xylenes), and halogen-benzene derivatives.

Adsorption phenomena are found in many domains including catalysis, pollution control, gas separation and storage. Recent environmentally driven applications have arisen using the hydrophobic molecular sieves as adsorbent, highly siliceous Y zeolite and silicalite, for the removal and recovery of volatile organic compounds (VOCs) which offer the promise of significant market growth. An exciting new scientific direction has emerged over the last few years for exploring molecular sieves as advanced solid state materials, this research includes zeolite electrodes; batteries and chemical sensors [13-14].

1.1.2 MESOPOROUS MATERIALS

A major advance in molecular sieve materials was reported in 1992 by researchers at Mobil. Kresge et al. and Beck et al. describe a new family of mesoporous silicate and aluminosilicate materials (Micelle-Templated Silicas, MTS), designated M41S. The most important members of the family include: MCM-41, with a unidimensional hexagonal arrangement of uniform open channels 0.2-10 nm in diameter and MCM-48, with a 3-dimensional channel system with pore sizes of 0.3 nm. The order in the structure is derived from the channel arrangement. The silica or aluminosilicate wall outlining the channel is disordered and exhibits properties much like amorphous silica or silica-alumina [14].

The properties of mesoporous materials have been explored in view of applications in fields as diverse as catalysis, biocatalysis, chromatography, sensing, photonics, optics, drug delivery, etc [15].

MCM-41 (Mesoporous Mobil catalytic materials) synthesis is possible due to unique self-assembly processes between surfactants and inorganic matter (see Figure 1.2). The formation of the hexagonal MCM-41 are consistent with the aggregation of $C_nH_{2n+1}(CH_3)N^+$ surfactant micelles into rods. These structures are known to exist in a hexagonal arrangement in solution. Inorganic silicate present in the reaction mixtures could then form around these arrays to produce an inorganic structure, reflecting the hexagonal micellar array (pathway 1 of Fig. 1.2). Another possible mechanism in which the silicate influences the formation of this liquid crystal phase (pathway 2 of Fig. 1.2). The carbon chain length of the quaternary ammonium surfactant plays a role in determining the dimensions of $C_nH_{2n+1}(CH_3)N^+$ micelles

and in the dimensions of the pores of MCM-41. MCM-41 usually have very high surface area of about 700 m^2/g and high hydrocarbon sorption capacity [16].

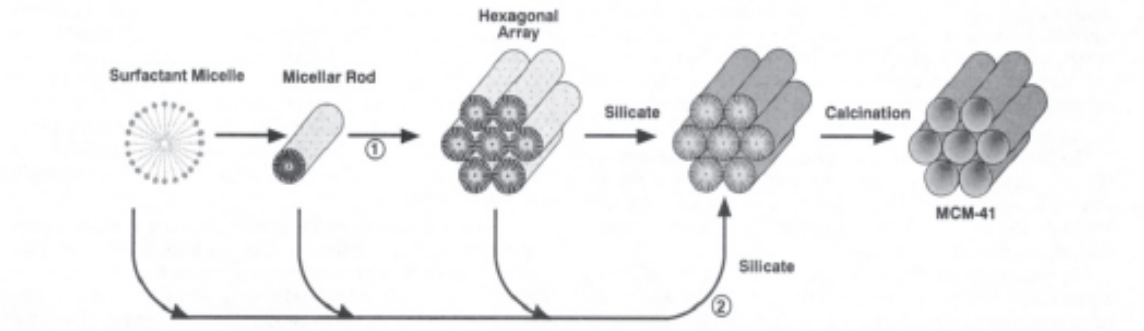

Figure 1.2: Possible mechanism pathways for the formation of MCM-41 (1) liquid crystal phase initiated and (2) silicate anion initiated [16].

In 2002 Galarneau and co-workers have developed a new method to transform amorphous mesoporous silicas into ordered materials maintaining the spherical morphology of the parent silica. It is based on the concept of pseudomorphic synthesis and allows a control of morphology from the nano to the microscale. The concept of pseudomorphic transformation has been applied to amorphous preshaped silica particles (5 to 800 μm) to produce Micelle-Templated Silicas (MTS) with the same morphology, using a mild alkaline solution to dissolve silica progressively and locally, and reprecipitate it at the same rate without modifying the global morphology of the grain. In particular the MTS material was synthesized by reacting the pre-shaped amorphous porous silica in alkaline solution ($NaOH+H_2O$) containing the surfactant and in the presence of swelling agent (1,3,5-trimethylbenzene, TMB) if necessary. The reaction mixture was stirred at 50°C and then placed in oven in stainless-steel reactor at 115°C for different days. The mesoporous obtained was filtrated and washed with water, dried overnight and calcinated at 550°C in air for 8h [15-17].

Another material belong to the MCM-41 class of molecular sieves is called HMS and it was described by Tanev and Pinnavaia for the first time. Hexagonal mesoporous materials are based on hydrogen bonding and self-assembly between neutral primary amine surfactants and neutral inorganic precursors. This neutral templating route has physical and catalytic properties substantially different from MCM-41 material prepared by electrostatic assembly. Indeed HMS has smaller domain size with shorter channels and larger textual mesoporosity than MCM-41 and these properties provide for the best access to the framework-confined

mesopores in adsorption and catalysis by guest molecules [18-19]. HMS molecular sieves were prepared by assembly pathways in water: ethanol solvent mixtures of differing composition and polarity. In both reactions media tetraethyl orthosilicate (TEOS) served as the neutral silica precursor and dodecylamine and tetradecylamine were the neutral structure directors. In a typical synthesis the surfactant was dissolved in ethanol, and then the desired amount of water was added under vigorous stirring to obtain a homogeneous solution. TEOS was added to the surfactant solution and the mixture was allowed to react under stirring at ambient temperature for about 18 h. When mesitylene was used as an auxiliary structure director, it was added to the surfactant solution and stirred for 15 min before the addition of TEOS. All of the HMS reaction products were filtered and dried in air. The surfactant can be readily removed from HMS mesostructures by solvent extraction or by calcination at 630°C in air for 4 h [19-20].

1.1.2a Characterisation techniques

The same technique described for the microporous materials was used to characterise the mesoporous materials, but it was possible to collect different information. In particular it has been used the scanning electron microscopy (SEM) techniques to obtain the particle morphology; the X-ray diffraction (XRD) pattern showed the specific peaks of all mesoporous materials; through Fourier transform infrared (FTIR) it was possible to observe the band characteristic of the silanol group, moreover this technique provided a rapid and effective method of following transformations occurring during the synthesis and allows a kinetic analysis, being indicative of the mechanical stability of the samples. Nitrogen sorption isotherms at 77K, determined with an apparatus from Micromeritics Instrument, were useful to measure the specific surface area, pore volume and pore size distribution [21-22-23].

1.2 ADSORPTION

Sorption phenomena play an important role in many fields of the natural sciences and underlie a number of extremely important processes. Applications of adsorption for chemical processing, air pollution control, and water treatment are well known. Adsorption is viewed as a superior method for wastewater treatment indeed. It has been demonstrated that adsorption is widely effective for removing dissolved organic substances from wastewaters. In such cases, the phenomena involved is the adsorption at different interfaces. This phenomenon causes a change in the concentration of the components at the interface with respect to their concentration in the bulk phase. Two adsorption processes may be distinguished: physical adsorption and chemical adsorption (chemisorption). Physical adsorption occurs when non-balanced physical forces appear at the boundary of the phases; and chemisorption occurs when atoms and molecules from adjacent phases form chemical bonds at the interface. The term “adsorption” is used most adequately with respect to sorption from gaseous and liquid phases on nonporous solids and on solids with large pores. A fluid (gas or liquid) in contact with the boundary surface of such solids may be divided into two regions with different physical properties; therefore, in a fluid-solid system, we distinguish three phase: the solid phase (inert adsorbent), the adsorbed (surface) phase formed on the surface of a solid, and the bulk (volume) phase (adsorbate) [24]. Theory underlying adsorption has been developed, however it is still unknown in many cases the mechanisms of interaction of pollutants with the solid sorbents. Consequently, many experiments are performed to compare the experimental data. For what concerns wastewater treatments, adsorption results in the removal of solutes from solution and their concentrations at a surface, until the amount of solute remaining in solution is in equilibrium with that at the surface. This equilibrium is described by expressing the amount of solute adsorbed per unit weight of adsorbent, q, as a function of C_e, the concentration of solute remaining in solution. An expression of this type is termed an adsorption isotherm.

1.2.1 STATIC AND FLOW METHODS

To determine adsorption isotherm is possible to use static methods (batch) or flow methods. The most common flow method is frontal analysis (FA). In many respects, the static method is comparable to FA, except that it is slower and usually requires larger amounts of material. The equilibrium adsorption isotherm is basically important in the design of adsorption system [25].

Batch method consists of immersing a known weight of adsorbent in a solution of known concentration in a closed vessel and waiting until equilibrium is reached. After a time, usually between in a few hours or in a few days, which depends on the size of the vessel and of the amount of adsorbent, a state close enough to equilibrium is reached. The solution at equilibrium is then analysed and the amount of solute adsorbed per unit weight of adsorbent (q) is calculated by

$$q = \frac{V(C_0 - C_e)}{w} \tag{1.1}$$

where V is the volume of solution (L), w is the mass of adsorbent (g), C_0 and C_e are the initial and equilibrium concentration of adsorbate in solution, respectively (mg L^{-1}) [26-27].

Frontal Analysis (FA) was originally proposed by James and Phillips and by Schay and Székely for the determination of adsorption isotherms. Its principle consists in replacing abruptly the mobile phase pumped into the column with a solution of the compound studied at a known concentration in the same mobile phase and in recording the composition of the column eluate. The profile recorded is called the breakthrough curve (see Figure 1.3). Frontal analysis (FA) of aqueous solution of contaminants on columns packed with zeolites particles allows directly data (adsorption isotherm) regarding the interactions between the microporous adsorbent materials and contaminants dissolved in the aqueous phase. FA permits the direct measurement of the equilibrium constant and the determination of the adsorbate-adsorbent interaction energy. The most important advantage of FA over other techniques is that, in a very wide concentration range, the precision of the data measured, the retention time of a breakthrough curve, are independent from the substrate concentration. Furthermore, FA measurements provide information on both the thermodynamic and the kinetic of the interactions studied (through the retention time and the shape of the breakthrough curve, respectively). The fundamental equation of FA stems from an integral mass balance throughout a column in equilibrium with a given mobile phase composition. The attainment of equilibrium is evidenced by an abrupt change in the concentration profile (breakthrough curve).

From the breakthrough volume, V_b, the amount adsorbed q^*(mol/g), corresponding to the mobile phase concentration C (mol/L), is calculated by:

$$q^* = \frac{C(V_b - V_0)}{w_{pack}} \tag{1.2}$$

where w_{pack} is the weight (g) of packing inside the column and V_0 the hold-up volume [25].

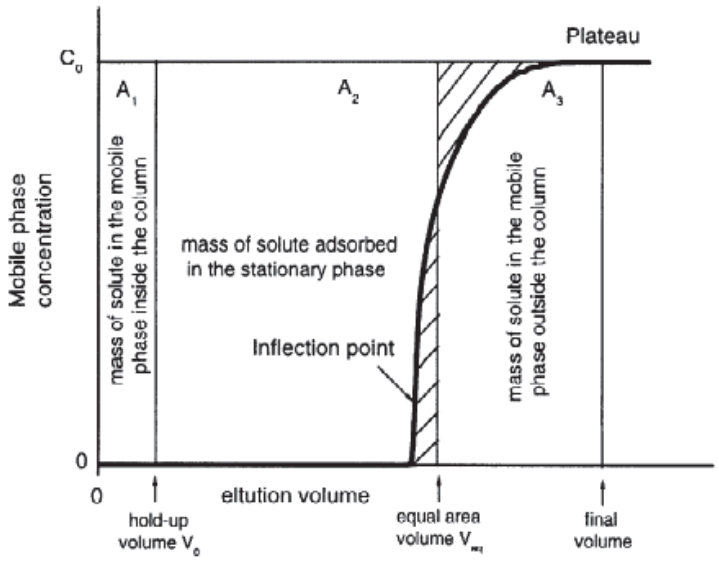

Figure 1.3: Frontal analysis method for determination of the equilibrium concentrations in the stationary phase. The breakthrough curve is represented by the thick solid line [28].

1.2.2 ADSORPTION MODELS

In this thesis adsorption phenomena of pollutants onto zeolites in aqueous phase was studied using both batch and flow method and the data were fitted with different equations describing diverse adsorption models. A considerable number of adsorption isotherm models have been suggested in order to account for extremely varied adsorption behaviour, depending on the nature of the adsorbent and of the adsorbate. These isotherm models can be divided into the following categories [25].

1- Isotherm models for ideal adsorption on homogeneous surfaces. The assumptions underlying that model are: 1) absence of adsorbate - adsorbate interactions, the adsorbed phase consists in a monolayer of adsorbate molecules and 2) the sorbent surface is homogenous, or in other worlds, there is solely one kind of interaction between the solid adsorbent and the contaminant in solution.

Surfaces are characterised by an adsorption energy distribution (AED) function, $F(\varepsilon)$, that may be broader or narrower, or that may have several more or less well resolved modes, each mode having a finite width. The experimental isotherm on such a surface is the sum of the isotherm contributions of each one of the different types of homogeneous sites that are covering the surface. Under the condition of a continuous adsorption energy distribution and assuming a Langmuir local isotherm model on each homogeneous patch of the surface, the experimental isotherm can be written:

$$q^*(C) = \int_0^\infty F(\varepsilon) \frac{b(\varepsilon)C}{1 + b(\varepsilon)C} d\varepsilon \tag{1.3}$$

$$b(\varepsilon) = b_0 \exp(\frac{\varepsilon}{RT}) \tag{1.4}$$

where $q^*(C)$ is the total amount of a solute adsorbed on the surface at equilibrium with a concentration C of this solute, ε is the binding energy between an adsorbed solute molecule and the surface of the adsorbent (the energy of adsorption), and $b(\varepsilon)$ is the associated binding constant related to ε. b_0 is a pre-exponential factor that can be derived from the molecular partition functions in both the bulk and the adsorbed phase [29].

The two important isotherms based on this model are the Langmuir and the Jovanović equations respectively. Jovanović model differs from Langmuir in the fact that the adsorption and the desorption processes are not supposed to be instantaneous.

The Langmuir isotherm is an isotherm model for ideal adsorption on homogeneous surfaces, the system can be described by a simple adsorbed monolayer. The expression of the isotherm is:

$$q = \frac{q_s K_L C_e}{1 + K_L C_e} \tag{1.5}$$

where q is defined in Eq. 1.1, C_e is the equilibrium concentration in solution (mg L^{-1}), K_L is the Langmuir coefficient and q_s is the saturation capacity (is the monolayer capacity of the adsorbent, mg g^{-1}). The ratio $\theta = q/q_s$ is called the fractional surface coverage. The Langmuir model appears the first-choice empirical equation to fit experimental results regarding the adsorption of single components. The Langmuir isotherm can be linearized in several ways, for example:

$$\frac{C_e}{q} = \frac{1}{K_L q_s} + \frac{C_e}{q_s} \tag{1.6}$$

Although these plots are convenient for checking the validity of the model in a particular case, nonlinear regression should be preferred for the determination of the best values of the parameters K_L and q_s.

The Jovanović isotherm was derived to account for the adsorption of a gas onto an homogeneous surface, with no adsorbate-adsorbate interactions. It is similar to the Langmuir model but it corrects for the error made in the derivation of this latter model when assuming that the adsorption and the desorption of the molecules of the solute considered are instantaneous. The isotherm equation becomes:

$$\theta = \frac{q}{q_s} = 1 - e^{-KC} \tag{1.7}$$

This equation has rarely been reported as accounting well for a set of experimental data [25].

2- Isotherm models for ideal adsorption on heterogeneous surfaces. In this models adsorbate - adsorbate interactions are assumed to be negligible, but they take into account for surface heterogeneity by considering adsorption sites characterised by various interaction energies between the sorbent and the contaminants. The most employed models belonging to this group are the bi-Langmuir, the Tóth, the Freundlich and the Langmuir-Freundlich isotherms. When different sites are considered the normalization condition for the adsorption energy distribution, $F(\varepsilon)$, can be considered:

$$q_s = \int_0^{\infty} F(\varepsilon) d\varepsilon \tag{1.8}$$

where q_s is the overall saturation capacity [25-29].

The bi-Langmuir isotherm was first suggested by Graham to account for adsorption behaviour on certain inhomogeneous surfaces. The surface is covered with two different kinds of sites that behave independently (and on each of which the two basic principles of the Langmuir model, local adsorption and lack of adsorbate - adsorbate interaction, apply), the equilibrium isotherm results from the addition of the two independent contributions of the two types of sites. The isotherm is:

$$\mathrm{q} = \frac{\mathrm{q_s K_L C_e}}{1 + \mathrm{K_L C_e}} + \frac{\mathrm{q_{s,1} K_{L,1} C_e}}{1 + \mathrm{K_{L,1} C_e}} \tag{1.9}$$

where the subscript refers to the type of adsorption sites. It usually used when the experimental data are acquired in a wide concentration range.

The Tóth Isotherm accounts for adsorption on a heterogeneous surface, with no adsorbate - adsorbate interactions. It has three parameters. The heterogeneous surface has a unimodal adsorption energy distribution with a width related to the value of the parameter *n*. The equation is:

$$\frac{q}{q_s} = \frac{KC}{[1 + (KC)^n]^{1/n}} \tag{1.10}$$

This isotherm is similar to the Langmuir model, to which it becomes identical for n=1. The parameters q_s and K have the same meaning as in the Langmuir isotherm model and n is the

heterogeneity parameter. The parameter *K* and *n* permit independent adjustment of the initial slope and curvature of the isotherm. It is frequently used because it is possible the determination of the adsorption energy distribution.

Boedeker proposed the following empirical isotherm equation:

$$q = K{C_e}^{1/n} \tag{1.11}$$

where *K* and *n* are the Freundlich constants characteristic of the system, indicators of adsorption capacity and adsorption intensity, respectively. The exponent *1/n* is smaller than unity (it was 0.5 in Boedeker's results). This isotherm is known as the Freundlich isotherm and it accounts for the adsorption of strongly polar compounds on polar or strongly polar adsorbents (inhomogeneous surface) in low- or medium polarity solvents, but it isn't restricted to the formation of monolayers [25]. If *n* is equal to unity the adsorption is linear. This means that the adsorption sites are homogeneous (as in the Langmuir model) in energy and no interaction take place between the adsorbed species. If the value of *1/n* is smaller than 1, reflecting favourable adsorption, then the sorption capacity increases and new adsorption sites occur. When the value of *1/n* is larger than 1, *1/n*>>1, the adsorption bond becomes weak; unfavourable adsorption take place, as a result of the decreasing adsorption capacities [26].

The Langmuir-Freundlich isotherm is an empirical isotherm and it is a combination of two classical models, the Langmuir and the Freundlich models discussed earlier:

$$\frac{q}{q_s} = \frac{(KC_e)^v}{1 + (KC_e)^v} \tag{1.12}$$

where *v* is the heterogeneity parameter. This model, at low concentration, reduces to the Freundlich isotherm, but it reduces to the Langmuir model for the case of a homogeneous surface. This model has been used in simple studies of the adsorption behaviour on heterogeneous surfaces.

There exists a great variety of adsorption isotherm models for heterogeneous surfaces without lateral interactions. Another important isotherm very useful for the characterisation of porous solids, and in particular microporous solids, is the Polanyi-Dubinin-Manes (PDM) model. The Dubinin–Astakhov (DA) or Dubinin–Radushkevich (DR) equation was derived from

Polanyi's potential theory for a vapour phase system and extended from Manes to aqueous systems by defining the Polanyi adsorption potential $\varepsilon_{sw} = RTln(S/C_e)$, where R is the ideal gas constant (8.314 J mol^{-1} K^{-1}), T the temperature (K), and S is the water solubility (mg L^{-1}). Polanyi adsorption potential describes heterogeneous adsorption phenomena. This equation is given by:

$$q = V_0 \rho_0 \exp\left[\frac{RTlnS/C_e}{E}\right]^b \tag{1.13}$$

where V_0 and ρ_0 are the maximum volume of adsorbed compound for unit mass of adsorbent (cm^3 g^{-1}) and compound density (mg cm^{-3}), respectively. E (kJ mol^{-1}) is the free energy of the adsorption process compared to that of a reference compound. b is an exponent which can be obtained by fitting or set to a given (integer) value, when b=2 it becomes the Dubinin–Radushkevich equation. From literature, the exponent values proposed are b>4 for zeolites, b=2-3 for homogeneous carbons, and b<2 for heterogeneous active carbons. But these values depend on both the adsorbate and the adsorbent and it is very difficult to have a universal exponent. As the zeolites and the activated carbons don't present comparable values of the characteristic energy, it isn't possible to compare the structure of the samples on the basic of the b exponent [30-31-32-33-34].

3- Isotherm models for nonideal adsorption on a heterogeneous surface. Besides the heterogeneity of the adsorbent surface above described, the second major reason for the adsorption of a compound to deviate from Langmuir isotherm behaviour is that the adsorbed molecules interact, we find the Fowler isotherm, the anti-Langmuirian isotherm, and several S-shaped isotherm models, including the BET isotherm models and the Moreau model [25]. The solution of the equations describing energy distribution, $F(\varepsilon)$, with the Fowler, the BET and the Moreau isotherms can be difficult due to the presence of a parameter (the adsorbate–adsorbate interaction coefficient, in addition to the equilibrium constant).

The Fowler-Guggenheim model isotherm model was introduced to correct for the first-order deviations from the Langmuir isotherm. It assumes ideal adsorption on a set of localized sites on a homogeneous surface, with weak interactions between molecules adsorbed on neighbouring sites. It assumes also that the interaction energy between two sorbate molecules is small enough that the random character of the sorbate molecule distribution on the

adsorbent surface is not significantly altered. Under these assumptions, the following liquid-solid isotherm is obtained:

$$K_{FG}C_e = \frac{\theta}{1-\theta}\exp\left(\frac{2\theta W}{RT}\right) \tag{1.14}$$

where K_{FG} is the equilibrium constant for adsorption of the adsorbate on an active site (L mol^{-1}), C_e is the concentration at equilibrium adsorption (mol L^{-1}), Θ is the degree of surface coverage and is the ratio q/q_s, W is the empirical interaction energy between two molecules adsorbed on nearest neighbouring sites (J mol^{-1}), 2 is the number of nearest-neighbour sites, R is the ideal gas constant and T is the thermodynamic temperature (K). The term $(2\Theta W/RT)$ is a measure of the average force field acting on an adsorbed molecule and created by the surrounding molecules on the nearest sites. Fowler-Guggenheir equation is one of the simplest equations taking into account the lateral interactions [25-35].

S-Shaped isotherms are sometimes referred to as anti-Langmuir isotherms because their initial curvature is convex down. The true anti-Langmuir isotherm, however, would have a vertical asymptote for some finite value of mobile phase concentration. The S-shaped isotherms belong to class V and are often called S-shaped isotherms. The curvature of these isotherms at the origin and at low concentrations is concave upward, which indicates that the amount adsorbed at equilibrium increases more rapidly than the concentration in the mobile phase [25].

BET isotherm developed by Brunauer et al. (1938) is one of the most successful isotherm models to express adsorption phenomena [36]. The BET isotherm describes well the adsorption behaviour corresponding to types II or III isotherms of the IUPAC classification of isotherms. It assumes that the solute molecules can be adsorbed from the solution onto either the bare surface of the adsorbent or a layer of solute already adsorbed. The expression after a rather lengthy derivation is:

$$q = q_s \frac{K_s C_e}{(1-K_l C_e)(1-K_l C_e + K_S C_e)} \tag{1.15}$$

where K_S and K_l are the equilibrium constants of adsorption of the compound on the bare surface and on a layer of adsorbate previously adsorbed, respectively. However, both

constants are related to the strength of the solute-solute interactions. If K_lC<<1, the system can be described by a simple adsorbed monolayer, that is the Langmuir isotherm.

The so-called Moreau isotherm is the simplest model for a homogeneous adsorbent surface with lateral interactions (i.e. adsorbate-adsorbate). The equation is:

$$\frac{q}{q_s} = \frac{K_r C_e + I\,(K_r C_e)^2}{1 + 2K_r C_e + I(K_r C_e)^2} \tag{1.16}$$

where q_s, K_r and I are the monolayer saturation capacity, the equilibrium constant at infinite dilution and the adsorbate-adsorbate interaction parameters, respectively. The equilibrium constant at infinite dilution K_r is associated with the adsorption energy ε through the following equation:

$$K_r = K_0 \exp(\frac{\varepsilon}{RT}) \tag{1.17}$$

where R is the universal gas constant, T is the absolute temperature and K_0 is a pre-exponent factor that could be derived from the molecular partition functions in the bulk and the adsorbed phase. K_0 is often considered to be independent of the adsorption energy ε. The adsorbate-adsorbate parameter I can be written as:

$$I = exp\left(\frac{\varepsilon_{AA}}{RT}\right) \tag{1.18}$$

Where ε_{AA} is the interaction energy (by convention $\varepsilon_{AA} \geq 0$) between two neighbour molecules of adsorbate A [25-37].

The Ruthven model was suggested to account for single-component adsorption in zeolitic system. In this system, each cage in the zeolite can contain a finite number of adsorbate molecules. For a cage which may accommodate up to two molecules of the adsorbate, the model gives for single-component adsorption:

$$\frac{q}{q_s} = \frac{K_r C_e + R\,(K_r C_e)^2}{1 + K_r C_e + R/2(K_r C_e)^2} \tag{1.19}$$

where R is the parameter accounting for adsorbate-adsorbate interactions in a cage and represent the corresponding configuration integral [37].

Adsorption isotherms are also classified according to their shape and in particular to the nature of slope of the initial portion of the curve, and thereafter into sub- groups depending on the slope of the isotherm in the high concentration range (see Figure 1.4). Briefly, the main classes are: S Curves, indicative of interactions between adsorbed molecules at the surface; L Curves, the normal or Langmuir isotherms, usually indicative of monolayers of molecules adsorbed on the surface; H Curves (high affinity), often given by solutes adsorbed as ionic micelles, and by high affinity ions exchanging with low affinity ions; C Curves (constant partition), linear curves, given by solutes which penetrate into the solid more readily than does the solvent [38].

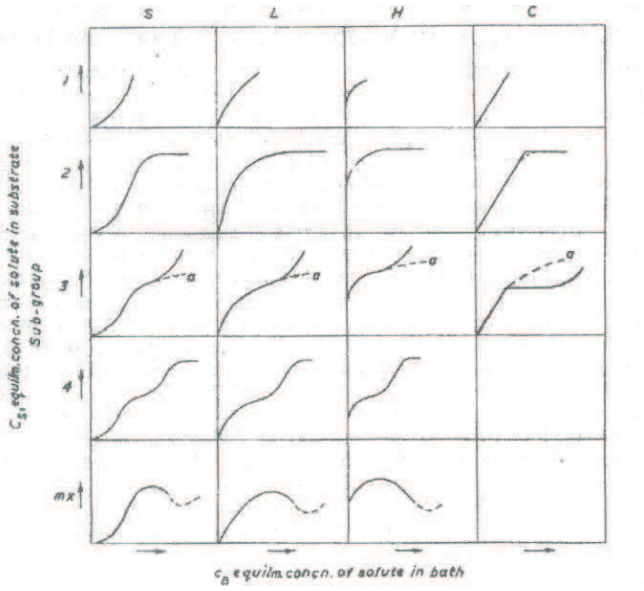

Figure 1.4: System of isotherm classification [38].

The isotherms, describe as far as here, can readily be extended to an n-component mixture. The equilibrium of multicomponent are more complex that single-component, this is due to the competition between the different components for interaction with the adsorbent, indeed molecules compete for access to the adsorption sites, and those of the more strongly adsorbed compounds tend to exclude the others. The amount of any component adsorbed at equilibrium depends on the concentration of all the other components present in the solution, for this reason multicomponents isotherms are often called competitive isotherms. The most common isotherms whose parameters can be determined directly from single-components data include the competitive Langmuir and the competitive Langmuir-Freundlich.

The competitive Langmuir isotherm is derived from the traditional Langmuir model (Eq. 1.5). However, when several components are simultaneously present in the solution, these compounds interfere. The amount of each of them that is adsorbed at equilibrium is smaller than if this compound were alone.

The amount, q_i, of the component i that is adsorbed at equilibrium is proportional to the surface area covered by its molecules so the competitive isotherm is written:

$$q_i = \frac{a_i C_i}{1 + \sum_{j=1}^{n} b_j C_j} \tag{1.20}$$

where n is the number of components in the system. The coefficients a_i and b_i are the coefficients of the single-component Langmuir equilibrium isotherm for component i. In a binary mixture it is possible to write the formula in:

$$q_i = \frac{q_{S,i} K_{L,i} C_i}{1 + K_{L,1} C_1 + K_{L,2} C_2} \tag{1.21}$$

The single-component isotherm is represented by a curve in the (q, C) plane. Binary competitive isotherms are represented by two surfaces, one in the three-dimensional space (q_1, C_1, C_2), the other one in the (q_2, C_1, C_2) space.

Also, the Langmuir-Freundlich equation (Eq. 1.12) can be extended to an n-component mixture:

$$q_i = \frac{a_{i,0} C_i^{Pi,0}}{1 + \sum_{j=1}^{n} a_{i,j} C_j^{Pi,j}} \tag{1.22}$$

This model, as for the description of single component, is based on heterogeneous surfaces [30].

1.3 KINETIC

Adsorption and desorption reactions are known to be important in many systems and were investigated recently for various adsorption systems. Adsorption and desorption are time-dependent processes. Therefore, it is necessary to evaluate the rate of these processes to compare adsorbents performances and to optimize adsorption and regeneration processes design. For these reasons, it is of interest to recognize the adsorption and desorption kinetics and determine their phenomenological coefficients characterising the transport of sorbate within sorbents [39].

To determine adsorption kinetic is possible to use static methods (batch) or flow methods (frontal analysis, FA).

1.3.1 KINETIC FOR STATIC METHOD

Many attempts have been made to formulate general mathematical expressions, which would be able to adequately describe the kinetics of sorption processes. The progress in this field appears to be limited by the fact that the description of sorption kinetics is a much more complicated problem than the theoretical description of sorption equilibrium. This is because the expressions describing the thermodynamic quantities at equilibrium are only limiting forms of those describing the time evolution of these quantities under non-equilibrium conditions. According to the present state of knowledge, the sorption process can be described by the following consecutive steps (i) transport of solute in the bulk of the solution; (ii) diffusion of solute across the so-called liquid film surrounding sorbent particles; (iii) diffusion

of solute in the liquid contained in the pores of sorbate particle and along the pore walls (intraparticle diffusion); (iv) adsorption and desorption of solute molecules on/from the sorbent surface. The overall sorption rate may mainly be controlled by any of these steps; a combined effect of a few steps is also possible. In many experimental sorption systems the effect of transport in the solution is eliminated by rapid mechanical mixing, thus, it is not assumed to be involved in controlling of the overall sorption rate and can be ignored, as a rule. In order to determine the contribution of the remaining steps, numerous kinetic models have been compared to predict the behaviour of the experimental data. The most widely used are those assuming that step (iv) makes a significant contribution in the kinetics of a process. Here, this step is referred to as the "surface reaction". The "surface reaction" term may not necessarily mean the actual chemical reaction occurring on the adsorbent surface involving the formation of chemical bonds. Interactions of physical nature (van der Waals forces, for instance) may also play a role. The crucial assumption behind this model is that the rate of the transfer of solute molecules from the solution (located in the direct vicinity of the surface) to the adsorbed phase either governs the overall rate of sorption process or at least is partially involved in it. The development of an appropriate model can be based on accepting a certain fundamental approach to interfacial kinetics, such as the Langmuir model, for instance, and its further modification in order to adopt it for a given sorption system. This method has led to propose many expressions related to the concept of a chemical reaction occurring on the surface and its order. These include Langmuir kinetics, first order and second-order reversible, and first-order and second-order irreversible reactions based on the solute concentrations. Simultaneously, many simple, compact formulas, such as the pseudo-first (Lagergren) and pseudo-second order equations or Elovich equations have been applied for correlating kinetic data measured in many different systems [40]. These formulas have usually been associated with the surface-reaction kinetic step as controlling the sorption rate and were done in equilibrium conditions; therefore the amount of solution adsorbed calculated in equilibrium (q_t) with batch method is determined as:

$$q_t = \frac{V(C_0 - C_t)}{w} \tag{1.23}$$

where C_0 and C_t are the initial and liquid-phase concentration of the solution at time t, respectively, V is the volume of the solution, and w is the mass of the adsorbent.

The first model for description of the kinetics of gases adsorption onto solid surfaces and adopted later for the solid/solution system was described by Langmuir and it is:

$$\frac{dq_t}{dt} = K_a C(q_m - q_t) - K_d q_t \tag{1.24}$$

in which C is the solute concentration in the bulk solution, q_t is the amount adsorbed at time t (Eq. 1.23). Further, K_a and K_d are some temperature-dependent constants and q_m is the monolayer capacity. This model is rather rarely used in its form given, however, when some assumptions are made, it can be reduced to other expressions, pseudo-second and pseudo-first order equations, commonly applied for the analysis of kinetic data. Langmuir kinetic model is related to the simple case of an ideal, energetically homogeneous solid surface and one-site occupancy adsorption model. The problem of incorporating the surface heterogeneity into the classical Langmuir kinetics is due to the existence of a two-dimensional different distribution of the K_a and K_d constants. In the early 1980s a new family of theoretical approaches appeared, among them the most important is the Statistical Rate Theory (SRT) approach that can further be generalized to describe the kinetics of adsorption in the gas/solid and solution/solid system with energetically heterogeneous solid surfaces, but one essential assumption of this model is that of a quasi- equilibrium on the solid surface. Besides SRT method has represented by complicated mathematical form. At present, the most popular expressions that describe the sorption of solutes from a liquid solution are the pseudo-second and pseudo-first order equations. Their main advantage is simplicity and easiness when applying to correlate the data without necessity of using advanced computational procedures. Most often many different rate equations are tested in parallel and the appropriate best-fit procedures are used to verify whether one is better than another. The linear least-squares method, applied to the transformed kinetic data is usually adopted for this purpose.

The pseudo-second order kinetics is usually associated with the situation when the rate of direct adsorption/desorption process (seen as a kind of chemical reaction) controls the overall sorption kinetics. In fact, the mathematical expression corresponding to this model was proposed by Blanchard et al. to describe the kinetics of heavy metal removal by natural zeolites. There was accepted the assumption that the rate of the ion exchange reaction occurring on the surface is responsible for the removal kinetic and that the kinetic order of this reaction is two with respect to the number of adsorption sites available for the exchange.

The most commonly-applied form of the pseudo-second order equation is that presented by Ho[41]. It can be written in its differential form as:

$$\frac{dq_t}{dt} = k_2(q_e - q_t)^2 \tag{1.25}$$

or, after integrating the above expression with the boundary condition q(t=0)=0 and then rearranging to obtain a linear form:

$$\frac{t}{q_t} = \frac{1}{k_2 q_e^2} + \frac{t}{q_e} \tag{1.26}$$

where k_2 is the pseudo-second-order rate constant of sorption. The procedure of applying the above expression for the analysis of the monitored kinetic data is usually based on plotting of t/q_t against t which should give a linear relationship. In this way the gram of solute sorbed per gram of sorbent at equilibrium (q_e) and sorption rate constant (k_2) can be determined directly from the slope and the intercept, respectively, of the linear plot [42-43] Many experimental studies and the extensive use of the pseudo-second order model have revealed that the value of k_2 strongly depends on the applied operating conditions, such as initial solute concentration, pH of solution, temperature and agitation rate. The k_2 constant value is usually strongly dependent on the applied initial solute concentration. It decreases with the increasing c_{in} as a rule, which is a commonly known fact related to the interpretation of k_2 as a time-scaling factor. The influence of pH and temperature on the k_2 value has not yet been theoretically studied, due to the complexity of the problem and numerous factors, importance of which can vary from one system to another, nevertheless both pH and temperature influence equilibrium system and therefore play an important role in the course of kinetic processes. It is important to know the agitation rate because it is possible the change of the transport of sorbate in the surface region of adsorbent when there is different rate. Another parameter present in Eq. 1.26 represents the amount of solute sorbed at equilibrium (q_e). Generally, its value should be equal to those determined from the measurements of the equilibrium adsorption isotherm, which can accompany the recording of the kinetic data.

At the end of 19th century, Lagergren presented the empirical rate equation for the adsorption of ocalic and malonic acids onto charcoal. This equation, called the pseudo-first order equation or the Lagergren equation, is probably the earliest known one describing the rate of sorption in the liquid-phase systems. Moreover, it has been one of the most widely used kinetic equations until now. Its differential form has the following formulation:

$$\frac{dq_t}{dt} = k_1(q_e - q_t) \tag{1.27}$$

when solving Eq. 1.27 with the boundary condition $q(t=0)=0$, one obtains:

$$\ln(q_e - q_t) = \ln q_e - k_1 t \tag{1.28}$$

where q_t and q_e are the grams of solute sorbed per gram of sorbent at any time and at equilibrium, respectively, and k_1 is the rate constant of first-order sorption [39]. The values of q_e and k_1 parameters are usually determined by applying the commonly accepted linear regression procedure, based on the above representation. The k_1 parameter is the time-scaling factor, the value of which decides how fast the equilibrium in the system can be reached (the tendency of the increasing k_1 value which results in shorter times required for a system to reach an equilibrium is maintained). As the similar observation has been made regarding the k_2 constant, it is worth noting that these resemblances are due to the mathematical differential forms of both the pseudo-first and the pseudo-second order equations. The experimental studies have confirmed that the value of k_1 parameter can be both dependent and independent of the applied operating conditions. The pseudo-first order equation is usually not able to describe the kinetic data equally well as the pseudo-second order equation. Examples of an opposite trend are rather sparse. The dependence of the k_1 constant value on the applied initial solute concentration varies from a system to another. It usually decreases with the increasing initial solute concentration in the bulk phase. This is understandable as k_1 can be treated as a time-scaling factor. Nevertheless, there are also systems whose behaviour can be predicted well by Eq. 1.28 and the obtained k_1 value is independent of c_{in}. However, as pseudo-second, the pseudo-first order equation is usually associated with the situation when the overall rate of sorption is determined by the rate of direct solute transfer from the solution to the adsorbed phase.

In conclusion, the pseudo-first order Eq. 1.28 can be treated as the expression corresponding to many different models when considering the range of high times, when the investigated system is close to equilibrium. Independently, several of narrower interpretations have been proposed. Many of them are connected with the assumption of time-independent solute concentration or linear equilibrium adsorption isotherm. There also exist some other approaches for which the pseudo-first equation is only a special case of more general kinetic expressions. The pseudo-second order equation Eq. 1.26 is able to simulate the behaviour characteristic of many different kinetic models very well and, one of the major advantages of the pseudo-second order equation over the pseudo-first order is its ability for "smoothing" the experimental data [39-40].

However, recent studies show that the pseudo-second order and the Elovich equation exhibit very similar behaviour under the assumption that the system is not close to equilibrium. The Elovich equation is the rate equation, proposed by Roginsky and Zeldovich in 1934 to describe the kinetics of adsorption of carbon monoxide on manganese dioxide. Its integral form reads:

$$q_t = \frac{1}{B}\ln(1 + ABt) \tag{1.29}$$

where A and B are the constants. The applicability of the Elovich equation is restricted to the initial times of sorption process, when the system is relatively far from equilibrium. There exist many different theoretical interpretations of that equation, most of them are directly connected with the assumption of strong heterogeneity of the sorbent surface [40].

1.3.2 KINETIC FOR FLOW METHOD

To determine the kinetic for flow methods several approach can be used, in our study it was utilized breakthrough curves (frontal analysis) and the zero length column method.
Kinetic studies of mass transfer in columns provide essential information on the separation mechanisms in chromatography. The most convenient approach for the kinetic study on column is obtained by analysing the dependence of the height equivalent to a theoretical plate (HETP, H) on the mobile phase flow velocity (u). It is generally assumed that mass transfer in chromatographic columns consists of several processes and the contributions of these processes to the total HETP are additive. The following four main processes are usually

considered, (i) axial dispersion, (ii) fluid-to-particle mass transfer, (iii) intraparticle diffusion, and (iv) adsorption/desorption.

The mass balance and the kinetic equations of the lumped kinetic model are:

$$\frac{\partial C}{\partial t} + u\frac{\partial C}{\partial z} + F\frac{\partial q}{\partial t} = D_L\frac{\partial^2 C}{\partial z^2} \tag{1.30}$$

$$\frac{\partial q}{\partial t} = k_m(q^* - q) \tag{1.31}$$

where q^* is the concentration of the solute in the stationary phase at equilibrium with C, t is the time, z the longitudinal distance along the column, and F the phase ratio [$F=(1-\epsilon)/\epsilon$ whit ϵ is the total column porosity]. The overall mass transfer rate in a column is represented by two kinetic parameters, D_L and k_m. The rate constant k_m accounts for the contributions of all the mass transfer processes contributing to peak broadening, except for axial dispersion (D_L). These include fluid-to-particle mass transfer, intraparticle diffusion, and adsorption/desorption. This model assumes that the driving force of the mass transfer between stationary and mobile phases is q^*-q, i.e., the deviation from equilibrium, and that the mass transfer rate is proportional to the driving force. Lapidus and Amundson derived an analytical solution for the set of Eqs. (1.30-1.31). On the basis of this result, Van Deemter et al. proposed the following plate height H equation which is valid for linear chromatography:

$$H = 2\frac{D_L}{u} + 2\left(\frac{k_0'}{1+k_0'}\right)^2\left[\frac{ud_p}{6Fk_f} + \frac{ud_p^2}{60FD_e} + \left(\frac{k_p}{1+k_p}\right)^2\frac{u}{Fk_{ads}}\right] \tag{1.32}$$

where k_o' is the retention factor at infinite dilution, d_p is the average particle diameter, k_f the external mass transfer coefficient, D_e the intraparticle diffusivity, k_{ads} the adsorption rate constant. The coefficient k_p is useful to simplify the formalist but it has no special physical meaning. In the general rate model of chromatography, the rate of adsorption or desorption are assumed to depend on the deviation of the local concentration from its equilibrium value. The mass transfer rate coefficient in the solid film linear driving force model (k_m) is related to three kinetic parameters, the external mass transfer coefficient, the intraparticle diffusivity, and the adsorption rate constant. The contributions of the corresponding three mass transfer processes are additive.

In the equilibrium-dispersive model, the contributions to band broadening of all the mass transfer processes active in the column are accounted for by one parameter only, D_a called apparent axial dispersion coefficient: the parameter D_L in Eq. 1.30 is replaced by D_a. It is assumed that the mass transfer kinetics between stationary and mobile phases is infinitely fast, therefore $k_m=\infty$. D_a was estimated from the breakthrough curve experimentally measured in the FA method (see the next paragraph). The HETP in the equilibrium-dispersive model becomes:

$$H_{Pe} = \frac{2L}{Pe_L} \tag{1.33}$$

where Pe_L is the column Peclet number, and $k_{m,L}$ is correlated with D_a as follows

$$k_{m,L} = \frac{u^2}{D_a}\frac{K}{(1+K)^2} \tag{1.34}$$

where K is the partition coefficient in nonlinear chromatography [44].

It is possible to have kinetic information, also, through the desorption curve of the zero length column method (see the next paragraph). In this model the overall mass transfer resistance (*1/k*) includes both external film and internal diffusional resistance:

$$\frac{1}{k} = \frac{R}{3k_f} + \frac{R^2}{15KD} \tag{1.35}$$

where R is the equivalent radius of adsorbent, k_f the fluid film mass transfer coefficient, K the dimensionless equilibrium constant and D intracrystalline diffusivity. For a liquid system, K is generally of order of unity, and the micropore diffusivity is always substantially smaller than the bulk diffusivity, it is reasonable to neglect the external resistance and assume:

$$k \approx 15D/R^2 \tag{1.36}$$

Therefore, for different value of D/R^2, it is possible to have similar general form of the desorption curves but with some quantitative differences. For small values of D/R^2 the desorption occurs in two distinct steps: an initially rapid step during which most of the sorbate

is removed, followed by a much slower final approach to equilibrium. As a result, the time for 95% completion passes through a maximum at an intermediate value of D/R^2 [45-46].

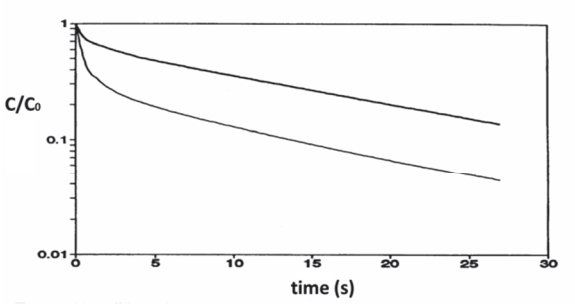

Figure 1.5: Typical time dependence of average adsorbed phase concentration calculated by integration of the desorption curve obtained with ZLC method.

1.4 DIFFUSION

Diffusion has been widely studied over the past 50 years to develop experimental methods for measurement of intracrystalline diffusion and to increase our basic understanding of the transport mechanism. Intracrystalline diffusion plays an important role in most of the practical applications of zeolites as adsorbents and catalysts. Indeed there are many examples, some of which have been commercialized to large processes, in which the catalyst selectivity depends on differences in diffusion rates between different species. The majority of adsorption separation processes depend on differences in equilibrium but some such processes depend on molecular sieving (size exclusion) or differences in sorption rates. These issues are especially important in zeolite membranes which are likely to see increasing commercialization over the next decade.

Diffusion is the macroscopic result of the sum of all molecular motions involved in the sample studied. Molecular motions are described by the general equation of dynamics. The classical Fick's first law explains the diffusional flux, *J*, in relation with the diffusivity or diffusion coefficient, $D_{A,B}$ through this equation:

$$J = -D_{A,B}\frac{dC}{dz} \tag{1.37}$$

where *dC/dz* is the concentration gradient along the column, $D_{A,B}$ the diffusivity of solute A in solvent B and *C* is the concentration of the component considered. As it is difficult to measure *J*, the Fick's second law is most widely used:

$$\frac{dC}{dt} = D_{A,B}\frac{d^2C}{dz^2} \tag{1.38}$$

There are several methods for obtaining an approximate value of the diffusion coefficient, one of which can be calculated with:

$$D_{A,B} = \frac{RT}{f} = \frac{RT}{6\pi\eta aN} \tag{1.39}$$

where *f* is the friction factor estimated by the Stokes-Einstein law of friction, *N* is Avogadro's number, η is the mobile phase viscosity, and *a* is the molecular radius, *R* the ideal gas constant and *T* the absolute column temperature [13-25].

The methods for measuring the diffusion coefficient value are divided into two broad categories; microscopic (sub-crystal scale) and macroscopic (many crystals) techniques depending on whether the technique measures a bulk flux or attempts to track and average the movement of individual molecules. The most used in this thesis are macroscopic techniques and in particular breakthrough curves and the zero length column (ZLC) method. The separation power of a column, under a given set of experimental conditions, is directly a function of the rate of the mass transfer kinetic and of the axial dispersion coefficient (D_L in the Eq. 1.32 HETP) [13].

Even if the ZLC method shows several advantages (i.e. small quantities, dilute aqueous solution), it is possible to determine diffusion coefficient by means of breakthrough curves.

Various mathematical models have been developed to describe the chromatographic process. The most important of these models are the equilibrium-dispersive (ED) model, the lumped kinetic model, and the general rate model (GRM) of chromatography. In the equilibrium-dispersive model, we assume that the mobile and the stationary phases are constantly in equilibrium. The model assumes an apparent axial dispersion coefficient, D_a, accounting for all the dispersive phenomena (molecular and eddy diffusion and non-equilibrium effects) that take place in a chromatographic column.

The apparent dispersion coefficient is:

$$D_a = \frac{H_{Pe} u}{2} = \frac{uL}{2N} = \frac{uL}{Pe_L} \tag{1.40}$$

where H_{Pe} is the column height equivalent to a theoretical plate (HETP) in this model, u is the mobile phase linear velocity, L the column length, and N the number of theoretical plates or apparent efficiency of the column. In this model, the mass balance equation for a single component is expressed as follows:

$$\frac{\partial C}{\partial t} + u\frac{\partial C}{\partial z} + F\frac{\partial q}{\partial t} = D_a \frac{\partial^2 C}{\partial z^2} \tag{1.41}$$

where q is the concentration of the solute in the stationary phase at equilibrium with C, t is the time, z the distance along the column and $F=(1-\epsilon)/\epsilon$ is the column phase ratio. q is related to C through the isotherm equation, $q=f(C)$. ϵ is the total column porosity or void volume fraction of the column packing [28].

The zero length column (ZLC) method is a chromatographic technique that eliminates the uncertainty due to axial dispersion. It depends on following the desorption of sorbate from a previously equilibrated (small) sample of adsorbent into a solution. The ZLC method was introduced, for gas phase adsorption systems, in the late 1970s, and then has been extended to the measurement of counter-diffusion in liquid phase adsorption systems by Ruthven and Stapleton. The actual ZLC column (see Figure 1.6) consists of a thin layer of adsorbent material placed into a small column. The individual particles (or crystals) are dispersed approximately as a monolayer across the area of the column. This minimizes the external resistances to heat and mass transfer, so that the adsorption cell can be considered as a perfectly mixed isothermal, continuous flow cell. Brandani and Ruthven have derived the

solution for the general mathematical model for such a system, including the capacity of the fluid phase as well as that of the adsorbent [47-48]. The mathematical description of the ZLC technique is also relatively simple and starts from an adsorbate mass balance across the column together with the diffusion equation written for a spherical crystal:

$$V_s \frac{\partial \bar{q}}{\partial t} + V_F \frac{\partial C}{\partial t} + FC = 0 \tag{1.42}$$

$$\frac{\partial q}{\partial t} = D\left(\frac{\partial^2 q}{\partial r^2} + \frac{2}{r}\frac{\partial q}{\partial r}\right) \tag{1.43}$$

The boundary and initial conditions are

$$q(r,0) = \bar{q}(0) = q_0 = KC_0 \qquad C(0) = C_0$$

$$\frac{\partial q}{\partial r}(0,t) = 0$$

The solution to this set of equation is given by

$$\frac{C}{C_0} = \sum \frac{2Lexp(-\beta_n^2 \tau)}{\beta_n^2 + (1 - L + \gamma\beta_n^2)^2 + L - 1 + \gamma\beta_n^2} \tag{1.44}$$

Where the β_n are the positive roots of:

$$\beta_n cot\beta_n + L - 1 - \gamma\beta_n^2$$

And the model parameters are:

$$L = \frac{1}{3}\frac{FR^2}{KV_sD};\ \gamma = \frac{1}{3}\frac{V_F}{KV_s};\ \tau = \frac{D}{R^2}t \tag{1.46}$$

where C_0 and C are the initial concentration and the concentration of adsorbate, respectively; t is time, r the radial coordinate in crystal, q the adsorbed phase concentration of adsorbate, D the diffusion coefficient, F the volumetric fluid flow rate, K the equilibrium constant, R the radius of adsorbent crystal, V_F the volume of fluid and V_s the volume of adsorbent in column. The key parameter is L which, from its definition (see Eq. 1.46), can be considered as the ratio of the diffusional and washout time constants, R^2/D and KV_s/F. This parameter is also

equal to the dimensionless adsorbed phase concentration gradient at the surface of the solid at the time zero. From either of these definitions it is evident that *L* gives an indication of how far removed the system is from equilibrium control. This parameter is proportional to the flow rate, so it can be easily varied and, in order to extract a reliable time constant, it is necessary to run the experiment with at least two different flow rates. The three model parameters (*L, γ, τ*) can be extracted from the experimental curves in two different ways. The simple analysis of the asymptotic behaviour shows two different possibilities depending on the time (short or long time), alternatively direct numerical fit of the experimental curves can be carried out using a non-linear regression algorithm [47-48-49]. A major advantage of the ZLC method is that, for any particular system, the validity of basic assumptions, under the experimental conditions, can be verified directly by a series of simple experimental tests. To establish the validity of the zero length limits, measurements are repeated with columns containing different amounts of adsorbent [13].

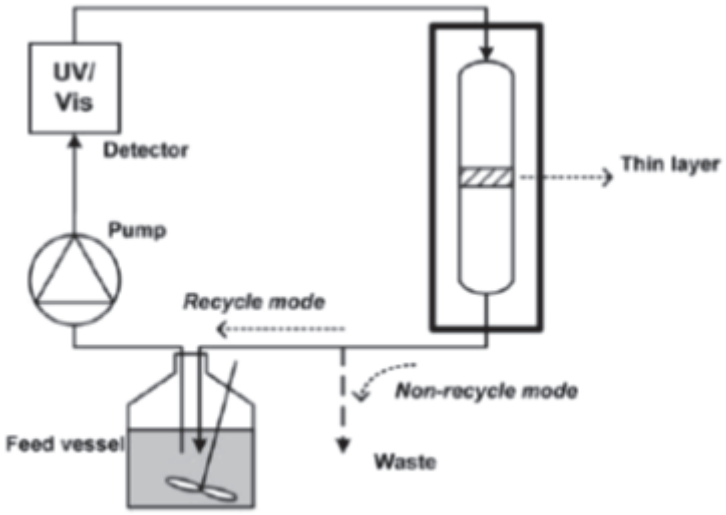

Figure 1.6: Schematic representation of the liquid ZLC [50].

Chapter 2

RESULTS AND DISCUSSION

Case I: Theory of reaction chromatography

One of the main industrial applications of synthetic zeolites is as catalysts in the petrochemical industry, such as in fluid catalytic cracking and hydrocracking. Zeolites confine molecules in small spaces, and, thanks to their acidic properties can facilitate a host of acid-catalyzed reactions, such as isomerisation, alkylation, and cracking. The specific activation modality of most zeolitic catalysts involves Lewis acid site reactions. Therefore, organic molecule reactions could, in some experimental conditions, take place during adsorption processes. In particular, since the main objective of the present work was to investigate adsorption of organic contaminants in zeolite, it could be possible that reaction occurs during adsorption processes. In such cases, different methods can be adopted to evaluate adsorption-reaction data and a comprehensive review of this topic can be found elsewhere [51].

One of these techniques is dynamic chromatography [52], which offers several advantages over other methodologies. Indeed, chromatography makes it possible to obtain mass transfer, adsorption and kinetics data and can be employed in non-linear conditions [53]. However, a prerequisite for employing this technique is that reactions must take place within the separation timescale (on-column reaction chromatography) [54-55].

This work, focuses on a description of dynamic chromatography from a microscopic point of view in order to provide a new method for determining the kinetic constant by dynamic chromatography experiments. In particular, the on-column reaction chromatography process is described by using the stochastic model of chromatography [56].

The main reason for this is that, when coupled with the so-called characteristic function (*CF*) approach, the solution found using this model can be expressed in the closed form in the frequency domain even when complex chromatographic cases are considered. The present work deals with isomerization reactions.

The system under consideration involves four different molecules, which are indicated as:

1) A_M lowest retained conformer in the mobile phase;

2) B_M highest retained conformer in the mobile phase;

3) A_S lowest retained conformer in the chiral stationary phase;

4) B_S highest retained conformer in the chiral stationary phase.

A standard reduction of the kinetic scheme from four states to two states (i.e. *A*, *B*) was followed.

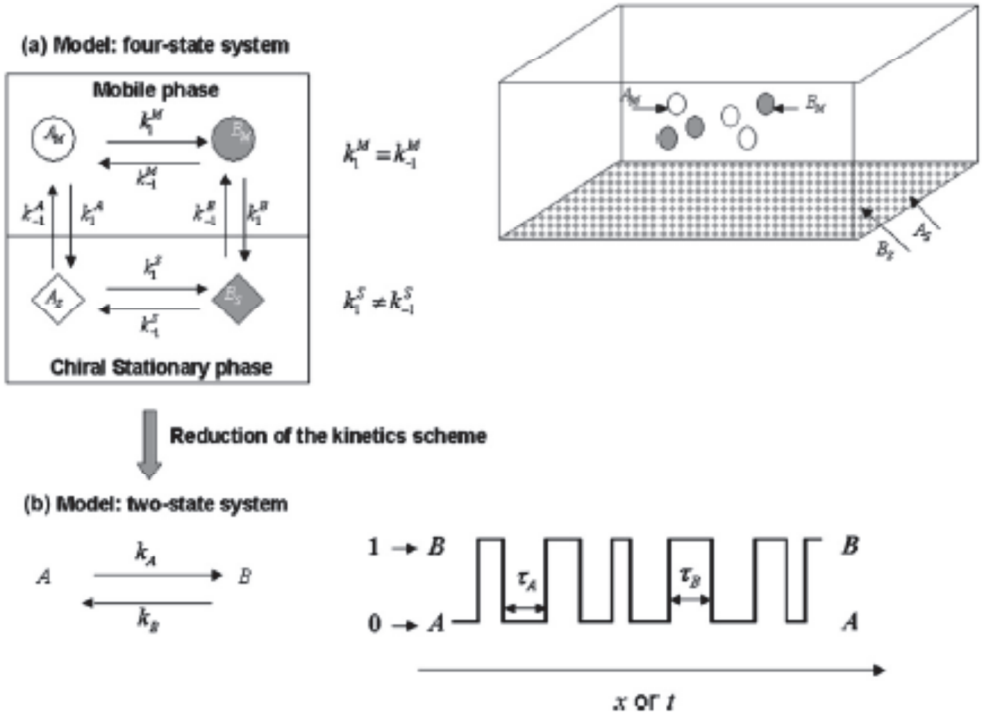

Figure 2.1: a) Kinetics scheme of a four states system and b) Kinetics scheme of a two states system.

1. REACTION MODEL

The main difference between a batch system and the corresponding chromatographic system is that, in the latter, it is important to evaluate the time evolution of a single molecule and its statistical properties instead of the molecular averaged chemical composition of the batch system at a given time. The batch results can be applied to the dynamic chromatographic process thanks to the ergodic hypothesis which states that the averages obtained from a large molecular population and over a long period of observation time are equivalent. In order to simplify the system, a new variable x was defined:

$$x = \frac{\left(t - t_{R,A}\right)}{\left(t_{R,B} - t_{R,A}\right)} = \frac{\left(t - t_{R,A}\right)}{\Delta t_R} = \frac{\left(t' - t'_{R,A}\right)}{\left(t'_{R,B} - t'_{R,A}\right)}$$

(2.1)

where $t_{R,i}$ and $t'_{R,i}$ are the retention times and the corrected retention times, respectively referred to the species in the conformation state *i* with: $i = A \quad and \quad B$.

The x variable represents the normalized time of the interconversion reaction within the limited interval of the chromatographic experiment, defined as the difference in the retention times of the two pure enantiomers, Δt_R, which is herein referred to as "observational time". Thus x represents the fraction of observational time Δt_R spent in the *B* state (in the stationary phase). It can be observed that x also represents the fraction of molecules which are in the *B* state at any given time (i.e. $P_B / \left(P_A + P_B\right)$). One can thus set the two following expressions:

$$a_A(x) = (1 - x)k_A$$

(2.2a)

$$a_B(x) = xk_B$$

(2.2b)

where $a_A(x)$ and $a_B(x)$ are the transition frequencies for the univariate processes $A \rightarrow B$ or $B \rightarrow A$, respectively. $a_A(x)$ and $a_B(x)$ are the so called "propensity functions". At equilibrium (i.e. $x = x_{eq}$), the process becomes stationary and has to satisfy the detailed

balance condition [57] - that is, the frequency transitions are the same in each direction for every pair of states (see Figure 2.2):

$$(1 - x_{eq})k_A = x_{eq}k_B \tag{2.3a}$$

By rearranging Eq. 2.3a one has:

$$x_{eq} = \frac{k_A}{k_A + k_B} \tag{2.3b}$$

which is the equilibrium condition of the *B* state occupancy in the system.

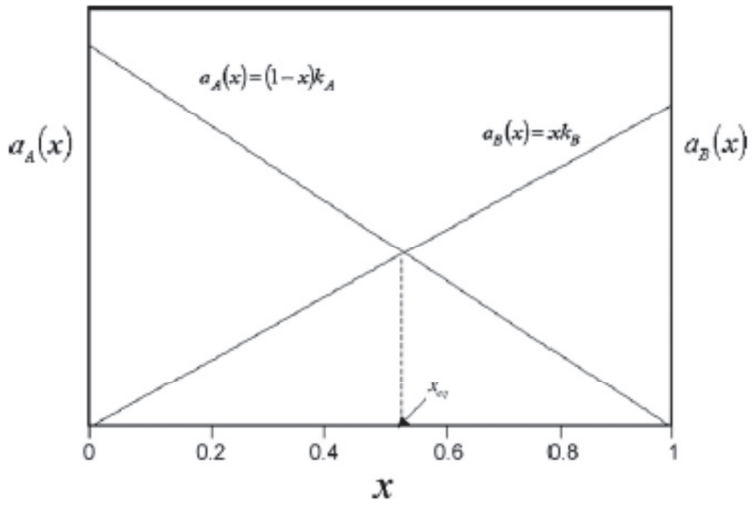

Figure 2.2: Scheme of the propensity functions of the process.

By assuming that the time spent in the mobile phase is constant for any eluted substance and that the forward and backward reaction rate constants in the mobile phase are equal, and by considering the relationships between the concentrations c_A and c_B, and the respective population P_A and P_B, a set of equations describing chromatographic peaks were obtained.

To take the reaction into account, we should consider that in the most general case, the reaction time scale may be similar to the separation time scale: each molecule spends part of the time in both conformations. Consequently, the average molecule migration velocity is expressed as a weighted sum of the migration velocity of the two pure components. The

weights are related to the fraction of time spent in each of the two states. To determine the latter quantities, a two-states jump model was employed. Such a two-states jump process is characterised by a single relaxation rate constant $k = k_A + k_B$, and by $p = k_A / k$, where the probability of finding the molecule in state *B* is equal to x_{ex}.

The solution to this problem (see Appendix D of paper I) can be obtained by following the method known as the Kubo and Anderson formalism [58-59], which has been extensively employed in developing the line shape theory of interconverting chromophores. The two-states enantiomeric interconversion and two-states dynamics processes of a chromophore molecule under stationary conditions [60] are, in fact, closely related from the stochastic-kinetic point of view because: i) they follow the same first order kinetic scheme (see Figs. 2.1 and 2.2); ii) they can be represented stochastically through two-states single molecule random trajectories; iii) the statistics of these random trajectories are the same; and iv) the probability density of trajectories at xT can be obtained as a sum of the two contributions. As mentioned above, the present approach can be applied to describe a macroscopic system which is made up of a large number of molecules or is observed for a long period of time vs. the reaction time scale. This description is mainly concerned with the derivation of the *B* state population at a given time *xT*, resulting from the isomerization reaction: $A_{M+S} \Leftrightarrow B_{M+S}$ under stationary conditions. The concept of the ''random trajectory'' of a single molecule $\xi(t)$ (see Fig. 2.1b) constitutes the starting point for calculating the fraction of average time spent in each state. $\xi(t)$ is the stochastic occupation variable which is set to *0* when the molecule is in state *A*, and *1* when the molecule is in state *B*. The time spent in state *A* or *B* is assumed to be exponentially distributed (corresponding to a first order kinetics). Consequently, the previously introduced quantity x (see Eq. 2.1) can now be expressed as:

$$x = \frac{\left(t - t_{R,A}\right)}{\left(t_{R,B} - t_{R,A}\right)} = \frac{1}{\Delta t_R} \int_{t_{R_B}}^{t_{R_B}} \xi(t)dt = \frac{1}{T} \int_{t_{R_A}}^{t_{R_B}} \xi(t)dt \tag{2.4}$$

where $\Delta t_R = t_{R,B} - t_{R,A} \equiv T$ - sake of notation simplicity equal to T - and x is the fractional time spent in *B* state and is now a stochastic variable characterised by its distribution, since the "histories" of a molecule, $\xi(t)$, giving an equal value to $(t - t_{R,A})$ as the integral in Eq. 2.4, can be more or less probable.

By following the above mentioned formalism the following equations were obtained (see Appendix D, paper I):

$$\hat{p}(\omega|T,A) == \exp\left(-\frac{kT-i\omega T}{2}\right)\left(\phi\cosh\frac{\phi T}{2}+(k+i\omega)\sinh\frac{\phi T}{2}\right)\Big/\phi \tag{2.5a}$$

$$\hat{p}(\omega|T,B) = \exp\left(-\frac{kT-i\omega t}{2}\right)\left(\phi\cosh\frac{\phi T}{2}+(k-i\omega)\sinh\frac{\phi t}{2}\right)\Big/\phi \tag{2.5b}$$

where:

$$\phi = \sqrt{\left(\left(\frac{k}{2}\right)^2 - i\left(p-\frac{1}{2}\right)k\omega - \left(\frac{\omega}{2}\right)^2\right)} \tag{2.5c}$$

$\omega = 2\pi/T$ is the frequency. $t = T + t_{R,A}$ since the time windows in the considered chromatographic experiment is, as specified above, $t_{R_A} \div t_{R_A} + T$.

The chromatographic process superimposes the reaction as a process of exchange between the mobile and stationary phases - $A_M \Leftrightarrow A_S$ and $B_M \Leftrightarrow B_S$ - and it contributes to broadening the elution band both because of the random nature of the stay of site *A* or *B* in the stationary phase and the random character of the interval between two subsequent adsorption processes from the mobile phase. The general solution of the problem was obtained by coupling the chromatographic band broadening process with the reaction process and was based on the assumption that the unitary band broadening contribution was constant within the domain $t_{R,B} \le t \le t_{R,B}$. The general treatment of the stochastic theory of chromatography can be found elsewhere. In the following a brief description is recalled.

2. CHROMATOGRAPHY MODEL

Let us describe briefly the dynamics of the chromatographic technique in one of its versions: the fundamental device is the so called “COLUMN” which is in practice a tube filled with granules (bed) here assumed as non-porous.

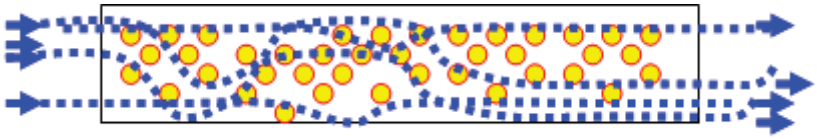

Figure 2.3: The chromatographic “COLUMN”.

A fluid is continuously flowing in the tube. Thus there are two types of zones:

1. the moving zone (fluid)
2. the stationary zone which is the active surface of the granules

The separation process consists in injecting a small volume containing one or more analytes into a fluid stream flowing through the bed.

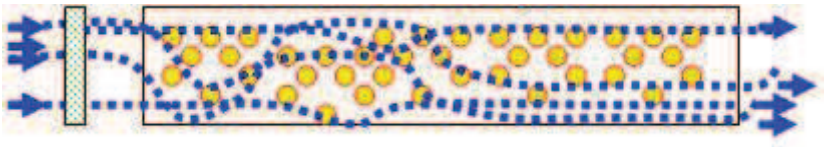

Figure 2.4: “INJECTION”: the Chromatographic experiment begins with the introduction of a pulse volume containing the analyte into the stream.

Let us consider firstly the case of injecting solely one analyte. This analyte volume contains a high number of identical molecules (several million). The analyte molecules can be captured by the active surface and can stay there for a random amount of time. After this time period they are released into the mobile zone. During their stay on the active surface, the analyte molecules are delayed in comparison with the main stream of the flowing mobile zone: their sojourn time undergoes random jumps. As a consequence, the analyte volume travels along the column with an average velocity which is lower than that of the main stream (blue streams). Moreover, the volume occupied by the analyte molecule (= band) will be enlarged because of the random nature of the capturing and releasing of the different analyte molecule by the surface:

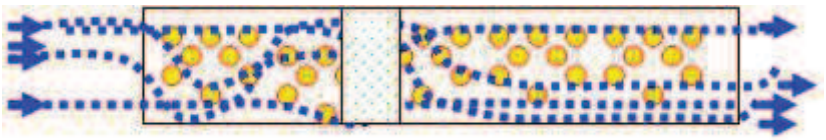

Figure 2.5: The chromatographic experiment is running.

If the injection volume contains two types of molecules:

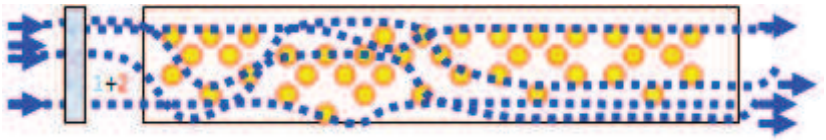

Figure 2.6: Injection of a volume containing two types of analytes.

These will travel at different velocities because the time spent during each single capturing step is different. The two species are thus separated.

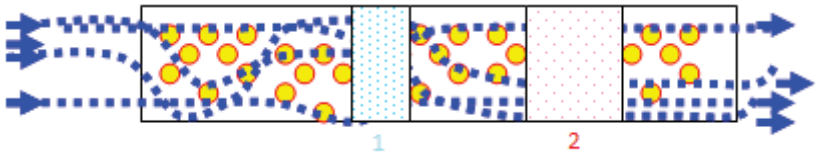

Figure 2.7: Separation of two types of analytes as a consequence of the different affinity of the two components for the stationary zone (surface).

The entire process of chromatographic migration is the result of a series of exchange processes regarding the analyte molecule between the moving zone and the stationary (or static zone).

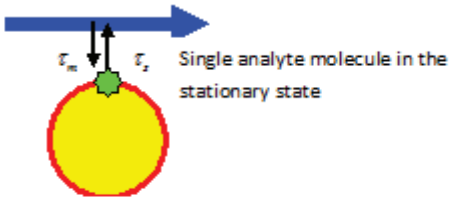

Figure 2.8: Exchange process of the analyte molecule between the moving zone and the stationary zone.

The essence of these exchange processes is stochastic: the time spent between the zone changes are random variables:

τ_m is the time spent in the mobile zone between a desorption and the consecutive adsorption;

τ_s is the time spent in the stationary site zone between the adsorption and the desorption;

The process is thus in essence the sum of random variables.

In the following we will focus on the behaviour of a single analyte chromatography. Moreover, a case where the number of identical species of the analyte is very high will be considering: by injecting a single component, in practice the same process is repeated millions of times and a posteriori behaviour is equal to the a priory probability.

A first approximation was made to consider that there is no dispersion in the fluid streams of the mobile phase:

Figure 2.9: Constant mobile zone velocity model of chromatography.

The model hypothesis is:

1st hypothesis: The velocity of molecules moving in the mobile phase is a unique constant value which is equal to ν_m (mobile phase velocity).

2nd hypothesis: The number of sites visited by a molecule (adsorption states) is a random variable (r.v.).

3rd hypothesis: The number of capturing steps experienced by a molecule is distributed according to a Poisson distribution.

4th hypothesis: The sorption sites of the column are equivalent i.e. the stationary zone is homogeneous.

5th hypothesis: The time spent in a given site is also a r.v. which is independent from the number of adsorption steps r.v.

6th hypothesis: The random variable sojourn time is assumed to be exponentially distributed.

Under these hypotheses the chromatographic process from a statistical point of view can be mathematically described as a random sum (i.e. the number of adsorption steps n is a r.v.) of random variables (i.e. the time spent in each adsorption step) equally distributed (4th hypothesis).

Under hypotheses 1 to 6, it can be demonstrated that the following relationships hold true for the II Characteristic Function (c.f.) of the r.v. t_r is:

$$\Psi_{t_r}(\xi) = \bar{n}\left[\frac{1}{1 - i\omega\bar{\tau}_s} - 1\right] + i\omega t_m \tag{2.6}$$

where t_m is the shift ["the inert tracer" retention time of the column = L/v_m a, (see comments at Fig. 2.8 and Eq. 2.7)], $\bar{n}$ and $\bar{\tau}_s$ are the expectation of the random variables n and τ_s, respectively.

It should be recalled that according to our system of hypotheses, n and τ_s are Poissonian and Exponentially distributed random variables, respectively. Eq. 2.6 is the well know II c.f. of the Poissonian mixture of the Gamma functions, plus the t_m shift.

When multiple-site chromatographic columns are employed the relationship is given by:

$$\varphi_t(\omega) = exp\left(t_m i\omega + \bar{n}\left(\sum_{i=1}^{m} \frac{p_i}{1 - i\omega\bar{x}_i} - 1\right)\right) \tag{2.7}$$

where p_i is the relative abundance of the *i-th* pore type and m the number of different types of pores. Finally, when continuous distributions of pore types are considered, the sum should be replaced by an integral and the relative abundances of pore types by the correspondent frequency distribution function. To take into account of the mobile zone, the new stochastic process describing the process Y(T(t)) is obtained by the subordination of the stationary zone jumps model Y(t), with the mobile phase process T(t) as a directing process.

In particular the general solution of Y(T(t)) is given by:

$$\varphi_{tot}(\xi) = \varphi_T\left(\frac{(\psi_S(\xi))}{i}\right)$$

(2.8)

where $\varphi_{tot}(\xi)$ and $\varphi_T(\xi)$ are the c.f of the whole and of the mobile zone stochastic processes respectively. The variance of this distribution can be expressed as a functions of the diffusion coefficient [61-62].

3. REACTION CHROMATOGRAPHY MODEL

The fundamental quantity x defined in Eq. 2.4 can be redefined as follows:

$$x = \frac{n(x)\overline{\tau}_{S.eq} - \overline{n}\,\overline{\tau}_{S,A}}{\overline{n}\left(\overline{\tau}_{S,B} - \overline{\tau}_{S,A}\right)}$$

(2.9a)

$$t \equiv n(x)\overline{\tau}_{S,eq}$$

(2.9b)

In Eq. 2.9a, one can see that for $x = x_{eq}$ one has $n(x_{eq}) = \overline{n}$. By rearranging Eq. 2.9a one obtains:

$$n(x) = \overline{n}\,\frac{\left(x\left(\overline{\boldsymbol{\tau}}_{S,B} - \overline{\boldsymbol{\tau}}_{S,A}\right) + \overline{\boldsymbol{\tau}}_{S,A}\right)}{\overline{\boldsymbol{\tau}}_{S,eq}}$$

(2.9c)

According to this equation, $n(x)$ is rescaled with respect to x and, since in Eq. 2.9c the averages terms ($\overline{\tau}_i$ and $\overline{n}$) are constants, $P(x)$ (or its CF $\hat{P}(x)$) can be directly transformed into a probability distribution of $n(x)$ (i.e. $P[n(x)]$) [63-64]. Note also that, according to Eq. 2.9c, $n(x)$ is a continuous variable as are x or t.

The retention profile for each t value is generated by the corresponding number of jumps, and the sorption time value given by $\bar{\tau}_{S,eq}$ is assumed to be common. The above assumption can be qualitatively explained by considering that the change in the probably of state occupation due to the system reaction can be viewed as a change in the number of jumps or, equivalently, in the corresponding change in permanence time, following the same approach proposed in the stochastic description of the chemical kinetics processes. In fact, in the chromatographic two-sites model, on one side it can be seen that the sorption time distributions do not change over time since the site adsorption properties are considered constant. Moreover, the number of type *A* and *B* sites in the stationary phase is also constant. On the other hand, the number of molecules which can specifically interact with sites *A* or *B* (see Fig. 2.1) evolves during the course of separation due to the interconversion reaction: the jump number is accordingly modulated (Eq. 2.9c).

The assumed hypothesis that expresses the t quantity as the product of two sole random quantities, n and $\bar{\tau}_{S,eq}$, allows us to obtain a solution for the coupled interconversion-phase exchange processes of dynamical chromatography by applying the mathematical formalism employed in handling the so-called stochastic dispersive model of chromatography [61]. In fact, in both cases, the band broadening due to reaction or inhomogeneous flow velocity is translated into a probability distribution for the jump number. The jump process acts as a process that directs the sorption process.

The presented approach can be applied only to systems containing a large number of molecules. In terms of *CF*, the solution is expressed as follows:

$$\varphi_{tot}(\omega) = \varphi_{dis}\left(\frac{\log(\varphi_u(\omega))}{i}\right) \tag{2.10}$$

where φ_u is the *CF* of the chromatographic retention process referred to either to $\bar{n}$ or t_M unit values and φ_{dis} is the *CF* of the probability dispersion function of either $n(x)$ or $t_M(x)$ (equal to $= n(x)\bar{\tau}_M$, see Eq. 2.9b).

In the present case, by assuming the initial condition corresponding to the condition of equilibrium, under conditions of $n = 1$, one obtains:

$$\varphi_u(\omega) = \exp\left(\frac{1}{(k_A + k_B)} \left(\frac{k_B}{(1 - i\omega\bar{\tau}_{S,A})} + \frac{k_A}{(1 - i\omega\bar{\tau}_{S,B})} - (k_A + k_B) \right) \right)$$

(2.11)

The final expression can obtained from the combination of the peak shape and number of jumps.

The previously described coupling of the chromatographic band broadening process with the reaction process was based on the assumption that the unitary band broadening contribution was constant within the domain $t_{R,B} \le t \le t_{R,B}$, The consequent approximation degree is here estimated as follows: peak variance and the number of theoretical plates in standard stochastic theory of chromatography [56-53] are given by:

$$\boldsymbol{\sigma}^2 = 2n\bar{\boldsymbol{\tau}}_S$$

(2.12a)

$$N = \left(\frac{t_R}{\sigma} \right)^2 = 2n$$

(2.12b)

In the present case from Eq. 2.9c one obtains, for x equal to *0*, x_{eq} and *1*, $n(0) = \bar{n} \times (\bar{\tau}_{S,A} / \bar{\tau}_{S,eq})$, $n(x_{eq}) = \bar{n}$ and $n(1) = \bar{n} \times (\bar{\boldsymbol{\tau}}_{S,B} / \bar{\boldsymbol{\tau}}_{S,eq})$, respectively. Consequently, since $\bar{\tau} \equiv \bar{\tau}_{S,eq}$, one has, by using Eq. 2.12a, $\boldsymbol{\sigma}^2(0) = 2\bar{n}\,\bar{\boldsymbol{\tau}}_{S,A}\bar{\boldsymbol{\tau}}_{S,eq}$, $\boldsymbol{\sigma}^2(x_{eq}) = 2\bar{n}\,\bar{\boldsymbol{\tau}}_{S,eq}{}^2$ and $\boldsymbol{\sigma}^2(1) = 2\bar{n}\,\bar{\boldsymbol{\tau}}_{S,B}\bar{\boldsymbol{\tau}}_{S,eq}$. By considering equations, the exact values should be $\sigma^2(0) = 2\bar{n}\,\bar{\tau}_{s,A}{}^2$, $\sigma^2(x_{eq}) = 2\bar{n}\,\bar{\tau}_{s,eq}{}^2$ and $\sigma^2(1) = 2\bar{n}\,\bar{\tau}_{s,B}{}^2$. Consequently, one can see that chromatographic band broadening calculated by using Eq. 2.10 is exact in the case of $x = x_{eq}$, and overestimated and underestimated in the domains $0 \le x < x_{eq}$ and $x_{eq} < x \le 1$, respectively. However, one should remember that, beside the chromatographic band broadening there is, in addition, the contribution due to the reaction and they are additive in variance. In most cases, the variance contribution due to reaction is the most important one. Consequently, the bias

should be of minor relevance. Alternatively, the whole process can be split into its two components labelled *A* and *B* and the solution is then given as a sum of the respective contributions, i.e.:

$$\varphi_{tot}(\omega) = \varphi_{tot,A}(\omega) + \varphi_{tot,B}(\omega)$$

(2.13)

The importance of this last equation is that it represents the correct expression for the peak shape in Fourier domain. The advantage of employing Eq. 2.13, expressed as separate components, is that it allows one to consider cases where the initial concentration of the two reacting species differ from one another (i.e. on-column reaction chromatography).

Several approximate or limit solutions were in addition obtained to describe the effect of moderately fast kinetics producing a unique Gaussian-like central peak. In comparison with the previously reported handlings, the present stochastic approach was able to obtain general and specific solutions in closed form under frequency domain, fully describing the dynamical chromatography (Eqs. 2.10 and 2.13). In Fig. 2.10 the time domain solution for the peak profile of two separated reacting species is plotted. Each profile represents the chromatographic peak corresponding to the elution of an injected solution containing only one component which reacts during the chromatographic run. They were obtained by numerical inversion of the function generated by summing the chromatographic peak profile in the Fourier domain for the pure enantiomers *A* and *B* with the corresponding peaks resulting from first order reaction chromatography (Eqs. 2.5a and 2.5b), i.e. the description of reaction chromatography, where only one of the species is present at the beginning of the separation process. One can see that the first enantiomer *A* appears as a peak at $t_R \cong 23\,\text{min}$ (which is product obtained by multiplying n (=9045) by the sum of $\bar{\tau}_M + \bar{\tau}_A$, according to Eqs. 2.2a and 2.2b). A decaying tail, corresponding to the transformation, follows this peak $A \rightarrow B$. In the same figure, the *B* peak appears with an increasing front followed by the peak located at t_B ($\cong 34\,\text{min}$). The reported example refers to a slow interconverting enantiomeric mixture ($k_A = 0.00042\ \text{s}^{-1}$, $k_B = 0.00037\ \text{s}^{-1}$). If the injected solution contains both the species *A* and *B*, the resulting peak profile can be obtained by summing the contribution of each.

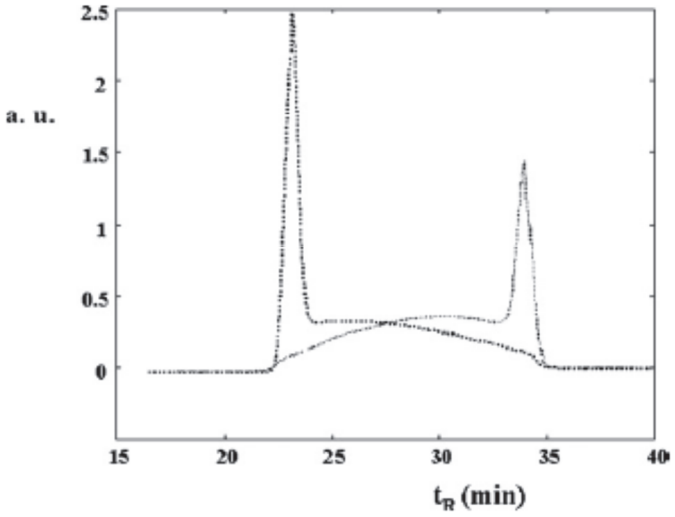

Figure 2.10: Simulated peak: a) $n = 9045$, $\tau_{S,A} = 0.1331$ s, $\tau_{S,B} = 0.2032$ s, $k_A = 0.00042$ s^{-1}, $T = 33.66$ min; b) $k_B = 0.00037$ s^{-1} [all other parameters have been kept constant and equal to a)].

The developed model allows for both general and specific solutions in frequency domain, fully describing the dynamic chromatography process. The general equation can be simplified in the limit cases: a) for slow reaction rate (compared to the adsorption kinetics) the chromatographic response is a sum of two separated peaks; b) very fast reaction rates generate just one peak having a retention related to the kinetic constants of the reaction (p); c) for intermediate rates, a peak cluster is generated. The model was able to describe both interconversion and reaction during separation. Some basic features of the process - such as interconversion kinetics constants - and/or operative variables - such as column length (or flow velocity) - and their influence on the chromatographic output have been exploited.

Case II: Adsorption of DCE in mordenite

In this work diffractometric, thermogravimetric and gas chromatographic techniques have been employed to investigate the adsorption process of 1,2-dichloroethane into mordenite (MOR), which is an organophilic zeolite, in order to quantitatively evaluate the adsorption and to elucidate its adsorption mechanism.

1,2-Dichloroethene (1,2-DCE) is a synthetic chemical with no known natural sources. It occurs in two forms known as *cis*- and *trans*- isomers that have similar properties. 1,2-DCE is a colourless, flammable liquid with a harsh odour. It is used as a chemical intermediate in the production of other chlorinated solvents. 1,2-DCE has also been used as a solvent in the extraction of rubber.

1,2-DCE may be released to the environment from manufacturing plants or from landfills where it had been disposed of. It can be released into the air from the burning of vinyl. Because the 1,2-DCE isomers are environmental breakdown products deriving from widely used chlorinated solvents trichloroethene (TCE) and tetrachloroethene (PCE), 1,2-DCE's detection in groundwater may often be due to the release of its parent compounds into the environment. Mordenite (MOR) (see Fig. 2.11) is a natural or synthetic zeolite, with an idealized chemical composition of $Na_8Al_8Si_{40}O_{96} * 24H_2O$, whose units of four 5-rings [5^4], of the framework type, are joined to one another via common edges to form chains. Mirror images of these chains are connected via oxygen bridges to form corrugated sheets (lying horizontally in Fig. 1.1 chapter1). These sheets, displaced by half a translation in *c*, are then connected to one another to form oval 12- and 8-rings along the corrugations. The lining of the 12-ring channels contains 8-rings, but the 8-ring openings of adjacent 12-ring channels are displaced in comparison with one another, so only very limited access from one channel to the next is possible. Consequently, the channel system is effectively one dimensional [13]. The experimental data have reported that the MOR particles are characterised by a lamellar or plated morphology. This morphology enables easy access to the large 12-membered ring channels, thus indicating that the sample has properties which are characteristic of Large Port mordenite.

MORDENITE (MOR)

Surface Area (BET, m^2/g)	Mean Particle Size (μm)	SiO_2/Al_2O_3
420	5-7	200

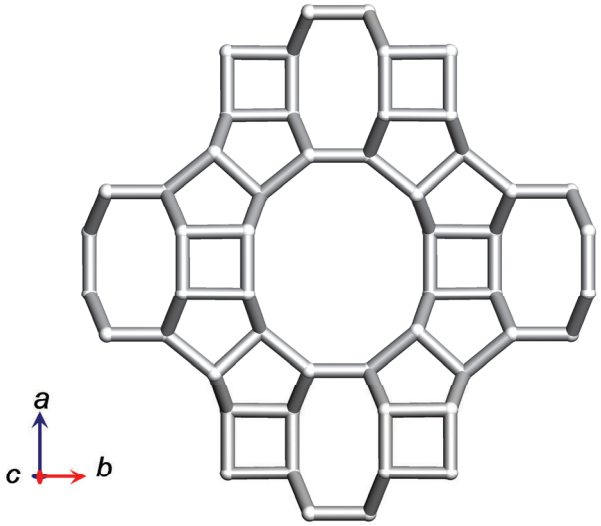

Channels (Atlas)[83]
[001] 12-ring 6.5 x 7.0Å<-> [001] 8 2.6 x 5.7Å

Figure 2.11: Structure and characteristics of zeolite mordenite.

Adsorption data were obtained using the batch method. Batch experiments were carried out in duplicate in 25 mL crimp top reaction glass flasks sealed with PTFE septa. The flasks were filled in order to have minimum headspace, a solid/solution ratio (mg mL^{-1}) of 1:4 was employed. After equilibration (24h) at a temperature of 25°C under stirring, the solids were separated from aqueous solution by centrifugation and analysed by headspace- solid phase microextraction- gas chromatography (HS-SPME-GC). The experimental details are reported in 'Experimental' of the Paper II.

The mathematic models used to fit the experimental data of the adsorption isotherm, obtained by HS-SPME-GC, are the Langmuir isotherm, the Freundlich equation and the Polanyi-Dubinin-Manes (PDM) model (please see Chapter 1)[25].

In Fig. 2.12 it can be seen that the experimental data are well fitted using the traditional Langmuir isotherm as well as the PDM model. From the data in Table 2.1, it is possible to infer some adsorption process properties. It can be noted that the saturation capacity evaluated from Langmuir equation is 71 mg g^{-1} and that this value is in agreement with the pore volume (V_0) obtained from fitting the PDM model, but that it is smaller than the mordenite pore

volume. The *b* value obtained for the zeolite is about 4. This result is indicative of relatively homogeneous adsorbents with narrow site energy distribution, and is in agreement with the literature. The exponent parameter of the Freundlich equation (*n*) is in agreement with those found in another works. In Table 2.1 it is notable that the goodness of fit (coefficient of determination, R^2) is similar for the three models employed. Therefore, the choice of a model based solely on statistical parameters of fitting seems to be arbitrary, for this reasons a structural investigation was performed to highlight the adsorption mechanism in order to select the appropriate isotherm model.

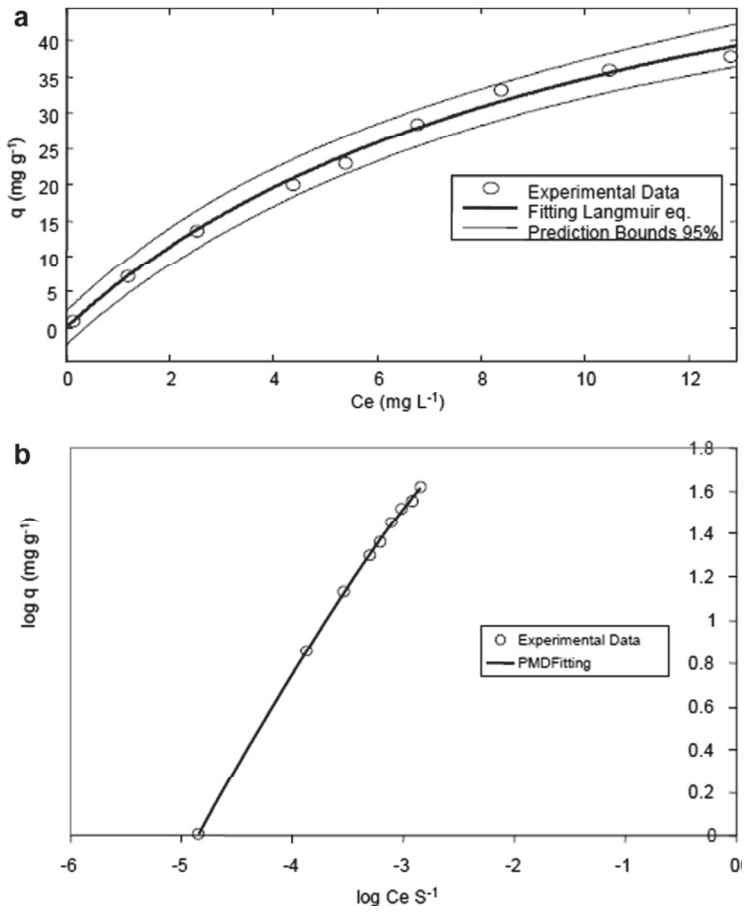

Figure 2.12: Adsorption isotherm of DCE on MOR: circle symbols: measured equilibrium concentration; (a) solid line: fitted Langmuir equation; (b) solid line: fitted PMD equation.

Table 2.1: Fitting isotherm parameters obtained by fitting the experimental data in Fig.2.12 The confidence limits at 95% of probability are reported in parentheses.

[1] q is the sorbed concentration, C_e is the concentration in the solution at equilibrium, K_L is the Langmuir coefficient, q_s is the saturation capacity; K and n are the Freundlich constants characteristic of the system; V_0 and ρ_0 are the maximum volume of adsorbed compound for unit mass of adsorbent and compound density, respectively. E is the free energy of the adsorption process compared to that of a reference compound.

ISOTHERM	Equation[1]	Parameters			
Langmuir	$\frac{C_e}{q} = \frac{1}{K_L q_s} + \frac{C_e}{q_s}$	K_L (L mg^{-1}) 0.09 (0.065, 0.12)	q_s (mg g^{-1}) 71 (59, 84)		R^2 0.9942
Freundlich	$q = KC_e^{1/n}$	K (mg g^{-1})(L g^{-1})^n 7.9 (6.0, 9.7)	n 1.6(1.3,1.8)		R^2 0.9832
PMD	$q = V_0\rho_0 \exp\left[\frac{RTlnS/C_e}{E}\right]^b$	V_0 (cm^3 Kg^{-1}) 62.5 (49.4, 74.0)	E(kJ mol^{-1}) 18 (11, 26)	b 4	R^2 0.9914

Thermogravimetric analysis (TG) was used to determine the amount of DCE molecules embedded in the mordenite framework, and to monitor the decomposition process of organic molecules during the heating procedure. TG analysis was carried out on saturated MOR-DCE system.

Thermogravimetric analysis (TG, see Fig. 2.13) curve of the MOR-DCE shows a sudden change in its slope at about 90°C, thus indicating the presence of molecules which are weakly bonded to the surface (water and/or DCE). The weight loss which occurred at higher temperatures (200-700°C), could indicate the decomposition and elimination of the organic molecules embedded in the mordenite channel system. Weight loss at 1000°C is about 10% in comparison to 7 % of the as-synthesized material at the same temperature.

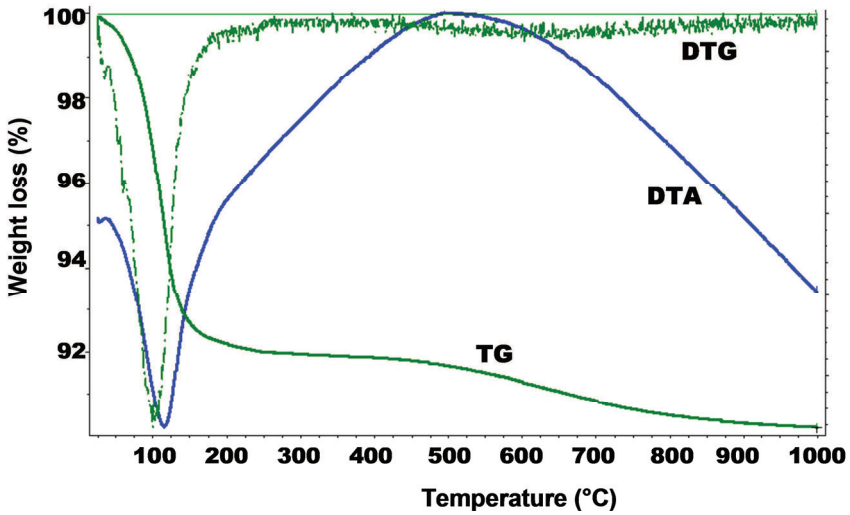

Figure 2.13: Thermogravimetric (TG), differential thermogravimetric (DTA) and differential thermal (DTA) curves in mordenite after DCE-dry air atmosphere adsorption.

A powder diffraction pattern (see Figure 2.14) can be used as a "fingerprint" to identify materials with, to determine unit cell parameters, to estimate the quality of the sample, to monitor phase transitions, to evaluate structural changes, to establish whether or not impurities are present, or to recognize the presence of faulting [13].

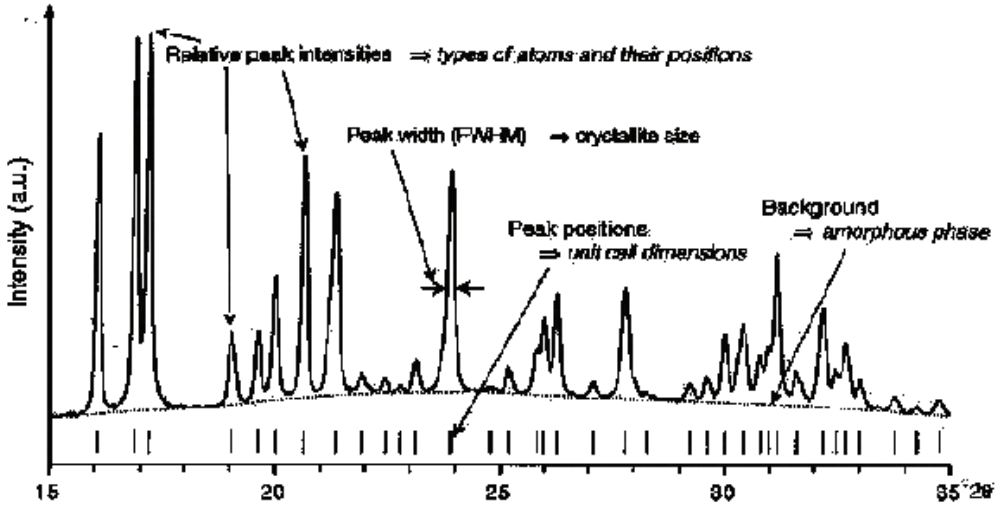

Figure 2.14: The relevant features of a power diffraction pattern and their origin [13].

Rietveld refinement revealed a remarkable increase in the dimensions of the 12-membered ring after adsorption, thus it is evident that DCE can penetrate micropores. Moreover, from the data of relative occupancy of the site it was possible to calculate an amount equating to 2.5 DCE molecules (which corresponds to about 7.7% in weight) and approximately 4 water molecules (which correspond to approximately 2.3% in weight) which were localised inside the mordenite channel system. Therefore, the structure refinement gave an extraframework content of about 10% in weight, which was in very good agreement with the weight loss given by the TG analysis and with the saturation capacity determined by the adsorption isotherm.

However, structure refinements have not allowed us to demonstrate whether only *trans*- or *gauche*-configurations are present or if both are present but in different frequencies, and consequently, the X-ray diffraction did not give a clear indication of the most well-favoured DCE configuration in mordenite structural confinement. The occupancy of Cl and C atoms is only 30%, and consequently, DCE molecules, whatever their configuration, alternate randomly with non-occupied positions. The Figure 2.15 shows that DCE molecules run parallel to the *c* direction, i.e. along the 12-ring channel. Nonetheless, this structural investigation can also explain the fact that the PDM model underestimates the adsorption capacity in comparison with that calculated from the solute density and adsorbent pore volume, especially as this finding has already been found in other studies. Indeed, from the structural investigation, it appears that DCE cannot completely displace water from the micropores.

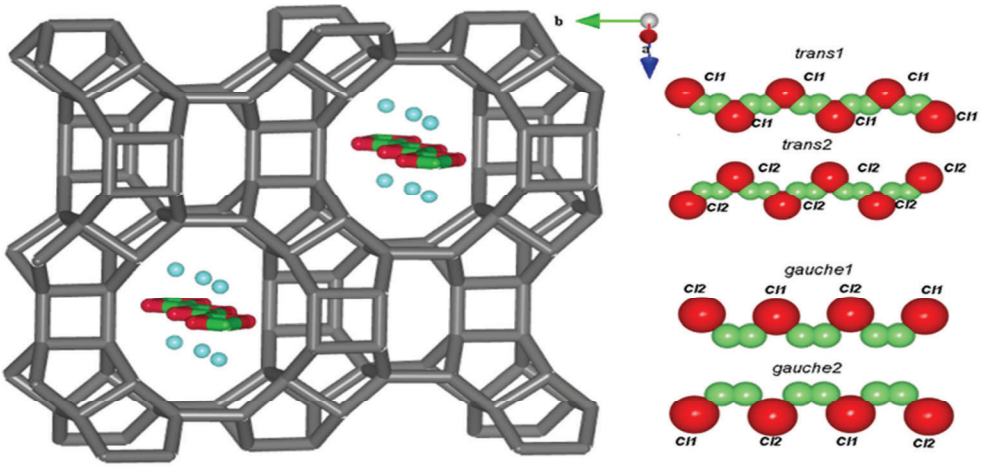

Figure 2.15: MOR-DCE projections along [001] shows DCE (Cl represented with red, C with green spheres) and water molecules (with blue spheres) which run parallel to the *c* direction.

Case 3: Role of water in the adsorption of organic contaminants in hydrophobic zeolites

In the previous work it was found that water is present inside the zeolite structures, indeed, in the MOR-DCE system, the water molecule oxygen atom distances from the organic molecule chlorine atoms (W – Cl1 = 2.34 Å, W – Cl2 = 2.53 Å) suggest that different DCE molecules could be connected by means of hydrogen bonds, to form a complex of DCE and water molecules independently by *gauche* or *trans* DCE sequencing. The fact that DCE cannot completely displace water from the micropores was also confirmed from the adsorption isotherm model. In this study, research was continued in order 1) to examine if the phenomena observed for DCE-MOR system can be generalised to other zeolite types and 2) to establish the role of water in the adsorption process. To accomplish this task, two different zeolites were employed: ZSM-5 and Y.

ZSM-5. ZSM-5 zeolite is the most important member of the MFI family. It is probably one of the most widely studied zeolite in the world. The ZSM-5 framework type (see Fig. 2.16) can be described in terms of [5^4] units, but it is easier to use pentasil units (Fig. 1.1 chapter 1). These [5^8] units are linked to form pentasil chains, and mirror images of these chains are connected via oxygen bridges to form corrugated sheets with 10-ring holes. Each sheet is linked by oxygen bridges to the next to form the 3-dimensional structure. Adjacent sheets are related to one another by an inversion centre. This produces straight 10-ring channels parallel to the corrugations (along y), and sinusoidal 10-ring channels perpendicular to the sheets (along x). The latter channels link the straight channels to one another to form a 3-dimensional 10-ring channel system. Because the pore openings are 10-rings rather than 12-rings, the shape selectivity for sorption and catalysis is distinctly different from other types of zeolites, and this fact is exploited in catalysis application. ZSM-5 has found many applications in refinery and petrochemical processes [13].

The Si/Al ratio of this zeolite type ranges from 20 to infinity for the pure silica form silicalite. When adsorbed on HZSM-5 zeolites (H denoting the hydrogen cation as the exchangeable cation in the structure), linear and branched hydrocarbons behave as condensed liquids, which are capable of filling the entire pore structure. Centi et al. (2002) found that the exchangeable cation of ZSM-5 zeolites plays a critical role in MTBE adsorption and hydrolysis. Centi et al. (2002) also found that a hydrogen-form ZSM-5 zeolite with a Si/Al ratio of 80 had an increased catalytic activity and adsorption capacity compared with the zeolite with a Si/Al

ratio of 25. Water adsorption studies have shown that the 3-dimensional array of hydrogen-bonded water molecules cannot easily penetrate the pores of ZSM-5 zeolites without considerable distortion of the hydrogen bonds, and that the quantity of adsorbed water in ZSM-5 zeolites is dependent on the zeolite hydrophobicity [12].

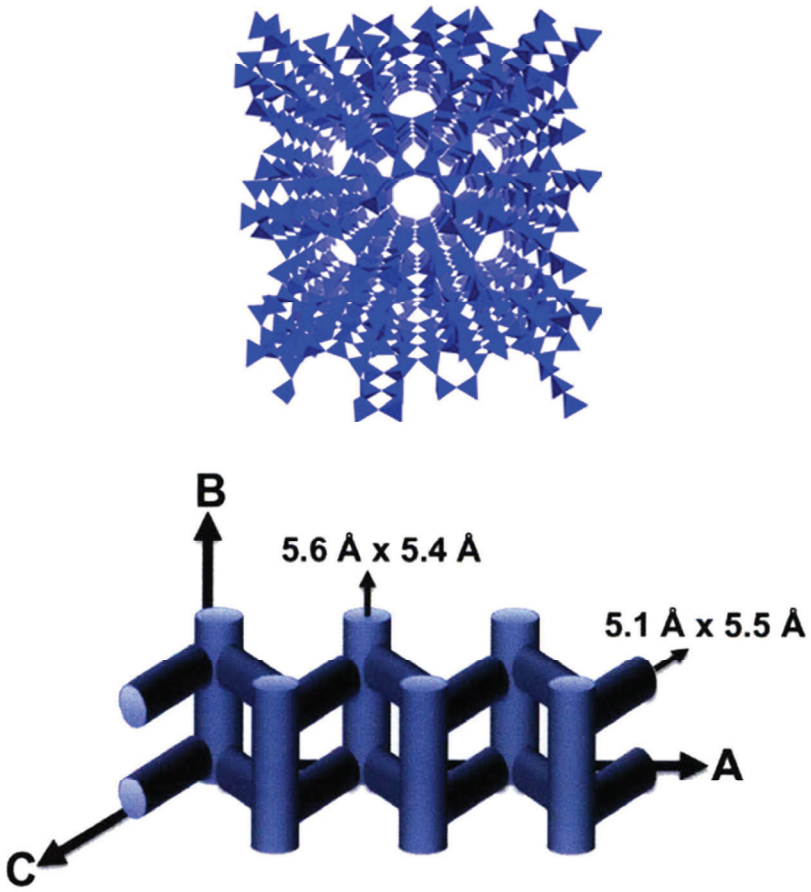

Figure 2.16: Structure of zeolite ZSM-5.

Y. In the Y (Faujasite, FAU) framework type there are sodalite cages (Fig. 2.17). In this case, they are arranged in the same way as the carbon atoms in a diamond, and are joined to one another via double 6-rings. This creates the so-called supercage with four, tetrahedrally oriented, 12-ring pore opening, and a 3-dimensional channel system along <110>. There is a centre of inversion in each of the double 6-rings, so the puckered layers of solidate cages are related to one another by inversion. The framework type can also be described as an ABCABC stacking of such layers. The combination of large void volume (Ca. 50%), 12-ring pore openings and 3-dimensional channel system makes the thermally stable silicate materials with the FAU framework type ideal for many catalytic applications [13].

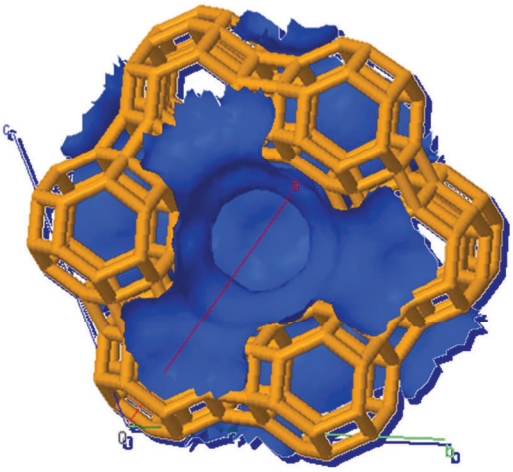

Figure 2.17: The FAU framework type and its supercage.

DCE uptake onto ZSM-5 as a function of time is plotted in Fig. 2.18a-b. It can be seen that for the studied zeolite the adsorption process is fast: equilibrium concentration is reached in just a few minutes. The data were fitted by a pseudo second order model, given by:

$$\frac{t}{q_t} = \frac{1}{k_2 q_e^2} + \frac{t}{q_e} \tag{2.14}$$

where q_t and q_e are the milligrams of solute sorbed per gram of sorbent at time t and at equilibrium, respectively, and k_2 is the second-order sorption rate constant. The equilibrium uptake and the adsorption rate constant, obtained by the slope and intercept of the linear fit of the data q_t/t vs. t, respectively, are reported in Table 2.2. Both pseudo first and second order equations are two extreme cases of a general rate equation when the initial adsorbate concentration is very high or very low, respectively. The pseudo second order model has been applied in order to analyse sorption kinetics from the liquid solutions of many adsorption systems [40]. However, it should be mentioned that the pseudo second order equation, like other commonly employed relationships (e.g. the pseudo-first order, the pseudo-second order and the Elovich equations) does not correspond only to one kinetic model, but is a more or less flexible mathematical formula, which is able to simulate the behaviour characteristic of physical kinetic processes of various kinds only adequately well. Moreover, the rate constant estimated from the fitting is a complex function of the initial concentration of solute [40].

In fact, it can be noted in Table 2.2 that the k_2 estimation depends on the initial concentration value. An approximate estimation of the general rate constant

$$k_2' = k_2 C_0^n \tag{2.15}$$

was evaluated by fitting. Similar results were also obtained using DCE onto Y adsorption kinetics (see Table 2.2 and Fig. 2.18c-d). Then, the adsorption isotherms for DCE-ZSM-5 and DCE-Y were analysed (see Fig. 2.19).

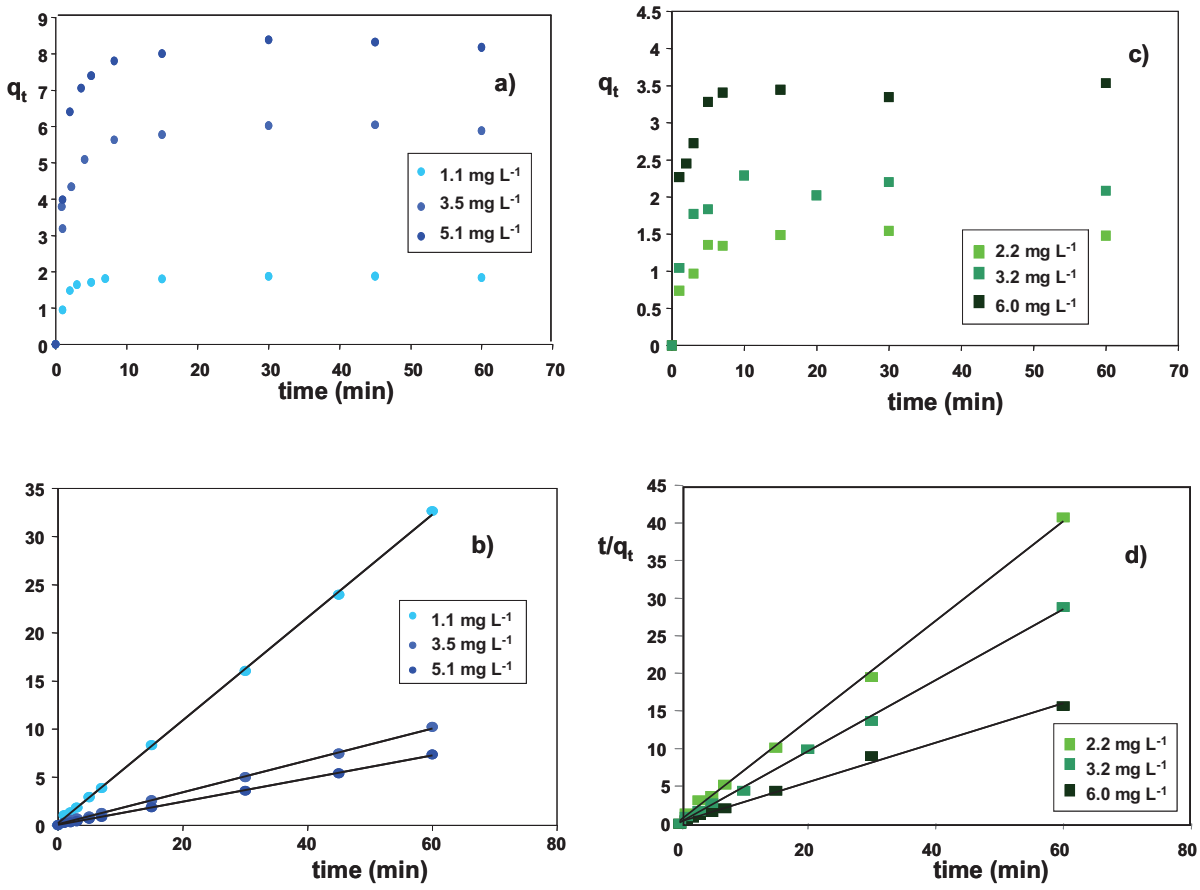

Figure 2.18: DCE uptake onto ZSM-5 (a-b) and Y (c-d) as a fuction of time a different concentrations.

Table 2.2: Uptake kinetics of DCE on ZSM-5 and Y (see Eq. 2.14).

[1] $t_{1/2}$ is calculated as the reciprocal of the product of k_2 and q_e.

Organic-Zeolite	C_0 mg L^{-1}	k_2 g mg^{-1} min^{-1}	q_e (kinetics) mg g^{-1}	q_e (equilibrium) mg g^{-1}	$t_{1/2}$ [1] min	k'_2 g mg^{n-1} L^{-n} min^{-1}	N
DCE-ZSM-5	1.1 3.5 5.1	1.33 0.32 0.24	1.9 6.2 8.3	2.3 6.3 9.3	0.40 0.51 0.53	1.45	1.14
DCE-Y	2.2 3.2 6	0.86 0.72 0.26	1.5 2.3 3.8	1.9 2.8 4.2	0.77 0.72 1.09	2.55	1.24

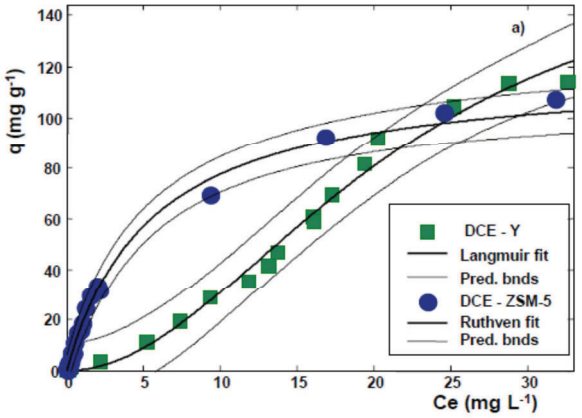

Figure 2.19a: Adsorption isotherms (at 298 K) of DCE on ZSM-5 (circle) and Y (square).

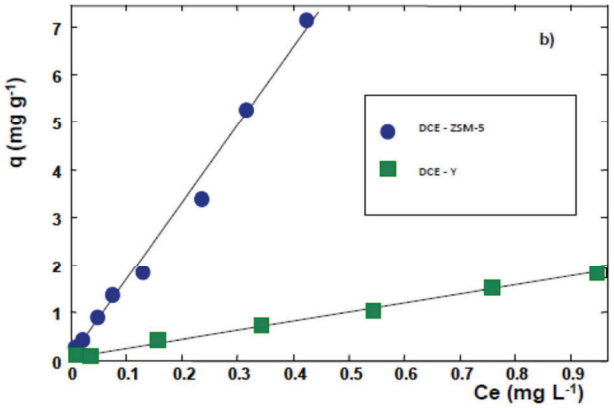

Figure 2.19b: Enlarged detail of data, in Fig. 2.19a above, in the low concentration range.

Different models of isotherms for these two pairs of organic-zeolite were considered. Besides the Langmuir isotherm, the bi-Langmuir isotherm, the Ruthven and the Fowler-Guggenheim models were used to fit the data obtained with batch method and analysed with HS-SPME-GC previously described in Case 2 (please see Table 2.3 and Chapter 1).

The bi-Langmuir isotherm was first suggested by Graham and is one of the isotherm models for ideal adsorption on heterogeneous surfaces, in this models adsorbate-adsorbate interactions are assumed to be negligible. The surface is covered with two different kinds of sites that behave independently and the equilibrium isotherm results from the addition of the two independent contributions of the two types of sites [25]. The Fowler-Guggenheim isotherm model was introduced to correct for the first-order deviations from the Langmuir isotherm. It assumes ideal adsorption on a set of localized sites on a homogeneous surface, with weak interactions between molecules adsorbed on neighbouring sites. It assumes also that the interaction energy between two sorbate molecules is small enough that the random character of the sorbate molecule distribution on the adsorbent surface is not significantly altered [35]. The Ruthven model was suggested to account for single-component adsorption in zeolitic system. In this system, each cage in the zeolite can contain a finite number of adsorbate molecules [37].

In Fig 2.19b it can be seen that, in the low concentration range, Y is less efficient in DCE removal from water solutions. The data in the low concentration range follow a linear trend ($q = KC_e$), but in a wide concentration range a different trend was observed for DCE on ZSM-5 and Y. In Fig. 2.19a, it can be seen that the adsorption data on ZSM-5 follows an L-class adsorption isotherm, whereas, the zeolite Y data follow an S-class isotherm. L-class data are typical for zeolite adsorption and can be fitted by different equations such as Langmuir (used in this case) or heterogeneous extended Langmuir models (e.g. Freundlich equation). These data were also fitted using a bi-Langmuir isotherm type and the fitting goodness is higher than that observed for Langmuir model, but it is due to the increase in the number of parameters in the isotherm equation. S-class data were fitted by Fowler-Guggenheim and Ruthven isotherms; these models have recently been employed to fit the adsorption of aromatics onto Y zeolite [35]. These types of isotherm are uncommon for hydrophobic zeolites, but recently different opinions have been expressed and it can be argued that the interaction mechanism is still a matter of debate. For a general adsorbent material, sigmoid isotherms have previously been observed as a result of lattice expansion and polymorph switching in porous materials, guest rearrangements in rigid hosts, and in the cooperative binding of substrates to protein [65].

Table 2.3: Fitting results of the adsorption data of DCE on ZSM-5 and Y.

[1] q (mg g^{-1}) is the sorbed concentration, C_e (mg L^{-1}) is the concentration in the solution at equilibrium, $K_{L,i}$ (L mg^{-1}) the Langmuir coefficient (binding constant), and $q_{s,i}$ (mg g^{-1}) the saturation capacity of site i. θ is the ratio q / $q_{s,}$ R the parameter accounting for adsorbate-adsorbate interactions in a cage and W the interaction energy (kJ mol^{-1}).

Organic – Zeolite	Equation[1]	Parameters				R^2
DCE-ZSM-5	Langmuir $q = \frac{q_s K_L C_e}{1+K_L C_e}$	K_L (L mg^{-1}) 0.19 (0.16,0.21)		q_s (mg g^{-1}) 120 (113,127)		0.9927
DCE-ZSM-5	Bi-Langmuir $q = \frac{q_s K_L C_e}{1+K_L C_e} + \frac{q_{s,1} K_{L,1} C_e}{1+K_{L,1} C_e}$	K_L (L mg^{-1}) 0.23 (0.18,0.28)	q_s (mg g^{-1}) 82 (73,91)	$K_{L,1}$ (L mg^{-1}) 0.11 (0.02,0.2)	$q_{s,1}$ (mg g^{-1}) 37 (33,42)	0.9987
DCE-ZSM-5	Linear $q = KC_e$	K (L mg^{-1}) 13 (12,14)				0.9929
DCE-Y	Ruthven $\frac{q}{q_s} = \frac{K_r C_e + R(K_r C_e)^2}{1+K_r C_e + R/2(K_r C_e)^2}$	K_r (L mg^{-1}) 0.014 (0.009,0.019)	q_s (mg g^{-1}) 175 (136,214)	R 4.3 (2.7,5.0)		0.9911
DCE-Y	Fowler-Guggenheim $K_{FG} C_e = \frac{\theta}{1-\theta} \exp\left(\frac{2\theta W}{RT}\right)$	K_{FG} (L mg^{-1}) 0.0923	q_s (mg g^{-1}) 178	W (kJ mol^{-1}) 5.2		0.9920
DCE-Y	Linear $q = KC_e$	K (L mg^{-1}) 2.0 (1.3,2.8)				0.9892

The saturation capacity obtained by fitting was is in good agreement with the TG data. The TG curves (see Fig. 2.20) of the zeolite sample after adsorption of DCE for both ZSM-5 and Y, showed that apart from the elimination of residual humidity, (T<100°C), a sudden change in its slope occurs at higher temperatures, which is probably due to the elimination of DCE and/or H_2O molecules trapped within the zeolite pores. Total weight loss of ZSM-5-DCE at 900°C is about 12% in comparison with 2.8% in the as-synthesised sample, for Y-DCE the weight loss at 900°C was higher than for ZSM-5, confirming the higher saturation capacity of this zeolite.

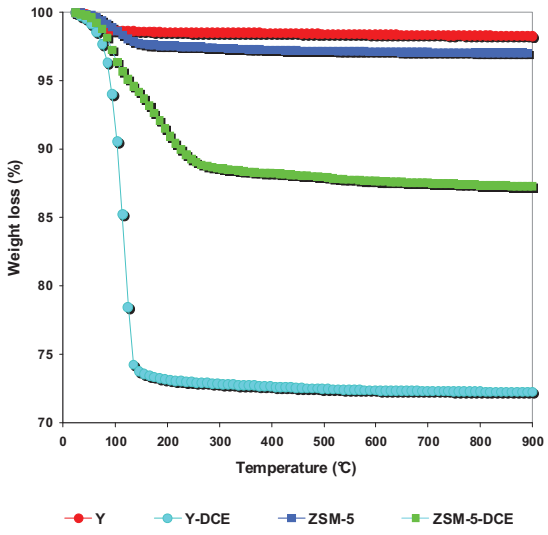

Figure 2.20: Thermogravimetric (TG) curves in ZSM5 and Y respectively, before and after DCE adsorption.

To further investigate the adsorption mechanism of DCE onto ZSM-5 and Y, structural analyses were carried out. Rietveld structure revealed that DCE adsorption caused a lowering in real *Fd-3m* symmetry in the Y zeolite to *Fd-3* and a remarkable increase in unit cell volume in comparison to those of untreated materials. These remarkable deformations can be explained on the basis of the presence of DCE- water complexes which strongly interact with framework oxygen via hydrogen bonding. The location of DCE molecules and symmetry elements for the *Fd-3* space group imposes the presence of both *trans-* and *gauche-* configurations (Fig. 2.21). As already mentioned, 1-2dichloroethane is present in a *trans-gauche-* conformational equilibrium. The DCE *trans-* conformer is generally preferred in the gas phase due to its steric effect, which is basically one of exchange and Coulombic repulsion. However, in the liquid or polar solvent phase, such as in water, the *gauche-*

conformer is stabilized when compared to the *trans*- conformer due to dipole-dipole interactions with neighbouring *gauche*- species or polar solvent molecules [66-67].

As far as concerns ZSM-5 (Fig. 2.22), it was found that all DCE molecules assume a *trans*-configuration, this is probably due to an energy landscape which has been defined by DCE low energy torsional motion in the zeolite channels. Even in this case, DCE-water complex were present, and adsorption occurred with a significant increase in the cell parameters without a simultaneous change in symmetry. All of these findings are important features in the adsorption process and suggest: a) flexibility in the framework should be included in modelling adsorption to correctly interpret the experimental findings; b) water molecules inside the porous framework lead to a multicomponent system being considered instead of a single component adsorption mechanism. Water effects cannot be neglected, especially when hydrogen bonds are involved; c) conformational selection in DCE on ZSM-5 has been observed and is probably due to an energy landscape which has been defined by DCE low energy torsional motion in the zeolite channels.

In conclusion, for DCE adsorption onto hydrophobic zeolites regardless of the framework type, isotherm modelling and/or simulation algorithms should be implemented to take system complexity into account.

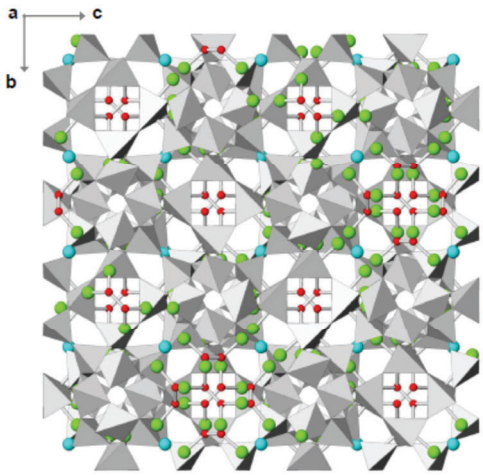

Figure 2.21: Projection along [001] showing DCE molecules in Y along the 12-ring channels. Chlorine (red circle), carbon (green circle) and water molecules (light blue) are reported.

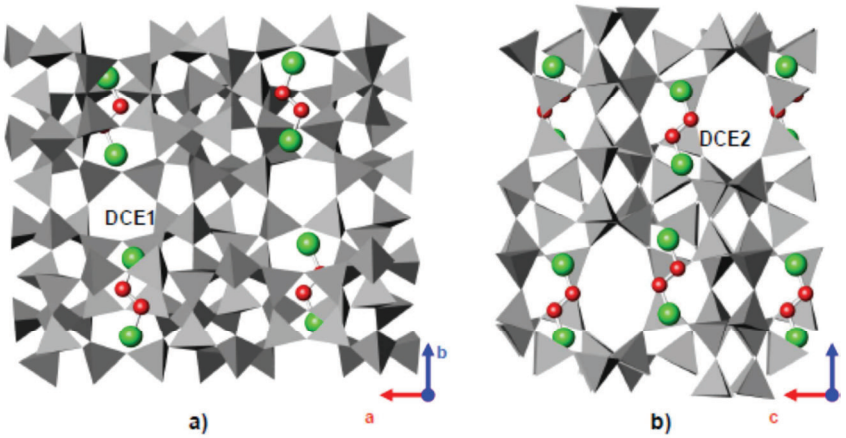

Figure 2.22: Projection along (a) [001] and (b) [010] showing DCE molecules in ZSM-5 along the 10-ring channels. Chlorine (red circle), carbon (green circle) and water molecules (light blue) are reported.

Case 4a: MTBE and TOL adsorption onto hydrophobic zeolites

The studies reported above showed that DCE adsorption from aqueous solutions onto hydrophobic zeolites leads to zeolite framework distortions and that both organic contaminant and water molecules are present inside the pore structure. To further generalize the obtained results, the adsorption of different organic contaminants onto zeolites, and in particular methyl tert-butyl ether (MTBE) and toluene (TOL), was investigated. Organic contaminants (i.e. MTBE and TOL) were chosen as representative of different classes, oxygenate compound and BTEX (benzene, toluene, ethylbenzene and xylene) respectively, both of them are often found in contaminated sites. To follow, a summary of the characteristics of the zeolites and properties of the pollutants considered in this study is represented. Zeolites materials were also characterized by Nitrogen adsorption isotherms at 77 K for what concerned pore diameter, pore size and surface area (see Fig. 2.23).

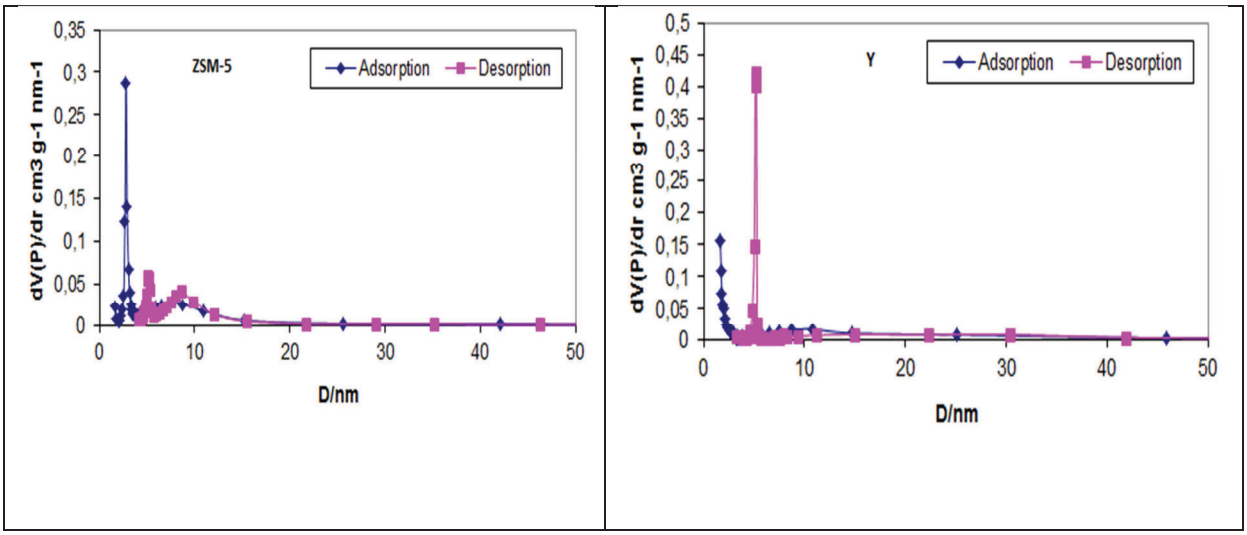

Figure 2.23: Particle size distribution of ZSM-5 and Y.

ZEOLITES

SAMPLE	**ZSM-5**	**Mordenite (MOR)**	**Y**
SUPPLIER AND SUPPLIER NAME	CBV 28014 Zeolyst	HSZ-690HOA Tosoh Corporation	HSZ-390HUA Tosoh Corporation
SiO_2/Al_2O_3	280	200	200
CHANNELS (ATLAS)	[100] 5.1x5.5Å<> (3-dimensional)	[001]12-ring 6.5x7.0Å<-> [001]8-ring 2.6x5.7Å (1-dimensional)	<111>12-ring 7.4x7.4Å (3-dimensional)
SURFACE AREA (BET m^2/g)	400	420	750
MEAN PARTICLE SIZE (µm)	3	5-7	6-8

POLLUTANTS

Name	**1,2-Dichloroethane (DCE)**	**Toluene (TOL)**	**Methyl tert-butyl Ether (MTBE)**
Supplier and supplier name	03522 Fluka - Sigma Aldrich	0713716 Carlo Erba Reagents	0923716 Carlo Erba Reagents
Molecular formula	$C_2H_4Cl_2$	C_7H_8	$C_5H_{12}O$
Molar mass (g mol^{-1})	98.96	92.14	88.15
Density (g cm^{-3})	1.253	0.87	0.74
Solubility in water (g L^{-1}) at 20°C	8.7	0.47	42
Boiling point	83°C	110-111°C	55.2°C
Appearance	Colorless liquid with characteristic odor	Colorless liquid	Colorless liquid
Main hazards	Toxic, flammable	Harmful, highly flammable	Irritant, highly flammable

MTBE is the most common oxygenate which is added to gasoline, is used extensively and has been the subject of frequent studies. It is used as a gasoline additive to reduce the levels of pollutants caused by automobile combustion emission and it is found in groundwater and surface water. MTBE is a potential carcinogen, currently listed on EPA's Drinking Water Contaminant Candidate List, it can adversely affect the taste and odour quality of water and it is difficult to remove from water because it has high water solubility and low volatility. In addition, MTBE is fairly resistant to biodegradation and chemical oxidation. Toluene belongs to the BTEX group since it is a typical organic compound that appears very often in chemical and petrochemical wastewaters due to its ready solubility, indeed toluene is usually used as a solvent and as an octane booster in gasoline fuels [68-69-70].

The contaminants differ from each other in structure and chemical properties, in particular toluene does not contain heteroatom, and doesn't form hydrogen bonds. These characteristics could be important for comparison DCE and MTBE in terms of adsorption behaviour.

1- MTBE and TOL on mordenite

The adsorption properties of MTBE and TOL on mordenite, an organophylic zeolite (described in the Case 2), were firstly investigated.

Adsorption kinetics and adsorption isotherms were studied for both MTBE and toluene on mordenite by using the experimental set up previously described (see Case 2). A pseudo-second-order equation (Eq. 2.14) was used to fit the data [40], in both cases the equilibrium was reached within few minutes. In the low concentration range, the adsorption data for the two contaminants showed analogous behaviour, i.e. a linear trend ($q = KC_e$). On the contrary, in the high concentration range different models (Langmuir and Freundlich) were used to fit the data. In Fig. 2.24 it can be seen that in the high concentration range, the saturation capacity is higher for TOL than for MTBE and in the low concentration range, the slope of linear fitting is less for TOL than for MTBE. These phenomena can be explained by stronger interactions between MTBE and mordenite than those of the TOL-MOR systems and by the hindered diffusion of MTBE due to the smaller mordenite channel.

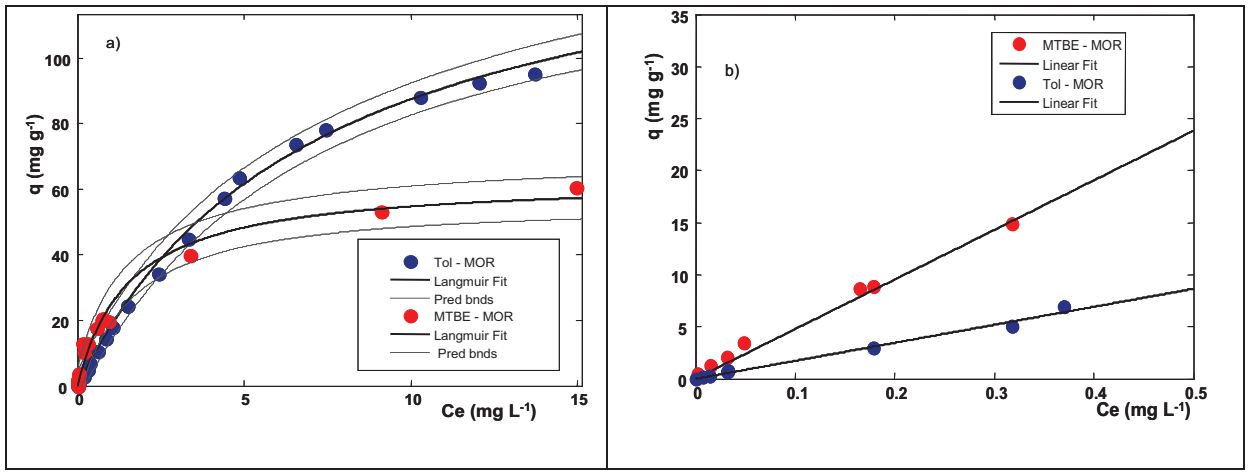

Figure 2.24: Adsorption isotherms (at 298 K) for MTBE (red) and TOL(blue) on MOR at high and low concentration ranges: the solid line is the fitted Langmuir equation and the dashed lines are the 95% confidence predictions bounds.

To obtain further information, thermogravimetric (Fig.2.25) and structural analysis were performed. The Rietveld refinement indicated partial MTBE occupancy as well as water molecules in the zeolite: 3 MTBE molecules and 2.5 water molecules per unit cell were found. The MTBE-MOR structure showed that the organic molecules were in the 12-membered ring channel and that after the adsorption of the pollutant the 12-ring channel was widened causing a narrowing and distortion of the 8-ring channel to accommodate the structural deformations (Fig. 2.26). These phenomena lead to small variations in the unit cell volume. For TOL-MOR, the Rietveld refinement showed a lowering of symmetry from the space group *Cmcm* to $Cmc2_1$ and toluene was localised in the 12-ring channel of the mordenite. 3.6 TOL molecules per unit cell were found and the toluene adsorption in the mordenite zeolite was very near to its maximum capacity. The short distance between the carbons of the toluene 6-ring and the oxygen atoms of the framework indicated possible strong interaction between the molecules and the guest zeolite, whereas the distances between the water molecule from one framework oxygen (W1-O5 = 3.13 Å) and one MTBE carbon atom (W-C1 = 3.17 Å) suggest that MTBE could be connected to the framework through water.

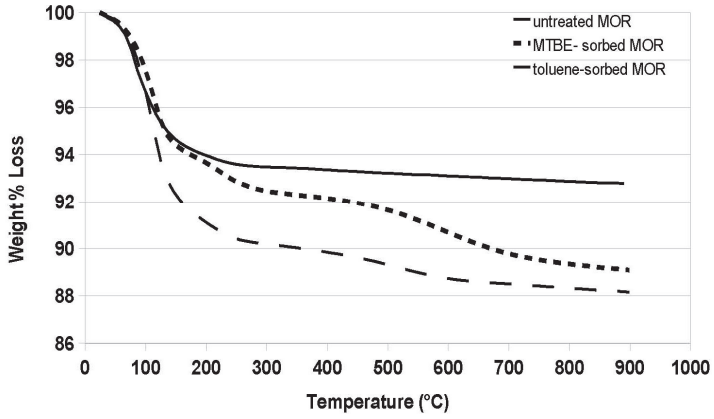

Figure 2.25: Thermogravimetric analyses of untreated, MTBE-sorbed and toluene-sorbed mordenite.

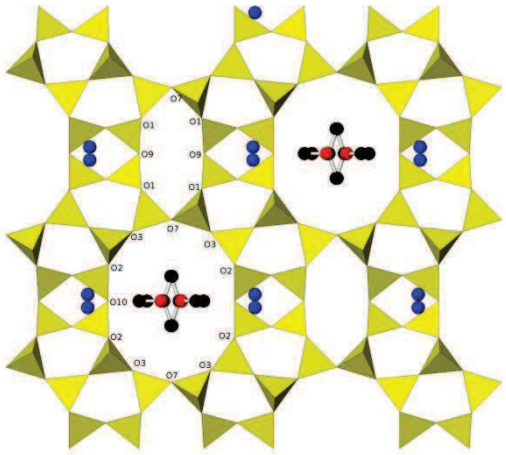

Figure 2.26: Projection of the MTBE sorbed mordenite.

The work on the adsorption of contaminants on hydrophobic zeolites was continued in order to explore the effects of framework types in terms of adsorption on both MTBE and TOL. In order to make easy the data comparison, the previously discussed adsorption data for mordenite, are reported here.

The aim of the present investigation was similar to that of the cases previously reported, in particular in evaluating the adsorption on MTBE and TOL on two hydrophobic zeolites (i.e. ZSM-5 and Y) and elucidating the mechanisms of adsorption. Moreover, a consideration of the data obtained in the present case highlighted the relevance of the number of systems organic contaminant-zeolite. This study also had the purpose of comparing the behaviour of the investigated adsorbent materials.

2- MTBE on ZSM-5 and Y

MTBE adsorption isotherms on both ZSM-5 and Y were determined in two different concentration ranges (Fig. 2.27), and different instrumental setups were adopted in order to guarantee the proper quality of the analytical data in terms of linearity and limit of detections.

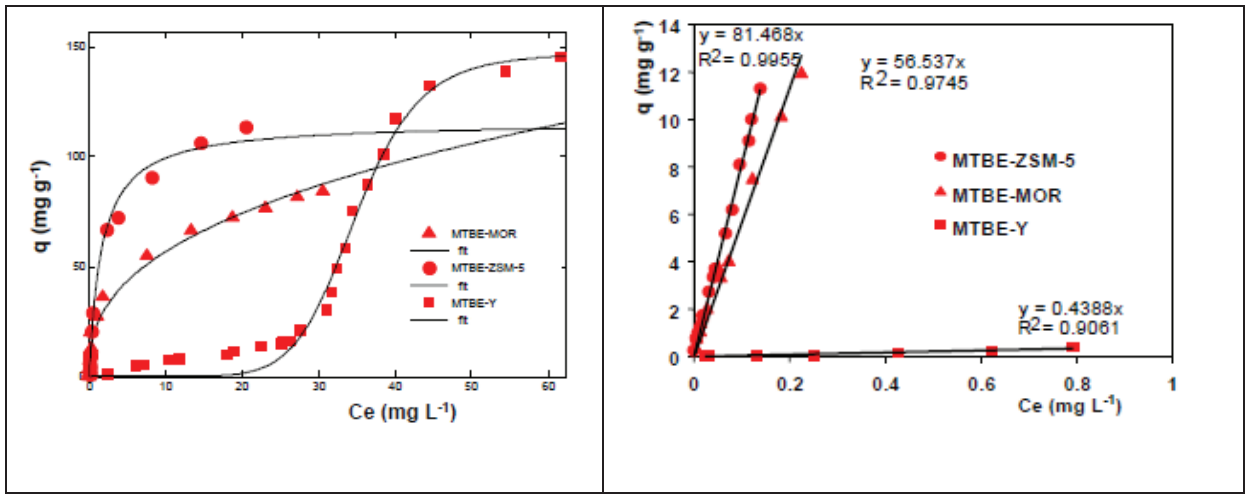

Figure 2.27: MTBE adsorption isotherms on MOR, ZSM-5 and Y in high and low concentration ranges.

It can be seen that the adsorption of MTBE on both Y and ZSM-5 follows a trend which is similar to that observed for DCE on the same zeolites. In particular, the adsorption data on ZSM-5 follow a classic L-class adsorption isotherm, whereas, the zeolite Y data follow a sigmoidal one. In this latter case, the adsorption of MTBE on Y zeolite is also scarce for the intermediate MTBE concentrations and not only for concentrations in the ppb range. The data for the MTBE-ZSM-5 system were fitted with both one and two sites Langmuir model (please see Table 2.4).

Table 2.4: Fitting results of the MTBE adsorption data on ZSM-5.

Organic - Zeolite	K_L (L mg^{-1})	q_s (mg g^{-1})	R^2
MTBE-ZSM-5	0.60	116	0.9927
Langmuir fit	(0.49, 0.72)	(110,121)	
MTBE-ZSM-5	1.2	65	0.9989
Dual-Langmuir fit	0.12	67	
MTBE-Mor	0.29	70.8	0.9826
Langmuir fit	(0.26, 0.32)	(57, 84.6)	
MTBE-Mor	2.2	36	0.9984
Dual-Langmuir fit	0.04	78	

From the data in Table 2.4, it can be seen that by increasing the number of sites the goodness of fit increases. However, this increase seems to be related to the higher flexibility of the two site models due to an increase of the fitting terms rather than to the physical meaning of the isotherm.

Thermal analyses confirmed the adsorption data. The TG curve of ZSM-5 after MTBE adsorption, showed that apart from the elimination of the species bonded to the surface of the grains (about 1% in weight) at T<100°C, a sudden change in its slope occurs at higher temperatures, which is probably due to the elimination of MTBE and/or H_2O molecules trapped within the zeolite pores. The total weight loss at 900°C is about 16%, in comparison with 2.8% in the as-synthesised material.

Powder diffraction data allow us to verify the effective incorporation of MTBE in the micro-porosities of ZSM-5 zeolite. The X-ray powder patterns of untreated and exhausted ZSM-5 are strongly different both in terms of intensity and the position of the diffraction peaks, indicating that the crystal structures were markedly modified by MTBE adsorption. The adsorption of MTBE causes small but significant variations of unit cell parameters in comparison to those of untreated materials, as well as a change in the geometry of the channel openings. Two crystallographically independent MTBE molecules were located in the ZSM-5 structure (Fig. 2.28), one (MTBE1) in the straight 10-ring channel parallel to *b* direction, the

other (MTBE2) in the sinusoidal 10-ring channel parallel to *a* direction. These two independent molecules, which are found in the zeolite, confirm the adsorption isotherm trend, in fact, precisely as before, the adsorption data fitted with the two site model had reported a greater value of goodness of fit. On the whole, 8 MTBE molecules were recognized (corresponding to 10% in weight). Difference Fourier maps revealed the presence of about 16 water molecules, corresponding to about 5% in weight, in very good agreement with the weight loss of the thermal analyses. MTBE strongly interacts with residual water molecules, which are H-bonded to the framework oxygen, thus explaining the distortions of the 10-ring channels. The difractometric analysis of the Y zeolite, before and after MTBE adsorption, confirms the saturation capacity obtained from the sigmoidal isotherm and permits MTBE molecules to be localised inside the supercage of this structure.

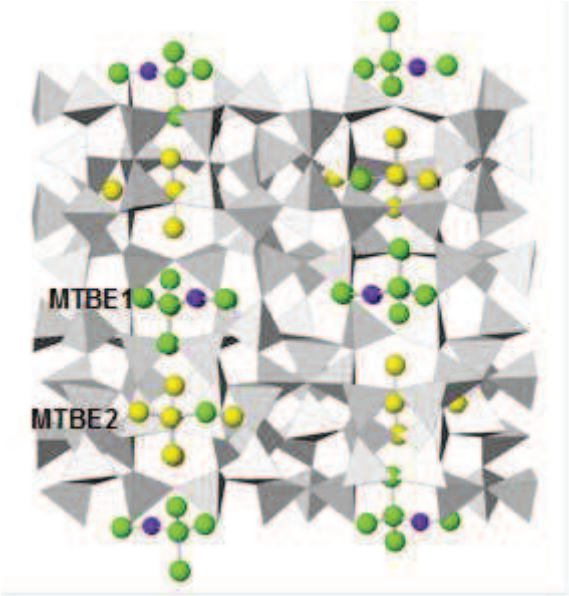

Figure 2.28: Two independent MTBE in the structure of ZSM-5.

3- TOLUENE on ZSM-5 and Y

Also in this case, adsorption isotherms showed very favourable adsorption kinetic for high-silica ZSM-5 (see Fig. 2.29). In particular, the effective and highly irreversible adsorption of TOL molecules into zeolite ZSM-5 pores make this material a tool with interesting applications for the removal of low concentrations of TOL from wastewater.

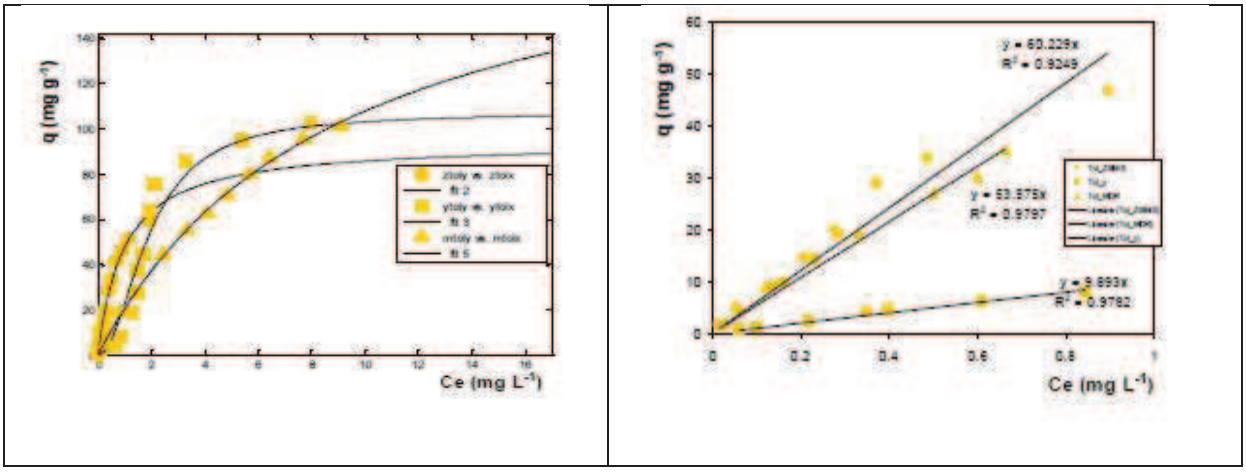

Figure 2.29: Adsorption isotherms for TOL on MOR, ZSM-5 and Y in high and low concentration ranges.

Thermal analyses confirmed the adsorption data. The TG curve of ZSM-5 after adsorption of TOL (Fig. 2.30) showed that apart from the elimination of the species bonded to the surface of the grains (about 9% in weight), (T<100°C), a sudden change in its slope occurs at higher temperatures, which is probably due to the elimination of TOL and/or H_2O molecules trapped within the zeolite pores. The total weight loss at 900°C is about 8%, in comparison with 2.8% in the as-synthesized material.

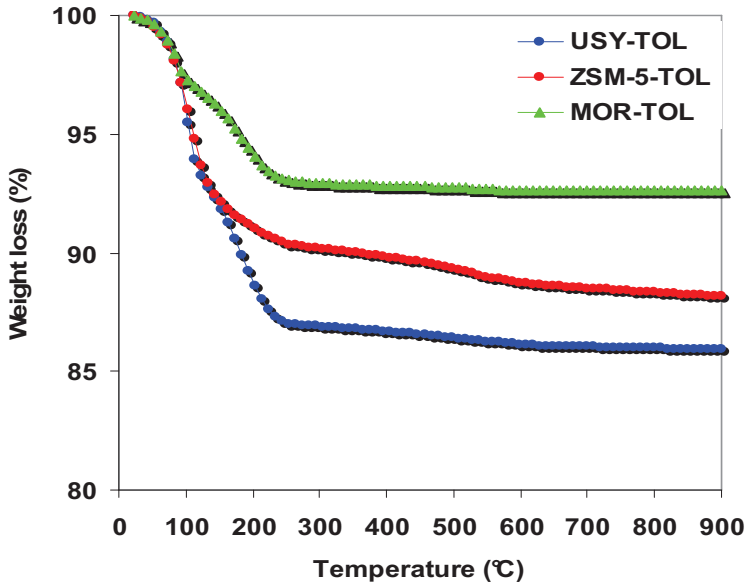

Figure 2.30: Thermogravimetric (TG) curves in Y, ZSM5 and MOR after adsorption of TOL.

The symmetry of ZSM-5 changes from monoclinic *P21/n* (before adsorption) to orthorhombic *P 21 21 21* (after adsorption), and consequently remarkable variations of unit cell parameters are detected. TOL adsorption strongly modifies the geometry of the channel systems, which become more elliptical. Rietveld refinement revealed the presence of 8 TOL molecules per unit cell, corresponding to about 9 % in weight, in good agreement with the TG analysis and adsorption capacity. Three disordered toluene sites were recognized. Two of these sites (TOL1 and TOL2) were located at the intersection of the straight and sinusoidal channels and the third (TOL3) in the sinusoidal channel (Fig. 2.31). The difference Fourier maps generated using GSAS, revealed the presence of a further extraframework site (fully occupied) which was attributed to water molecules. Dipole-dipole interactions occur between water and TOL 1 and TOL3 molecules thus forming TOL-water complexes which interact with framework oxygens. Rietveld refinement of TOL-Y revealed the presence of 24 TOL molecules/ u.c. (about 15 % in weight) which are located at the centre of the supercage.

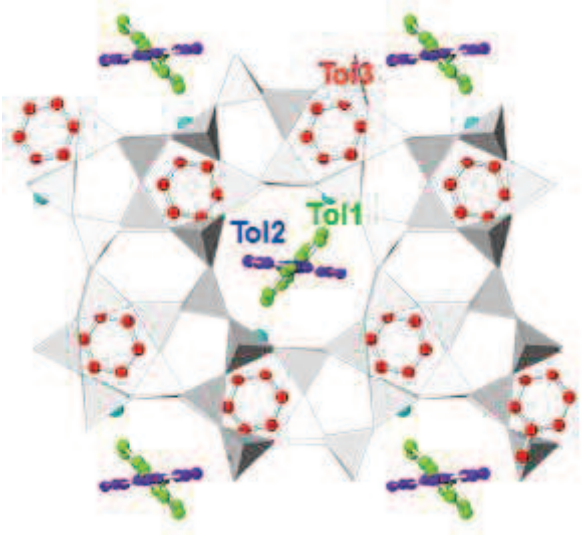

Figure 2.31: TOL in the ZSM-5 structure.

In conclusion, it was possible to exactly localize the contaminants in the zeolites framework and to determine the adsorption mechanism.

Case 4b: Additional analyses

1- BREAKTHROUGH CURVES

The use of zeolites as adsorbent materials may be an interesting alternative since these materials are stable at high temperatures and experimental data have demonstrated that zeolites have good adsorption capacities. Now, it is necessary to improve the industrial design of these adsorbents and to find the best operating conditions. As a result, adsorption processes needed to be modelled. In order to obtain further results, equilibrium data were obtained by dynamic analysis, therefore creating a breakthrough curve. Indeed only the start of this curve, and in particular the very initial part, is of interest for evaluating the performance of the adsorption process [35-70]. In the present study the breakthrough curves for two pollutants, TOL and MTBE, on a fixed bed of ZSM-5 zeolite were studied.

The experiments were performed using a 2mm x 2cm stainless steel column packed with ZSM-5. The packing of the column with zeolite was carefully carried out in order to minimise band spreading and to prevent the presence of air bubbles. The column contained 61 mg of packing materials and an aqueous solution of pollutant was pumped into the column until the concentration front broke through. The toluene concentration was measured using a UV-VIS Dionex detector at its maximum of adsorption (λ = 220nm), while the MTBE concentration was measured using a RID Agilent detector, which was coupled with the other detector. The amount of pollutant adsorbed by the stationary phase at equilibrium was derived through the standard equation:

$$q^* = \frac{C(V_b - V_0)}{w_{pack}} \tag{2.15}$$

where q^* is the amount adsorbed on the solid phase when it reaches equilibrium with the concentration C in the fluid phase, V_b is the retention volume of the half-height of the breakthrough curve, V_0 is the column hold-up volume and w_{pack} is the volume of adsorbent in the column. The breakthrough curve of toluene and MTBE was analysed at different flow rate and concentration (Fig. 2.32 and 2.33) to understand the interaction mechanism with the zeolite.

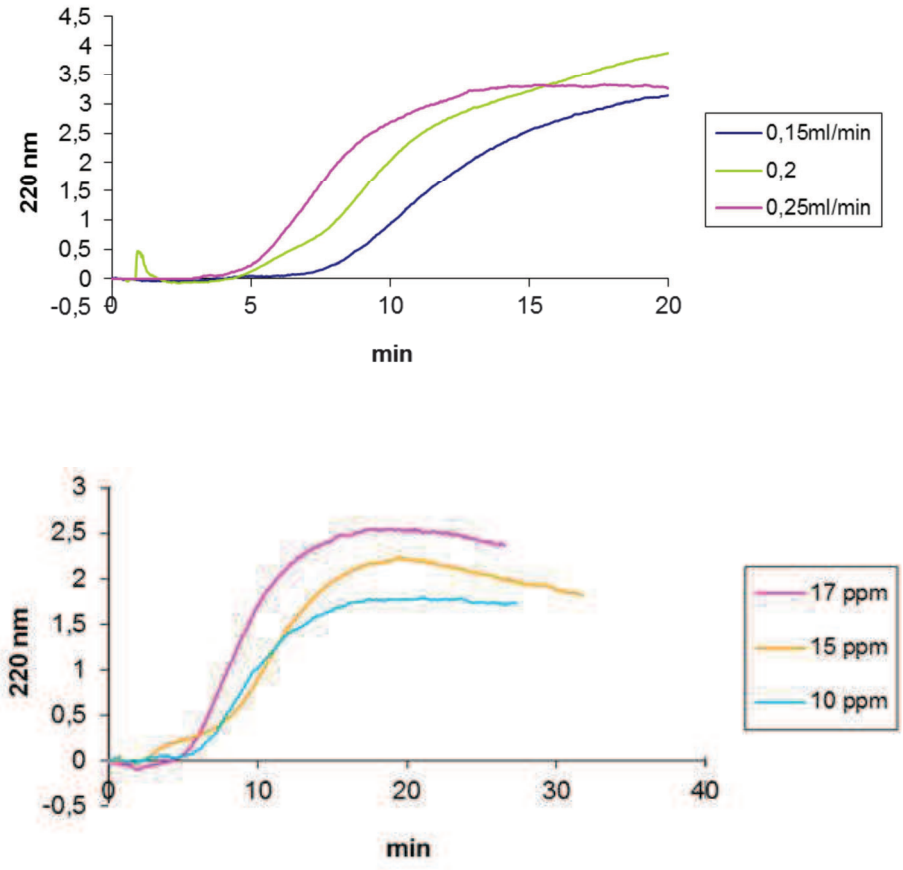

Figure 2.32: Experimental breakthrough curves for toluene (20ppm) at various flow rates and for toluene (0.2ml/min) at different concentrations.

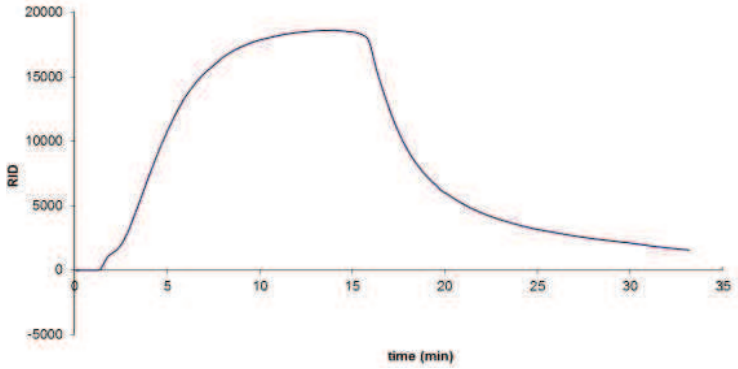

Figure 2.33: Experimental breakthrough curve for MTBE at 25 ppm.

Isotherm data obtained by means of column method were in good agreement with those gathered with batch method.

2- COMPETITION

The results obtained for a single component adsorption on hydrophobic zeolites were used as a basis for studying the adsorption process of mixtures of hydrocarbons on zeolites (i.e. TOL+MTBE, MTBE+DCE, DCE+TOL) with concentrations in the ppb and ppm range. In most environmental applications, these pollutants are present in the form of mixtures in very dilute aqueous solutions, indeed. ZSM-5 was chosen as adsorbent material since previous studies on single components had demonstrated that this zeolite has good adsorption capacities and affinity for these compounds even at low concentration levels.

In multicomponent equilibria, different molecules can compete for access to the adsorption sites, and those from more strongly adsorbed compounds tend to exclude others. The amount of any component adsorbed at equilibrium depends on the concentration of all the other components in the solution [25].

The batch method was used in order to study the equilibrium competition of toluene and MTBE on ZSM-5: different aqueous solutions were prepared with zeolite and, in all samples, the same concentration of toluene was kept fixed, while the concentration of MTBE was varied. In this way, it was possible to see the change in the adsorption isotherm of toluene when it was both alone and part of a mixture.

The adsorption isotherms of a mixture were obtained using the competitive Langmuir isotherm model since it has been proved that the traditional Langmuir model (see above) described the adsorption of contaminants on ZSM-5 well. The competitive model differs from the traditional one since, when several components are simultaneously present in the solution, the amount of each that is adsorbed at equilibrium can be smaller than that of the compound alone. In a binary mixture, it is possible to write the formula of the competitive Langmuir isotherm as:

$$q_i = \frac{q_{S,i} K_{L,i} C_i}{1 + K_{L,1} C_1 + K_{L,2} C_2} \tag{2.16}$$

The single-component isotherm is represented by a curve in the (q, C) plane. Binary competitive isotherms are represented by two surfaces, one in the three-dimensional space (q_1, C_1, C_2), the other one in (q_2, C_1, C_2) space [25].

The experimental data (see Table 2.5) had showed that both pollutants were adsorbent on ZSM-5. MTBE had a bigger saturation capacity than toluene when they were in a mixture and

even more so when the pollutants were studied as single component. The adsorption results indicate that competition exists between the organic compounds and that it occurs at low co-solute concentrations. Competitive adsorption in ZSM-5 in the medium-high concentration range was also observed.

Table 2.5: Isotherm parameter values for MTBE and TOL sorption in single and mixture adsorption experiments.

Pollutant-Zeolite	K_L (L mg^{-1})	q_s (mg g^{-1})	R^2
MTBE ZSM-5	0.60	116	0.9927
TOL ZSM5	0.51	96	0.9989
MTBE+TOL ZSM-5	0.60 0.51	68 33	0.9787

The TG curves for the ZSM-5 sample before and after MTBE and TOL adsorption showed that apart from the elimination of residual humidity, (T<100°C), a sudden change in their slope occurs at higher temperatures, which is probably due to the elimination of hydrocarbon species and/or H_2O molecules trapped within the MFI pores. Total weight loss at 900°C is about 7% for ZSM-5-TOL and 16% for ZSM-5-MTBE, respectively, in comparison to 3% of the as synthesised material at the same temperature. The weight loss after adsorption of the TOL and MTBE mixtures at the same temperature is about 13 %, thus confirming competitive adsorption in ZSM-5 at high concentration ranges (Fig. 2.34).

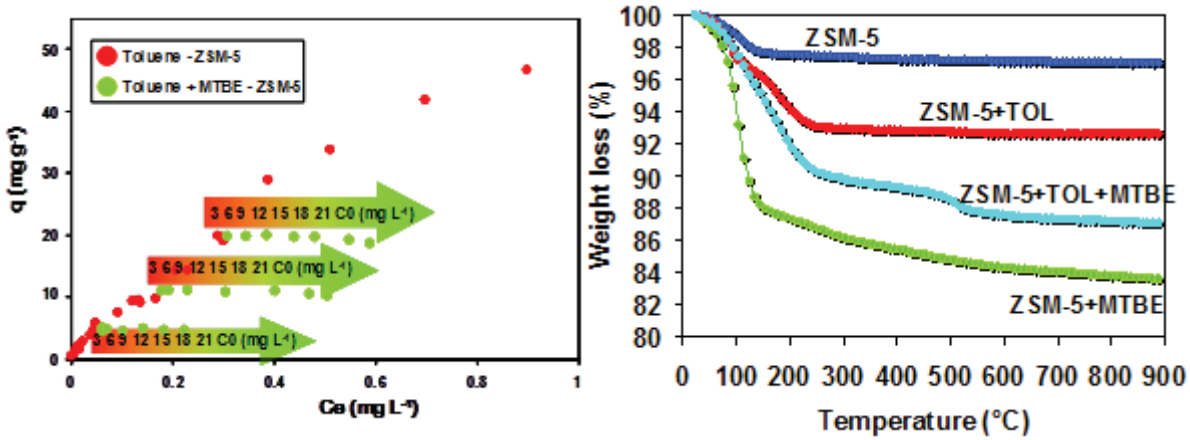

Figure 2.34: Competitive adsorption isotherm and TG curves.

Diffractometric data allowed us to obtain clear evidence of the adsorption of both MTBE and toluene molecules in the ZSM-5 channels as well as to exactly localise the organic species in the structure. The X-ray powder patterns of ZSM-5, before and after adsorption of the hydrocarbon mixtures, are strongly different both in terms of intensity and the position of the diffraction peaks, indicating that the crystal structure was markedly modified by hydrocarbon adsorption. Unit cell parameters do not change significantly. Only a slight increase in the volume can be observed. Deformations in the 10-ring windows were particularly highlighted by variations in both the CFA and ellipticity indexes. Both parameters indicate an enlargement in all channel systems to favour the adsorption of hydrocarbons molecules.

The 10-ring channels became more elliptical when compared with those found in the parent zeolite as a consequence of the diffusion and adsorption of organic complexes.

After adsorption the hydrocarbon mixtures, the TOL1 and TOL2 sites are emptied. The TOL molecules diffuse into the sinusoidal channel and are only confined in the TOL3 site. Its occupancy factors are unchanged (0.45). On the whole, about 2 TOL molecules per unit cell are recognised. These molecules interact with the framework oxygens.

Two crystallographically independent MTBE sites were again located in the structure of ZSM-5. The first one (MTBE1) in the straight 10-ring channel is fully occupied by 4 MTBE molecules. This result clearly indicates that MTBE molecules are preferably adsorbed and diffused into the straight 10-ring channel with respect to the TOL molecules. The second MTBE molecules (MTBE2) in the sinusoidal 10-ring channel are now only partially occupied by about 2 MTBE molecules. On the whole, 6 MTBE molecules (corresponding to 7.8% in weight) and 2 TOL molecules (corresponding to 2.5% in weight) are recognized. These molecules strongly interact with the framework oxygens, thus explaining the distortions in the 10-ring channels (Fig. 2.35).

Another extraframework site was recognized and attributed to water molecules (4 molecules, corresponding to about 1.3 % in weight). These water molecules can form chains which connect MTBE1 and MTBE2 molecules in the straight 10-ring channel.

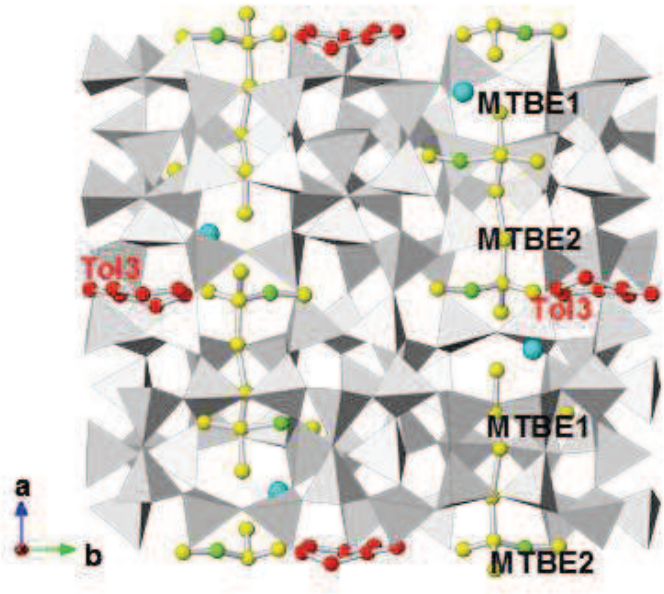

Figure 2.35: MTBE and TOL in ZSM-5 framework.

Similar adsorption results were found for the TOL-DCE and MTBE-DCE systems, as can be seen, competition exists because the saturation capacity is lower in the mixture than when the pollutants are alone (see Table 2.6 and Fig. 2.36). In these cases too, the diffractometric analysis was able to recognise differences in the occupation site of the multicomponent systems compared to single component adsorption.

Furthermore from the data obtained, the affinity order of adsorption was found to be: MTBE>DCE>TOL.

Table 2.6: Isotherm parameter values for DCE/TOL and DCE/MTBE sorption in single and mixture adsorption experiments on ZSM-5.

Pollutant-Zeolite	K_L (L mg^{-1})	q_s (mg g^{-1})	R^2
DCE ZSM-5	0.19	120	0.9927
TOL ZSM5	0.51	96	0.9989
DCE+TOL ZSM-5	0.19 0.51	58 50	0.9817
DCE ZSM-5	0.19	120	0.9927
MTBE ZSM5	0.6	116	0.9989
DCE+MTBE ZSM-5	0.19 0.60	53 49	0.9883

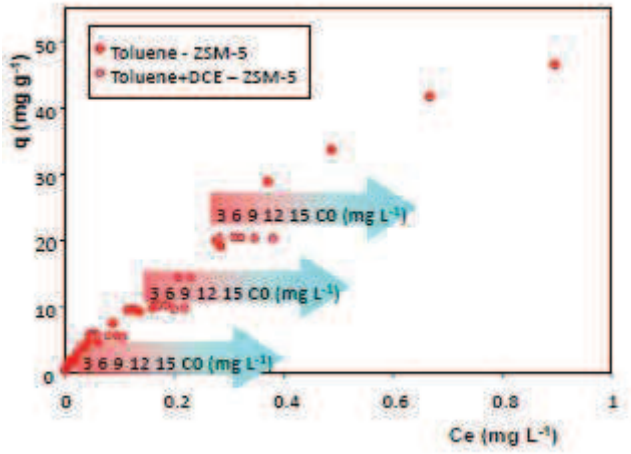

Figure 2.36: Competitive adsorption isotherm.

In conclusion, for both the two components systems studied, the competitive adsorption on ZSM-5 was observed.

3- LIQUID PHASE DIFFUSION MEASUREMENTS

An understanding of the transport properties of the adsorbed species in microporous solids is required in order to accurately design adsorption and catalytic reaction processes. The zero length column method (ZLC) represents a simple and relatively inexpensive technique to obtain the required physical properties. It is essentially a chromatographic technique, which eliminates uncertainty due to axial dispersion and requires only a small amount of adsorbent. ZLC has been widely used to measure intracrystalline diffusivities in zeolitic adsorbents and other microporous solids. In order to obtain the diffusion coefficients, the model equation solution, proposed by Ruthven to describe ZLC, is matched to the experimental desorption curves.

This technique is an extension of the gas phase ZLC method; in the gas phase zero length column method the hold-up in the fluid phase can usually be neglected, while in the liquid phase adsorption system, the hold-up in the fluid phase can be of the same order of magnitude as the hold-up in the adsorbed phase. This was accounted for in the extended model for liquid systems as reported by Brandani and Ruthven, which showed that the long-time slope of the desorption curve is relatively unaffected by interstitial hold-up [45-49].

In this study the diffusivity of toluene and MTBE in water solution was determined using the ZLC method with ZSM-5 as the adsorbate. The ZLC desorption curve, including the effect of interstitial fluid, is given by applying the formula:

$$\frac{c}{c_0} = \sum \frac{2Lexp(-\beta_n^2 \tau)}{\beta_n^2 + (1 - L + \gamma\beta_n^2)^2 + L - 1 + \gamma\beta_n^2} \tag{2.17}$$

This equation is described in the Chapter 1 (Eq. 1.44) about the diffusion phenomena.
Over long times periods, and assuming that L is large (in comparison to $\gamma\beta^2$), the equation reduces to the form [71]:

$$ln\frac{C}{C_0} = ln\frac{2}{L} - \pi^2 \frac{D}{R^2} t \tag{2.18}$$

From Eq. 2.18 it may be seen that diffusivity (D) may be extracted from the slope over the long time period region of a semi-logarithmic plot of normalised concentration versus time. The assumption of large L implies, physically, that intracrystalline diffusion is slow relative to the removal of sorbate from the crystal surface. Please note that the long time period slope of the desorption curve is independent from the value of γ; this implies that the diffusional time constant can be measured reliably even in the presence of fluid phase hold-up if L is large.
The experimental set-up consisted of two HPLC Waters 515 pumps, a six-way Rheodyne valve, which a ZLC column was installed on, and a diode array UV-VIS Waters detector. The ZLC column was made out of stainless steel (1/2''OD; 1cm length). One of the major prerequisites of the ZLC method is the use of a small zeolite bed. For these purposes, only a small amount of zeolite is generally necessary, indeed in this work 700 mg of ZSM5 were used.
The MTBE or toluene aqueous solution was pumped through the ZLC column; the transient desorption of the MTBE or toluene was monitored as a function of time after switching the mobile phase to the pure solvent, water. The diffusion coefficient was determined using the long time period solution of the ZLC model.
The blank response of the system was evaluated, replacing the zeolite with glass beads.
Blank and pollutant responses showed different behaviour, since glass represents a non-adsorbing system; indeed the Fig. 2.37 shows non-ideal flow behaviour indicating non-

negligible fluid hold-up in the lines, valve and/or detector. The parameter D/R^2 was determined by considering the Eq. 2.18 and was obtained from the slope of the long-time period region of the C/C_0 plot vs. time. The resulting parameter values are summarized in the Table 2.7 and the model fit to the experimental curves is shown in Fig. 2.38.

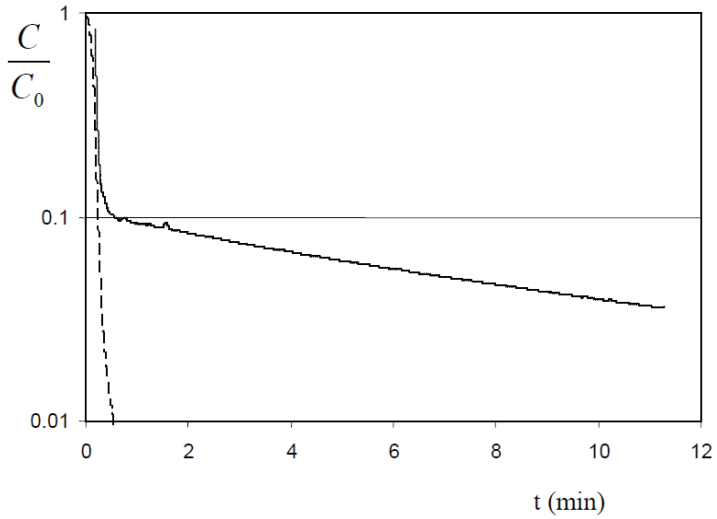

Figure 2.37: Comparison of experimental ZLC curves for glass beds (dashed line) and ZSM5 (continuous line).

Table 2.7: Diffusivity coefficient of toluene and MTBE in ZSM-5.

Pollutant	**D (m^2/s)**
Toluene	9,1 x 10^{-17}
MTBE	5,4 x 10^{-16}

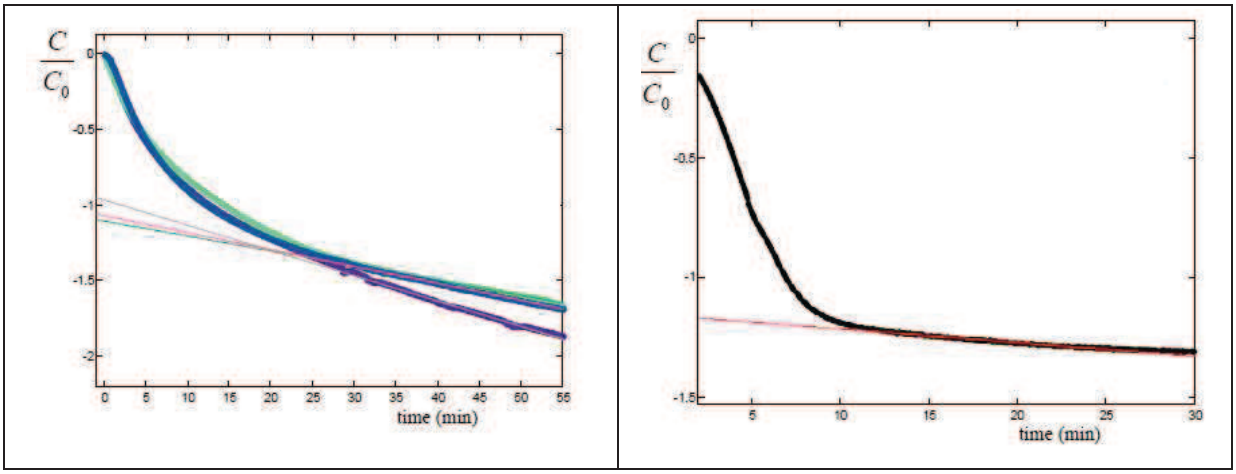

Figure 2.38: Experimental ZLC desorption curve for toluene (blue) and MTBE (black) diffusion in ZSM-5.

The diffusivity of toluene in water is slower than that of MTBE. Wilkenhöner et al. found similar diffusion coefficient values, of the same magnitude order (10^{-16}- 10^{-17}), in particular the diffusivity of Phenol in titano-silicates TS-1 and Al-free Ti-beta and of Phenol, Catechol and Hydroquinone in titano-silicates TS-1 were compared using water as a solvent. The high polarity enables the formation of associated complexes e.g. between Phenol and solvent, within the pores TS-1, and thus reducing the mobility of Phenol in the pores of TS-1 with water as a solvent [71].

Case 5: Study of adsorption of perfluorooctanoic acid onto mesoporous materials

Perfluororinated compounds (PFCs) have been widely used in industrial and commercial applications for about 50 years as surfactants, emulsifiers, fire retardants, polymer additives and etc. In this study, perfluorooctanoic acid (PFOA) has been considered. PFOA is also known as C8 and is found in the environment since it may be directly discharged from pollution sources or generated by the microbial degradation of other perfluorinated compounds. PFOA is environmentally persistent, bio accumulative, potentially toxic and has high solubility. Due to this, it has been detected in surface water and groundwater. PFOA is difficult to analyse because it is found in low concentration ($\mu L\ g^{-1}$) in groundwater. Therefore, the development of effective techniques to remove it from water becomes crucial. Different technologies have already been tested to remove PFOA from water such as UV-visible light irradiation, photochemical decomposition with persulfate ions, membrane processes and sonochemical degradations, but most of these methods were ineffective [72].

It has been demonstrated in many cases that sorption is an effective and economical method for the removal many pollutants [73-74]. In this paper, the adsorption behaviour of PFOA on mesoporous materials has been investigated. Mesoporous materials, as described previously (see Chapter 1), have been utilized as they have bigger channels than zeolites and adsorption of large molecules is possible. MCM-41 and HMS were synthesised and characterised in the 'Institut Charles Gerhardt (ICG), Matériaux Avancés pour la Catalyse et la Santé (MACS)' at Montpellier (France) with the supervision of Prof. Francesco di Renzo and Dr. Anne Galarneau.

The pseudomorphic synthetic procedure was applied to a silica source to obtain MCM-41. The silica source for the synthesis, called "Aerosil", was used in a mixture of final molar composition $Si_2O/NaOH/C_{16}TAB$ = 0.1:0.25:0.1 ($C_{16}TAB$ is cetyltrimethyl ammonium bromide) with 50 H_20, which was stirred and then heated at 115°C without stirring for various time [15]. HMS, on the other hand, was synthetized following the procedure provided by Tanev and Pinnavaia [19] and, in particular, TEOS (tetraethyl orthosilicate) was added to a vigorously stirred solution of amine in ethanol and deionized water in the following molar composition $TEOS/C_{16}H_{33}NH_2/EtOH/H_2O$ = 1:0.25:7:36. The materials characterisation was followed by Nitrogen sorption at 77 K and IR analysis. From Nitrogen sorption (Fig. 2.39), it was possible to determine surface area (S_{BET}), pore volume (V_L) and pore size (D BdB)

(Table 2.8) and it was found that MCM-41 had a smaller surface area and pore size than HMS according with the synthesis properties.

In order to obtain the specific surface area, the Brunauer-Emmet-Teller (BET) method was applied. This consists in considering the BET equation:

$$\frac{\frac{P}{P_0}}{V_{ads}\,(1-\frac{P}{P_0})} = \frac{1}{V_m C} + \frac{C-1}{V_m C} \times \frac{P}{P_0} \tag{2.19}$$

where V_m is the monolayer volume and C is the BET coefficient (C_{BET}). The C_{BET} parameter was measured from the linear fit, in the $0.15<P/P_0<0.26$ range of the Nitrogen adsorption isotherm, $(P/P_0)/(V_{ads}[1-P/P_0])$ versus (P/P_0). C_{BET} = [(S/I)+1], where S is the slope of the linear fit and I is the intercept with the y-axis. By means of the intercept and slope values it was possible to obtain V_m = [1/(S+I)], which was necessary to determine S_{BET}, indeed $S_{BET} = N_m * V_m$ was calculated by multiplying the number of molecules adsorbed in the first monolayer (N_m) by the surface area (V_m) covered by each molecule. The most widely used value for N_2 is 16.2 $Å^2$, which was obtained by attributing the density of liquid N_2 to the first monolayer, after which N_m is taken as a constant value of 4.36 [75-76-77].

Pore volume (V_L) was determined by considering the volume of the mesoporous materials at the top of the adsorption step and then dividing by 646 (the ratio between the liquid and gas densities of Nitrogen) [75].

In order to determine pore size, the Broekhoff and de Boer method was applied. Using this method, hexagonal pores of mesoporous materials were assimilated to cylindrical pores, by a theoretical studies of capillary-condensed liquid from a cylindrical pore; by making use of a mathematical formula this method was useful in determining the correlation between the pore diameter (D BdB) and P/P_0 [77-78].

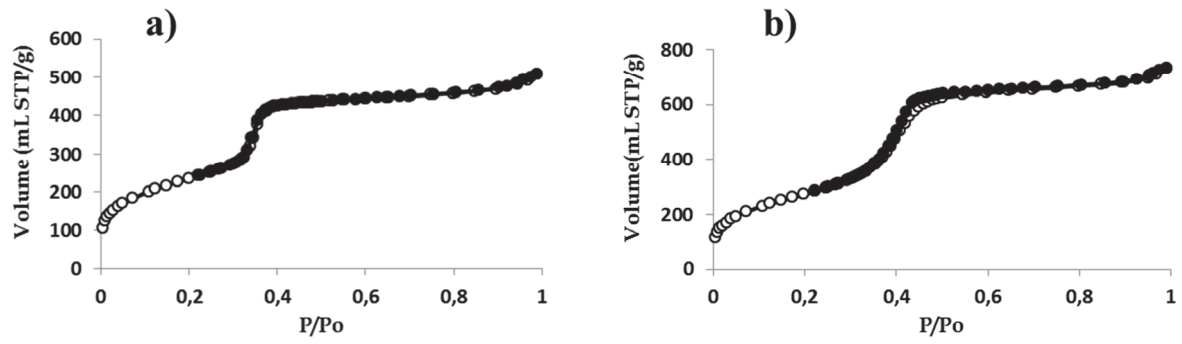

Figure 2.39: Nitrogen adsorption/desorption isotherm at 77 K of a) MCM-41 and b) HMS. White circles are adsorption, black circles are desorption.

Table 2.8: Values obtained by Nitrogen adsorption isotherm at 77 K.

Sample name	MCM-41	HMS
S_{BET} (m^2/g)	856	1019
V_L (mL/g)	0.66	0.96
D BdB (nm)	3.75	4.2

In all the experiments adsorption was obtained using the batch method, therefore a given amount of mesoporous materials was equilibrated with a note volume of PFOA in an aqueous solution. After equilibration, the solid was separated from aqueous solution and, the PFOA in the aqueous solution at the equilibrium was analysed through the HPLC-MS. The adsorption kinetic tests showed that about 70 h of agitation are required to reach adsorption equilibrium for both mesoporous materials. The kinetic was slow compared to that of microporous materials. However, previous studies had demonstrated the same time or a time longer period than ours [72]. The data at low concentrations were fitted using a pseudo-second order equation [40]: MCM-41 and HMS had similar high correlation coefficients (R^2 > 0.99), indicating that chemical interactions were possibly involved in the sorption processes. The adsorption isotherms were fitted by Langmuir model (see Fig. 2.40) and it can be seen that MCM-41 and HMS had the same adsorption capacity value (q_s ~6 mg g^{-1}) therefore the same adsorption behaviour. In the literature, when alumina or GAC were used as adsorbents, a lower adsorption capacity value was found [73-74], therefore MCM-41 and HMS can be considerated good adsorbents for removing perfluorooctanoic acid from water, but other analysis are required in order to understand the mechanism of interaction between the pollutant and mesoporous materials.

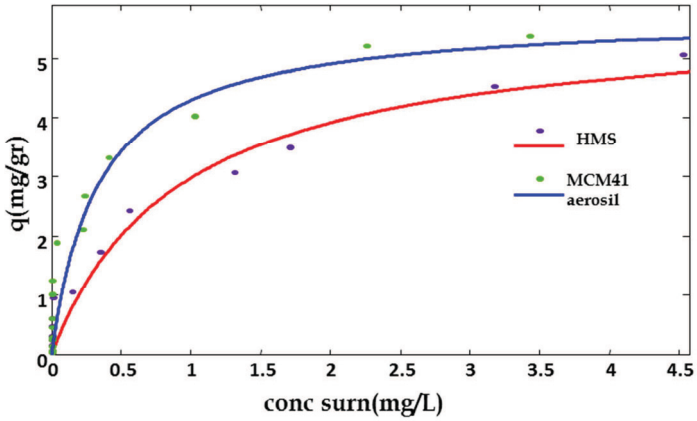

Figure 2.40: PFOA adsorption isotherm on HMS (red) and MCM-41 (blue).

CONCLUSIONS

The results of the adsorption of contaminants on hydrophobic zeolites enable a comprehensive characterisation of the adsorption process:

- The adsorption process was fast for all the contaminant-zeolite systems investigated: equilibrium concentration was reached in few minutes.
- High adsorption efficiency of Y and ZSM-5 zeolites in adsorbing MTBE, DCE and toluene was observed from the saturation capacity data.
- The isotherm model type depends more on the zeolite characteristics than on the contaminant structure.
- Evaluation of zeolite selectivity based on the binding constant values, which were obtained by fitting the adsorption data for the given zeolites- organic system.
- The locations of contaminants in different zeolite frameworks were established.
- The interactions between organic species, water molecules and framework oxygen atoms were investigated. The water-organic material complexes strongly interacted with the framework, thus justifying the deformation of the 10-ring channel systems. Water effects cannot be neglected especially when hydrogen bonds are involved. The presence of water should be considered as a multicomponent system instead of a single component adsorption mechanism.
- The competitive adsorption of the investigated contaminants in mixtures was proved. The competitive process induces diffusion of molecules through the zeolite channel systems thus causing the reorientation of the extraframework species.

These results show that the adsorption properties of zeolitic materials are difficult to determine “a priori” based only on the SAR and the size of the micropores; indeed, the structural features of zeolite materials strongly affect zeolite selectivity.

Since zeolites are known to be powerful catalysts for different organic reactions, a novel mathematical model to describe the flow reaction systems was proposed. The model is able to describe both the interconversions and the reactions during separation. Some basic features of the process - such as the interconversion kinetics constants - and/or operative variables - such as column length (or flow velocity) – and their influence on the chromatographic can be obtained from experimental data by fitting with the proposed equations.

Finally, in the present thesis the efficiency of synthesized mesoporous materials in the adsorption of perflourinated acids contaminants was also proved.

Chapter 3

REFERENCES

[1] R. Vignola, G. Grillo, R. Sisto, G. Capotorti, P. Cesti, M. Molinari, in: G.A. Boshoff, B.D. Bone (Eds.), Permeable Reactive Barriers, IAHS Publ 298, 2005, pp. 105–109.

[2] R. Vignola, U. Cova, F. Fabiani, G. Grillo, R. Sbardellati, R. Sisto, Stud. Surf. Sci. Catal. 174 (Part 1) (2008) 573–576.

[3] R. Vignola, R. Sisto, G. Grillo, U. Cova, P. Cesti, US2009/0014390 A1 Patent, (2009).

[4] R. Vignola, U. Cova, G. Della Penna, R. Sisto, WO 2005/06361 A2 Patent (2005).

[5] Berrin Tansel, Recent Patents on Chemical Engineering 1 (2008) 17-26.

[6] J. Lemić, M. Tomašević-Čanović, M. Adamović, D. Kovačević and S. Milićević, Microporous and Mesoporous Materials 105 (2007) 317-323.

[7] C.M.M. Almeida and L.V. Boas, J. Environ. Monit. 6 (2004) 80-88.

[8] A. Giaya, R.W. Thompson and R. Denkewicz Jr., Microporous and Mesoporous Materials 40 (2000) 205-218.

[9] V. Matamoros, C. Arias, H. Brix and J.M. Bayona, Environ. Sci. Technol. 41 (2007) 8171-8177.

[10] M.F. Rahman, E.K. Yanful and S.Y. Jasim, Desalination 248 (2009) 578-585.

[11] M. F. Rahman, E.K. Yanful and S.Y. Jasim, Journal of Water and Health (2009) 224-243.

[12] A. Pfenninger, 'Manufacture and Use of Zeolites for Adsorption Processes' Molecular Sieves, Vol.2 (1999) 164-198.

[13] J. Čejka, H. van Bekkum, A. Corma, F. Schüth, Introduction to Zeolite Science and Practice, 3RD revised edition, Elsevier, Vol.168, 2007.

[14] H.van Bekkum, E.M. Flanigen, P.A. Jacobs and J.C. Jansen, Studies in Surface Science and Catalysis 137 (2001) 11-35 (Chapter 2).

[15] A. Galarneau, J. Iapichella, K. Bonhomme, F. Di Renzo, P. Kooyman, O. Terasaki and F. Fajula, Adv. Funct. Mater. 16 (2006) 1657-1667.

[16] J.S. Beck, J.C. Vartuli, W.J. Roth, M.E. Leonowicz, C.T. Kresge, K.D. Schmitt, C.T-W. Chu, D.H. Olson, E.W. Sheppard, S.B. McCullen, J.B. Higgins and J.L. Schlenker, J. Am. Chem. Soc. 114 (1992)10834-10843.

[17] J. Iapichella, J.-M. Meneses, I. Beurroies, R. Denoyel, Z. Bayram-Hahn, K. Unger and A. Galarneau, Microporous and Mesoporous Materials 102 (2007) 111-121.

[18] R.T. Yang, T.J. Pinnavaia, W. Li and W. Zhang, Journal of Catalysis 172 (1997) 488-493.

[19] P.T. Tanev and T.J. Pinnavaia, Chem. Mater. 8 (1996) 2068-2079.

[20] W. Zhang, T.R. Pauly and T.J. Pinnavaia, Chem Mater. 9 (1997) 2491-2498.

[21] S.M. Holmes, V.L. Zholobenko, A. Thursfield, R.J. Plaisted, C.S. Cundy and J. Dwyer, J. Chem. Soc., Faraday Trans. 94(14) (1998) 2025-2032.

[22] K.R. Kloetstra, H.W. Zandbergen, M.A. van Koten and H. van Bekkum, Catalysis Letters 33 (1995) 145-156.

[23] X.S. Zhao, G.Q. Lu and X. Hu, Microporous and Mesoporous Materials 41 (2000) 37-47.

[24] M. Jaroniec, Physical Adsorption on Heterogeneous Solids, Elsevier, 1988.

[25] G. Guiochon, A. Felinger, D.G. Shirazi, A.M. Katti, Fundamentals of Preparative and Nonlinear Chromatography, Second Edition, Elsevier, 2006.

[26] A. Safa Özcan, B. Erdem and A. Özcan, Journal of Colloid and Interface Science 280 (2004) 44-54.

[27] C.Y. Chang, W.T.Tsai, C.H.Ing and C.F. Chang, Journal of Colloid and Interface Science 260 (2003) 273-279.

[28] F. Gritti, W. Piatkowski and G. Guiochon, Journal of Chromatography A 978 (2002) 81-107.

[29] F. Gritti, G. Gotmar, B.J. Stanley and G. Guiochon, Journal of Chromatography A 988 (2003) 185-203.

[30] I. Quinones and G. Guiochon, Journal of Chromatography A 796 (1998) 15-40.

[31] A. Gil and P. Grange, Colloids and Surfaces A: Physicochemical and Engineering Aspects 113 (1996) 39-50.

[32] R.M. Allen-King, P. Grathwohl and W.P. Ball, Advances in Water Resources 25 (2002) 985-1016.

[33] R. Pelech, Ind. Eng. Chem. Res. 47 (2008) 5615-5622.

[34] E. Bi, S.B. Haderlein and T.C. Schmidt, Water Research 39 (2005) 4164-4176.

[35] B. Koubaissy, G.Joly, I.Batonneau-Gener and P.Magnoux, Ind. Eng. Chem. Res. 50 (2011) 5705-5713.

[36] A. Ebadi, J.S. Soltan Mohammadzadeh and A. Khudiev, Adsorption 15 (2009) 65-73.

[37] I. Quinones and G. Guiochon, Langmuir 12 (1996) 5433-5443.

[38] Giles, MacEwan, Nakhwa and Smith, Studies in Adsorption Part XI 786 (1960) 3973-3993.

[39] S. Azizian, Journal of Colloid and Interface Science 276 (2004) 47-52.

[40] W. Plazinski, W. Rudzinski, A. Plazinska, Advances in Colloid and Interface Science 152 (2009) 2-13.

[41] Y.S. Ho, Water Research 40 (2006) 119-125.

[42] Y.S. Ho, G. McKay, Process Biochemistry 34 (1999)451-465.

[43] W. Rudzinski and W. Plazinski, J. Phys. Chem. B 110 (2006) 16514-16525.

[44] K. Miyabe and G. Guiochon, Journal of Chromatography A, 890 (2000) 211-223.

[45] D.M. Ruthven and P. Stapleton, Chemical Engineering Science, 48 (1993) 89-98.

[46] L. Boulicaut, S. Brandani and D.M. Ruthven, Microporous and Mesoporous Materials 25 (1998) 81-93.

[47] P. Cherntongchai and S. Brandani, Adsorption 9 (2003) 197-204.

[48] S. Brandani and D.M. Ruthven, Chemical Engineering Science 50 (1995) 2055-2059.

[49] J.R. Hufton and D.M. Ruthven, Ind. Eng. Chem. Res. 32 (1993) 2879-2386.

[50] K. Babić, L.G.J. van der Ham and A.B. de Haan, Adsorption 14 (2008) 357-366.

[51] O. Trapp, G. Schoetz, V. Schurig, Chirality 13 (2001) 403.

[52] W. Bürkle, H. Karfunkel, V. Schurig, J. Chromatogr. 288 (1984) 1.

[53] G. Guiochon, A. Felinger, A.M. Katti, D. Shirazi, Fundamentals of Preparative and Nonlinear Chromatography, 2nd ed., Elsevier, The Netherlands, 2006.

[54] R. Thede, Encyclopedia of Chromatography: Rate Constants: Determination from On-Column Chemical Reactions, 2nd ed., Taylor & Francis, 2006.

[55] O. Trapp, Chem. Today 26 (2008) 26.

[56] N.G. Van Kampen, Stochastic Processes in Physics and Chemistry, North Holland, Amsterdam, 1981.

[57] D.T. Gillespie, J. Chem. Phys. 113 (2000) 297.

[58] R. Kubo, J. Phys. Soc. Jpn. 9 (1954) 935.

[59] P.W. Anderson, J. Phys. Soc. Jpn. 9 (1954) 316.

[60] Y. Jung, E. Barkai, R.J. Silbey, Chem. Phys. 284 (2002) 181.

[61] L. Pasti, A. Cavazzini, A. Felinger, M. Martin, F. Dondi, Anal. Chem. 77 (2005) 2524.

[62] William Feller, An Introduction to Probability Theory and Its Applications, Vol. 2, Second Edition.

[63] R.N. Bracewell, The Fourier Transform and Its Applications, 2nd ed., McGraw- Hill, NY, 1978.

[64] W.C. Hamilton, Statistics in Physical Science Estimation, Hypothesis Testing, and Least Squares, The Ronal Press Company, NY, USA, 1964.

[65] J. Rabone, Y.-F. Yue, S. Y. Chong, K. C. Stylianou, J. Bacsa, D. Bradshaw, G. R. Darling, N. G.Berry, Y. Z. Khimyak, A. Y. Ganin, P. Wiper, J. B. Claridge, M. J. Rosseinsky, Science 329 (2010)1053-1057.

[66] L. Y. Lee, N. Yoshida, F. Hirata, J. Phys. Chem. B 110 (2006) 16018-16025.

[67] B. Cohen, S. Weiss, J. Phys. Chem. 87 (1983) 3606-3610.

[68] M. A. Anderson, Environ. Sci. Technol. 34 (2000) 725-727.

[69] I. Arambarri, M.Lasa, R.Garcia and E.Millan, Journal of Chromatography A 1033 (2004) 193-203.

[70] L. Abu-Lail, J.A. Bergendahl and R.W. Thompson, Journal of Hazardous Materials 178 (2010) 363-369.

[71] U. Wilkenhöner, W.L. Duncan, K.P. Möller and E. van Steen, Microporous and Mesoporous Materials 69 (2004) 181-186.

[72] S.T.M.L.D. Senevirathna et al., Chemosphere 80 (2010) 647-651.

[73] Q. Yu, R.Zhang, S. Deng, J. Huang and G. Yu, Water Research 43 (2009) 1150-1158.

[74] Fei Wang and Kaimin Shih, Water Research 45 (2011) 2925-2930.

[75] A. Galarneau, H. Cambon, F. Di Renzo and F. Fajula, Langmuir 17 (2001) 8328-8335.

[76] Kenneth Sing, Colloids and Surfaces A: Physicochem. Eng. Aspects 187-188 (2001) 3-9.

[77] A. Galarneau, D. Desplantier, R. Dutartre and F. Di Renzo, Microporous and Mesoporous Materials 27 (1999) 297-308.

[78] J.C.P. Broekhoff and J.H. De Boer, Journal of Catalysis 10 (1968) 377-390.

Chapter 4

PAPERS

1- L. Pasti, A. Cavazzini, M. Nassi, F. Dondi, *Dynamic chromatography: A stochastic approach,* Journal of Chromatography A, 1217 (2010) 1000-1009.

2- A. Martucci, L. Pasti, M. Nassi, A. Alberti, R. Arletti, R. Bagatin, R. Vignola, R. Sticca, *Adsorption mechanism of 1-2-dichloroethane into an organophilic zeolite mordenite: A combined diffractometric and gas chromatographic study*, Microporous and Mesoporous Materials 151 (2012) 358-367.

3- L. Pasti, A. Martucci, M. Nassi, A. Cavazzini, A. Alberti, R. Bagatin, *The role of water in DCE adsorption from aqueous solutions onto hydrophobic zeolites* (manuscript).

4- R. Arletti, A. Martucci, A. Alberti, L. Pasti, M. Nassi, R. Bagatin, *Location of MTBE and Toluene in the channel system of the zeolite mordenite: adsorption and host-guest interactions* (manuscript).

Journal of Chromatography A, 1217 (2010) 1000–1009

Contents lists available at ScienceDirect

Journal of Chromatography A

journal homepage: www.elsevier.com/locate/chroma

Dynamic chromatography: A stochastic approach

Luisa Pasti*, Alberto Cavazzini, Marianna Nassi, Francesco Dondi

Department of Chemistry, University of Ferrara, Via L. Borsari, 46, I-44100 Ferrara, Italy

ARTICLE INFO

Article history:
Available online 17 October 2009

Keywords:
Dynamic chromatography
Reaction chromatography
Enantiomers separation
Chiral chromatography
Reaction rate

ABSTRACT

During the chromatographic separation process, analyte reactions are often observed leading to band broadening and/or elution of peak clusters. For many different chemical compounds the reaction can be reduced to a simple isomerisation kinetic scheme where elution is the result of adsorption–desorption on the surface stationary phase coupled with a flipping two-level reaction system. In this paper, the chromatographic peak shape for a reacting analyte is calculated in frequency domain when the reaction follows a simple reversible first order scheme. Both reaction and dynamic chromatographic systems have been considered. The derived solutions are expressed in closed form in the Fourier domain. Several limit solutions obtained under conditions of very slow and moderately fast kinetics are exploited. The effects of both kinetics rate constants and retention time on the chromatographic peak shape are singled out.

1. Introduction

Efficient, economical product or process design requires accurate fundamental data values such as transport properties, adsorption energy and kinetic rate. Likewise, the fundamental understanding of many processes requires the use of thermodynamics, mass transfer with chemical reaction in nonideal systems [1,2]. Moreover in product design, it is well known that the stability of certain chemicals is an important issue in chemical and pharmaceutical studies, since most biochemical processes or chemical properties are stereochemically controlled. Different methods can be adopted to evaluate these data and a comprehensive review of these can be found elsewhere [3].

One of these techniques is dynamic chromatography studied by Bürkle et al. [4], which offers several advantages over other methodologies. Indeed, chromatography makes it possible to obtain mass transfer, adsorption and kinetics data and can be employed in non-linear conditions [5]. However, a prerequisite for employing this technique is that reaction must take place within the separation timescale (on-column reaction chromatography) [6–12]. Different methods can be employed to extract kinetic parameters from the experimental chromatograms [3,4,13–16].

The focus of the present work is to represent the dynamic chromatography from a microscopic point of view in order to provide a new method for determining the kinetic constant by dynamic chromatography experiments. In particular, the on-column reaction chromatography process is described by using the stochastic model of chromatography [17]. Originally developed by Keller and Giddings [18], there has been renewed interest in this model since it makes it possible to correlate macroscopic classical chromatographic parameters with the behavior properties of individual molecules [19,20]. These arguments partially support the use of the stochastic approach even to study interconversion phenomena. The main reason for this is that, when coupled with the so-called characteristic function (*CF*) approach, the solution found using this model can be expressed in closed form in the frequency domain even when complex chromatographic cases are considered [19–25].

The theoretical dynamic chromatography model, here developed, follows the general formalism proposed for the photon statistics model of single molecule observation [26–28]. Since in this last case the model solution is available in terms of *CF*, the model of dynamic chromatography will be obtained by coupling the reaction kinetics description with the stochastic model of two sites chromatography [22]. By this way, the representation of the chromatography profile will be available in the Fourier domain, as a function of the process parameters: this makes it possible to estimate the kinetic constants of reaction–elution processes by fitting the whole experimental chromatographic profile in the Fourier domain [20]. Thus, the methodological approach followed here differs from both the original theoretical plate model of chromatography [4,24], and its extensions based on the introduction of stochastic terms describing the peak band broadening [29–31].

In the present approach to on-column reaction chromatography, the classical reduction of the kinetic scheme from the four states to two states will be followed [16,32,33]. This will imply a certain

* Corresponding author. Tel.: +39 0532 455346; fax: +39 0532 240709.
E-mail address: l.pasti@unife.it (L. Pasti).

0021-9673/$ – see front matter © 2009 Elsevier B.V. All rights reserved.
doi:10.1016/j.chroma.2009.10.036

degree of approximation. Moreover, the focus will be essentially on the band broadening coming from the phase exchange kinetics and reaction, neglecting other significant aspects such as the mobile phase diffusion and eddy diffusion. The aim of this study is, in fact, to explore the potential advantages of using a stochastic description of dynamic chromatography.

2. Theory

The theory section of the present paper starts by recalling some basics of the stochastic model of chromatography and ends with a treatment of the chromatographic elution of molecules undergoing first order reaction. Description of the model follows the general formalism for a four-states kinetics system [4,16,33] and then this kinetics scheme is reduced to obtain a two-states system. Finally, the general expression for the chromatographic peak in reaction chromatography is derived together with particular solutions valid for given reaction kinetics in the separation time considered (reaction time scale). The obtained solution does not account for important chromatographic phenomena, such as mobile phase and eddy diffusion, responsible for peak broadening. Details of the mathematical description of the process are reported in the Appendixes A–D given in Supporting Information.

2.1. Dynamic microscopic description of the chromatographic process

In chromatographic separation, analyte molecules can be captured by the active surface sites and they can stay there for a random amount of time (τ_s); while they remain on the sites, the molecules are delayed vs. the main stream of the flowing mobile zone. After this time has elapsed they revert to the mobile phase until a new sorption event (n) occurs: the sojourn time undergoes to random jumps process. As a consequence, the analyte volume travels along the column at an average velocity, which is lower than that of the main stream. Moreover, the mobile phase volume occupied by the molecules is enlarged as a result of the random nature of the capturing and releasing processes (chromatographic band broadening).

The one site model of chromatography describes a chromatographic process involving solely a single kind of site (i.e. surface site homogeneity) (see Appendix A). In chiral chromatography at least two different active site types are present on the surface of the stationary phase and molecules could interact with both. The distribution of the time spent on each site is related to the molecule interaction energy on these two different sites. In chromatography literature the latter model is the so-called two sites model or biLangmuir model [5] and it is generally used to interpret enantiomeric separation. In enantiomeric chromatographic separation both enantiomers may be present in the mobile phase and they undergo different interactions with the two active stationary phase sites. In a simplified model, each enantiomer interacts selectively with just one site. If the two enantiomers can interconvert during the separation, then each molecule can be present in four different situations which correspond to the four states of the system (see Fig. 1a).

2.2. Model of first order dynamic chromatography

Let us consider an experimental interconversion batch involving enantiomers A and B partitioned between the M phase—a non-chiral homogenous phase and the S phase—the chiral phase (see Fig. 1a) The achiral and chiral phases are, respectively, the mobile and stationary phases in the chromatographic column corresponding to the batch system.

The considered system involves four different conformer types, which, in agreement with Refs. [4,29–31], are indicated as:

(1) A_M, lowest retained conformer in the mobile phase;
(2) B_M, highest retained conformer in the mobile phase;
(3) A_S, lowest retained conformer in the chiral stationary phase;
(4) B_S, highest retained conformer in the chiral stationary phase.

This model is a four-states system: at a given time t, a given molecule can be in one of the four above-described states. When the reaction rate constants are employed to describe the system, one should also consider the relationships existing between these constants. The principle of microscopic reversibility [4,29,34] states that, when a batch system is at equilibrium, the transition frequency is the same in both directions for each individual reaction step. Consequently, in any cyclic reaction the product of the rate constants going one way around the cycle is equal to the product of the kinetic constants describing the reverse reaction going the other way. With reference to Fig. 1 one has:

$$k_{-1}^{B} k_{-1}^{M} k_{1}^{A} k_{1}^{S} = k_{1}^{B} k_{1}^{M} k_{-1}^{A} k_{-1}^{S} \tag{1}$$

where k_1^j, and k_{-1}^j with $j = M, S$ are the forward and backward reaction rate constants in the mobile (M) and stationary (S) phase, respectively; k_1^j, and k_{-1}^j with $j = A, B$ are the sorption and desorption rate constants of the species A and B, respectively.

The main difference between a batch system like the one described above and the corresponding chromatographic system is that, in the latter, it is important to evaluate the time evolution of a single molecule and its statistical properties instead of the molecular averaged chemical composition of the batch system at a given time. The batch results can be applied to the dynamic chromatographic process thanks to the ergodic hypothesis which states the averages obtained from a large molecular population and over a long observation time are equivalent.

In a macroscopic chromatographic system, under linear conditions, the microscopic reversibility principle holds true [4,16,34]. Under the hypothesis that $k_{-1}^M = k_1^M$, Eqs. (1) and A-6b show that this condition is verified in a chromatographic separation of enantiomers using an achiral mobile phase (see Fig. 1a) and, after rearrangement (see Appendixes B and C), one obtains:

$$K^S = \frac{k_1^S}{k_{-1}^S} = \frac{K_B}{K_A} = \frac{k'_B}{k'_A} = \frac{\bar{\tau}_{S,A}}{\bar{\tau}_{S,B}} \tag{2}$$

where $\bar{\tau}_{S,A}$ and $\bar{\tau}_{S,B}$ are the average time spent during one species A or B sojourn step in the stationary phase (S). Likewise, k'_A and k'_B are the capacity factors of the pure enantiomer A or B, respectively (see Eq. A-6a). K_B and K_A are the stationary-to-mobile phase partition coefficients for species B and A, respectively, and $K^S = B_S/A_S$.

Eq. (2) is obtained under the hypothesis that the mean time spent in the mobile phase (see Eq. A-2) is constant for all species involved. Moreover, Eq. (2) shows that, in the stationary phase, the interconversion rate is inversely proportional to a molecule's mean residence time in the corresponding conformational state in the stationary phase:

$$k_1^S \propto \frac{1}{\bar{\tau}_{S,B}} \tag{3}$$

2.3. Reduction of the kinetic scheme

In a chromatographic experiment it is only possible to observe the history of the molecule inside the column as a whole—that is, the sum of the times spent in each of the four possible system states. The kinetic scheme can be simplified as a two states system: each

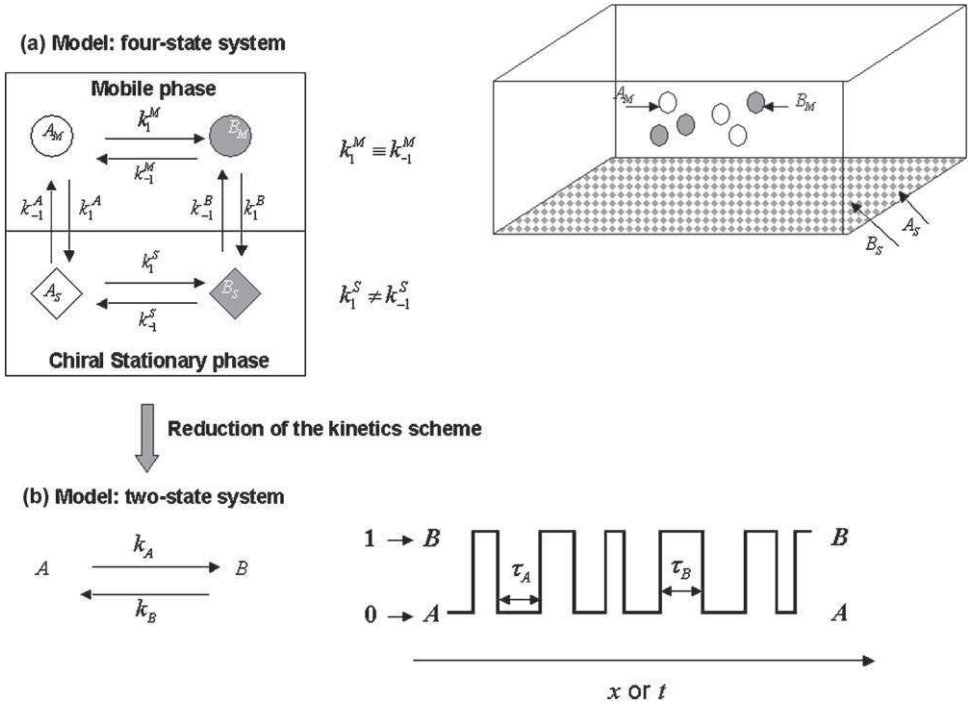

Fig. 1. (a) Kinetics scheme of a four-state system and (b) kinetics scheme of a two-state system.

containing, respectively, the mobile and stationary phase states of the enantiomers *A* and *B*:

$$\frac{dP_A}{dt} = k_B P_B - k_A P_A \tag{4a}$$

$$\frac{dP_B}{dt} = k_A P_A - k_B P_B \tag{4b}$$

where k_A and k_B are the two observed reaction rate constants and P_A and P_B are the molecular populations (i.e. the number of species) of the two states (enantiomers) *A* and *B* independently of their stay in the *M* or *S* phases (i.e. their sum).

The reduction of the four-state scheme to the two-state system in Fig. 1b can be achieved using different approaches, each implying different degrees of approximation [35–37]. Details of the approach adopted here are reported in Appendix C.

The apparent kinetic constants, already derived for a macroscopic system [31,38–40], in the case of the simplified two-states microscopic model are (see Appendix C):

$$k_B = \frac{(\bar{\tau}_{S,B} k_{-1}^S + \bar{\tau}_M k_{-1}^M)}{\bar{\tau}_M + \bar{\tau}_{S,B}} = \frac{1}{1+k'_B} k_{+1}^M + \frac{k'_B}{1+k'_B} k_{-1}^S \tag{5a}$$

$$k_A = \frac{(\bar{\tau}_{S,A} k_{-1}^S + \bar{\tau}_M k_{-1}^M)}{\bar{\tau}_M + \bar{\tau}_{S,A}} = \frac{1}{1+k'_A} k_1^M + \frac{k'_A}{1+k'_A} k_1^S \tag{5b}$$

Reaction dynamic chromatography experiments generally yield a peak cluster composed of two peaks of the unconverted enantiomers and a large central peak formed by the molecules involved in the interconversion reaction. Thus, it is conceptually useful to divide the chromatograms into two parts: one for the unconverted species, the other for the converted species.

2.4. Peak generated from reaction chromatography

In chromatographic experiments, retention times are the functions of numerous variables. Different instrumentation parameters such as flow velocity, column length, temperature can influence the eluted species peak profile as well as the contribution due to the chemical interaction between the analyzed species and both the stationary and mobile phases. In order to simplify the mathematical handling and unify the model description of these processes, changing the process time variable is convenient. Subsequently, a peak profile description for unreacted species is derived and finally a general expression for the profile of reacted species is obtained.

2.4.1. Change of the process variable

Let us define *x* as follows:

$$x = \frac{(t - t_{R,A})}{(t_{R,B} - t_{R,A})} = \frac{(t - t_{R,A})}{\Delta t_R} = \frac{(t' - t'_{R,A})}{(t'_{R,B} - t'_{R,A})} \tag{6}$$

where $t_{R,i}$ and $t'_{R,i}$ are the retention times and the corrected retention times, respectively referred to the species in the conformation state *i* with *i* = *A* or *B*.

The *x* variable represents the normalized time of the interconversion reaction within the limited interval of the chromatographic experiment, defined as the difference in retention times of the two pure enanatiomers, Δt_R, here referred as "observational time", in analogy with single molecule photon transition experiments [26] (see in the following). We can thus consider a molecule of enantiomer *A* (less retained enantiomer) which is eluted at $t_{R,A}$ as a molecule that never visited a type *B* site and thus never remained in molecular state *B*, in the stationary phase. Note that the mobile phase is, in fact, assumed achiral and thus it is not possible to detect any interconversion process occurring therein. Conversely, a molecule of enantiomer *B* (most retained enantiomer) which is eluted at $t_{R,B}$ is a molecule that never visited site *A* and thus was never in the state *A*, in the stationary phase. Consequently, we can associate a molecule eluting at $t_{R,A}$ with a zero probability of transition from *A* to *B*. In fact, by substituting $t = t_{R,A}$ in Eq. (6) one has $x = 0$. Likewise, a molecule of enantiomer *B*, which is eluted at $t_{R,B}$, has a zero probability of transition from *B* to *A*.

Thus *x* represents the fraction of the observational time Δt_R spent in the *B* state (in the stationary phase). It can be observed that *x* also represents the fraction of molecules which are in state *B* at any given time (i.e. $P_B/(P_A + P_B)$). One can thus set the two following

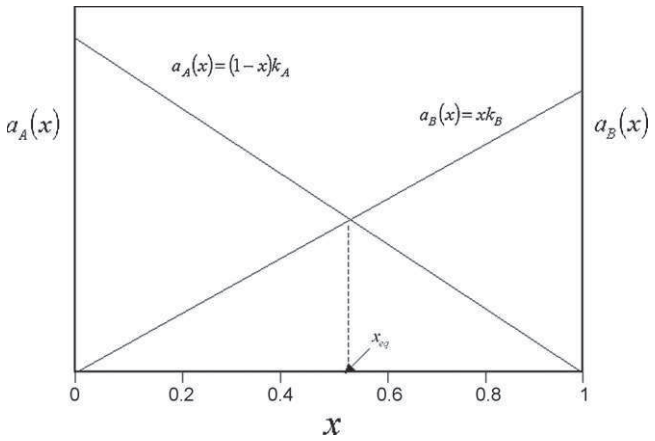

Fig. 2. Scheme of the propensity functions of the process.

expressions:

$$a_A(x) = (1-x)k_A \tag{7a}$$

$$a_B(x) = xk_B \tag{7b}$$

where $a_A(x)$ and $a_B(x)$ are the transition frequencies for the univariate processes $A \rightarrow B$ or $B \rightarrow A$, respectively. $a_A(x)$ and $a_B(x)$ are the so-called "propensity functions" characterizing, from a stochastic point of view, the reversible isomerisation reaction in Eq. (4a) as proposed by Gillespie [41] (see Appendix C). It is important to underline that the propensity functions here introduced do not include concentration of reacting species.

At the equilibrium (i.e. $x = x_{eq}$), the process becomes stationary and it has to satisfy the detailed balance condition [41]—that is, the frequency transitions are the same in each direction for every pair of states (see Fig. 2):

$$(1-x_{eq})k_A = x_{eq}k_B \tag{8a}$$

By rearranging Eq. (8a) one has:

$$x_{eq} = \frac{k_A}{k_A + k_B} \tag{8b}$$

which is the equilibrium condition of state B occupancy in the system.

The concentrations c_A and c_B can be obtained from the respective population P_A and P_B by dividing by the system volume. For $x = 1$ and $x = 0$ Eqs. (4a) and (4b) expressed in concentration units become:

$$\frac{dc_A}{dt} = -k_A c_A(t) \tag{9a}$$

$$\frac{dc_B}{dt} = -k_B c_B(t) \tag{9b}$$

The solution of the differential equations in the time domain are given, respectively, by

$$c_A(t_{R,A}) = c_A^0 \exp(-k_A t_{R,A}) \tag{10a}$$

$$c_B(t_{R,B}) = c_B^0 \exp(-k_B t_{R,B}) \tag{10b}$$

Eqs. (10a) and (10b), obtained in the framework of the kinetic microscopic description (see Appendixes B and C), correspond to those achieved by discontinuous equilibrium models based on the description of the chromatographic column as a sequence of theoretical plates [4,16]. However, a detailed comparison between the present approach and that presented in Refs. [29–31,38–40] would deserve a specific study, especially for that which concerns the introduced approximations, the limit conditions of the model and the applicability of limit solutions.

2.5. Case a: peaks generated from unconverted molecules

By combining Eqs. (10a) and (10b) with Eqs. A-6c, d and e, one obtains:

$$c_A(t_{R,A}) = c_A^0 \exp(-k_A t_{R,A}) = c_A^0 \exp(-k_1^S t'_{R,A} - k_{-1}^M t_M) \tag{11a}$$

$$c_B(t_{R,B}) = c_B^0 \exp(-k_B t_{R,B}) = c_B^0 \exp(-k_{-1}^S t'_{R,B} - k_1^M t_M) \tag{11b}$$

By assuming that the time spent in the mobile phase is constant for any eluted substance and that the forward and backward reaction rate constants in the mobile phase are equal (i.e. $k_{-1}^M = k_1^M$), it follows that:

$$\exp(-k_{-1}^M t_M) = \exp(-k_1^M t_M) = \text{const} \tag{11c}$$

The time spent in the mobile phase is constant for unreacting molecules. On the other hand, molecules involved in on-column reaction, are allowed to spend a variable amount of time in mobile phase (see Section 2.7 Eqs. (28a)–(28c)).

The above-defined quantities c_A and c_B are the concentration or number of species partitioned between the mobile and stationary phases in any given conformation (i.e. A or B, respectively). These molecules spent time only in one of the pairs of states related to a given conformation (i.e. A or B). In the stochastic description of chromatography, these molecules behave as though retained on a one-site chromatographic column since they only interact with one site of the stationary phase. This one-site model of chromatography (described in Appendix A) [19] can thus be applied to model the unconverted species and the functions describing the peak profile in frequency domain – scaled with respect to t_M – are:

$$\Phi(\omega)_{S,A}\big|_{unc} = c_A(t_{R,A}) \exp\left\{\bar{n}\left[\frac{1}{1 - i\omega\bar{\tau}_{S,A}} - 1\right]\right\} \tag{12a}$$

$$\Phi(\omega)_{S,B}\big|_{unc} = c_B(t_{R,B}) \exp\left\{\bar{n}\left[\frac{1}{1 - i\omega\bar{\tau}_{S,B}} - 1\right]\right\} \tag{12b}$$

$\Phi(\omega)_{S,A}\big|_{unc}$ and, $\Phi(\omega)_{S,B}\big|_{unc}$ are the *CFs* of the chromatographic process, over the sites A and B, respectively. Eqs. (12a) and (12b) do not account for any band broadening phenomena with the only exclusion of that coming from the randomness of the sorption–desorption process.

The chromatographic elution peaks for the unconverted species in the time domain can be obtained from the *CF* (Eqs. (12a) and (12b)) by a Fast Fourier Transform (*FFT*) algorithm as described elsewhere [19]. Alternatively, the parameters defining the peak (i.e. $\bar{n}$ and $\bar{\tau}_{S,A}$) can be estimated by fitting in the frequency domain [21]. The corresponding time domain solution is reported in Appendix A (see Eqs. A-5a and b).

2.6. Peaks generated from molecules that react during column migration

2.6.1. Case b: fast interconversion kinetic

Let us now consider molecules that react very fast vs. the separation process time scale. Such molecules can be present in both conformational states A and B in the stationary phase, and they interact with the corresponding sites of the stationary phase. During the time spent inside the column, those highly reacting molecules perform a high number of jumps (n) between the mobile and stationary phases and are in a stationary or equilibrium position, as above-described with reference to Eqs. (8a) and (8b). Consequently, by considering the equivalence between chromatographic site and molecular conformational state, the chromatographic process can be fully described by the two-sites stochastic model of chromatography [22].

At the equilibrium condition, the fraction of visits to B site is given by Eq. (8b). The corresponding two-sites chromatographic process can be described by:

$$\begin{cases} \Phi_S(\omega)\big|_{fast} = \exp\left[\bar{n}((1-x_{eq})\varphi_{S,A}(\omega) + x_{eq}\varphi_{S,B}(\omega)) - 1\right] \\ 1 - x_{eq} = \dfrac{k_B}{k} = 1 - p \\ x_{eq} = \dfrac{k_A}{k} = p \\ k = k_A + k_B \end{cases} \tag{13}$$

where $\varphi_{S,A}(\omega)$ and $\varphi_{S,B}(\omega)$ – given by Eqs. (12a) and (12b) with $c_A(t_{R,A}) = 1$ and $c_B(t_{R,B}) = 1$, respectively – are the *CFs* of the chromatographic process for a unit amount of species, over sites A and B, respectively (see Eq. (6b)). We observe that quantities x_{eq} and $1 - x_{eq}$ just correspond to the fraction of the two site types, p and $(1-p)$, in the two-sites stochastic model of chromatography [19,22].

Under the hypothesis that the number of jumps in the stationary phase is a Poissonian variable of average $\bar{n}$, in the case of a two-site model the probability density functions describing the number of jumps to sites A and B will have averages equal to $\bar{n}_A$ and $\bar{n}_B$, respectively. This hypothesis does not hold for slow reactions. In such cases, changes in the average number of jump of reacting species have to be accounted for (see Section 2.7). The retention time of the peak described by Eq. (13) can be expressed as:

$$t'_{R,eq} = \bar{n}\bar{\tau}_{S,eq} = \bar{n}\left(\frac{k_B}{k_A + k_B}\bar{\tau}_{S,A} + \frac{k_A}{k_A + k_B}\bar{\tau}_{S,B}\right) \tag{14a}$$

$t'_{R,eq}$ corresponds to the weighted retention time of a mixture of enantiomers, having weights equal to the equilibrium states population. The quantity $\bar{\tau}_{S,eq}$:

$$\bar{\tau}_{S,eq} = \left(\frac{k_B}{k_A + k_B}\bar{\tau}_{S,A} + \frac{k_A}{k_A + k_B}\bar{\tau}_{S,B}\right) \tag{14b}$$

is the corresponding "equilibrium" average sorption time of a single sorption step characteristic of the fast interchanging species.

Eq. (13) is the *CF* referred to a unit amount of species. The total amount of interconverting enantiomers c^* corresponds to the amount not eluted as pure enantiomers A or B at $t_{R,A}$ and $t_{R,B}$, respectively, and thus, from Eqs. (11a) and (11b), we get:

$$c^* = c_A^* + c_B^* = c_A^0(1 - \exp(-k_A^S t_{R,A})) + c_B^0(1 - \exp(-k_B^S t_{R,B})) \tag{15}$$

The searched solution of the peak profile in the Fourier domain, obtained from Eqs. (13) and (15) is

$$\Phi_S^*(\omega)\big|_{fast} = c^* \exp\left[\bar{n}((1-x_{eq})\varphi_{S,A}(\omega) + (x_{eq})\varphi_{S,B}(\omega)) - 1\right] \tag{16}$$

2.6.2. Case c: low interconversion kinetics

In the most general case, the reaction time scale can be similar to the separation time scale: each molecule spends part of the time in both conformations. Consequently, the average molecule migration velocity is expressed as a weighted sum of the migration velocity of the two pure enantiomers. The weights are related to the fraction of time spent in each of the two states. To determine the latter quantities, a two-states jump model is employed. Such a two-states jump process is characterized by a single relaxation rate constant $k = k_A + k_B$, and by $p = k_A/k$, the probability of finding the molecule in state B which is equal to x_{eq} (see Eq. (8)).

The concept of the "random trajectory" of a single molecule $\xi(t)$ (see Fig. 1b) constitutes the starting point for calculating the fraction of average time spent in each state. $\xi(t)$ is the stochastic occupation variable which is set to 0 when the molecule is in state A, and 1 when the molecule is in state B. The time spent in the state A or B is assumed to be exponentially distributed (corresponding to a first order kinetics). Consequently, the number of jumps between the two states follows Poisson statistics (see Eq. A-1, with $\mu = 1/k$). For a given trajectory lasting t, the time spent in state B is the integral of $\xi(t)$ over t. Consequently, the previously introduced quantity x (see Eq. (6)) can now be expressed as:

$$x = \frac{(t - t_{R,A})}{(t_{R,B} - t_{R,A})} = \frac{1}{\Delta t_R}\int_{t_{R_A}}^{t_{R_B}} \xi(t)dt = \frac{1}{T}\int_{t_{R_A}}^{t_{R_B}} \xi(t)dt \tag{17}$$

where $\Delta t_R = t_{R,B} - t_{R,A} \equiv T$ – sake of notation simplicity equal to T – and x is the fractional time spent in the state B and it is now a stochastic variable and is characterized by its distribution, since the "histories" of a molecule, $\xi(t)$, giving a value equal to $(t - t_{R,A})$ as the integral in Eq. (17), can be more or less probable.

The probability density associated with x and notated as $P(x|T)$ can be obtained as a sum of two contributions:

$$P(x|T) = ap(x|T, A) + bp(x|T, B) \tag{18}$$

where $p(x|T,A)$ and $p(x|T,B)$ are a molecule's probability density of spending xT time in state B for molecules initially in the states A and B, respectively ($x = 0$, with $t = t_{R_A}$, see Eq. (6)); a and b are the fractional populations of the states A and B at the initial condition ($a + b = 1$).

The solution of the problem (see Appendix D) can be obtained by following the method known as the Kubo and Anderson formalism [42,43], extensively employed in developing the line shape theory of interconverting chromophores [26–28,44,45]. The two-states enantiomeric interconversion and two-states dynamics processes of a chromophore molecule under stationary conditions [46] are, in fact, closely related from the stochastic–kinetic point of view because: (i) they follow the same first order kinetic scheme (see Figs. 1 and 2); (ii) they can be represented stochastically through two-states single molecule random trajectories (Eq. (17)); (iii) the statistics of these random trajectories are the same; and (iv) the probability density of trajectories at xT can be obtained as a sum of two contributions (Eq. (18)). As mentioned above in Section 2.2, the present approach can be applied to describe a macroscopic system composed of a large number of molecules or observed for a long period of time vs. the reaction time scale.

By applying the Fourier–Stiltjes transform to Eq. (18) one obtains:

$$\hat{P}(x|T) = a\hat{p}(x|T, A) + b\hat{p}(x|T, B) \tag{19}$$

where $\hat{P}(x|T)$, $\hat{p}(x|T, A)$ and $\hat{p}(x|T, B)$ are the *CFs* of $P(x|T)$, $p(x|T,A)$ and $p(x|T,B)$, respectively. $\hat{p}(x|T, A)$ and $\hat{p}(x|T, B)$ were solved in Ref. [47] (see Appendix D):

$$\hat{p}(\omega|T, A) == \exp\left(-\frac{kT - i\omega T}{2}\right)\left(\phi\cosh\frac{\phi T}{2} + (k + i\omega)\sinh\frac{\phi T}{2}\right)/\phi \tag{20a}$$

$$\hat{p}(\omega|T, B) = \exp\left(-\frac{kT - i\omega t}{2}\right)\left(\phi\cosh\frac{\phi T}{2} + (k - i\omega)\sinh\frac{\phi t}{2}\right)/\phi \tag{20b}$$

where

$$\phi = \sqrt{\left(\left(\frac{k}{2}\right)^2 - i\left(p - \frac{1}{2}\right)k\omega - \left(\frac{\omega}{2}\right)^2\right)} \tag{20c}$$

$\omega = 2\pi/T$ is the frequency. $t = T + t_{R,A}$ since the time windows in the considered chromatographic experiment is, as specified in Appendix D, $t_{R_A} \div t_{R_A} + T$.

By considering Eq. (19) and given the linearity properties of the Fourier transform, by combining Eqs. (20a) and (20b) one obtains:

$$\hat{P}(x|T) = \exp\left(-\frac{kt - i\omega t}{2}\right) \times \left(\cosh\frac{\phi t}{2} + \frac{(k - i(p - (1/2))\omega)}{\phi}\sinh\frac{\phi t}{2}\right) \quad (21)$$

i.e. the *CF* total probability of being in the *B* state.

Eq. (21) was originally derived by Reilly and Skinner [47] to interpret chromophore transition of a two-level system. The probability density *CF* associated to *x* due solely to interconversion can be obtained from Eq. (21) by applying the following relationship:

$$\Phi_2(\omega|T) = \hat{P}(\omega|T) - \Phi_A^*(\omega) - \Phi_B^*(\omega) \quad (22)$$

where $\Phi_A^*(\omega)$ and $\Phi_B^*(\omega)$ are the *CFs* of the probability density functions of the fraction of unconverted molecules in *A* and *B*, respectively. The unconverted quantities in concentration units were discussed in paragraph 2.5 (Eqs. (12a) and (12b)). Thus the pertinent expressions – as fractional units and starting from equilibrium conditions in Fourier domain [48] – are:

$$\Phi_A(\omega) = (1 - p)\exp(-pkt) \quad (23a)$$

$$\Phi_B(\omega) = p\exp(-(1 - p)kt)\exp(-i\omega) \quad (23b)$$

Starting from Eq. (22), other useful relationships can be obtained, in particular:

2.6.3. Limit solutions

If $kt \gg 1$, which corresponds to moderately fast kinetics, Eq. (21) becomes:

$$\hat{P}(\omega|T) = \exp(i\omega pt)\exp\left(-\frac{p(1-p)}{kt}\omega^2\right) \quad (24)$$

which is the *CF* of a Gaussian function [47] having a mean equal to *p* and variance σ:

$$\sigma = \frac{2p(1-p)}{kt} \quad (25)$$

The limit for $kt \to \infty$, i.e. for very fast interconversion kinetics (see Section 2.6.1) one has:

$$\hat{p}(\omega|T) = p \quad (26a)$$

$$P(x|T) = \delta(x - p) \quad (26b)$$

Eq. (26a) is, in fact, the *CF* of a Dirac function (Eq. (26b)). The probability density $P(x|T)$ thus consists of a single spike located at $x = p$. In this case all the molecules rapidly interconvert vs. the separation time scale and the result here obtained confirms what was previously found in Section 2.6.1. The main difference between Eq. (26a) and Eq. (16) is that Eq. (26a) does not take into account the chromatographic band broadening contribution that will be considered later on.

The limit of Eq. (21) for $kt \to 0$ is [47]:

$$P(x|T) = (1 - p)\delta(x) + p\delta(1 - x) \quad (27)$$

Eq. (27) represents two spikes positioned at the extremes of the *x* domain and having abundances equal to the thermodynamic limit $(1 - p)$ and *p*, respectively. These functions correspond to the spikes of the non-reacting molecules handled in Section 2.5 and again do not include the contribution of the chromatographic sorption/desorption process.

2.7. From the probability distribution to the chromatographic peaks

The discussion developed in the previous paragraph (i.e. 2.6) was mainly concerned with the derivation of the *B* state population at a given time *xT*, resulting from the isomerisation reaction: $A_{M+S} \Leftrightarrow B_{M+S}$ (see Fig. 1b) under stationary conditions. The chromatographic process superimposes the reaction as a process of exchange between the mobile and stationary phases – $A_M \Leftrightarrow A_S$ and $B_M \Leftrightarrow B_S$ – and it contributes to broadening the elution band both because of the random nature of the stay of site *A* or *B* in the stationary phase and the random character of the interval between two subsequent adsorption processes from the mobile phase (see Section 2.2). Other band broadening processes, that can be significant and/or prevailing in chromatographic experiments [5], will be not handled in the present work. For each *x* (or *xT*) value, the number of jumps between the two states $n(x)$ is a Poisson variable (see Eq. A-1) which, when combined with the distribution of time spent in one state, gives the peak shape function in either the time domain, as developed by Giddings [18], Kramer [24] and Cremer [25], or in frequency domain (see Appendix A). This was essentially the result for fast reaction chromatography, when the equilibrium approximation $x = x_{eq}$ was adopted. Now, the approach must be extended to account for the distribution of *x* values (see Eq. (21)). The stochastic theory of dynamical chromatography includes this second stochastic variability thus far developed. The band broadening process in the interval $t_{R,B} \le t \le t_{R,B}$, i.e. in $0 \le x \le 1$ (see Eq. (6)) will be applied by rescaling this interval as number of jump units ($n(x)$). The chosen unit, as will be showed in the following, will be equal to $\bar{\tau}_{S,eq}$ since for it the chromatographic band broadening function is accessible in the Fourier domain (see Eq. (13) with $\bar{n} = 1$).

The fundamental quantity *x* defined in Eq. (17) can be redefined (see Eq. A-6d) as follows:

$$x = \frac{n(x)\bar{\tau}_{S.eq} - \bar{n}\bar{\tau}_{S,A}}{\bar{n}(\bar{\tau}_{S,B} - \bar{\tau}_{S,A})} \quad (28a)$$

$$t \equiv n(x)\bar{\tau}_{S,eq} \quad (28b)$$

In Eq. (28a), one can see that for $x = x_{eq}$ one has $n(x_{eq}) = \bar{n}$. By rearranging Eq. (28a) one obtains:

$$n(x) = \bar{n}\frac{(x(\bar{\tau}_{S,B} - \bar{\tau}_{S,A}) + \bar{\tau}_{S,A})}{\bar{\tau}_{S,eq}} \quad (28c)$$

According to this equation, $n(x)$ is rescaled with respect to *x* and, since in Eq. (28c) the averages terms ($\bar{\tau}_i$ and $\bar{n}$) are constants, $P(x)$ (or its *CF* $\hat{P}(x)$) can be directly transformed to a probability distribution of $n(x)$ (i.e. $P[n(x)]$) [48,49]. Note also that, according to Eq. (28c), $n(x)$ is a continuous variable like *x* or *t*.

The retention profile for each *t* value is generated by the corresponding number of jumps, and the sorption time value given by $\bar{\tau}_{S,eq}$ is assumed to be common (see Eq. (14b)). The above assumption can be qualitatively explained by considering that the change in probably of state occupation due to system reaction can be viewed as a change in the number of jumps or, equivalently, in the corresponding change in permanence time, following the same approach proposed in the stochastic description of chemical kinetics processes [45]. In fact, in the chromatographic two-sites model (see paragraph 2.1), on one side the sorption time distributions do not change in time since the site adsorption properties are considered constant. Moreover, the number of type *A* and *B* sites in the stationary phase is also constant. Instead, the number of molecules which can specifically interact with sites *A* or *B* (see Fig. 1) evolves during the course of separation due to the interconversion reaction: the jump number is accordingly modulated (Eq. (28c)).

The assumed hypothesis that expresses the *t* quantity as the product of two sole random quantities, *n* and $\bar{\tau}_{S,eq}$, allows us to

obtain a solution for the coupled interconversion-phase exchange processes of dynamical chromatography by applying the mathematical formalism employed in handling the so-called stochastic dispersive model of chromatography [19]. In fact, in both cases, the band broadening due to reaction or to inhomogeneous flow velocity is translated into a probability distribution for the jump number. The jump process acts as a process that directs the sorption process.

The presented approach can be applied only to systems containing a large number of molecules. In terms of *CF*, the solution is expressed as follows:

$$\varphi_{tot}(\omega) = \varphi_{dis}\left(\frac{\log(\varphi_u(\omega))}{i}\right) \tag{29}$$

where φ_u is the *CF* of the chromatographic retention process referred to either to $\bar{n}$ or t_M unit values and φ_{dis} is the *CF* of the probability dispersion function of either $n(x)$ or $t_M(x)$ (equal to $= n(x)\bar{\tau}_M$, see Eq. (28b)).

In the present case, by assuming the initial condition corresponding to condition of equilibrium, under conditions of $n = 1$, Eq. (13) becomes:

$$\varphi_u(\omega) = \exp\left(\frac{1}{(k_A + k_B)}\left(\frac{k_B}{(1 - i\omega\bar{\tau}_{S,A})} + \frac{k_A}{(1 - i\omega\bar{\tau}_{S,B})} - (k_A + k_B)\right)\right) \tag{30}$$

The *CF* of the directing process (i.e. $\varphi_{dis}(\omega)$ in Eq. (29)) is obtained from Eq. (21) and by performing the variable change from x to $n(x)$ [46] one obtains:

$$\varphi_{dis}(\omega) = \hat{P}(x|T)\frac{p}{\bar{n}} = \exp\left(-\frac{kt - i\omega t}{2}\right)\left(\cosh\frac{\phi t}{2} + \frac{(k - i(p - (1/2))\omega)}{\phi}\sinh\frac{\phi t}{2}\right)\frac{p}{\bar{n}} \tag{31}$$

The final expression is obtained from the combinations of Eqs. (28)–(31). In particular the argument of φ_{dis} in Eq. (29) should be $\log(\varphi_u(\omega)/i)$.

The previously described coupling of the chromatographic band broadening process with the reaction process was based on the assumption that the unitary band broadening contribution was constant within the domain $t_{R,B} \le t \le t_{R,B}$, The consequent approximation degree is here estimated as follows: peak variance and the number of theoretical plates in standard stochastic theory of chromatography (e.g. Eq. (12a) or (12b)) [17,5] are given by

$$\sigma^2 = 2n\bar{\tau}_S \tag{32a}$$

$$N = \left(\frac{t_R}{\sigma}\right)^2 = 2n \tag{32b}$$

In the present case from Eq. (28c) one obtains , for x equal to 0, x_{eq} and 1, $n(0) = \bar{n} \times (\bar{\tau}_{S,A}/\bar{\tau}_{S,eq})$, $n(x_{eq}) = \bar{n}$ and $n(1) = \bar{n} \times (\bar{\tau}_{S,B}/\bar{\tau}_{S,eq})$, respectively. Consequently since $\bar{\tau} \cong \bar{\tau}_{S,eq}$, one has, by using Eq. (32a), $\sigma^2(0) = 2\bar{n}\bar{\tau}_{S,A}\bar{\tau}_{S,eq}$, $\sigma^2(x_{eq}) = 2\bar{n}\bar{\tau}^2_{S,eq}$ and $\sigma^2(1) = 2\bar{n}\bar{\tau}_{S,B}\bar{\tau}_{S,eq}$. By considering Eqs. (12a) and (12b), (13), (14b), and (32a)), the exact values should be $\sigma^2(0) = 2\bar{n}\bar{\tau}^2_{s,A}$, $\sigma^2(x_{eq}) = 2\bar{n}\bar{\tau}^2_{s,eq}$ and $\sigma^2(1) = 2\bar{n}\bar{\tau}^2_{s,B}$. Consequently one see that chromatographic band broadening calculated by using Eq. (29) is exact in the case of $x = x_{eq}$, and overestimated and underestimated in the domains $0 \le x < x_{eq}$ and $x_{eq} < x \le 1$, respectively. However one should remember that, beside the chromatographic band broadening there is, in addition, the contribution due to the reaction (see e.g. Eq. (25) in the case of fast kinetics) and they are additive in variance. In most cases the variance contribution due to reaction the most important one (see Section 4). Consequently the bias should be of minor relevance Alternatively, the whole process can be split into its two components labelled *A* and *B* (see Eqs. (19)–(21)) and the solution is then given as a sum of the respective contributions, i.e.:

$$\varphi_{tot}(\omega) = \varphi_{tot,A}(\omega) + \varphi_{tot,B}(\omega) \tag{33}$$

where the argument of $\varphi_{tot,A}$ and $\varphi_{tot,B}$ (see Eqs. (21) and (22) and D-9 a and b, respectively) are $\log(\varphi_{S,A}(\omega)/i)$ and $\log(\varphi_{S,B}(\omega)/i)$ with $\varphi_{S,A}(\omega)$ and $\varphi_{S,B}(\omega)$ given by Eqs. (12a) and (12b) when $c_A(t_{R,A})$ $c_B(t_{R,B})$ are both equal to one. The importance of Eq. (33) is that it represents the correct expression for the peak shape in Fourier domain. Its meaning will be thoroughly described in the discussion. The advantage of employing Eq. (33), expressed as separate components, instead of Eq. (31) is that it allows one to consider cases where the initial concentrations of the two reacting species differ from one another (i.e. on-column reaction chromatography).

Finally, the general solution is obtained by multiplying Eq. (31) by the total amount of the interconverting enantiomers c^* (see Eq. (15)).

3. Computation

Computations were done by using Mathematica version 4.1 or Matlab version 5.0 routines. The numerical FFT inversion procure was described elsewhere [17].

4. Results and discussion

Eqs. (12a) and (12b) represent the chromatographic peak profile in Fourier domain of the pure enantiomers *A* and *B*, and Eqs. (33) the corresponding peaks due to first order reaction chromatography. By summing the contributions due to only one enantiomer *A* (or *B*) it is thus possible to obtain the equations describing the chromatographic response of a single species. The peak profile in the time domain can be obtained as numerical inversion of the abovementioned equations. This set of equations (i.e. Eqs. (12a) and (12b) and (33)Eqs. (12) and (33)) represent thus a solution of the on-column reaction chromatography model, however, they appear mathematically cumbersome to be applied to experimental chromatograms. For this reason several approximate or limit solutions were in addition obtained. In particular, a simplified solution that describes the effect of fast or moderately fast kinetics (i.e. $kt \gg 1$, see Eq. (24)) under linear elution condition, can be approximated by a Gaussian-like central peak. With respect to the previously reported handlings, the present stochastic approach was able to obtain general and specific solutions in closed form under frequency domain, fully describing the dynamical chromatography (Eqs. (29) and (33)). In the following basic features of dynamical chromatography and its dependence on interconversion kinetics and operative variables such as column length are exploited. The retention time data and column efficiency values of the selected examples were chosen in order to mimic real cases.

In Fig. 3 the time domain solution for the peak profile of two separated reacting species is plotted. Each profile represents the chromatographic peak corresponding to the elution of an injected solution containing only one component which reacts during the chromatographic run. They were obtained by numerical inversion of the function generated by summing the chromatographic peak profile in the Fourier domain for the pure enantiomers *A* and *B* (Eqs. (12a) and (12b)) with the corresponding peaks resulting from first order reaction chromatography (Eqs. (20a) and (20b)), i.e. the description of reaction chromatography, where only one of the species is present at the beginning of the separation process. One can see that the first enantiomer A appears as a peak at $t_R \cong 23$ min (which is product obtained by multiplying n(=9045) by the sum of $\bar{\tau}_M + \bar{\tau}_A$, according to Eqs. (7a) and (7b)Eq. (7e)). A decaying tail,

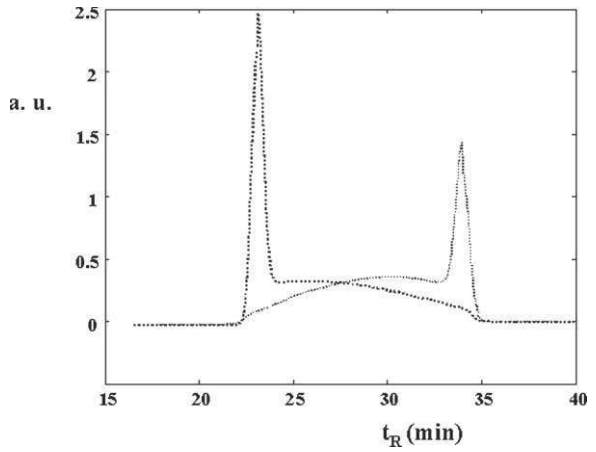

Fig. 3. Simulated peak: (a) $n = 9045$, $\tau_{S,A} = 0.1331$ s, $\tau_{S,B} = 0.2032$ s, $k_A = 0.0252\ \text{min}^{-1}$, $T = 33.66$ min; (b) $k_B = 0.0222\ \text{min}^{-1}$ (all other parameters have been kept constant and equal to (a)).

corresponding to the transformation, follows this peak $A \rightarrow B$. In the same figure, the B peak appears with an increasing front followed by the peak located at t_B (≅34 min). The reported example refers to a slow interconverting enantiomeric mixture ($k_A = 0.0252\ \text{min}^{-1}$, $k_B = 0.0222\ \text{min}^{-1}$). If the injected solution contains both the species A and B, the resulting peak profile can be obtained by summing the contribution of each.

In dynamic chromatography experiments the observation time T plays a key role in determining the shape of the resulting chromatographic peak for a given reactive substance. In fact, the quantity kT characterizes the reaction kinetic time scale (k, see Eq. (13)) vs. separation time scale (T). Fig. 4 provides an example of simulated chromatograms corresponding to increasing k values from a to f while keeping T constant. In this series of chromatograms, the retention time for the pure enantiomers is kept constant by fixing the values of $T\ (=t_{R,B} - t_{R,A})$, $\bar{n}$, $\bar{\tau}_B$ and $\bar{\tau}_A$ for all simulations. In Fig. 4a no interconversion takes place (see paragraph 2.5); in Fig. 4b–d interconversion rates are steadily increasing and all the components due to pure enantiomers and reacting species are present. Finally, in Fig. 4e and f, only one central peak is present. These last two cases correspond to the moderately fast kinetics discussed in Section 2.6.3. By comparing the peak shapes seen in Fig. 4e and f, one can see that peak width decreases as kinetics constant values increase and this is in agreement with what has been predicted from theory.

Increasing the observation time of moderately fast reactions should lead to a decrease in peak variance; this follows from the inverse proportionality relationship between kinetics constant and observation time. In chromatographic practice, a species' residence time in a column is related to column length or mobile phase velocity, two related variables (see Appendix A). Fig. 5 reports simulated chromatographic peaks obtained for different separation times, thus providing an example of the influence of this feature. It can be observed that peak band broadening increases with time. Two factors have to be considered in evaluating the band broadening in reaction chromatography, namely: (1) chromatographic (i.e. sorption/desorption) band broadening and (2) the global process separation time. From stochastic theory of chromatography one knows that peak variance for a one-site column is given by Eq. (32a). Therefore band broadening increases with n. Figs. 4 and 5a reports the peak corresponding at the highest n value. In this case, the calculated chromatographic band broadening was found to be $\sigma^2 = 0.188\ \text{min}^2$ (for $n = 10{,}000$, tau = $0.1838\ \text{s}^{-1}$), a small value when compared to the total peak variance $\sigma^2 = 2.25\ \text{min}^2$. It follows

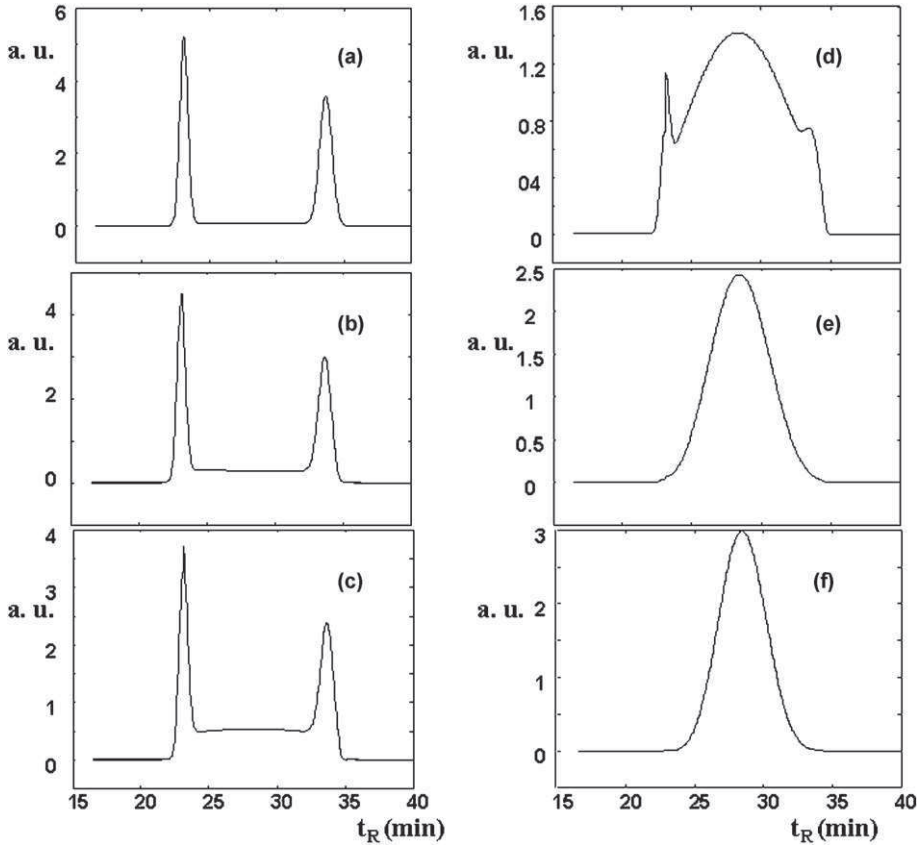

Fig. 4. Simulated chromatograms. Effect of increasing k value: $n = 9045$, $\tau_{S,A} = 0.1331$ s, $\tau_{S,B} = 0.2032$ s, $p = 0.53$ (a) $kT = 0.16$, (b) $kT = 0.8$, (c) $kT = 1.6$, (d) $kT = 8$, (e) $kT = 16$, and (f) $kT = 24$.

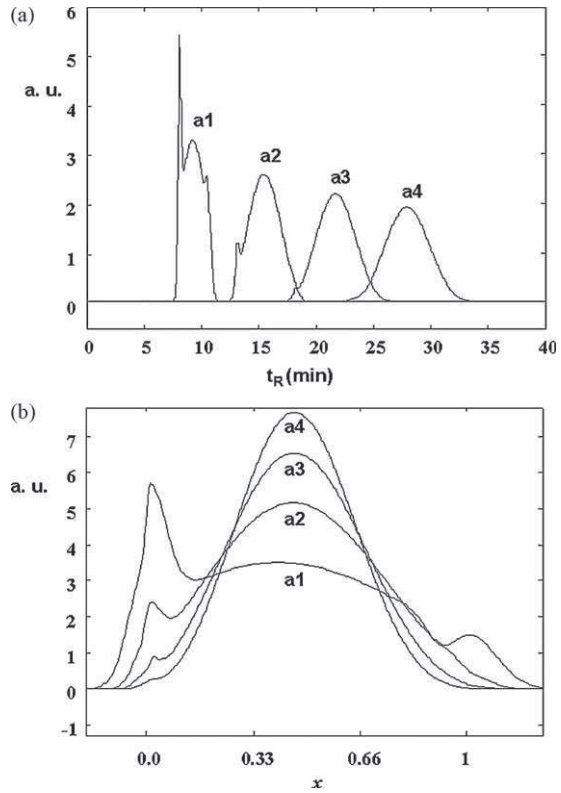

Fig. 5. a) Simulated chromatograms. Effect of increasing process time: $\tau_{S,A}$ = 0.1204 s, $\tau_{S,B}$ = 0.1838 s, p = 0.47, k = 0.474 min^{-1}, (a1) $\bar{n} = 2500$ (solid line), (a2) $\bar{n} = 5000$ (dashed line), (a3) $\bar{n} = 7500$ (dotted line) and (a4) $\bar{n} = 10000$ (dash-dot line). (b) Simulated chromatograms of (a) scaled by the process time.

that, for the reported cases, kinetics makes the main contribution to peak width. In fact, by plotting the simulated chromatograms in the normalized x-axis (see Eq. (6).) one obtains Fig. 5b.

The simulated chromatograms do not account for axial and eddy diffusion contributions to the overall to peak band broadening which, in experimental chromatograms, can be relevant. When the above-mentioned additional band broadening contributions are negligible, the proposed procedure makes it possible to obtain the kinetic parameters by non-linear fitting of the acquired chromatogram. This procedure has to be applied in the Fourier domain where the solution is available in closed form. The topic lies beyond the aim of the present study since it requires a specific extended numerical handling. Nonetheless some simple computations in order to allows one to obtain preliminary kinetic data is selected cases is presented in the following.

For moderately fast reactions vs. elution time scale, once the retention times of the two pure enantiomers are available, it is possible to obtain an approximated value of the kinetic constant (see paragraph 2.6.3). Experimental chromatograms satisfying such requirements have been already reported in the literature [50,51]. In such cases the following procedure can be applied:

(a) Normalization of the retention times:

$$x_A = \frac{t_{R,eq} - t_{R,A}}{T} = \frac{(\bar{\tau}_{S,eq} - \bar{\tau}_{S,A})}{\bar{\tau}_{S,B} - \bar{\tau}_{S,A}} \tag{34a}$$

$$x_B = 1 - x_A = \frac{t_{R,B} - t_{R,eq}}{T} = \frac{(\bar{\tau}_{S,B} - \bar{\tau}_{S,eq})}{\bar{\tau}_{S,B} - \bar{\tau}_{S,A}} \tag{34b}$$

where $t_{R,eq}$ is the retention time of the Gaussian peak of the two interconverted species.

Form Eq. (13) one has:

$$x_A = 1 - p = \frac{k_B}{k} \tag{35a}$$

$$x_B = p = \frac{k_A}{k} \tag{35b}$$

(b) Evaluation of normalized standard deviation.

When limit condition 2.6.3 is applicable and the band broadening of the reaction is the most important contribution to the peak variance, after subtraction of the chromatographic band brading contribution (see Eq. (32a)) from the peak variance one has:

$$\sigma(x) = \frac{2p(1-p)}{kt} = 2\frac{x_A x_B}{kt} \tag{36}$$

By substituting Eqs. (35a) and (35b) in Eq. (36) one has:

$$k_A = \frac{2x_A x_B^2}{\sigma(x)t} \tag{37a}$$

$$k_B = \frac{2x_A^2 x_B}{\sigma(x)t} \tag{37b}$$

The outlined theoretical model can be thus the basis for setting up and validating a numerical procedure based on least square fitting in the Fourier domain for determining the kinetic constants of the reaction.

5. Conclusions

To summarize, the developed model allows for both general and specific solutions in frequency domain, fully describing the dynamic chromatography process. The general equation can be simplified in the limit cases: (a) for slow reaction rate (compared to the adsorption kinetics) the chromatographic response is a sum of two separated peaks; (b) very fast reaction rates generate just one peak having a retention related to the kinetic constants of the reaction (p); (c) for intermediate rates, a peak cluster is generated. The model was able to describe both interconversion and reaction during separation. Some basic features of the process – such as interconversion kinetics constants – and/or operative variables – such as column length (or flow velocity) – and their influence on the chromatographic output have been exploited.

Acknowledgments

This work has been supported by the Italian University and Scientific Research Ministry (CHEM-PROFARMA-NET, RBPR05NWWC_008) and by PRRIITT (ER) misura 4 azione 2.

Appendix A. Supplementary data

Supplementary data associated with this article can be found, in the online version, at doi:10.1016/j.chroma.2009.10.036.

References

[1] D. Do Duong, Adsorption Analysis: Equilibria and Kinetics, Imperial College Press, 1998.
[2] I.M. Richard, Principles of Adsorption and Reaction on Solid Surfaces, Wiley–IEEE, 1996.
[3] O. Trapp, G. Schoetz, V. Schurig, Chirality 13 (2001) 403.
[4] W. Bürkle, H. Karfunkel, V. Schurig, J. Chromatogr. 288 (1984) 1.
[5] G. Guiochon, A. Felinger, A.M. Katti, D. Shirazi, Fundamentals of Preparative and Nonlinear Chromatography, 2nd ed., Elsevier, The Netherlands, 2006.
[6] R. Thede, Encyclopedia of Chromatography: Rate Constants: Determination from On-Column Chemical Reactions, 2nd ed., Taylor & Francis, 2006.
[7] C. Wolf, Dynamic Stereochemistry of Chiral Compounds—Principles and Applications, RSC Publishing, Cambridge, 2008.
[8] C. Wolf, Chem. Soc. Rev. 34 (2005) 595.

[9] O. Trapp, S.K. Weber, S. Bauch, W. Hofstadt, Angew. Chem. Int. Ed. 46 (2007) 7307.
[10] O. Trapp, J. Chromatogr. A 1184 (2008) 160.
[11] O. Trapp, S.K. Weber, S. Bauch, T. Baecker, W. Hofstadt, B. Spliethoff, Chem. Eur. J. 14 (2008) 4657.
[12] O. Trapp, Chem. Today 26 (2008) 26.
[13] J. Krupcik, P. Oswald, P. Màjek, P. Sandra, D.W. Armstrong, J. Chromatogr. A 1000 (2003) 779.
[14] B. Lina, F. Songa, G. Guiochon, J. Chromatogr. A 1003 (2003) 91.
[15] J. Veciana, M.I. Crespo, Angew. Chem. Int. Ed. 30 (1991) 74.
[16] O. Trapp, V. Schurig, Comput. Chem. 25 (2001) 187.
[17] N.G. Van Kampen, Stochastic Processes in Physics and Chemistry, North Holland, Amsterdam, 1981.
[18] R.A. Keller, J.C. Giddings, J. Chromatogr. 3 (1960) 205.
[19] L. Pasti, A. Cavazzini, A. Felinger, M. Martin, F. Dondi, Anal. Chem. 77 (2005) 2524.
[20] A. Felinger, L. Pasti, F. Dondi, M. van Hulst, P.J. Schoenmakers, M. Martin, Anal. Chem. 77 (2005) 3138.
[21] A. Felinger, A. Cavazzini, M. Remelli, F. Dondi, Anal. Chem. 71 (1999) 4472.
[22] A. Cavazzini, M. Remelli, F. Dondi, A. Felinger, Anal. Chem. 71 (1999) 3453.
[23] F. Dondi, A. Cavazzini, L. Pasti, J. Chromatogr. A 1126 (2006) 257.
[24] R. Kramer, J. Chromatogr. 107 (1975) 241.
[25] E. Cremer, R. Kramer, J. Chromatogr. 107 (1975) 253.
[26] A.M. Berezhkovskii, A. Szabo, G.H. Weiss, J. Chem. Phys. 110 (1999) 9145.
[27] I. Gopich, A. Szabo, J. Chem. Phys. 122 (2005) 014707.
[28] E. Barkai, Y. Jung, R.J. Silbey, Phys. Rev. Lett. 87 (2001) 207403.
[29] O. Trapp, V. Schurig, J. Chromatogr. A 911 (2001) 167.
[30] O. Trapp, V. Schurig, Chirality 14 (2002) 465.
[31] O. Trapp, Anal. Chem. 78 (2006) 189.
[32] K. Cabrera, M. Jung, M. Fluck, V. Schurig, J. Chromatogr. A 731 (1996) 315.
[33] M. Jung, V. Schurig, J. Am. Chem. Soc. 114 (1992) 529.
[34] R.C. Tolman, Proc. N.A.S. 11 (1925) 436.
[35] M. Scappin, P. Canu, Chem. Eng. Sci. 56 (2001) 5157.
[36] G. Zumofen, J. Klafter, Chem. Phys. Lett. 219 (1994) 303.
[37] J. Cao, Chem. Phys. Lett. 327 (2000) 38.
[38] O. Trapp, Electrophoresis 27 (2006) 2999.
[39] O. Trapp, Electrophoresis 27 (2006) 534.
[40] O. Trapp, Chirality 18 (2006) 489.
[41] D.T. Gillespie, J. Chem. Phys. 113 (2000) 297.
[42] R. Kubo, J. Phys. Soc. Jpn. 9 (1954) 935.
[43] P.W. Anderson, J. Phys. Soc. Jpn. 9 (1954) 316.
[44] M. Boguñá, J. Masoliver, G.H. Weiss, Physica A 289 (2001) 307.
[45] I. Gopich, A. Szabo, J. Chem. Phys. 124 (2006) 154712.
[46] Y. Jung, E. Barkai, R.J. Silbey, Chem. Phys. 284 (2002) 181.
[47] P.D. Reilly, J.L. Skinner, J. Chem. Phys. 101 (2) (1994) 959.
[48] R.N. Bracewell, The Fourier Transform and Its Applications, 2nd ed., McGraw-Hill, NY, 1978.
[49] W.C. Hamilton, Statistics in Physical Science Estimation, Hypothesis Testing, and Least Squares, The Ronal Press Company, NY, USA, 1964.
[50] D.H. Hochmuth, W.A. Konig, Lieb. Ann. 6 (1996) 947.
[51] R. Cirilli, R. Costi, R. Di Santo, F. La Torre, M. Pierini, G. Siani, Anal. Chem. 81 (2009) 3560.

Supporting Information

Dynamic Chromatography: a stochastic approach.

Luisa Pasti*, Alberto Cavazzini, Marianna Nassi, Francesco Dondi

Department of Chemistry, University of Ferrara, Via L. Borsari, 46, I-44100 Ferrara, Italy.

* Corresponding author: Department of Chemistry, University of Ferrara, Via L. Borsari, 46, I-44100 Ferrara, Italy. E-mail: l.pasti@unife.it, Phone: +39 0532 455346, Fax: +39 0532 240709.

Appendix A

Let us consider a two-states system. For a batch experiment this system corresponds to the partition of a species between two homogeneous phases. Because of the homogeneity of the two phases, the corresponding chromatographic process is called one site model [19]. Since this model represents the starting point of the approach here presented, some basic relations previously obtained will be herein recalled.

In chromatography retention time are made up of numerous sorption desorption steps or jumps, the large number of them allowing the long time approximation, and the ergodic hypothesis. The present theoretical development is based on the assumption that transition between states follows a first-order kinetics, consequently the number of jumps (n) between the states follow a Poisson distribution :

$$P(n) = \frac{(\mu t_M)^n}{n!} e^{(-\mu t_M)} \tag{A-1}$$

where:

$$t_M = \frac{L}{u_M} \tag{A-2}$$

t_M is the hold up time, u_M is the mobile phase velocity, L the column length and μ the frequency of adsorption events. $P(n)$ is the probability that during time t_M a given molecule will adsorb n times, assuming constant both u_M and t_M.

The average values of $\overline{n}$ during the time t_M is:

$$\overline{n} = t_M \mu = \frac{t_M}{\overline{\tau}_M} \tag{A-3}$$

where:

$$\overline{\tau}_M = \frac{1}{\mu} \tag{A-4}$$

is the average time spent by a molecule in the mobile phase between a desorption event from the stationary phase and the subsequent event of adsorption in the stationary phase.

Under the assumption that the band broadening process is determined by the sole mobile to stationary phase kinetics, i.e. that the species in the mobile phase do not undergo to longitudinal diffusion and that move at constant u_M value (see eq. A-2) the following relationships, describing a chromatographic peak profile –scaled by the quantity t_M - in either the time domain or in the in the frequency (ω) domain – i.e. the CF - is derived respectively :

$$f(t_S) = \exp\left(-\frac{t}{\overline{\tau}_{S,1}} - \overline{n}\right)\sqrt{\frac{\overline{n}}{\overline{\tau}_{S,1} t}}\mathrm{I}_1\left(\sqrt{\frac{4\overline{n}}{\overline{\tau}_{S,1}} t_S}\right) \tag{A-5a}$$

$$\varphi_S(\omega) = \exp\left(\overline{n}\left(\frac{1}{1 - i\omega\overline{\tau}_S} - 1\right)\right) \tag{A-5b}$$

where $\overline{\tau}_S$ is the average time spent during one sojourn step in the adsorbed state, under the hypothesis of homogeneous adsorption site. I_1 is the Bessel function of first order of imaginary argument. t_S in eqs. A-5a, b is the time spent in the stationary phase and it is the stochastic variable corresponding to the time axis value of the chromatographic peak profile, scaled by the t_M value.

The definition of the capacity k' is recalled:

$$k' = \frac{(t_R - t_M)}{t_M} = \frac{t'_R}{t_M} \quad \text{(A-6a)}$$

being t_R is the retention time, i.e. the average time spent in the mobile and in the stationary phase and t'_R. the net retention time, i.e. the average time spent in the stationary phase.

In the followings, we limit ourselves to the linear chromatographic retention in absence of mobile phase dispersions. In such a case, it has been demonstrated [21] that from eq A-3 one has:

$$k' = \frac{\overline{\tau}_S}{\overline{\tau}_M} \quad \text{(A-6b)}$$

$$t_M = \overline{n}\,\overline{\tau}_M \quad \text{(A-6c)}$$

$$t'_R = \overline{n}\,\overline{\tau}_S \quad \text{(A-6d)}$$

$$t_R = \overline{n}(\overline{\tau}_M + \overline{\tau}_S) \quad \text{(A-6e)}$$

Appendix B

The principle of microscopic reversibility [4, 35] states that when a system is at equilibrium the frequency of transition is the same in both directions for each individual reaction step. As a consequence any cyclic reaction the product of the rate constants going in one way around the cycle is equal to the product of the kinetic constants describing the other way of the reversible reaction.

$$k_{-1}^{B} k_{-1}^{M} k_{1}^{A} k_{1}^{S} = k_{1}^{B} k_{1}^{M} k_{-1}^{A} k_{-1}^{S} \quad \text{(B-1)}$$

when a non-chiral mobile phase is considered the rate constant in mobile phase are equal to each others:

$$k_{-1}^{M} = k_{1}^{M} \quad \text{(B-2)}$$

By substituting eq. B-2 in B-1 one obtains:

$$k_{-1}^{B} k_{1}^{A} k_{1}^{S} = k_{1}^{B} k_{-1}^{A} k_{-1}^{S} \quad \text{(B-3)}$$

and after rearrangement eq B-3 becomes:

$$\frac{k_{1}^{S}}{k_{-1}^{S}} = \frac{k_{1}^{B}}{k_{-1}^{B}} \frac{k_{-1}^{A}}{k_{1}^{A}} \quad \text{(B-4)}$$

Some important relationships linking chromatographic and equilibrium thermodynamical quantities are reported:

$$K = \frac{k'}{\phi} \quad \text{(B-5)}$$

where K is the partition constant between stationary and mobile phase, i.e. the equilibrium $A_M \leftrightarrow A_S$, i.e, the ratio of the stationary and mobile phase concentrations of the species considered (A_S and A_M):

$$K = \frac{A_S}{A_M} \tag{B-6}$$

k' in eq. B-5 is the capacity factor (see eq. A-6a.in Appendix A) and ϕ the column phase ratio:

$$\phi = \frac{V_S}{V_M} \tag{B-7}$$

wth V_S and V_M the volumes of the stationary phase and mobile phase.

It must also be remembered the relationship between equilibrium constant K and reaction constant:

$$K = \frac{k_1^A}{k_{-1}^A} \tag{B-8}$$

where k_1^A and k_{-1}^A are the reaction rates for $A_M \rightarrow A_S$ and $A_M \leftarrow A_S$, respectively

With reference to the reaction $A_S \leftrightarrow B_S$ (see Fig. 1), at the system equilibrium one has thus

$$K^S = \frac{B_S}{A_S} = \frac{k_1^S}{k_{-1}^S} \tag{B-9}$$

where K_S is the equilibrium constant of the $A_S \leftrightarrow B_S$ reaction and k_1^S and k_{-1}^S are the pertinent rate constants (see Fig. 1). From eq B-4, by using eqs. B-5 and B-6, one has:

$$K^S = \frac{k_1^S}{k_{-1}^S} = \frac{K_B}{K_A} = \frac{k_B'}{k_A'} \tag{B-10}$$

where the equilibrium constants K_A and K_B in eq. B-10 are the phase partition coefficients:

$$K_B = \frac{k_1^B}{k_{-1}^B} = \frac{B_S}{B_M} \qquad K_A = \frac{k_1^A}{k_{-1}^A} = \frac{A_S}{A_M} \tag{B-11}$$

which in turn, according to eq. B-5, are related to the capacity factor (k') by:

$$K_A = \frac{k_A^{'}}{\phi} = \frac{\left(t_{R,A} - t_M\right)}{t_M}\frac{1}{\phi} = \frac{t'_{R,A}}{t_M}\frac{1}{\phi} \quad \text{(B-12a)}$$

$$K_B = \frac{k_B^{'}}{\phi} = \frac{\left(t_{R,B} - t_M\right)}{t_M}\frac{1}{\phi} = \frac{t'_{R,B}}{t_M}\frac{1}{\phi} \quad \text{(B-12b)}$$

In eqs are $t_{R,A}^{'}$ and $t_{R,B}^{'}$ the corrected retention time of the species A .and B , respectively.

Appendix C

The dynamic process underlying to the batch description of Fig. 1 can be mathematically described by [4]:

$$\frac{dP_{A_M}}{dt} = k_{-1}^{A} P_{A_S} + k_{-1}^{M} P_{B_M} - k_{1}^{A} P_{A_M} - k_{1}^{M} P_{A_M} \tag{B-1}$$

$$\frac{dP_{A_S}}{dt} = k_{1}^{A} P_{A_M} + k_{-1}^{S} P_{B_S} - k_{-1}^{A} P_{A_S} - k_{1}^{S} P_{A_S} \tag{C-2}$$

$$\frac{dP_{B_M}}{dt} = k_{1}^{B} P_{B_S} + k_{1}^{M} P_{A_M} - k_{-1}^{B} P_{B_M} - k_{-1}^{M} P_{B_M} \tag{C-3}$$

$$\frac{dP_{B_s}}{dt} = k_{-1}^{B} P_{B_M} + k_{1}^{S} P_{A_S} - k_{1}^{B} P_{B_S} - k_{-1}^{S} P_{B_S} \tag{C-4}$$

where general symbol P_{E_i} is the molecular population (i.e. the number of species) of the species E (in the two sates A or B) in the phase i (M or S), which can be related to the concentration under well defined conditions (see the paper by Gillespie in ref. [42] for a detailed discussion).

By summing the above equations for each species (i.e. C-1 + C-2 and C-3 + C-4), the A and B states process dynamics given by:

$$\frac{dP_{A_M}}{dt} + \frac{dP_{A_S}}{dt} = \frac{d\left(P_{A_M} + P_{A_S}\right)}{dt} = \frac{dP_A}{dt} = k_{-1}^{S} P_{B_S} + k_{-1}^{M} P_{B_M} - k_{1}^{S} P_{A_s} - k_{1}^{M} P_{A_M} \tag{C-5a}$$

$$\frac{dP_{B_M}}{dt} + \frac{dP_{B_S}}{dt} = \frac{d\left(P_{B_M} + P_{B_S}\right)}{dt} = \frac{dP_B}{dt} = k_{1}^{S} P_{A_S} + k_{1}^{M} P_{A_M} - k_{-1}^{S} P_{B_S} - k_{-1}^{M} P_{B_M} \tag{C-5a}$$

with :

$$P_A = P_{A_M} + P_{A_S} \tag{C-6a}$$

$$P_B = P_{B_M} + P_{B_S} \tag{C-6b}$$

By putting:

$$k_A = k_1^S \frac{P_{A_S}}{P_A} + k_1^M \frac{P_{A_M}}{P_A} \quad \text{(C-7a)}$$

$$k_B = k_{-1}^S \frac{P_{B_S}}{P_B} + k_{-1}^M \frac{P_{B_M}}{P_B} \quad \text{(C-7b)}$$

and by combining eqs C-5a and C-5b with eqs C-7a and C-7b, one obtains:

$$\frac{dP_A}{dt} = k_B P_B - k_A P_A \quad \text{(C-8a)}$$

$$\frac{dP_B}{dt} = k_A P_A - k_B P_B \quad \text{(C-8b)}$$

Eqs C-8a, and b together with eqs. 7a, and b can be interpreted as the mathematical representation of the four state system of Fig. 1a reduced as two state system of Fig. 1b, being thus k_A and k_B the observed rate constants for the formation of each of the two enantiomers.

It is possible to further simplify the model by assuming that the sorption desorption process is fast when compared to the interconversion reaction, i.e. with reference to Fig. 1:

$$k_{\pm 1}^S \;\; k_{\pm 1}^M \;<<\; k_{\pm 1}^A, \; k_{\pm 1}^B \quad \text{(C-9)}$$

and, in such conditions, the equilibrium approximation can be assumed, i.e. the equality between molecular population ratio and equilibrium concentration:

$$\frac{P_{A_S}}{P_{A_M}} = \frac{A_S V_s}{A_M V_M} = \frac{A_S}{A_M}\phi \quad \text{(C-10)}$$

where A_S, A_M, V_S, V_M and ϕ are defined in Appendix A. By combining eq. C-10 and eq. A-11 one obtains:

$$K_A = \frac{k_1^A}{k_{-1}^A} = \frac{P_{A_S}}{P_{A_M}} \frac{1}{\phi} \tag{C-11}$$

and, by considering eq. A-5, one has from eq. C-11:

$$k'_A = \frac{k_1^A}{k_{-1}^A} = \frac{P_{A_S}}{P_{A_M}} \tag{C-12}$$

From eq. C-12, the probabilities of A of being in the M or in the S phases, p_{A_M} and p_{A_S}, respectively, are obtained:

$$p_{A_M} = \frac{P_{A_M}}{P_{A_M} + P_{A_S}} = \frac{1}{1 + k'_A} \tag{C-13a}$$

$$p_{A_S} = \frac{P_{A_s}}{P_{A_M} + P_{A_S}} = \frac{k'_A}{1 + k'_A} \tag{C-13b}$$

By considering eq. C-7b, eqs. C-13 a and b become:

$$p_{A_M} = \frac{\overline{\tau}_{M,A}}{\overline{\tau}_{M,A} + \overline{\tau}_{S,A}} \tag{C-14a}$$

$$p_{A_S} = \frac{\overline{\tau}_{S,A}}{\overline{\tau}_{M,A} + \overline{\tau}_{S,A}} \tag{C-14b}$$

The identity of eqs. C-14 and C-15 referred to the same phase, express the ergodic condition that the averages performed in time and in the phase state are the same under long time observation.

Equations holding true for the second eluted enantiomer B similar to those reported for the first eluted enantiomer, A – eqs C-10 to C-14 – can be written. Moreover it can be assumed that the average time spent in the mobile phase by both enantiomer are equal, i.e.:

$$\overline{\tau}_M = \overline{\tau}_{M,A} = \overline{\tau}_{M,B} \tag{C-15}$$

Finally by substituting in eqs. C-7a and C-7b in eqs C-13-a, b and eqs C-6a, b in eqs. C-14a, b one has:

$$k_B = \frac{\left(\bar{\tau}_{S,B} k_{-1}^{S} + \bar{\tau}_M k_{-1}^{M}\right)}{\bar{\tau}_M + \bar{\tau}_{S,B}} = \frac{1}{1+k_B^{'}} k_{-1}^{M} + \frac{k_B^{'}}{1+k_B^{'}} k_{-1}^{S} \qquad \text{(C-16a)}$$

$$k_A = \frac{\left(\bar{\tau}_{S,A} k_{-1}^{S} + \bar{\tau}_M k_{-1}^{M}\right)}{\bar{\tau}_M + \bar{\tau}_{S,A}} = \frac{1}{1+k_A^{'}} k_1^{M} + \frac{k_A^{'}}{1+k_A^{'}} k_1^{S} \qquad \text{(C-16b)}$$

An analogous result can be obtained by assuming equilibrium conditions. In this case the instantaneous rate of change of the species is equal to zero:

$$\frac{d\left(P_{A_M} + P_{A_S}\right)}{dt} = \frac{d\left(P_{B_M} + P_{B_S}\right)}{dt} = 0 \qquad \text{(C-17)}$$

Eq. C-17 indicates that the total concentration of both the enantiomers does not change with time. By combining eq C-17 with eq. C-5 a or C-5b one obtains:

$$k_{-1}^{S} P_{B_S} + k_{-1}^{M} P_{B_M} = k_1^{S} P_{A_s} + k_1^{M} P_{A_M} \qquad \text{(C-18)}$$

Likewise, by combining eq. C-8a or C-8b, with eq. C-18 and taking into account eqs. C-6 a, b one has:

$$k_B P_B = k_A P_A \qquad \text{(C-19)}$$

By rearranging eq. C-18 with eq. C-19, one obtains:

$$P_B\left(k_{-1}^{S}\frac{P_{B_S}}{P_B} + k_{-1}^{M}\frac{P_{B_M}}{P_B}\right) = P_A\left(k_1^{S}\frac{P_{A_s}}{P_A} + k_1^{M}\frac{P_{A_M}}{P_A}\right) \qquad \text{(C-20)}$$

By introducing eqs. C-6a,b in eq. C-20, one has,

$$P_B\left(k_{-1}^{S}\frac{P_{B_S}}{P_{B_M}+P_{B_S}} + k_{-1}^{M}\frac{P_{B_M}}{P_{B_M}+P_{B_S}}\right) = P_A\left(k_1^{S}\frac{P_{A_s}}{P_{A_M}+P_{A_S}} + k_1^{M}\frac{P_{A_M}}{P_{A_M}+P_{A_S}}\right) \qquad \text{(C-21)}$$

and, by introducing eqs C-14 a and b, eq. C-21 becomes:

$$\left(k_{-1}^{S}\frac{k'_{B}}{1+k'_{B}}+k_{-1}^{M}\frac{1}{1+k'_{B}}\right)P_B=\left(k_{1}^{S}\frac{k'_{A}}{1+k'_{A}}+k_{1}^{M}\frac{1}{1+k'_{A}}\right)P_A \tag{C-22}$$

By comparing eq. C-22 and eq. C-19, one obtains

$$k_B=\frac{\left(\overline{\tau}_B k_{-1}^{S}+\overline{\tau}_M k_{-1}^{M}\right)}{\overline{\tau}_M+\overline{\tau}_B}=\frac{1}{1+k_B^{'}}k_{-1}^{M}+\frac{k_B^{'}}{1+k_B^{'}}k_{-1}^{S} \tag{5a}$$

$$k_A=\frac{\left(\overline{\tau}_A k_{-1}^{S}+\overline{\tau}_M k_{-1}^{M}\right)}{\overline{\tau}_M+\overline{\tau}_A}=\frac{1}{1+k_A^{'}}k_{1}^{M}+\frac{k_A^{'}}{1+k_A^{'}}k_{1}^{S} \tag{5b}$$

which are equal to eqs. C-16 a) and b).

Additionally, in term of propensity functions (see main text eqs. 7a, b) eqs 8a, b become:

$$\frac{dP_A}{dt}=k_B P_B-k_A P_A=(P_A+P_B)\left[a_B(x)-a_A(x)\right] \tag{C-23a}$$

$$\frac{dP_B}{dt}=k_A P_A-k_B P_B=(P_A+P_B)\left[a_A(x)-a_B(x)\right] \tag{C-23b}$$

Equations C-23a, b are the well known reaction rate equations of chemical kinetics, and they can be included as a part of the stochastic description of the chromatographic jumps processes $A \Leftrightarrow B$ under the long time approximation, when fluctuations are negligible. $a_A(x)dt$ and $a_B(x)dt$ represent in fact the number of reactions $A \to B$ and $B \to A$ in the time interval dt, respectively. These numbers are stochastic variables which are assumed to follow the Poisson Statistics (see eq. A-1).

Appendix D

The two states system characterized by the probability density $p(x|T,A)$ and $p(x|T,B)$ - describing the probability of a molecule to spend xT time in state B for molecules initially in the state A and B respectively – has been solved in frequency domain by Kubo and Andersen [43, 44].

The master equations that describe the dynamics of the kinetic scheme are (see eqs. C-8 a and b in Appendix C):

$$\frac{dp_A}{dt} = k_B p - k_A P_A \tag{C-8a}$$

$$\frac{dP_B}{dt} = k_A P_A - k_B P_B \tag{C-8b}$$

In the following the original treatment proposed by Anderson is reported.

For the two states system with jumps following a Poissonian distribution (first order kinetic) and the Fourier transform of the probability density functions satisfy to a master equation.

$$\frac{dg_A(\omega|T,A)}{dT} = g_A(\omega|T,A)(i\omega - k_A) + g_B(\omega|T,A)k_B \tag{D-1}$$

$$\frac{dg_B(\boldsymbol{\omega}|T,A)}{dT} = g_A(\boldsymbol{\omega}|T,A)(i\boldsymbol{\omega} - k_A) + g_B(\boldsymbol{\omega}|T,A)k_B \tag{D-2}$$

where $g_A(\boldsymbol{\omega}|T,A)$ and $g_B(\boldsymbol{\omega}|T,A)$ are the Fourier Tranform of P_A and P_B, with initial condition in state A.

Eqs. D-1 and D-2 can be solved in the Laplace domain. The Laplace transform with respect to T is given by:

$$L_A(\omega|s,A)=\int_0^{\infty}\exp(-sT)g_A(\omega|T,A)dT \tag{D-3}$$

By substituting eq. D-1 in D-3 and under initial conditions $g_A(\omega|0,A)=1$ and $g_B(\omega|0,A)=0$ one has:

$$L_A(\omega|s,A)(s+k_A-i\omega)-k_BL_B(\omega|s,A)=1 \tag{D-4a}$$

$$k_AL_A(\omega|s,A)-(s+k_B)L_B(\omega|s,A)=0 \tag{D-4b}$$

By solving the linear system of eqs. D-4a and b one obtains:

$$L_A(\omega|s,A)=\frac{s+k_B}{(k_A+s-i\omega)(k_B+s)-k_Ak_B} \tag{D-5a}$$

$$L_B(\omega|s,A)=\frac{k_A}{(k_A+s-i\omega)(k_B+s)-k_Ak_B} \tag{D-5b}$$

and by considering that:

$$L(\omega|s,A)=L_A(\omega|s,A)+L_B(\omega|s,A) \tag{D-6}$$

one has:

$$L(\omega|s,A)=\frac{s+k_B+k_A}{(k_A+s-i\omega)(k_B+s)-k_Ak_B} \tag{D-7}$$

The Fourier Transform of the probability density can be obtained by inverting the Laplace transform of eq. D-7:

$$\Phi(\omega|T,A)=\int_0^T\frac{s+k_B+k_A}{(k_A+s-i\omega)(k_B+s)-k_Ak_B}\exp(-sT)dT \tag{D-8}$$

The integration of eq. D-8 was resolved in Refs. [26, 48] .

$$\hat{p}(\omega|T,A)=exp\left(-\frac{kt-i\omega t}{2}\right)\left(\phi\cosh\frac{\phi t}{2}+(k+i\omega)\sinh\frac{\phi t}{2}\right)\Big/\phi \tag{D-9a}$$

Analogously, by setting initial conditions $g_A(\omega|0,A)=0$ and $g_B(\omega|0,A)=1$ and solving the correspondent liner system (eqs. D-1 and D-2) one obtains:

$$\hat{p}(\omega|T,B)=exp\left(-\frac{kt-i\omega t}{2}\right)\left(\phi\cosh\frac{\phi t}{2}+(k-i\omega)\sinh\frac{\phi t}{2}\right)\Big/\phi \tag{D-9b}$$

Microporous and Mesoporous Materials 151 (2012) 358–367

Contents lists available at SciVerse ScienceDirect

Microporous and Mesoporous Materials

journal homepage: www.elsevier.com/locate/micromeso

Adsorption mechanism of 1,2-dichloroethane into an organophilic zeolite mordenite: A combined diffractometric and gas chromatographic study

Annalisa Martucci [a,*], Luisa Pasti [b,*], Marianna Nassi [b], Alberto Alberti [a], Rossella Arletti [c], Roberto Bagatin [d], Rodolfo Vignola [d], Rosalba Sticca [d]

[a] Earth Sciences Department, University of Ferrara, Via G. Saragat 1, 44100 Ferrara, Italy
[b] Department of Chemistry, University of Ferrara, Via L. Borsari 46, 44100 Ferrara, Italy
[c] Dipartimento di Scienze Mineralogiche e Petrologiche, University of Torino, Via Valperga Caluso 35, I-10125 Torino, Italy
[d] Research Centre for Non-Conventional Energy – Istituto Eni Donegani Environmental Technologies, Via Fauser 4, I-28100 Novara, Italy

ARTICLE INFO

Article history:
Received 23 July 2011
Received in revised form 7 October 2011
Accepted 8 October 2011
Available online 17 October 2011

Keywords:
Mordenite
1,2-Dichloroethane
Adsorption
Gas chromatography
X-ray diffraction

ABSTRACT

We investigated the 1,2-dichloroethane (DCE) adsorption process into an organophilic zeolite mordenite. A combined diffractometric, thermogravimetric and gas chromatographic approach enabled to obtain clear evidence of DCE adsorption in mordenite channels as well as to pinpoint the exact location of the organic species found in the structure. Rietveld refinement revealed the incorporation of 2.5 DCE molecules and approximately 4 water molecules within the mordenite channel system, in very good agreement with the weight loss given by TG analysis and the saturation capacity determined by the adsorption isotherm. This relevant incorporation of DCE molecules caused a remarkable increase in the dimension of the 12-ring, when compared to the parent zeolite. The distances between the oxygen atoms of the water molecules from the chlorine atoms of the organic molecule (W–Cl1 = 2.34 Å, W–Cl2 = 2.53 Å) suggest that different DCE molecules could be connected by means of hydrogen bonds through water, to form a DCE and water molecule complex. The isotherm adsorption model for organic compounds from an aqueous dilute solution was selected based on the results of the structural investigation.

1. Introduction

Chlorinated volatile organic compounds (VOCs), such as dichloromethane (DCM) and 1,2-dichloroethane (DCE) constitute an important environmental pollutants class due to their high toxicity, inertness and widespread application in industry. Such compounds are typically carcinogens, mutagens and teratogens, and, furthermore, are involved in the destruction of the ozone layer. Substantial quantities of DCE are generated in vinyl chloride production plants [1] and are present in air stripping and soil venting remediation off-gases [2]. Other sources of entry into the ecosystem include effluent discharge from industries that use or produce DCE, effluents from the treatment of contaminated groundwater, air emissions and leachates from waste disposal sites, and long-range atmospheric transportation from remote sources. Despite DCE being the most abundant chlorinated groundwater pollutant on Earth, an efficient reductive in situ detoxification technology for this compound is not known. For instance, zero-valent iron (ZVI), which directly degrades several contaminants appears to be ineffective on irreducible compounds such as DCE, chlorobenzenes, as well as hydrocarbons [3,4]. Granular activated carbon (GAC) has been shown to be only slightly effective in treating water containing very soluble compounds, such as oxygenated organics, or low molecular weight compounds, such as DCE and vinyl chloride (VC) [5]. Recently Vignola et al. [6] have demonstrated that hydrophobic zeolites are able to effectively adsorb molecules against which ZVI or GAC are totally ineffective. In particular, ZSM-5 zeolite turned out to be suitable for mono-aromatic molecules, such as BTEX (benzene, toluene, ethylbenzene and xylene) and halogen–benzene derivatives [6].

The DCE molecule has been the subject of a considerable number of studies because of interest in its restricted internal rotation and the nature of the potential barrier associated with this motion. DCE is a small, flexible molecule which occurs in two stable conformations, namely *gauche* (with a Cl–C–C–Cl dihedral angle of ±60°) and *trans* or *anti* (with a Cl–C–C–Cl dihedral angle of 180°), respectively. Experimental and theoretical molecular conformational studies in ambient conditions have revealed that in the gaseous phase, DCE exists mainly in the *trans* conformer, due to the steric effect, which is basically composed of exchange and Coulombic repulsion [7–12]. In the liquid phase or in a polar solvent media, such as water, the dipole–dipole interactions with neighbouring species (in liquid) or polar solvent molecules (in solutions) stabilise the *gauche* conformer (with a dipole moment of 3.5 Debye) when

* Corresponding authors. Tel.: +39 (0)532 974730; fax: +39 (0)532 974767 (A. Martucci), tel.: +39 (0)532 455346; fax: +39 (0)532 240709 (L. Pasti).
E-mail addresses: mrs@unife.it (A. Martucci), luisa.pasti@unife.it (L. Pasti).

1387-1811/$ - see front matter © 2011 Elsevier Inc. All rights reserved.
doi:10.1016/j.micromeso.2011.10.010

compared to the *trans* conformer (with a near to zero dipole moment) [13–17].

It is well known that the conformational equilibrium of molecules or atomic clusters can show strong differences in confinement, due to reduced dimensionality and large interface effects. In particular, the present work deals with the confinement effect of zeolite materials. Due to their confinement effect, zeolites and inorganic mesoporous materials can be described as solid solvents, as the electronegative charge on their framework can polarise adsorbed molecules as with any polar solvent [18]. The wide applicability of zeolites stems from their structural and compositional properties, such as their pore structures, acidic properties, good thermal stability and ion exchange properties [19–23]. The ability of zeolites with a low Si/Al ratio to remove cations by ionic exchange has been largely demonstrated and utilised in water treatment plants producing drinking water [24]. In contrast, zeolites characterised by a high Si/Al ratio are hydrophobic and organophilic materials which are widely used in adsorption-related applications [25–27]. In fact, zeolitic networks of well-defined micropores may act as adsorption and reaction sites whose selectivity and activity can be modulated by acting on their structure and chemical composition. In selecting adsorbent materials, it is important to characterise their sorbent properties and this is usually done by modelling the experimental data with an adsorption isotherm model. However, to date several isotherms have been employed to interpret this phenomenon and in many cases the choice of model is based solely on the goodness of fit. In the present work, a structural investigation was performed to highlight the adsorption mechanisms in order to select the appropriate isotherm model.

X-ray and neutron diffraction techniques are usually employed to characterise the structure of zeolites loaded with hydrocarbon guest species in order to clearly locate their position inside the channel system [28–36]. Unfortunately, these experiments are generally performed at low temperatures by incorporating hydrocarbons using the gas phase. However, pore diffusion through the gas phase is much faster than the liquid phase, especially in the case of highly volatile hydrocarbons which have rather large distribution coefficients. To date, studies and applications on organic pollutant adsorption in microporous zeolitic materials from aqueous media have been relatively scarce [26,27,37,38]. The presence of a small amount of water reduces the adsorption capacity of alkanes and olefins in zeolites, especially at low adsorbate concentration [39]. In particular, water decreases saturated hydrocarbons diffusivity, thus acting as a screen between the cationic sites of the zeolite and the hydrocarbon molecules (screening effect) and reducing both the sorption volume (steric effect) and the zeolite window apertures of the (blocking effect) [40–42]. Beauvais et al. [42] reported a Monte Carlo molecular simulation study of the equilibrium adsorption of water and aromatics in zeolite faujasite NaY and observed cation redistribution upon water adsorption. The authors observed the same phenomenon in the presence of adsorbed xylene molecules in the noted. These results clearly show that the location of hydrocarbons and of chlorinated organics in zeolites has not been explored in detail, especially in the presence of water.

H-mordenite and chemically dealuminated H–Y zeolites resulted as the most active catalysts for chlorinated VOC destruction due to the presence of strong Brønsted acidity [22,23]. Mordenite (MOR) is a natural or synthetic zeolite, with an idealised chemical composition $Na_8Al_8Si_{40}O_{96} \cdot 24H_2O$ whose framework can be built up by the assembly of single 6-ring sheets linked by single 4-rings, or else by a combination of 5–1 secondary building units (SBUs). Its structure is characterised by straight 12-membered and 8-membered rings running along the *c* axis, and sinusoidal 8-membered rings running along the *b* axis; these channels accommodate extra framework cations and water molecules. The 12-ring channels are interconnected along [0 1 0] through 8-ring side pockets. In naturally occurring mordenites, the Si/Al ratio is within the range 4.3–6.0, whereas in synthetic mordenites this ratio varies from less than 5.0 up to 200 [54]. From a technical point of view, two different varieties of mordenite can be distinguished: Large Port (LPM) and Small Port Mordenites (SPM). Large Port Mordenites are hydrothermally synthesised in the Na-form between 75 and 260 °C, whereas Small Port Mordenites are usually hydrothermally synthesised between 275 and 300 °C [43]. Molecules with a diameter >4.5 Å can be introduced into large LPM channels, whereas SPM only accepts molecules with a diameter <4.2 Å and is thus less favourable for industrial applications [44]. As far as concerns its morphology, natural mordenite is characterised by acicular crystals with *c*-elongation, which are usually thin in the [0 1 0] direction, whereas synthetic mordenite commonly crystallises as large platelets with dominant (0 0 1) faces [45]. It seems that morphology is an additional parameter influencing small-port and large-port behaviour; in fact, platy mordenite enables easy access to large 12-membered ring channels, whereas long prismatic or fibrous (along *c*) crystals have fewer large-channel openings and diffusion is more sluggish [46,47]. In addition, most natural mordenites have properties which are characteristic of small-port mordenite.

The aluminosilicate framework of mordenite has orthorhombic topology with C*mcm* symmetry and includes four symmetrically independent tetrahedral cation sites and 10 framework oxygen sites. In the natural mineral real symmetry is reduced to C*mc*2_1 [48,49] in order not to constrain the O8 oxygen on the inversion centre, and consequently, to avoid a straight T–O–T angle. However, the crystal structure remains strongly C*mcm* pseudo-centrosymmetric so that all structure refinements of natural, synthetic and H-mordenite were performed in this space group [50–52]. Dehydrated, cation-exchanged mordenite occurs with a P*bcn* space group [52,53] whereas hydrated, cation- and molecule-exchanged samples have been refined in lower monoclinic symmetry with the C*c* space group [49,54].

Recently, it has been proved that host–guest interactions in zeolitic systems have a strong influence on the conformational properties of adsorbed organic molecules due to the effect of the zeolite framework [55]. Therefore, it is important to understand the guest molecules behaviour inside the zeolite hosts in applications involving guest species adsorption in zeolitic frameworks, since it can influence the thermodynamics and kinetics of the adsorption processes.

For the first time this study reports the adsorption of both 1,2-dichloroethane and water into an organophilic zeolite mordenite from dilute solutions. To date, no information is available on the mechanisms and effectiveness of high-silica mordenite for DCE removal from water and no studies have investigated the effects of adsorbed DCE on the zeolite pore size. These results enabled an isotherm model which better explains the experimental adsorption data to be selected. A combined diffractometric, thermogravimetric and gas chromatographic study was used to:

(1) Investigate the adsorptive properties of hydrophobic synthetic mordenite.
(2) Characterise its structure after DCE adsorption.
(3) Localise the organic species in the mordenite channel system.
(4) Investigate DCE conformational equilibrium in this organophilic zeolite.
(5) Probe the interactions between DCE molecules, water molecules and framework oxygen atoms.

2. Experimental

2.1. Materials

1,2-Dichloroethane (purity 99.8%) and sodium chloride (purity 98%) were obtained from Sigma–Aldrich (Steinheim, Germany). The as-synthesised mordenite sample is a hydrophobic commercial adsorbent, which is synthesised with SiO_2/Al_2O_3 as equal to 200, and was purchased in its protonated form (HSZ-690HOA Tosoh Corporation). Its Na_2O content was lower than 0.1 wt.%. The material characteristics are reported in Fig. 1. The water used was filtered and purified by reverse osmosis using Milli-Q apparatus (Millipore, MA, USA).

The solid-phase microextraction (SPME) fibres which were used were coated with polydimethylsiloxane (PDMS) at 100 μm thickness (supplied by Supelco, PA, USA) and housed in a manual holder (Supelco, PA, USA). The fibre sorbent was selected due to its high versatility; in fact, it is generally used for the extraction of a wider range of analytes with differing polarity and volatility. Following the guidelines, the fibres were conditioned under helium at a flow-rate of approximately 1.0 mL/min with the split valve open (to reduce the amount of impurities entering the column) in the hot injection port of a gas chromatograph at 250 °C for 1 h prior to use. Additionally, the SPME fibres were conditioned for 15 min at 250 °C every day before use and were systematically cleaned at 250 °C for 20–30 min after every extraction. The blanks were tested by thermal desorption (5 min in the injection port) followed by gas chromatography (GC).

2.2. Scanning electron microscopy (SEM)

SEM images of the zeolites were acquired using a Zeiss EVO 40 XVP scanning electron microscope. To prepare the sample for SEM, a drop of dilute colloidal solution of the sample was dripped onto the SEM sample stud surface and the sample stud was then dried at 60 °C for 3 h. Shortly before SEM image acquisition, the latter was coated with gold. The SEM zeolite image reported in Fig. 2 indicated that mordenite is composed of particles with lamellar or plated morphology, the lamella lengths are in the 2–3 μm range.

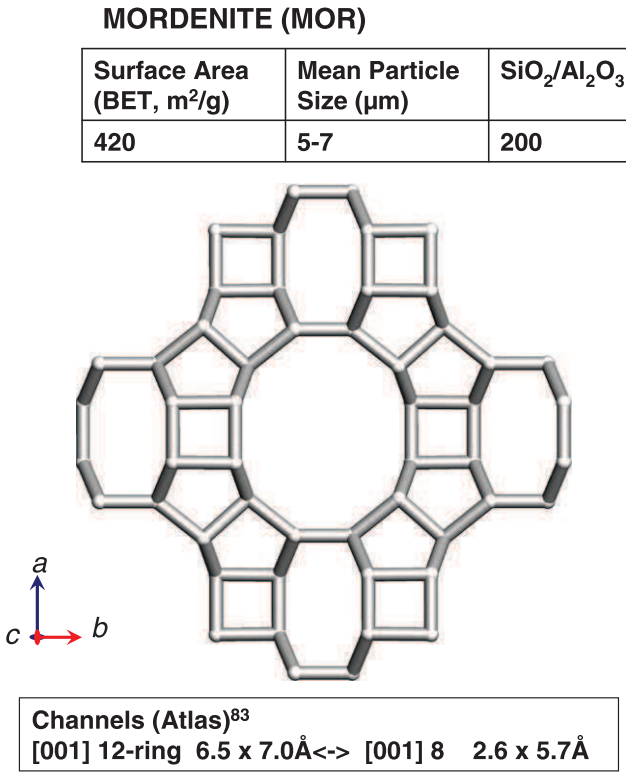

Fig. 1. Structure and characteristics of zeolite mordenite under investigation.

2.3. X-ray diffraction

A mordenite powder pattern after DCE adsorption (MOR-DCE) was measured on a Bruker D8 Advance Diffractometer equipped with a Sol-X detector, using Cu $K_{\alpha1,\alpha2}$ radiation in the 4–116° 2θ range and a counting time of 12 s/step.

2.4. Structure determination and refinement strategy

The diffraction pattern was firstly indexed using the DICVOL program [56] in an orthorhombic cell [a = 18.041 Å, b = 20.212 Å, c = 7.447 Å, V = 2715.5 Å^3]. Rietveld structure refinement was therefore performed, using the GSAS package [57] with the EXPGUI interface [58]. The framework atoms for hydrophobic mordenite reported by Martucci et al. [27] provided the initial parameters for structure determination. All tetrahedral sites were modelled with Si atoms, while the amount of Al atoms were neglected. In all the Rietveld structure refinement, the Bragg peak profile was modelled using a pseudo-Voigt peak-shape function [59] with 0.01% cut-off peak intensity. The background curve was fitted using a Chebyschev polynomial with 20 variable coefficients. The 2θ-zero shift was accurately refined into the data set pattern. The scale factor and unit-cell parameters were allowed to vary in all the cycles. The refined structural parameters for the data histogram were the following: fractional coordinates and isotropic displacement factors for all atoms (one for each tetrahedral site and framework oxygen atom), and occupancy factors for the extraframework ions. Occupancy factors and isotropic displacement factors were varied in alternate cycles. Soft constraints were imposed on the tetrahedral cations and coordinated framework oxygen atom T–O distances during the first stages of refinement, and left free in the last cycles. The positions of the extraframework sites were determined by the Fourier and Difference Fourier maps. The crystallographic data and refinement details are reported in Table 1. The final atomic positions, thermal parameters and occupancies are given in Table 2, the interatomic distances and angles in Table 3. The final observed and calculated patterns are shown in Fig. 3.

2.5. Thermal analyses

Thermogravimetric (TG), differential thermogravimetric (DTG) and differential thermal analyses (DTA) measurements of exhausted sample were performed in air at up to 1000 °C using an STA 409 PC LUXX® – Netzch at a 10 °C/min heating rate. The thermal curves are reported in Fig. 4.

2.6. Gas chromatography

Headspace-gas chromatography (HS-SPME-GC) solid phase-micro extraction was used to extract 1–2-dichloroethane from each aqueous sample and to subsequently perform to GC analysis. Preliminary experiments were done in order to evaluate extraction conditions. The headspace (HS) mode was used for extraction from a sample volume of 10 mL of DCE solutions. The addition of an inorganic salt has often been used in order to enhance the activity coefficients of volatile components in aqueous solutions, increasing the concentration in the headspace vapour. In the present work, 2 mL of a sodium chloride solution (300 g/L) were added to the sample which was placed in 25 mL glass flasks sealed with Teflon screw caps. After equilibration at 40(±0.5) °C, for 10 min, the

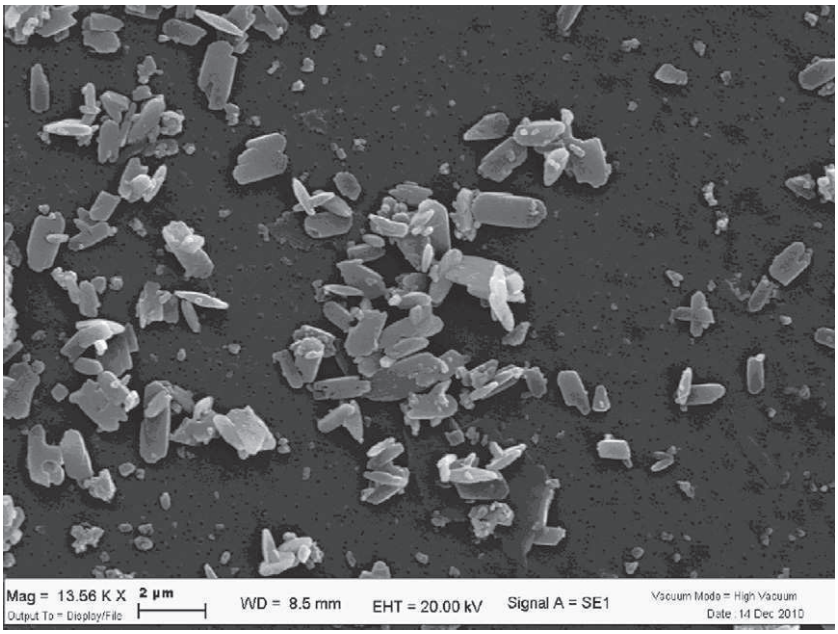

Fig. 2. Scanning electron microscopy (SEM) image of zeolite mordenite showing large platelets with dominant (001) faces.

Table 1
Lattice parameters and refinement details for mordenite before (MOR) and after DCE adsorption (MOR-DCE).

	MOR	MOR-DCE
Space group	Orthorhombic, C*mcm*	Orthorhombic, C*mcm*
a (Å)	18.069(1)	18.075(1)
b (Å)	20.219(1)	20.234(1)
c (Å)	7.456(3)	7.4602(2)
$\alpha = \beta = \gamma$ (°)	90	90
V (Å^3)	2723.9(2)	2728.3(2)
Wavelength of incident radiation (Å)	1.5417(1)	1.5417(1)
Refined pattern 2θ range (°)	4–116	4–116
Profile function	T–C–H pseudo-Voigt correction	T–C–H pseudo-Voigt correction
H-atom treatment	Not refined	Not refined
R_{wp} (%)	9.82	12.6
R_p (%)	7.45	9.8
R_F^2 (%)	6.42	8.4
No. of contributing reflections	2246	2302
N_{obs}	5665	5584
N_{var}	47	65

Estimated standard deviations in parentheses refer to the last digit.

SPME was inserted and the samples were maintained under controlled agitation with a magnetic stirrer (300 rpm) for 10 min. Finally, the fibre was inserted into the GC injector for analysis. The desorption time was 1 min.

The GC used in this work was an HRGC 5160 MEGA SERIES Instrument (Carlo Erba, Mi, I) equipped with a split/splitless injector and an electron capture detector (ECD, ^{63}Ni). A fused-silica DB-5 capillary column (60 m × 0.25 mm ID: 0.25 μm film thickness; J&W Scientific, USA) was employed. Helium (99.999%) was used as a carrier gas at a constant head pressure of 50 kPa and nitrogen (196 kPa) was employed as a make-up gas at a constant flow-rate (1 mL/min). The detector and injector temperatures were held constant at 250 °C. The GC oven was programmed as follows: 40 °C (5 min), 5 °C/min–80 °C (5 min), 30 °C/min–100 °C (5 min). The linearity of the quantitative analysis method was tested by evaluating the calibration curves: standard solutions of DCE in MilliQ water were analysed at varying concentration levels in the range 0.1–30 ppm. Each concentration was analysed twice. The linearity range as well as the method detection limit (LOD) were evaluated and computed from the calibration line. Good linearity was observed with a correlation coefficient of 0.993.

2.7. Adsorption isotherm

The adsorption equilibrium isotherm was determined using the batch method. Batch experiments were carried out in duplicate in 25 mL crimp top reaction glass flasks sealed with PTFE septa (Supelco, PA, USA). The flasks were filled in order to have minimum headspace, a solid/solution ratio (mg mL^{-1}) of 1:4 was employed. After equilibration (24 h) at a temperature of 25.3 ± 0.5 °C under stirring, the solids were separated from the aqueous solution by centrifugation (10,000 rpm for 30 min) and analysed by HS-SPME-GC, as above described.

3. Results and discussion

As described in the experimental section, the MOR particles are characterised by lamellar or plated morphology. This morphology enables easy access to the large 12-membered ring channels, thus indicating that the sample has properties which are characteristic of Large Port Mordenite.

The experimental data of the adsorption isotherm are reported in Fig. 5. In this work, the experimental sorption data were modelled using the traditional Langmuir isotherm [60]:

$$q = \frac{q_s K_L C_e}{1 + K_L C_e} \quad (1)$$

where q (mg g^{-1}) is the equilibrium adsorbed concentration, C_e (mg L^{-1}) is the equilibrium concentration in water, K_L (L mg^{-1}) is the Langmuir coefficient (binding constant), and q_s (mg g^{-1}) the saturation capacity. K_L and q_s, were determined by non-linear least squares data fitting. It can be seen that the examined concentration range is well fitted using the Langmuir equation (see Fig. 5a). The parameters obtained by fitting the Freundlich equation $q = KC_e^{1/n}$

Table 2
MOR-DCE atomic coordinates, occupancies and thermal parameters.

Atom	x/a	y/b	z/c	Multiplicity	Fraction	Uiso
T1	0.3068(3)	0.0752(2)	0.0401(5)	16	1.0	0.010(1)
T2	0.3051(3)	0.3103(2)	0.0447(6)	16	1.0	0.010(1)
T3	0.0852(4)	0.3786(4)	0.25	8	1.0	0.010(1)
T4	0.0843(4)	0.2205(4)	0.25	8	1.0	0.010(1)
O1	0.1190(4)	0.4076(5)	0.4326(9)	16	1.0	0.014(2)
O2	0.1229(4)	0.1874(5)	0.4212(11)	16	1.0	0.014(2)
O3	0.2368(4)	0.1215(4)	0.9973(13)	16	1.0	0.014(2)
O4	0.0910(7)	0.2959(3)	0.25	8	1.0	0.014(2)
O5	0.1676(7)	0.1898(10)	0.75	8	1.0	0.014(2)
O6	0.1727(8)	0.4216(8)	0.75	8	1.0	0.014(2)
O7	0.2158(8)	0.5	0.5	8	1.0	0.014(2)
O8	0.25	0.25	0.5	8	1.0	0.014(2)
O9	0	0.4011(10)	0.25	4	1.0	0.014(2)
O10	0	0.1957(11)	0.25	4	1.0	0.014(2)
Cl1	0.5	0.4287(17)	0.25	4	0.30(1)	0.16(1)
Cl2	0.5	0.5566(26)	0.25	4	0.31(1)	0.15(1)
C	0.5	0.4927(21)	0.0918(13)	8	0.33(1)	0.14(1)
W	0.3861(15)	0.4840(17)	0.25	8	0.48(1)	0.09(1)

Table 3
Selected bond distances (Å) and angles (°) for mordenite before (MOR) and after DCE adsorption (MOR-DCE).

	MOR	MOR-DCE		MOR	MOR-DCE
T1–O1	1.599(2)	1.602(2)	T2–O2	1.600(2)	1.597(2)
T1–O3	1.605(2)	1.607(2)	T2–O3	1.606(2)	1.606(3)
T1–O6	1.613(1)	1.610(2)	T2–O5	1.601(2)	1.610(2)
T1–O7	1.599(2)	1.602(2)	T2–O8	1.605(2)	1.608(3)
T3–O1 [x2]	1.602(2)	1.603(2)	T4–O2[x2]	1.606(2)	1.602(2)
T3–O4	1.610(2)	1.604(2)	T4–O2	1.609(2)	1.605(2)
T3–O9	1.613(2)	1.605(2)	T4–O10	1.610(2)	1.604(3)
T1–O1–T3	151.3(8)	145.5(8)	T1–O6–T1	147.4(11)	153.0(12)
T2–O2–T4	143.4(8)	143.4(8)	T1–O7–T1	142.6(10)	150.5(11)
T1–O3–T2	152.5(7)	155.7(7)	T2–O8–T2	180	180
T3–O4–T4	172.5(9)	171.9(9)	T3–O9–T3	162.8(16)	147.2(17)
T2–O5–T2	150.1(8)	144.2(10)	T4–O10–T4	135.2(16)	143.6(18)
C–Cl1		1.75(1)	Cl1–Cl2		2.59(2)
C–Cl2		1.75(1)	Cl2–W		2.53(4)
C–C		1.40(1)	Cl1–W		2.34(4)
Cl2–O10		2.81(5)	C–W		2.38(3)

are also reported in Table 4. In several papers devoted to adsorption from dilute solutions, Dubinin–Astakhov (DA) or Dubinin–Radushkevich (DR) adsorption isotherms have been applied. The Dubinin–Astakhov equation was derived from Polanyi's potential theory for a vapour phase system and extended from Manes [61] to aqueous systems by defining the Polanyi adsorption potential $\varepsilon_{SW} = RT\ln(S/C_e)$, where R is the ideal gas constant ($J\,mol^{-1}\,K^{-1}$), T the temperature (K), and S is the water solubility ($mg\,L^{-1}$). The Polanyi–Dubinin–Manes (PDM) model [62] is given by:

$$q = V_0\rho_0 \exp\left[\frac{RT\ln S/C_e}{E}\right]^b \quad (2)$$

where V_0 and ρ_0 are the maximum volume of adsorbed compound for unit mass of adsorbent ($cm^3\,g^{-1}$) and compound density ($mg\,cm^{-3}$), respectively. E ($kJ\,mol^{-1}$) is the free energy of the adsorption process compared to that of a reference compound [63]. b is an exponent which can be obtained by fitting or set to a given (integer) value, when $b = 2$ it becomes the Dubinin–Radushkevich equation. To apply Eq. (2), the water solubility of 1,2-dichloroethane was set to 8700 $mg\,L^{-1}$, DCE had a vapour pressure of 81 hPa at 20 °C, a $\log K_{ow}$ of 1.45, and a density of 1.25 ($g\,cm^{-3}$) [64]. In Fig. 5b it can be seen that the experimental data are well fitted using the PDM model. From the data in Table 4, it is possible to infer some adsorption process properties. It can be noted that the saturation capacity evaluated from Eq. (1) is 71.5 $mg\,g^{-1}$ and that this value is in agreement with the pore volume obtained from fitting the PDM model Eq. (2), but that it is smaller than the mordenite pore volume. The b value Eq. (2) obtained for the zeolite is about 4. This result is indicative of relatively homogeneous adsorbents with narrow site energy distribution, and is in agreement with the literature data on Y zeolite [65]. The exponent parameter of the Freundlich equation is in agreement with those found for VOC [66]. In Table 4, it is notable that the goodness of fit (coefficient of determination) for the three models employed are similar. Therefore, the choice of the model based solely on statistical parameters of fitting seems to be arbitrary. From the literature data, it seems that the micropore-filling-based PDM isotherm should theoretically be the best model to describe the sorption process on microporous materials. However, it has been found that the PDM isotherm underestimates pore volume at a low aqueous concentration range (<2 mg/L). This result was also found in TCE sorption on other adsorbents [67]. This was supposed to be due to another sorption mechanism in addition to micropore-filling at low concentrations, in particular due to specific sorbent sites of high adsorption energies. Moreover, loading results for trichloroethylene from both the liquid and vapour phase indicated that the liquid phase did not penetrate the silicalite-1 pores. However, it did enter the dealuminated NaY pores, even if theoretically, trichloroethylene can penetrate the pores of both the studied zeolites [67]. Finally, one unresolved issue from the aqueous solution adsorption experiments was if the presence of water affected the adsorption capacity, and whether or not the water actually entered the micropores. Therefore, there is no clear piece of evidence on which isotherm model to choose out of all these experimental results. This is mainly as a result of a lack of knowledge about adsorption mechanisms. In order to highlight the adsorption mechanism in use, a structural investigation was carried out.

Thermogravimetric analysis (TG) was used to determine the amount of DCE molecules embedded in the mordenite framework, and to monitor the decomposition process of organic molecules during the heating procedure. The TG curve of the MOR-DCE shows a sudden change in its slope at about 90 °C, thus indicating the presence of molecules which are weakly bonded to the surface

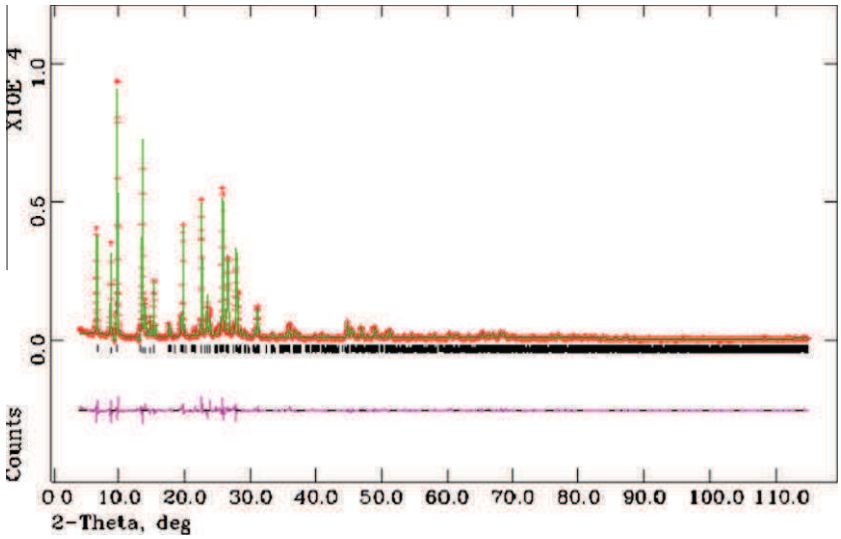

Fig. 3. The observed (red), calculated (green), and difference (pink) profiles of MOR-DCE. (For interpretation of the references to colour in this figure legend, the reader is referred to the web version of this article.)

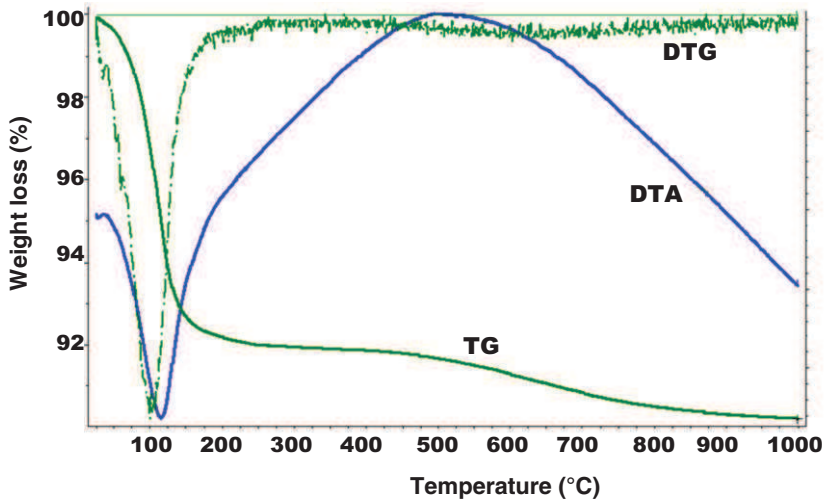

Fig. 4. Thermogravimetric (TG), differential thermogravimetric (DTG) and differential thermal (DTA) curves in mordenite after DCE-dry air atmosphere adsorption.

(water and/or DCE). The weight loss which occurred at higher temperatures (temperature range 200–700 °C), could indicate the decomposition and elimination of the organic molecules embedded in the mordenite channel system. Weight loss at 1000 °C is about 10% (see Fig. 4) in comparison to 7% of the as-synthesised material at the same temperature [27]. The question is, whether this variation is really due to DCE adsorption, which remarkably or completely substitutes H_2O in the as-synthesised material, or to a trapping of further water molecules from the aqueous solution.

A comparison of the X-ray diffraction patterns of as-synthesised (MOR) and mordenite after DCE adsorption (MOR-DCE) shows relevant differences both in the intensity and position of the diffraction peaks (Fig. 6), indicating that the mordenite crystal structure was markedly modified by the DCE adsorption experiment. Rietveld structure refinement indicated a small but significant increase of unit cell parameters in comparison to those of the untreated material (see Table 1) and revealed a relevant modification in the channel system (see Fig. 7). The 12-membered ring strongly increased and its Crystallographic Free Area (C.F.A.) *sensu* Baerlocher et al. [68] became 35.9 $Å^3$ as compared with the 33.0 $Å^3$ C.F.A. of the untreated mordenite. This increase was remarkably compensated by a decrease in the 8-membered ring (C.F.A. = 10.4 $Å^2$ in MOR-DCE, 11.8 $Å^2$ in MOR). These results clearly indicated that the increase in weight loss resulting from the DCE adsorption experiment was not only due to the trapping of other water molecules from the aqueous solution but also to a remarkable modification in the extraframework content, i.e. to the adsorption of a significant amount of DCE molecules.

The difference Fourier map generated using the GSAS package, revealed the presence of a number of extraframework ions inside the 12-ring channel. The two largest peaks in the difference Fourier map were attributed to chlorine atoms of encapsulated DCE molecules (Cl1 and Cl2 in Tables 2 and 3). With this assumption, it was easy to localise a third peak to be attributed to a carbon atom (C in Tables 2 and 3). Moreover, using this assumption, reasonable values were also obtained for C–C and C–Cl bond distances in the DCE molecule. The geometry of the DCE molecule, which was very near to ideal, as well as the very similar occupancy values (around 30%) and isotropic displacement parameters (Uiso ≈ 0.15 A^3) obtained for the carbon and chlorine atoms confirmed that the observed peaks had been correctly attributed to the DCE compound. Fig. 8 shows the location of these sites in the *Cmcm*

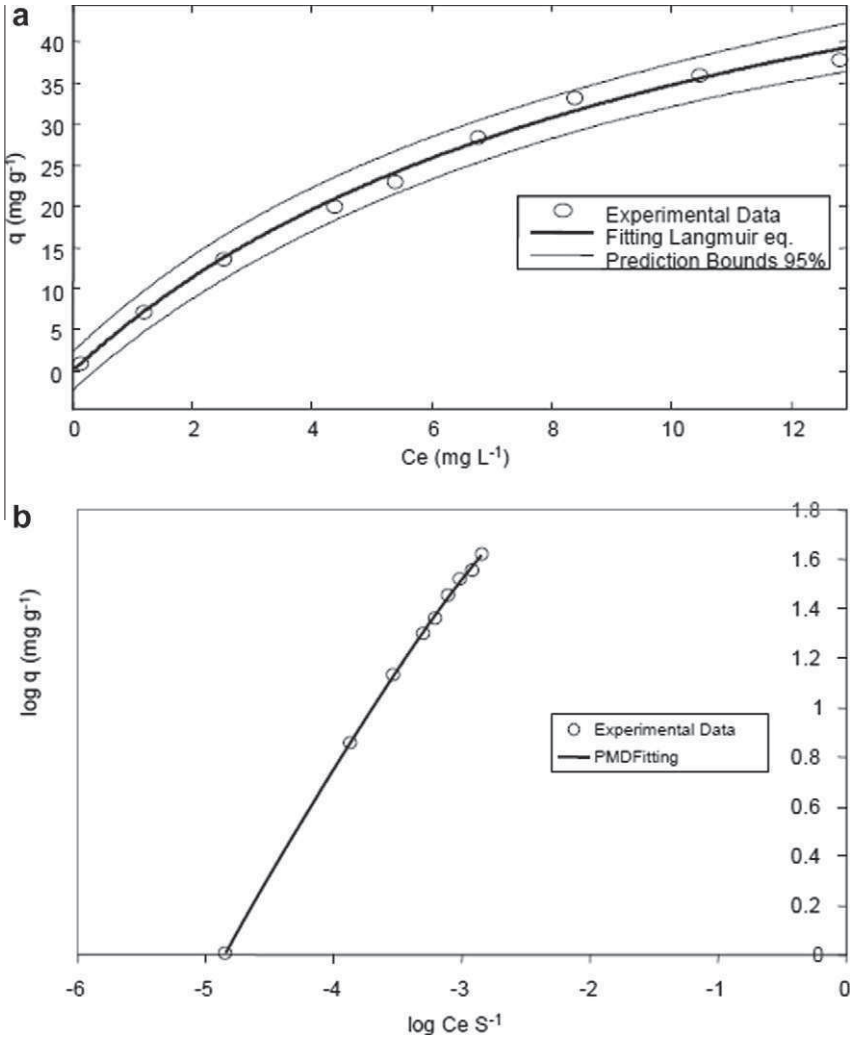

Fig. 5. Adsorption isotherm of DCE on MOR: Circle symbols: measured equilibrium concentrations; (a) solid line: fitted Langmuir equation; dashed lines: 95% confidence prediction bounds. (b) Solid line: fitted PMD equation.

Table 4
Fitting isotherms parameters obtained by fitting the experimental data in Fig. 5. The confidence limits at 95% of probability are reported in parentheses.

Langmuir			
K_L (L mg^{-1})	q_S (mg g^{-1})		R^2
0.09	71		
(0.065, 0.12)	(59, 84)		0.9942
Freundlich			
K (mg g^{-1})(L g^{-1})^n	n		R^2
7.9	1.6		
(6.0, 9.7)	(1.3, 1.8)		0.9832
PMD			
V_0 (cm^3 kg^{-1})	E (kJ mol^{-1})	b	R^2
62.5	18	4	0.9914
(49.4, 74.0)	(11, 26)		

space group. If Cl atoms only occupy Cl1 or Cl2 sites (referred to as "trans1" and "trans2", respectively in Fig. 8) DCE occurs in *trans*-configuration. Trans1 and trans2 configurations are not constrained by symmetry elements, so that only one of these could be present. However, the very similar occupancy levels for the Cl1 and Cl2 sites (Table 2) exclude this possibility. The dihedral angle between the Cl–C–C–Cl atoms, commonly referred to as ϕ, is 180°. On the contrary, when the Cl1 and Cl2 sites are contemporarily occupied, DCE occurs in *gauche*-configurations. The presence of symmetry elements of the *Cmcm* space group (inversion centre at ½, ½, ½ and diad at *x*, ½, ½) imposes the presence of two *gauche*-configurations, which are obviously not occupied at the same time, and are referred to as gauche1 and gauche2, respectively in Fig. 8. The dihedral angle between the Cl1–C–C–Cl2 atoms, is 60°. In conclusion, Rietveld structure refinements of exhausted mordenite, did not demonstrate whether only *trans*- or *gauche*-configurations were present or if both were present in different frequencies. Consequently, X-ray diffraction does not give a clear indication on the most favoured DCE configuration in mordenite structural confinement, but this is beyond the scope of this work. As reported previously, the occupancy of Cl and C atoms is only 30%, and consequently, DCE molecules, whatever their configuration, alternate randomly with non-occupied positions. Fig. 8 shows that DCE molecules run parallel to the *c* direction, i.e. along the 12-ring channel.

In MOR-DCE, the DCE molecule distance from the framework oxygens is larger than 3.5 Å, thus indicating the absence of electrostatic interaction with the framework. Only a few examples of molecule-framework contacts in zeolite or layered materials have been reported [[69] and references therein]. Most of them concern systems where the guest molecules are usually the templates used during the synthesis (often amine). When the guest molecules are introduced after synthesis, they are frequently disordered

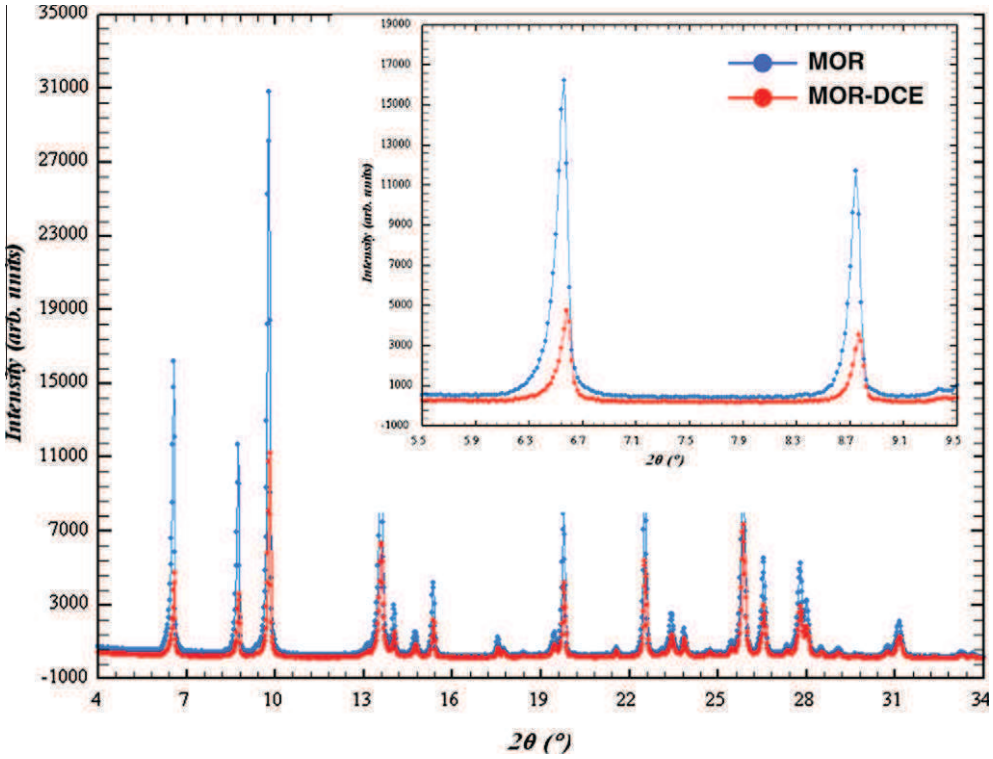

Fig. 6. Observed powder diffraction patterns of MOR (blue line), and MOR-DCE (red line), at low and intermediate 2θ angles, showing strong differences both in the intensity and position of the diffraction peaks. (For interpretation of the references to colour in this figure legend, the reader is referred to the web version of this article.)

12-RING	MOR	MOR-DCE
O10-O10	5.74(1)	6.10(1)
O2-O2	6.14(1)	6.17(1)
O3-O3	6.91(1)	7.17(1)
O7-O7	7.15(1)	7.59(1)
8-RING	MOR	MOR-DCE
O7-O7	5.41(1)	5.08(1)
O9-O9	3.01(1)	2.76(1)
O1-O1	3.20(1)	3.09(1)

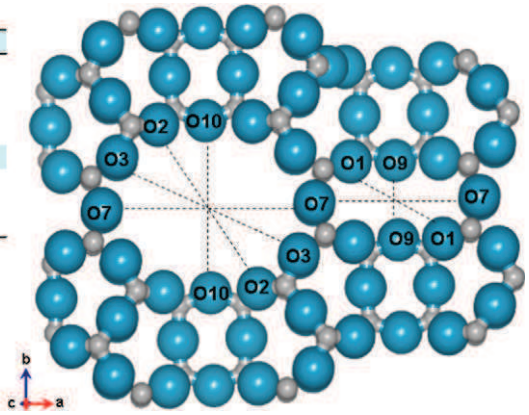

Fig. 7. Free diameter (Å) of the 12- and 8-ring channels of MOR and MOR-DCE, viewed normal to [001]. Oxygen is assumed to have an ionic radius of 1.35 Å.

and, when localised, establish interactions with framework oxygen atoms which can be classified as medium to weak [[27] and references therein]. In particular, Porcher et al. [69] determined the crystal structure of mordenite after the inclusion of *p*-*N*,*N*-dimethylnitroaniline using synchrotron powder diffraction and showed that the guest molecules are located in the large 12-membered ring channel at the intersection with the 8-membered channel and form hydrogen bonds with the framework oxygens which delimitate the channels. The 12-membered-ring channels also host both thionin blue [49] and methylene blue molecules [54] which interact with the framework and show a strongly disordered arrangement.

The difference-Fourier map revealed the presence of a further extraframework site which was attributed to water molecules (W site). This site has a slightly higher level of occupancy than that of the organic molecules (Table 2). The importance of this W site is immediately clear: the distance of the oxygen atom in the water molecule from the organic molecule chlorine atoms (W–Cl1 = 2.34 Å, W–Cl2 = 2.53 Å, see Table 3) suggests that different DCE molecules could be connected by means of hydrogen bonds through W to form a complex of DCE and water molecules independently by *gauche* or *trans* DCE sequencing.

On the whole, 2.5 DCE molecules (which correspond about to 7.7% in weight) and approximately 4 water molecules (which correspond to approximately 2.3% in weight) were localised inside the mordenite channel system. Therefore, the structure refinement gave an extraframework content of about 10% in weight, which was in very good agreement with the weight loss given by TG analysis and with the saturation capacity determined by the adsorption isotherm.

To summarise, Rietveld refinement revealed a relevant level of incorporation of DCE molecule incorporation in the mordenite

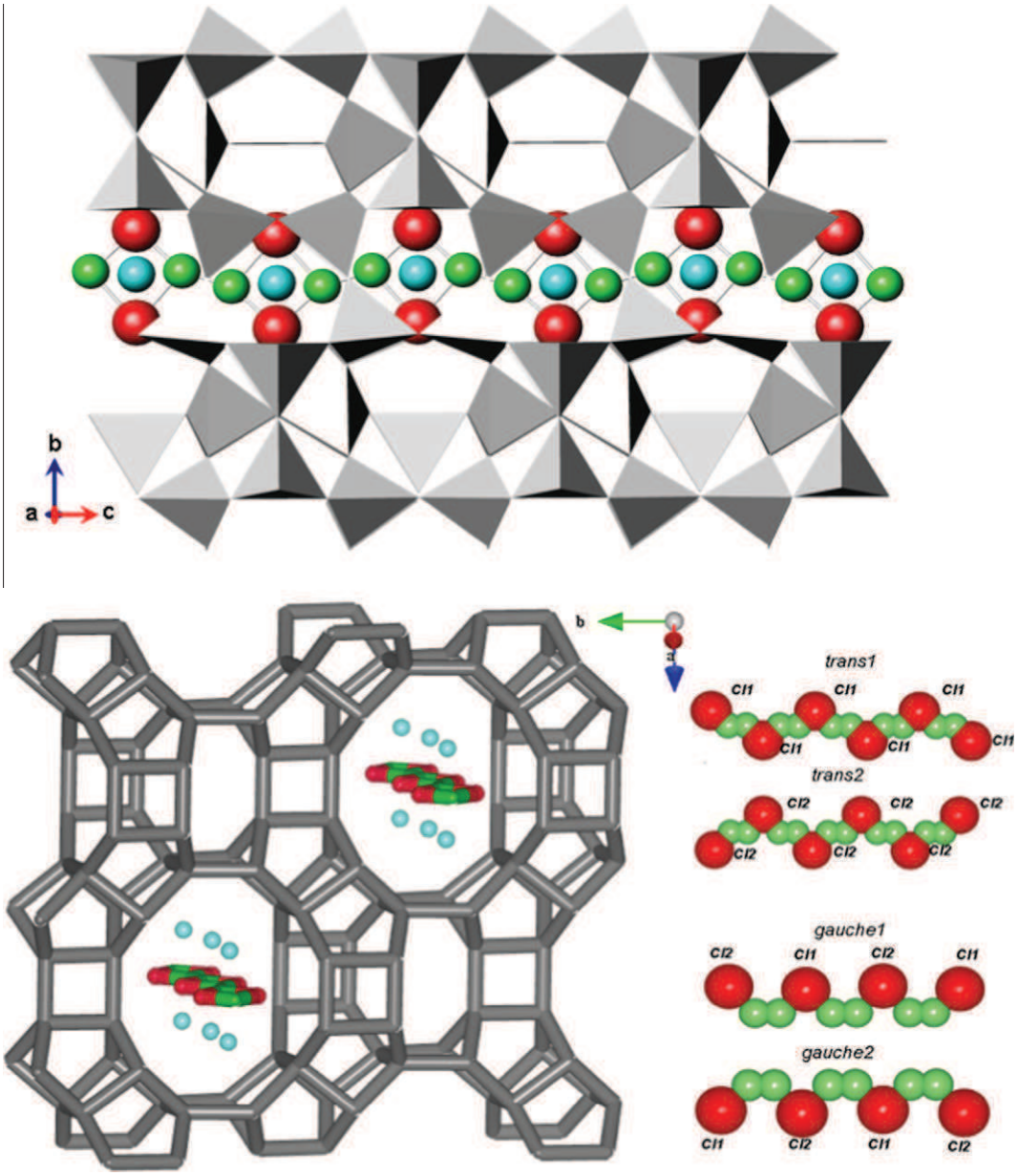

Fig. 8. MOR-DCE projections along [100] (top) and [001] (bottom) showing DCE (Cl represented with red, C with green spheres) and water molecules (with blue spheres) which run parallel to the *c* direction, i.e. along the 12-ring channel. (For interpretation of the references to colour in this figure legend, the reader is referred to the web version of this article.)

structure which caused a remarkable increase in the dimensions of the 12-membered ring where the DCE molecules were hosted (see Fig. 7 for details) when compared with those found in the parent zeolite. This clearly indicates that both *gauche*- and *trans*-conformers can be present. Wang and Huang [70] found that the *anti* or *trans* rotational conformer of 1-Bromo-2-chloroethane in organophilic silicalite-1 and siliceous Y zeolites prevails at room temperature, whereas the *gauche* conformer is the dominant conformer in hydrophilic L and Na-Y zeolites. Since 1-bromo-2-chloroethane differs from DCE only by one Br atom and consequently, has a lower dipole moment and higher steric hindrance, it seems reasonable to assume a *trans* (*anti*) conformation for DCE in MOR. Moreover, a *trans* DCE conformer is favoured in other organophobic zeolites such as ferrierite and L zeolites [71].

From the structure refinement, it is thus evident that DCE can penetrate micropores, giving an indication that PDM isotherm models should be employed to fit the adsorption data. Moreover, this structural investigation can also explain the fact that the PDM model underestimates the adsorption capacity in comparison with that calculated from the solute density and adsorbent pore volume, especially as this finding has already been found in other studies [71]. Indeed, from the structural investigation, it appears that DCE cannot completely displace water from the micropores.

4. Conclusions

In this study, we investigated the adsorption process of 1,2-dichloroethane in an organophilic zeolite mordenite. A combined diffractometric, thermogravimetric, adsorption and gas chromatographic approach enabled clear evidence of DCE adsorption in the mordenite channel system to be obtained as well as to be localised

the exact position occupied by the organic species in the structure. Rietveld refinement revealed the incorporation of 2.5 DCE molecules and approximately 4 water molecules per unit cell inside the mordenite channel system (about 10% in weight), in very good agreement with the weight loss given by TG analysis and with the saturation capacity which was determined from the adsorption isotherm. The water molecule oxygen atom distances from the organic molecule chlorine atoms (W–Cl1 = 2.34 Å, W–Cl2 = 2.53 Å) suggest that different DCE molecules could be connected by means of hydrogen bonds through W, to form a complex of DCE and water molecules independently by *gauche* or *trans* DCE sequencing.

The relevant incorporation of DCE molecules in the mordenite structure causes distortions of the 12-membered ring, where DCE are hosted, when compared to the parent zeolite. Structure refinement does not give clear indications as to whether only one or both *gauche*- and *trans*-conformers are present. Nevertheless, according to the results reported on 1-bromo-2-chloroethane in organophilic other zeolites [70] at room temperature, it is reasonable to assume a *trans* (*anti*) conformation for DCE in MOR.

Acknowledgment

The authors wish to thank Eni spa for their financial support. This work was also supported by PRRIITT (Emilia Romagna Region) misura 4 azione A.

References

[1] H. Muller, B. Deller, B. Despeyroux, E. Peldszud, P. Kammerhofer, W. Kuhn, R. Spielmannleitner, M. Stoger, Catal. Today 17 (1993) 383–390.
[2] T.D. Hylton, Environ. Progr. 11 (1992) 54–57.
[3] R. Vignola, U. Cova, F. Fabiani, G. Grillo, R. Sbardellati, R. Sisto, Stud. Surf. Sci. Catal. 174 (Part 1) (2008) 573–576.
[4] R. Vignola, G. Grillo, R. Sisto, G. Capotorti, P. Cesti, M. Molinari, in: G.A. Boshoff, B.D. Bone (Eds.), Permeable Reactive Barriers, IAHS Publ 298, 2005, pp. 105–109.
[5] M.L. Occelli, H.E. Robson, Zeolite Synthesis, ACS Symposium Series American Chemical Society, Washington, DC, 1989.
[6] R. Vignola, R. Bagatin, A. De Folly D'Auris, C. Flego, E. Previde Massara, M. Nalli, R. Sisto, in: C. Colella, P. Aprea, B. De Gennaro, B. Liguori (Eds.), IZC-IMMS 2010, A. De Fedre, Napoli, 2010, p. 51.
[7] S. Mizushima, Y. Morino, S. Noziri, Nature 137 (1936) 945.
[8] I. Nakagawa, S. Mizushima, J. Chem. Phys. 21 (1953) 2195–2198.
[9] S. Mizushima, T. Shimanouchi, I. Harada, Y. Abe, H. Takeuchi, Can. J. Phys. 53 (1975) 2085–2094.
[10] G. Georgieva, T. Dudev, B. Galabov, J.R. Durig, Vib. Spectrosc. 3 (1992) 9–21.
[11] R.J. Sabharwal, Y. Huang, Y. Song, J. Phys. Chem. B 111 (2007) 7267–7273.
[12] J. Ainsworth, J. Karle, J. Chem. Phys. 20 (1952) 425–427.
[13] J.Y. Lee, N. Yoshida, F. Hirata, J. Phys. Chem. B 110 (2006) 16018–16025.
[14] N.A. Murugan, H. Ågren, J. Phys. Chem. B Lett. 113 (2009) 3257–3263.
[15] R.J. Sabharwal, Y. Huang, Y. Song, J. Phys. Chem. B 111 (2007) 7267–7273.
[16] M.W. Wong, M.J. Frisch, K.B. Wiberg, J. Am. Chem. Soc. 113 (1991) 4776–4782.
[17] B. Cohen, S. Weiss, J. Phys. Chem. 87 (1983) 3606–3610.
[18] E.G. Derouane, J. Mol. Catal. A Chem. 134 (1998) 29–45.
[19] M. Tajima, M. Niwa, Y. Fujii, Y. Koinuma, R. Aizawa, S. Kushiyama, S. Kobayashi, K. Mizuno, H. Ohuchi, Appl. Catal. B 9 (1996) 167–177.
[20] J.R. González-Velasco, R. López-Fonseca, A. Aranzabal, J.I. Gutiérrez-Ortiz, P. Steltenpohl, Appl. Catal. B 24 (2000) 233–242.
[21] E. Finocchio, C. Pistarino, S. Dellepiane, B. Serram, S. Braggio, M. Baldi, G. Busca, Catal. Today 75 (2002) 263–267.
[22] R. López-Fonseca, S. Cibrián, J.I. Gutiérrez-Ortiz, J.R. González-Velasco, Stud. Surf. Sci. Catal. 142 (2002) 847–854.
[23] R. López-Fonseca, J.I. Gutiérrez-Ortiz, J.L. Ayastui, M.A. Gutiérrez-Ortiz, J.R. González-Velasco, Appl. Catal. B: Environ. 45 (2003) 13–21.
[24] C. Colella, Stud. Surf. Sci. Catal., in: J. Čejka, H. van Bekkum, A. Corma, F. Schueth (Eds.), Introduction to Zeolite Science and Practice, third Rev.ed., Elsevier, Amsterdam, 2007, pp. 999–1035. No. 168.
[25] M.A. Anderson, Environ. Sci. Technol. 34 (2000) 725–727.
[26] I. Braschi, S. Blasioli, L. Gigli, C.E. Gessa, A. Alberti, A. Martucci, J. Hazard. Mater. 178 (2010) 218–225.
[27] A. Martucci, L. Pasti, N. Marchetti, A. Cavazzini, F. Dondi, A. Alberti, Micropor. Mesopor. Mater. 148 (2012) 174–183.
[28] H. Van Koningsveld, F. Tuinstra, H. Van Bekkum, J.C. Jansen, Acta Crystallogr. B 45 (1989) 423–431.
[29] D.H. Olson, G.T. Kokotailo, S.L. Lawton, W.M. Meier, J. Phys. Chem. 85 (1981) 2238–2243.
[30] G.D. Price, J.J. Pluth, J.V. Smith, J.M. Bennett, R.L. Patton, J. Am. Chem. Soc. 104 (1982) 5971–5977.
[31] H. Van Koningsveld, Acta Crystallogr. B 43 (1987) 127–132.
[32] Y. Yokomori, S. Idaka, Micropor. Mesopor. Mater. 28 (1999) 405–413.
[33] H. Van Koningsveld, J.C. van Jansen, Micropor. Mesopor. Mater. 6 (1996) 159–167.
[34] G. Reck, F. Marlow, J. Kornatowski, W. Hill, J. Caro, J. Phys. Chem. 100 (1996) 1698–1704.
[35] B.F. Mentzen, J. Appl. Crystallogr. 22 (1989) 100–104.
[36] K. Nishi, A. Hidaka, Y. Yokomori, Acta Crystallogr. B61 (2005) 160–163.
[37] A. Rossner, S.A. Snyder, D.R.U. Knappe, Water Res. 43 (2009) 3787–3796.
[38] D.R.U. Knappe, A. Rossner, S.A. Snyder, C. Strickland, American Water Works Association Research, Foundation, Denver, Colorado, 2007.
[39] A. Malka-Edery, K. Abdallah, Ph. Grenier, F. Meunier, Adsorption 7 (2001) 17–25.
[40] O.H. Tezel, D.M. Ruthven, D.L. Wernick, in: D. Olson, A. Bisio (Eds.), Proc. 6th Intern Conf Zeolites, Butterworth, Guildford, UK, 1984, pp. 232–241.
[41] A. Germanus, J. Kärger, H. Pfeifer, Zeolites 4 (1984) 188–190.
[42] C. Beauvais, A. Boutin, H. Fuchs, Adsorption 11 (2005) 279–282.
[43] T. Tsuda, B.-W. Lu, H. Sasaki, Y. Oumi, K. Itabashi, T. Teranishi, T. Sano, Stud. Surf. Sci. Catal. 154 (2004) 224–232.
[44] L.B. Sand, Molecular Sieves, Conference Papers, 1967, Society of Chemical Industry, London, 1968, pp. 71–77.
[45] V. Sanders, Zeolites 5 (1985) 81–90.
[46] F. Hamidi, A. Bengueddach, F. Di Renzo, F. Fajula, Catal. Lett. 87 (2003) 149–152.
[47] T. Armbruster, M.E. Gunter, in: D.L. Bish, D.W. Ming (Eds.), Reviews in Mineralogy and Geochemistry Natural Zeolites: Occurrence Properties Use, vol. 45, Mineralogical Society of America, Washington, 2001, pp. 1–67.
[48] A. Alberti, P. Davoli, G. Vezzalini, Zeit. Kristallogr. 175 (1986) 249–256.
[49] P. Simoncic, T. Armbruster, Am. Miner. 89 (2004) 421–431.
[50] W.J. Mortier, J.J. Pluth, J.V. Smith, Mater. Res. Bull. 10 (1975) 1319–1326.
[51] A. Martucci, G. Cruciani, A. Alberti, C. Ritter, P. Ciambelli, M. Rapacciuolo, Micropor. Mesopor. Mater. 35–36 (2000) 405–412.
[52] A. Martucci, M. Sacerdoti, G. Cruciani, C. Dalconi, Eur. J. Miner. 15 (2003) 485–493.
[53] J.L. Schlenker, J.J. Pluth, J.V. Smith, Mater. Res. Bull. 14 (1979) 751–758.
[54] P. Simoncic, T. Armbruster, Micropor. Mesopor. Mater. 71 (2004) 185–198.
[55] H. Wang, Y. Huang, Langmuir (2009) 8042–8050.
[56] A. Boultif, D. Louër, J. Appl. Crystallogr. 24 (1991) 987–993.
[57] A.C. Larson, R.B. Von Dreele, General Structure Analysis System (GSAS), Los Alamos National Laboratory Report LAUR, 2000, pp. 86–748.
[58] B.H. Toby, J. Appl. Crystallogr. 34 (2001) 210–213.
[59] P. Thompson, D.E. Cox, J.B. Hastings, J. Appl. Crystallogr. 20 (1987) 79–83.
[60] M. Jaroniec, R. Madey, Physical Adsorption on Heterogeneous Solid, Studies in Physical and Theoretical Chemistry, vol. 59, Elsevier, Amsterdam, The Netherlands, 1988, pp. 317–341.
[61] M. Manes, in: R.A. Meyers (Ed.), Encyclopedia of Environmental Analysis and Remediation, John Wiley, New York, 1998, pp. 26–68.
[62] R.M. Allen-King, P. Grathwohl, W.P. Ball, Adv.Water Res. 25 (2002) 985–1016.
[63] http://www.inchem.org/pages/sids.html.
[64] S. Kleineidam, C. Schüth, P. Grathwohl, Environ. Sci. Technol. 36 (2002) 4689–4697.
[65] S.W. Davis, S.E. Powers, J. Environ. Eng. 126 (2000) 354–360.
[66] G.R. Parker, Adsorption 1 (1995) 113–132.
[67] A. Giaya, R.W. Thompson, R. Denkewicz, Micropor. Mesopor. Mater. 40 (2000) 205–218.
[68] Ch. Baerlocher, L.B. McCusker, D.H. Olson, Atlas of Zeolite Framework Types, sixth Rev ed., Elsevier, Amsterdam, 2007.
[69] F. Porcher, E. Borissenko, M. Souhassou, M. Takata, K. Kato, J. Rodriguez-Carvajal, C. Lecomte, Acta Crystallogr. B64 (2008) 713–724.
[70] J.H. Leech, H. Wang, C. Granger, T. Woo, Y. Huang, in: Proceedings of the 19th Int Conference on Raman Spectroscopy, ICORS, 2004, Gold Coast, Queensland, Australia, 8–13 August 2004. (http://www.publish.csiro.au/issue/1051.htm).
[71] E. Bi, S.B. Haderlein, T.C. Schmidt, Water Res. 39 (2005) 4164–4176.

The role of water in DCE adsorption from aqueous solutions onto hydrophobic zeolites

Luisa Pasti [*,‡], Annalisa Martucci [*,†], Marianna Nassi [‡], Alberto Cavazzini [‡], Alberto Alberti [†], Roberto Bagatin [§]

[‡] *Department of Chemistry, University of Ferrara, Via L. Borsari, 46, 44100 Ferrara, Italy*

[†] *Earth Sciences Department, University of Ferrara, Via G. Saragat 1, 44100 Ferrara, Italy*

[§] *Research Centre for Non-Conventional Energy - Istituto Eni Donegani Environmental Technologies Via Fauser 4, I-28100 Novara, Italy*

Title Running Head: The role of water in DCE adsorption onto hydrophobic zeolites.

[*]**Corresponding Authors:**

Luisa Pasti

Department of Chemistry, University of Ferrara, Via L. Borsari, 46, 44100 Ferrara, Italy

Tel. +39 0532 455346

Fax:+39 0532 240709

e-mail: luisa.pasti@unife.it

Annalisa Martucci,

Earth Sciences Department, University of Ferrara, Via G. Saragat 1, 44100 Ferrara, Italy

Tel. +39-532-974730

Fax. +39-532-974767

e-mail: mrs@unife.it

Abstract. In this study, we have investigated the adsorption processes of 1,2-dichloroethane (DCE) from aqueous solutions onto ZSM-5 and Y organophilic zeolites. The presence of this organic molecule in the zeolite channel systems was revealed by X-ray structure analyses carried out using the Rietveld method. Difference Fourier maps allowed us to determine the exact location of these DCE molecules, as well as that of the water molecules inside extraframework sites. Rietveld refinement revealed the incorporation of approximately 38 DCE molecules within Y and 5 in the ZSM-5 zeolites, respectively, which is in very good agreement with the weight loss given by TG analyses and with the saturation capacity determined by the adsorption isotherms. The distances between the oxygen atoms in the water molecules and the chlorine atoms in the DCE solutions suggest that different DCE molecules could be connected by means of hydrogen bonds through water, to form DCE-water complexes influencing the DCE *trans– gauche* conformational equilibrium. The presence of these complexes causes variations in unit cell parameters as well as remarkable framework deformations, clearly indicating that water strongly controls diffusion and adsorption processes in zeolite materials.

KEYWORDS: Water Remediation; Adsorption; Organophilic zeolites; 1,2-dichloroethane

1. Introduction

Chlorinated volatile organic compounds (VOCs) constitute a significant portion of hazardous air and water pollution [1]. Since many of them have been found to be toxic and potentially carcinogenic several treatment technologies based on advanced oxidation, air stripping, reverse osmosis, ultra filtration, and adsorption processes have been proposed for their removal from the environment. Recently, zeolites with good mechanical and hydrothermal stability have been employed as adsorbents for the removal of mono-aromatic molecules, such as BTEX (Benzene, Toluene Ethylbenzene, Xilenes) methyl tertiary butyl ether (MTBE) and halogen-benzene derivatives in water remediation [2]. Furthermore, it has been shown that zeolites are more effective in removing certain organic molecules from water than activated carbon [3-8] and are less sensitive than GAC to the presence of dissolved natural organic matter in the water stream being treated [9,10]. The adsorption of several organic pollutants onto zeolites has already been investigated in several works [1,11]. However, while gas phase system adsorption mechanisms have been deeply investigated for many organic compounds [12, 13], there is not yet a univocally accepted interpretation for the adsorption of organics from aqueous media, and indeed, those systems which have been studied (sorbate - zeolite) are relatively few. Adsorption from gas phase systems can significantly differ from that of corresponding aqueous solutions due to the highly polar nature of water molecules. In fact, it has been proved that interactions between water molecules and the zeolite framework are especially crucial in adsorption simulations [14, 15]. Consequently, to better simulate such systems more information on the adsorption sites and their interactions is required. Indeed, Krishna and van Baten [16] have demonstrated that the adsorption behaviour of water-alcohol mixtures on zeolites is markedly different from that of the respective pure components. These observed differences have been ascribed to the hydrogen bonds [16]. The authors suggested that estimating the adsorption and diffusion behaviour of water-alcohol mixtures using only pure component data on adsorption isotherms and diffusivities is impossible. Generally, it has been shown that large amounts of co-adsorbed water decreases the adsorption of unsaturated hydrocarbons such as ethylene and butene in zeolites [17-19].

Furthermore, this finding was confirmed by molecular simulation for hydrophilic silica micropores. On the contrary, the mobility of pyrene, naphthalene, butane, and trichloroethylene increases upon addition of small amounts of water to the zeolite, due to the attractive forces between water and organics [2, 20]. Likewise, the adsorption of water in silicalites seems to be controversial. In fact, it has been reported that para-cresol facilitates the penetration of water into silicalite-1 due to a cooperative phenomenon in the co adsorption process, [21], whereas Ref. [3] reports that the organophilic environment in the silicalite-1 pores brought about the concentration of VOC by preferential water exclusion. The adsorption mechanism of organics from aqueous solutions onto hydrophobic zeolites has also been interpreted on the basis of the displacement of loosely bound water molecules by organic compounds [22]. This explanation does not include any modifications in the crystalline structure of the adsorbent phase which, if considered, could modify the results of these studies. Recently, the effective adsorption of 1,2-dichloroethane (DCE) when dissolved in the aqueous matrix in highly siliceous mordenite (MOR) zeolite has been demonstrated and the position of this pollutant in the zeolite framework has been localized exactly by combining diffractometric and gas chromatographic techniques [23]. The authors have demonstrated that MOR adsorbed readily a relevant amount of DCE molecules at room temperature [23] and the adsorption into the pores modified significantly the unit cell parameters as well as the dimensions of the zeolite channel systems. DCE was studied as a VOCs adsorbate probe molecule since its *trans– gauche* conformational equilibrium has been one of the most frequently studied systems [24], mainly since the two conformers have different polarity. The DCE trans conformer is generally preferred in the gas phase due to its steric effect, which is basically one of exchange and Coulombic repulsion. However, in the liquid or polar solvent phase, such as in water, the gauche conformer is stabilized when compared to the trans conformer due to dipole-dipole interactions with neighbouring gauche species or polar solvent molecules [25-29].

In this work, an approach similar to that employed in Ref. [23], was employed to get a better understanding of the host–guest interactions which occur during the adsorption processes of organics

from aqueous solutions onto zeolites. In particular, we focused our investigation on: 1) the adsorptive properties of Y and ZSM-5 hydrophobic synthetic zeolites towards DCE, 2) the localisation and conformation of the organic species in the channel systems and 3) establishing the role of water in their adsorption process.

2. Experimental section

2.1 Materials. 1-2 Dichloroethane (purity 99.8%) and sodium chloride (purity 98%) were obtained from Sigma-Aldrich (Steinheim, Germany). The as-synthesised ZSM-5 sample is a hydrophobic commercial adsorbent, synthesised with SiO_2/Al_2O_3 equal to 280, and purchased in its ammonium forms (CBV28014, Zeolyst International). The Na_2O content was lower than 0.05 wt%. The Surface Area is 400 m^2/g. The as-synthesized Y zeolite powder (code HSZ-390HUA) with a 200 SiO_2/Al_2O_3 (mol/mol) ratio, was purchased in its protonated form from the Tosoh Corporation (Japan). The Na_2O content was lower than 0.1 wt%. The Surface Area is 750 m^2/g.

2.2 Gas Chromatography. The DCE concentration in the water was determined using a Gas Chromatography – Electron Capture Detector (GC- ECD). Prior to this, the DCE was extracted from the water sample by Head Space - Solid Phase Micro Extraction (HS-SPME).

The head space mode was used for DCE extraction from a sample volume of 10 ml of water in 25-ml glass flasks sealed with Teflon screw caps. 2 mL of a 300 g L^{-1} NaCl solution were added to the sample. Samples were immersed in a thermostatic water bath at 40 °C (±0.5 °C) and maintained under controlled agitation with a magnetic stirrer (300 rpm) for 10 min to equilibrate before SPME insertion.

The fibre was inserted into the GC injector for analysis and kept at 250 °C. The desorption time was 1 min. The GC used in this work was an HRGC 5160 MEGA SERIES Instrument (Carlo Erba, Mi, I) equipped with a split/splitless injector and an electron capture detector (ECD,^{63}Ni). A fused-silica

DB-5 capillary column (60 m X0.25 mm I.D:, 0.25 μm film thickness; J&W Scientific, USA) was employed. Helium (99.999%) was used as a carrier gas at a constant head pressure of 50 kPa and nitrogen (196KPa) was employed as a make-up gas at a constant flow-rate (1 mL min^{-1}). The detector temperatures was kept constant at 250°C. The GC oven was programmed as follows: 40°C (5 min), 5°C min^{-1} to 80°C (5 min), 30°C min^{-1} to 100°C (5 min).

The linearity of the method for quantitative analysis was tested by the evaluation of the calibration curves: standard solutions of DCE in MilliQ water were analysed at varying concentration levels in the range 0.1 to 30 ppm. Each concentration was analysed twice. The linearity range was evaluated, as well as the method detection limit (LOD) and computed from the calibration line. Good linearity was observed with a correlation coefficient of 0.993.

2.3 Adsorption Isotherm. An adsorption isotherm was determined using the batch method. Batch experiments were carried out in duplicate in 25 ml crimp top reaction glass flasks sealed with PTFE septa (Supelco, PA, USA). The flasks were filled in order to have the minimum headspace, a solid/solution ratio of 1:4 (mg mL^{-1}) was employed. After equilibration, (24 hours) at a temperature of 25.3 ± 0.5 °C under stirring, the solids were separated from the aqueous solution using centrifugation (10000 rpm for 30 min) and analysed by HS-SPME-GC as above described. The DCE concentration in the solutions was quantified at equilibrium conditions using the HS-SPME-GC technique.

2.4 Thermal analyses. Thermogravimetric (TG) and differential thermal analysis (DTA) measurements of the exhausted sample were performed in air at up to 900°C using an STA 409 PC LUXX® - Netzch at 10 °C/min heating rate. The thermal curves are reported in Figure 1.

2.5 X-ray Diffraction. Exhausted ZSM-5 and Y samples were prepared by repeating the batch adsorption steps on the same zeolite sample until the concentration of the solution in contact with the zeolites no longer changed. In particular, 1 g of zeolite was placed in a 2 L vessel and equilibrated,

(12 hours) at a temperature of 25.3±0.5°C under continuous stirring (400 rpm). The solids separated from the solution by filtration constituted the exhausted zeolite samples. The concentration of DCE in the aqueous solution was analyzed by HS-SPME-GC and this operation was repeated until the concentration of DCE in the solution no longer decreased after contact with the zeolite.

ZSM-5 and Y Powder patterns after DCE adsorption (ZSM-5-DCE and Y-DCE, respectively) were measured on a Bruker D8 Advance Diffractometer equipped with a Sol-X detector, using Cu $K_{\alpha 1, \alpha 2}$ radiation in the 3°-110° 2ϑrange and a counting time of 12 s/step. The GSAS [30] computer program with the EXPGUI interface [31] was used (see Table 1 for Rietveld refinement details) with atomic scattering factors for neutral atoms. Full matrix least-square refinements of exhausted zeolites were carried out in the P 2_1/n (for ZSM-5-DCE) and F d-3 (for Y-DCE) space groups, respectively.

In all the Rietveld structure refinements, the Bragg peak profile was modelled using a pseudo-Voigt function with 0.01% cut-off peak intensity. The background curve was fitted using a Chebyschev polynomial with 20 variable coefficients. The 2θ-zero shift was accurately refined into the data set pattern. The scale factor and unit-cell parameters were allowed to vary for all the histograms. The refined structural parameters for each data histogram were the following: fractional coordinates and isotropic displacement factors for all atoms (one for each tetrahedral site and framework oxygen atom), and occupancy factors for the extraframework ions. The occupancy factors and isotropic displacement factors were varied in alternate cycles. Soft constraints were imposed on the tetrahedral cations and coordinated framework oxygen atom distances during the first stages of refinement, and left free in the last cycles. The position of the C and Cl extra-framework atoms were determined with the help of difference Fourier maps. The C–C and C–Cl bond distances were constrained at 1.40 and 1.70 Å, respectively, in the first stage of refinement and set free in the final stages. Atomic coordinates, fractions and thermal factors are reported in Tables S1 and S2 (see Supplementary Information), respectively. Tetrahedral bond distances and angles are given in Tables S3, S4 and S5 (see Supplementary Information), respectively.

3. Results and Discussion

3.1 Adsorption Isotherms

DCE uptake onto ZSM-5 as a function of time is plotted in Fig. 2a. It can be seen that for the studied zeolite the adsorption process is fast: equilibrium concentration is reached in few minutes. The data were fitted by a pseudo second order model - as suggested by Azizian when initial concentrations are significantly lower than the saturation concentration [32, 33] - which is given by:

$$\frac{t}{q_t} = \frac{1}{k_2 q_e^2} + \frac{1}{q_e} t \qquad (1)$$

where q_t and q_e are the milligrams of solute sorbed per gram of sorbent at time t and at equilibrium, respectively, and k_2 is the second-order sorption rate constant. The equilibrium uptake and the adsorption rate constant, obtained from the slope and intercept of the linear fit of the data q_t/t vs. t, respectively, are reported in Table 2. Both pseudo first and second order equations are two extreme cases of a general rate equation when the initial adsorbate concentration is very high or very low respectively. The pseudo second order model has been applied in order to analyse sorption kinetics from the liquid solutions of many adsorption systems [34]. However, it should be mentioned that the pseudo second order equation, like other commonly employed relationships (e.g. the pseudo-first order, the pseudo-second order and the Elovich equations) does not correspond to one kinetic model only, but is a more or less flexible mathematical formula, which is able to simulate the behaviour characteristic of physical kinetic processes of various kinds only adequately well [35]. Moreover, the rate constant estimated from the fitting is a complex function of the initial concentration of solute [35]. In fact, it can be noticed in Table 2 that the k_2 estimation depends on the initial concentration value. An approximate estimation of the general rate constant $k_2' = k_2 C_0^n$ was evaluated by fitting. Similar results were also obtained using DCE onto Y adsorption kinetics (see Table 2).

The adsorption rate k_2' constants for DCE on Y and ZSM-5 are different (see Table 2), therefore it would seem that k_2' relates to zeolite structure and morphology.

Figure 3 a) shows DCE adsorption isotherms on ZSM-5 and Y, respectively. It can be seen that Y is less efficient in DCE removal from water solutions in the low concentration range (see Fig. 3 b). In fact, adsorption onto Y is low for the most dilute solutions. The data in the low concentration range follows a linear trend as is shown in Fig. 3 b. Similar adsorption behaviour for Y and ZSM-5 when compared to different organic molecules in both the liquid and gas phases, has already been observed, and reported in the literature [4, 20, 36-37], and different models have been employed to interpret this phenomenon. Essentially, for aqueous systems, this behaviour has been ascribed to the competitive role played by water molecules on the adsorption of organic compounds in the Y framework. It has already been shown that the presence of water vapour decreases TCE adsorption by up to 83% compared to dry conditions, and that this decrease in TCE adsorption was less than that observed for adsorption from bulk water solutions [20]. This latter effect has been explained by Giaya et al. [4] who demonstrated that the pore size and strength of fluid-wall interactions determine the density of water in adsorbent micropores. DAY (De Alluiminated Y) pores were shown to be sufficiently large to accommodate water with a liquid-like density when liquid water was present outside the pores, while silicalite-1 was not supposed to be able to assure the same interactions between water molecules in the pore. The adsorption data of DCE onto Y obtained in a wide range of concentrations shows (see Fig. 3a) a different trend when compared to DCE on ZSM-5. In Fig. 3a, it can be seen that the adsorption data on ZSM-5 follows an L-class or type I adsorption isotherm, whereas, the Y data follows an S-class or type V isotherm in line with the Giles [38] and IUPAC [39] classification, respectively.

The adsorption behaviour of water pollutants is generally studied in the low concentration range, close to that found in real applications [6]. However, in practical applications of adsorbent materials the whole working range should be explored. Generally, once adsorption equilibrium data

are obtained they should be represented by a specific mathematical model (i.e., an isotherm equation). This allows one to obtain physical parameters of a model used over a wide range of concentrations. Furthermore, an adsorption model is essential in calculating the breakthrough curve in adsorptive separation process simulations [40]. Type I data are typical for zeolite adsorption and can be fitted by different equations such as Langmuir, or heterogeneous extended Langmuir models, Freundlich, or Virial equations [41]. In such models, each zeolite cage is considered as an independent site or subsystem and the interaction between molecules in neighbouring cages is neglected [42]. Adsorption from dilute solutions into porous materials can be also described by the Polanyi-Dubinin-Manes (PDM) model [4], however, this model cannot adequately describe trichloroethylene-Y adsorption behaviour on wet Y zeolites [20]. Isotherm models can, in turn, be related to the interaction energy of solute-sorbent systems. Type I data for zeolites has been attributed to adsorption energy generated by the potential fields of the atoms in the walls of the nanopores, and are mainly fitted using Langmuir and Langmuir-Freundlich equations [41]. It can be seen that this is the case for the DCE-ZSM-5 system (Table 3). The data are also fitted using a bi-Langmuir isotherm type. The increase in the fitting goodness seems to be related to the increase in the numbers of parameters in the isotherm equation. However, these above mentioned models cannot fit S-shaped data because of a lack of flexibility in their mathematical formula. Moreover, deviations of DCE-Y data from L-class models, can occur due to differences in the adsorption mechanisms such as: site heterogeneity or to interaction between adsorbed molecules. It should be borne in mind that isotherm equations must reflect the physical processes involved rather than just fit the (complete) isotherm [43].

Type V data are uncommon for hydrophobic zeolites, as underlined in the article title by Halasz [44], dealing with adsorption of methanol on Y in the gas phase. Recently, type V isotherms were also found for paracresol-water systems [21] and for the adsorption of phenol and aniline derivates from aqueous solutions onto Y [36]. For the above mentioned cases, different explanations have been provided: the microporous structure and network force field were proposed as explanations in [44], whereas hydrogen bonds between organic and water molecules were hypothesized in [21], and

hydrogen bonding between zeolite framework oxygen and organic molecules have been invocated in [36]. The formation of hydrogen bonds between water and alcohol molecules have also been recently reported by Krishna and van Baten [16]. The above mentioned works have investigated different molecules and have obviously arrived at different interpretations. Therefore, it can be argued that the interaction mechanism is still a matter of debate [41]. For a general adsorbent material, sigmoidal isotherms have previously been observed as a result of lattice expansion and polymorph switching in porous materials, guest rearrangements in rigid hosts, and in the cooperative binding of substrates to proteins [45]. For porous adsorbents, the adsorption data were fitted using Fowler –Guggenheim, and Ruthven models (see Table 3), this former has recently been employed to fit the adsorption of aromatics onto Y zeolite [36]. The assumptions underlying the Fowler model are that adsorbed molecules form a localized monolayer on an energetically homogenous surface and that each adsorbed molecule interacts with a limited number of other adsorbed molecules distributed randomly on the nearest-neighbour sites. The Ruthven model has been suggested to account for adsorbate-adsorbate interactions in the zeolite cage [42]. For the DCE-Y system there is no clear evidence for the model choice. In fact, it should be considered that a comparison of isotherm models based on the fitting goodness is not always significant in interpreting adsorption mechanisms. Moreover, it is sometimes possible to obtain more than one model which accurately describes the experimental data, and it is not always possible to distinguish which model to use on the basis of thermodynamic analyses [42].

In conclusion, further investigations are required to elucidate adsorption mechanisms. Several approaches can be followed to accomplish this task, one of which consists in localising the molecules in the framework. The main advantage of structural investigations is that they furnish a visual result of the experimental data without requiring an ‘a priori’ hypothesis to be formulated.

3.2 Thermogravimetric and structural analyses.

3.2.1 Y zeolite.

This zeolite (FAU-type framework topology [46]) is of the utmost importance in heterogeneous catalysis [47]. Its pore structure is relatively spacious and is characterized by cuboctahedral sodalite cages (β-cages), which are linked together by hexagonal prisms to form large cavities referred to as "supercages", with a diameter of approximately 12 Å (Figure 4a). Each supercage is joined to four others via circular windows that are delimited by 12 rings of tetrahedra with a free diameter of about 7.5 **Å.** Zeolite Y is therefore classified as possessing a three-dimensional, 12-membered-ring pore system.

Thermogravimetric analysis (TG) was used to determine the amount of DCE molecules embedded in the Y framework, and to monitor the decomposition process of organic molecules during the heating procedure. The TG curve of the Y-DCE (Figure 1) showed that, apart from the elimination of residual humidity (T<100°C, weigh loss (7%), a sudden change in its slope occurs at higher temperatures, which is probably due to the elimination of DCE and/or H2O molecules trapped within the zeolite pores. Total weight loss at 900°C is about 27.7.% compared to 1.8 % in the as-synthesized sample [23].

The question is, whether this variation is really due to DCE adsorption, which remarkably or completely substitutes the H_2O in the as-synthesised material, or to the trapping of further water molecules from the aqueous solution, even if this last hypothesis appears improbable considering the hydrophobicity of the studied zeolite.

In order to verify the effective incorporation of DCE in Y-porosities, powder diffraction data were analyzed. A comparison of the X-ray powder diffraction patterns of Y zeolite before and after DCE adsorption clearly highlighted that the peak intensities in the two patterns are markedly different mainly in the low 2θ region (Figure 5a). This effect is typical of structural modifications, in particular (it indicates an) increased disorder, in the extraframework region. At the same time, the diffraction positions in the two patterns are slightly different. Rietveld structure refinement revealed that DCE adsorption caused a lowering in real *Fd-3m* symmetry in the parent Y zeolite [8] to *Fd*-3 and a remarkable increase in unit cell volume (Y-DCE: a =b=c= 24.2767(6) Å Cell volume = 14307.6(6) $Å^3$

Table 1) in comparison to those of the untreated materials (a=b=c= 24.259(4) Å, Cell Volume= 14277.1(4) $Å^3$ [8]). At the same time, the opening of the zeolite framework pore system strongly increased (see Figure 6) and consequently, its Crystallographic Free Areas (C.F.A.) *sensu* Baerlocher [46] also increased when compared with the as-synthesized materials. These results clearly indicated that the increase in weight losses resulting from both the adsorption experiments and TG analyses were not only due to the trapping of additional water molecules from the aqueous solution but also to a strong modification in the extraframework content, i.e. to the adsorption of a significant amount of DCE molecules.

According to both the TG and adsorption data, Rietveld refinement confirmed the most relevant level of incorporation of DCE molecules in the Y zeolite. The difference Fourier maps generated using GSAS package [30], revealed the presence of the largest peak in the difference Fourier map which was attributed to chlorine atoms of encapsulated DCE molecules (see Table 4). With this assumption, it was easy to localise the peak corresponding to the carbon atoms (Table 4). The location of DCE molecules and the symmetry elements for the *Fd-3* space group imposes the presence of both *trans*-and *gauche*-configurations (Figure 7). Consequently, X-ray diffraction does not give any clear indication of the most well-favoured DCE configuration and both *trans*-and *gauche*-configurations seem to be possible.

The partial occupation of DCE molecule sites (0.43 of occupancy, see Table S1), giving a total of about 38 DCE/u.c (corresponding to about 24.3% in weight). Two further extraframework sites were localised, and attributed to water molecules (W1 and W2 sites, respectively, corresponding to a total of about 12 H_2O/u.c (and to about 1.4% in weight).

The distances between water molecules from the organic molecule chlorine atoms (Table 4 and Figure 8) indicate that different DCE molecules could be connected by means of hydrogen bonds through W1, to form a DCE-water molecules complexes (clusters or short chains). Moreover the W2-Cl bond distance suggests that DCE molecules are connected to framework oxygens through W2 (Figure 8) thus justifying the symmetry lowering as well as the deformations of the 12-ring channel

systems (Figura 7). The presence of DCE and water molecules complexes was recently observed in organophylic mordenite by Martucci et al.[23]: in that case, the distances between water molecules from the framework oxygens suggest that these complexes strongly interact with the framework, thus justifying the lowering in symmetry as well as the deformations in the 12-ring mordenite channel systems. An analogous behaviour was also found for Y zeolite, as explained before. The complexation of water molecules with organic compounds via hydrogen bonding was also predicted by theoretical calculations and confirmed by spectroscopic studies [48-53].

3.2.2 ZSM-5

The zeolite (MFI-type framework topology [46]) is probably one of the most widely studied zeolites. The MFI framework pore structure system consists in two intersecting sets of tubular channels, a linear one parallel to the [010] direction, with an opening of about 5.4 -5.6 Å, and a sinusoidal one parallel to the [100] direction, with an opening of 5.1 -5.5 Å [46] (Figure 4b-c). These channels are delimited by 10-membered rings of TO_4 tetrahedra. From the crystallographic point of view, all synthetic MFI zeolites show a polymorphic orthorhombic-to-monoclinic phase transition. The polymorphism mechanism is complex and depends on the Si/Al ratio, the defect density of the tetrahedral framework, the temperature, the synthesis conditions, the nature and the amount of extra-framework (i.e. nature of sorbate), post synthesis treatment (calcination, ion exchange, etc) and the loading/unloading of organic molecules [54-55]. At room temperature, the as-synthesized samples of hydrogen free MFI type materials are orthorhombic, with a P*nma* space group, whereas the hydrogen-containing ZSM-5 are monoclinic $P2_1/n$ [54-55]. The orthorhombic form can also be stabilized by the insertion of structural defects [56] or by the absorption of organic molecules such as benzene [57], aniline, or naphthalene in the channels [58]. In particular, low loading ZSM-5 (4 or less sorbate per unit cell) are orthorhombic P*nma* or P$n2_1a$ (i.e. 2.6*p*-dichlorobenzene, *p*-nitroaniline3.7-ZSM-5, naphtalene3.7-ZSM-5), whereas high loading ZSM-5 (over 4 sorbate per unit cell) are orthorhombic *P* $2_12_12_1$ (i.e. 8 p-xylene, 8 *p*-dichlorobenzene and 6.4 toluene [54 59 60]. Orthorhombic *Pnma*

symmetry was also found in mutinaite, the natural counterpart of ZSM-5 [61]. According to the literature, our H-ZSM-5 sample is monoclinic, space group $P\,2_1/n$ (Table 1).

Also for ZSM-5, strong differences in both the positions and intensity of diffraction peaks were detected after DCE incorporation throughout the 2θ range under investigation, when compared to the as-synthesized material, thus indicating strong structural rearrangement (Figure 5b).

The most probable symmetry may still be considered monoclinic, with the $P2_1/n$ space group. Rietveld refinement of the unit cell parameters indicated small but significant variations in comparison to those of the untreated material (ZSM-5-DCE: a= 20.117(1) Å, b= 19.899(1) Å, c= 13.389(1) Å, α = 90.55(1), Cell volume= 5359.9(1) $Å^3$; untreated ZSM-5 a= 20.109(1) Å, b= 19.897(1) Å, c= 13.380(1) Å, α= 90.54(1), Cell volume = 5353.3(3) $Å^3$). The α values as well as a/b and a/c unit-cell parameter ratios confirm the assumption of the monoclinic symmetry [54] of ZSM-5 before (a/b=1.0106, a/c= 1.577) and after DCE adsorption (ZSM-5-DCE) (a/b=1.011, a/c=1.503).

Two crystallographically independent DCE sites were located in the structure of ZSM-5, one (DCE1) (Figure 9a), the other in the sinusoidal 10-ring channel parallel to [100] direction (Figure 9b). The sorbate molecules located near the channel-intersections are isolated one from each other and do not present any interactions through the straight-channels thus confirming the monoclinic symmetry [56].

According to our results, all DCE molecules assume a *trans* (anti) configuration. The DCE molecules display planar geometry, which was very near to ideal, with C–C–CL angles of about 114°. The very similar values for the occupancy and isotropic temperature factor obtained for carbon and chlorine atoms confirmed that the observed peaks were correctly attributed to the ZSM-5-DCE compound. All sites are partially occupied, giving a total of about 5 DCE/u.c (which correspond to about 8% in weight). No short distances between C and Cl atoms and framework oxygens were observed (Table 4).

Two further extraframework sites have been localised, and were attributed to water molecules (W1 and W2 sites, respectively). On the basis of the occupancies, the water content corresponds to a

total of about 5 H_2O/u.c (and to about 1.4% in weight (Table S2). On the whole, the amount of DCE and H_2O obtained from Rietveld refinement is in very good agreement with that reported from TG weight loss at 900°C (Figure 1).

In ZSM-5, the short distances between the W2 water molecules from the framework oxygens and DCE1 molecules suggest that these complexes strongly interact with the framework, thus justifying the deformations in the 10-ring channel systems (Figure 10). The relevant incorporation of DCE molecules in the ZSM-5 structure is confirmed by a change in the dimension of the ten-membered rings, when compared to the parent zeolite (see Figure 11 for details). To note that DCE1 and DCE2 molecules are connected to each others through W1 (Figure 10). As can be clearly seen, the ring shapes became more elliptical when compared with those found in the parent zeolite ZSM-5 as a consequence of the strong interaction between DCE-water molecules complexes and framework oxygens. Therefore, ZSM-5 is able to adsorb water molecules, and this adsorption modifies the zeolite structure.

4. Conclusions

In the present work, it is shown that after the adsorption of organic molecules from aqueous solutions on zeolitic materials, strong framework distortions occur depending on the flexibility and/or the accessibility of the channel systems to the host molecules. These remarkable deformations can be explained on the basis of the presence of DCE- water complexes which strongly interact with framework oxygens via hydrogen bonding. A similar result was recently observed in organophilic mordenite after DCE adsorption [23].

All of these findings are important features in the adsorption process and suggest that: a) framework flexibility was found to be insignificant for the adsorption of n-alkane on silicalite-1 and that generally, it influences transport properties to a lesser degree than thermodynamic properties. However, recently it has been shown that adsorption of VOC on MFI zeolites is affected by structural

changes [41]. Therefore, flexibility in the framework should be included in modelling adsorption to correctly interpret the experimental findings. b) Water molecules inside the porous framework lead to a multicomponent system being considered instead of a single component adsorption mechanism. Water effects cannot be neglected, especially when hydrogen bonds are involved. c) Conformational selection in DCE on ZSM-5 has been observed and is probably due to an energy landscape which has been defined by DCE low energy torsional motion in the zeolite channels.

In conclusion, for DCE adsorption onto hydrophobic zeolites regardless of the framework type, isotherm modelling and/or simulation algorithms should be implemented to take system complexity into account.

5. Acknowledgements

The authors wish to thank Eni spa for the financial support. This work was also partially supported by MIUR project PRIN 2009 grant N. 2009ZSC5K2_004. Thanks to Georgia Emma Gili for the revision of the English language.

References

[1] A. R. Gavaskar, B. C. Kim, S. H. Rosansky, S. K. Ong and E. G.Marchand, Environ Prog. 14 (1995) 33–40.

[2] R. Vignola, R. Sisto, G. Grillo, U. Cova, P. Cesti, US2009/0014390 A1 Patent, (2009)

[3] L. Abu-Lail, J. A. Bergendahl, R. W. Thompson, *J. Hazard. Mater.* 178 (2010**)** 363-369.

[4] A. Erdem-Senatalar, J. A. Bergendahl, A. Giaya, R. W. Thompson, Environ. Eng. Sci. 21 (2004**)** 722-729.

[5] A. Rossner, D. R. U. Knappe, Water Res. 42 (2008**)** 2287-2299.

[6] M. A. Anderson, Environ. Sci. Technol. 34 (2000**)** 725-727.

[7] I. Braschi, S. Blasioli, L. Gigli, C. E. Gessa, A. Alberti, A. Martucci , J. Hazard. Mater. 178, (2010) 218–225.

[8] A. Martucci, N. Marchetti, A. Cavazzini, F. Dondi, A. Alberti, L. Pasti, in press, doi:10.1016/j.micromeso.2011.07.009.

[9] D. Z. Chen, J. X. Zhang, J. M. Chen, Int. J. Environ. Sci.Tech. 7 (2010**)** 235-242.

[10] A. Giaya, R. W. Thompson, R. W., R. Denkewicz Jr., Micropor. Mesopor. Mat. 40 (2000**)** 205-218.

[11] S. S. Rayalu, S. U. Meshram, R. B. Biniwale, A. Srivasatava, P. D. Jadhav and S. Devotta, Res. Commun. 91(4) (2006) 497-503.

[12] M. F. Ciraolo, J. C. Hanson, P. Norby, C. P. Grey, J. Phys. Chem. B 105 (2001) 2604-2611.

[13] J. A. Ritter, S. J. Bhadra, A. D. Ebner, Langmuir 27 (2011) 4700–4712.

[14] P. A. Bonnaud, B. Coasne, R. J-M. Pellenq, J. Phys.: Condens. Matter 22 (2010) 284110-284125.

[15] M. G. Ahunbay, Langmuir 27 (2011) 4986–4993

[16] R. Krishna, J. M. van Baten, Langmuir 26(13) (2010) 10854–10867

[17] A. Germanus, J. Karger, H. Pfeifer, Zeolites 4, (1984) 188-190.

[18] J. Karger, H. Pfeifer, Zeolites 7 (1987) 90-107.

[19] E. H. Ellison, J. Phys. Chem. B 103 (1999) 9314-9320.

[20] J. Farrell, C. Manspeaker and J. Luo. Microporous Mesoporous Mater., 59 (2003) 205–214

[21] L. Narasimhan, P. Boulet, B. Kuchta, O. Schaef, R. Denoyel, P. Brunet, Langmuir 25(19), (2009) 11598–11607.

[22] H. Cheng, M. Reinhard, Environ. Sci. Technol. 40(24) (2006) 7694–7701.

[23] A. Martucci, L. Pasti, M. Nassi, A. Alberti, R. Arletti, R. Bagattin, R. Vignola, R. Sticca, available on line doi:10.1016/j.micromeso.2011.10.010.

[24] P. Jedlovszky, A. Vincze, G. Horvai, J. Chem. Phys. 117 (2002) 2271-2281.

[25] L. Y. Lee, N. Yoshida, F. Hirata, J. Phys. Chem. B 110 (2006) 16018-16025.

[26] N. A. Murugan, H Ågren, J. Phys. Chem B 113 (2009) 3257-3263.

[27] R. J. Sabharwal, Y. Huang, Y. Song, J. Phys. Chem. B 111 **(**2007*)* 7267-7273.

[28] M. W. Wong, M. J. Frisch, K. B. Wiberg, J. Am. Chem. Soc. 113 (1991) 4776-4782.

[29] B. Cohen, S. Weiss, J. Phys. Chem. 87 **(**1983) 3606-3610.

[30] A. C. Larson, R. B. Von Dreele, "General Structure Analysis System (GSAS)", Los Alamos National Laboratory Report LAUR (2000) 86-748.

[31] B. H. Toby, J. Appl. Cryst. 34 (2001) 210-213.

[32] S. Azizian, J. Coll. Int. Sci., 276(1) (2004) 47-52.

[33] W. Rudzinski, W. Plazinski, J. Phys. Chem. B 110, (2006) 16514-16525.

[34] Y. S. Ho, Water Res. 40, (2006) 119-125.

[35] W. Plazinski, W. Rudzinski, A. Plazinska, Adv. Coll. Interf. Sci. 152 (2009) 2–13.

[36] B. Koubaissy, G. Joly, I. Batonneau-Gener, P. Magnoux, Ind. Eng. Chem. Res. 50, (2011) 5705–5713.

[37] S. Kleineidam, C. Schüth, P. Grathwohl, Environ. Sci. Technol. 36, (2002) 4689-4697.

[38] C. H. Giles, T. H. Macewan, S. N. Nakhwa, D. Smith, J. Chem. Soc. 4 (1960) 3973-3993.

[39] K. S. W. Sing, D. H. Everett, R. A. W. Haul, L. Moscou, R. A. Pierotti, J. Rouquerol, T. Siemieniewska, Pure & Appl. Chem. 57(4) (1985) 603—619.

[40] J. H. Yun, D. K. Choi, J. Chem. Eng. Data 42 (1997) 894-896.

[41] B. A. De Moor, M-F. Reyniers, O. C. Gobin, J. A. Lercher, G. B. Marin, J. Phys. Chem. C, 115(4) (2011) 1204-1219.

[42] D. G. Ruthven, Principles of adsorption and adsorption processes, Wiley-Interscience; John Wiley & Sons, N.Y. (USA), 1984.

[43] J. P. Mota, S. Lyubchik (Eds), Recent Advances in Adsorption Processes for Environmental Protection and Security NATO Science for Peace and Security, Series C: Environmental Security, Springer, The Netherlands, 2008.

[44] I. Halasz, S. Kim, B. Marcus, J. Phis. Chem. B 105, (2001) 10788-10796.

[45] J. Rabone, Y.-F. Yue, S. Y. Chong, K. C. Stylianou, J. Bacsa, D. Bradshaw, G. R. Darling, N. G. Berry, Y. Z. Khimyak, A. Y. Ganin, P. Wiper, J. B. Claridge, M. J. Rosseinsky, Science 329 (2010) 1053-1057.

[46] Ch. Baerlocher, W.M. Meier, D.H. Olson, Atlas of Zeolite Framework Types, 5th ed., Elsevier, Amsterdam, 2001.

[47] M. Guisnet, J. P. Gilson, Eds., Zeolites for Cleaner Technologies, Imperial College Press, 2002,

[48] Z. Li, J. Singh, J. Phys. Chem. A 112 (2008) 8593-8599.

[49] L. Wang, J. Phys. Chem. A 111 (2007) 3642-3651.

[50] R. Iwamoto, T. Matsuda, T. Sasaki, J. Phys. Chem. B 2003, 107, 7976-7980.

[51] M. P. Conrad, H. L. Strauss, J. Phys. Chem. 91 (1987) 1668-1673.

[52] M. Besnard, Y. Danten, T. Tassaing, J. Phys. Chem. 113 (2000) 3741-3748.

[53] H. C. Allen, E. A. Raymenod, G. L. Richmond, J. Phys. Chem. A 105 (2001) 1649-1655.

[54] B. F. Mentzen, Mat. Res. Bull., 27 (1992) 831-838.

[55] E. L. Wu, S. L. Lawton, D. H. Olson, A. C. Rohrman, Jr., and G. T. Kokotailo J. Phys. Chem., 83 (1979) 2777-2781.

[56] H. van Koningsveld , J.C. Jansen, H. van Bekkum Zeolites 10(4) (1990) 235-242

[57] G. Marra, G. Tozzola, G. Leofanti, M. Padovan, G., Petrini, F. Genoni, B. Venturelli, A. Zecchina, S. Bordiga, G. Ricchiardi, Stud. Surf. Sci. Catal. 84 (1994) 559-566.

[58] N. Kamiya, W. Iwama, T. Kudo,T. Nasuno, S. Fujiyama, K. Nishi and Y. Yokomori *Acta Cryst.*. B**67** (2011) 508-515

[59] H. Van Koningsveld, J. C. Jansen, Microporous Mater., 6(3) (1996) 159-167.

[60] K.Nishi , A.Hidaka, and Y. Yokomori, *Acta Cryst.* B61, (2005) 160-163.

[61] G. Vezzalini, S. Quartieri, E. Galli, A. Alberti, G. Cruciani, and Å. Kvik**,** Zeolites**.** 19**,** (1997) 323-325.

FIGURE CAPTIONS

Figure 1. Thermogravimetric (TG) curves in ZSM5 and Y respectively, before and after DCE adsorption.

Figure 2. a) Uptake of DCE on ZSM-5 data b) Pseudo second order linear fit of data in a), c) Uptake of DCE on Y data, d) Pseudo second order linear fit of data in c),

Figure 3. a) Adsorption isotherms (at 298 K) of DCE on ZSM-5 (circle) and Y (square). b) Enlarged detail of data in a) in the low concentration range

Figure 4. Representation of Y (a) and MFI (b-c) frameworks, showing both the straight channel parallel to the [100] direction, and the tubular channels, parallel to the [010] direction.

Figure 5. Observed powder diffraction patterns of Y-DCE (a) and ZSM-5-DCE (b) respectively, showing strong differences both in intensity and the position of the diffraction peaks.

Figure 6. Oxygen-oxygen distance (Å) of the apertures in Y zeolite before and after DCE adsorption, assuming an oxygen ionic radius of 1.35 Å. Crystallographic Free Areas (C.F.A.) *sensu* Baerlocher [46] are also reported.

Figure 7. Projection along [001] showing DCE molecules in Y along the 12-ring channels. Chlorine (red circle), carbon (green circle) and water molecules (light blue) are reported.

Figure 8. DCE-water complexes in Y cage. Chlorine (red circle), carbon (green circle), framework oxygens (yellow circle) and water molecules (light blue) are reported. Bond distances are in Table 4

Figure 9. Projection along [001] (a) and [010] (b) showing DCE molecules in ZSM-5 along the 10-ring channels. Chlorine (red circle), carbon (green circle) and water molecules (light blue) are reported.

Figure 10. DCE-water complexes in ZSM-5. Chlorine (red circle), carbon (green circle), framework oxygens (yellow circle) and water molecules (light blue) are reported. Bond distances are in Table 4.

Figure 11. Dimensions (Å) of the apertures in ZSM-5 zeolite before and after DCE adsorption, viewed normal to [100] and [010], assuming an oxygen ionic radius of 1.35 Å. The ellipticity index (l/s= largest/shortest oxygen-oxygen distances) was also reported.

Figure(s)

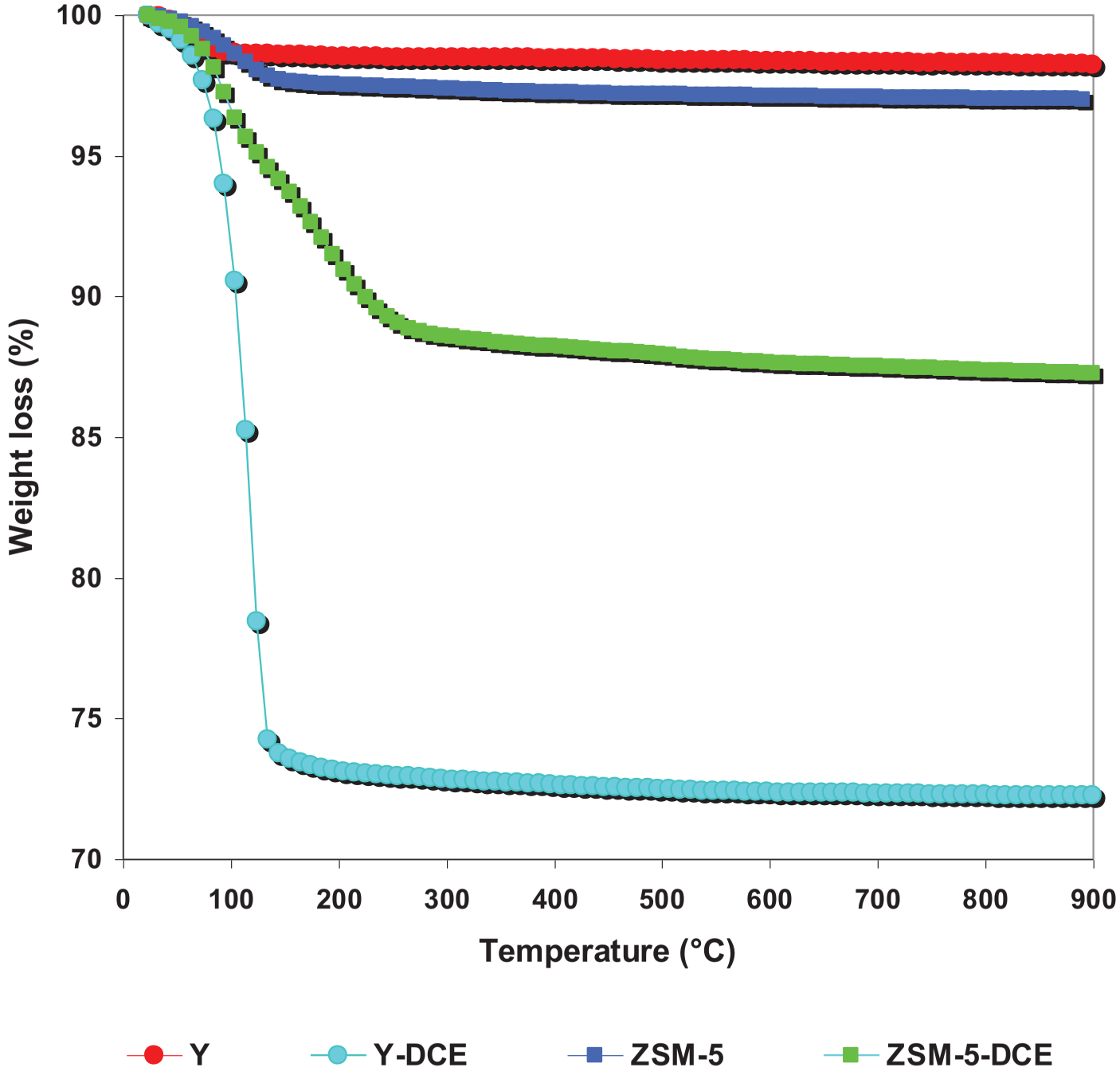

Figure 1

Figure(s)

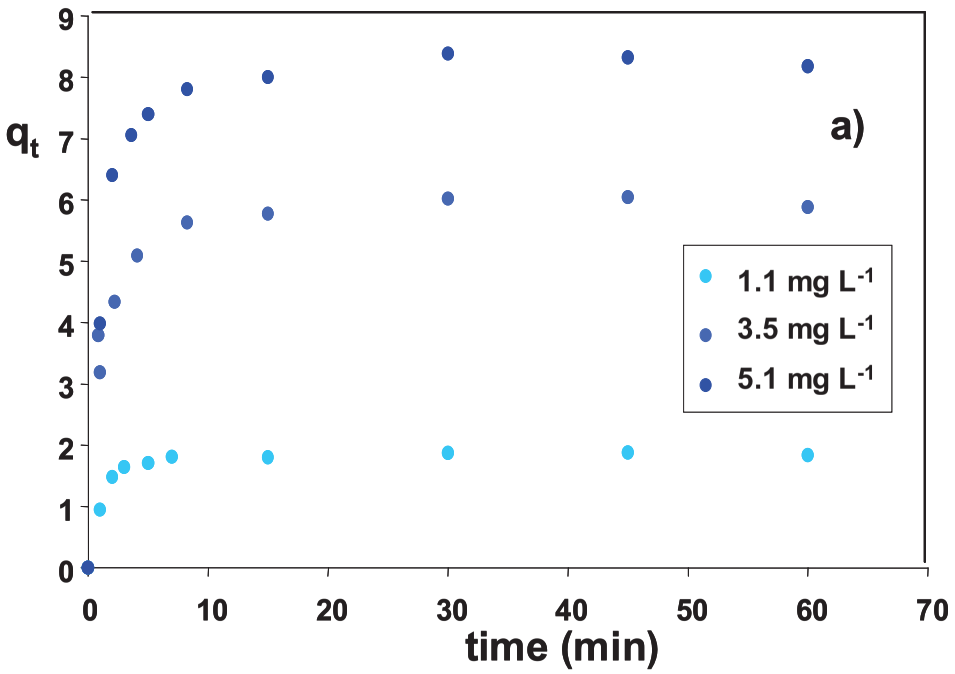

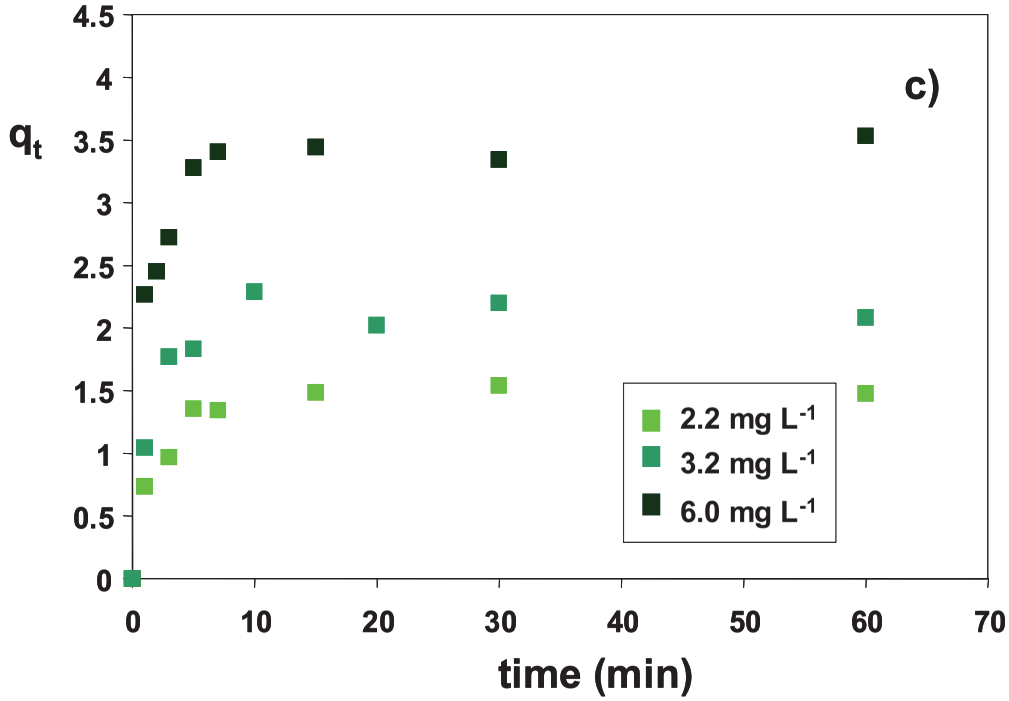

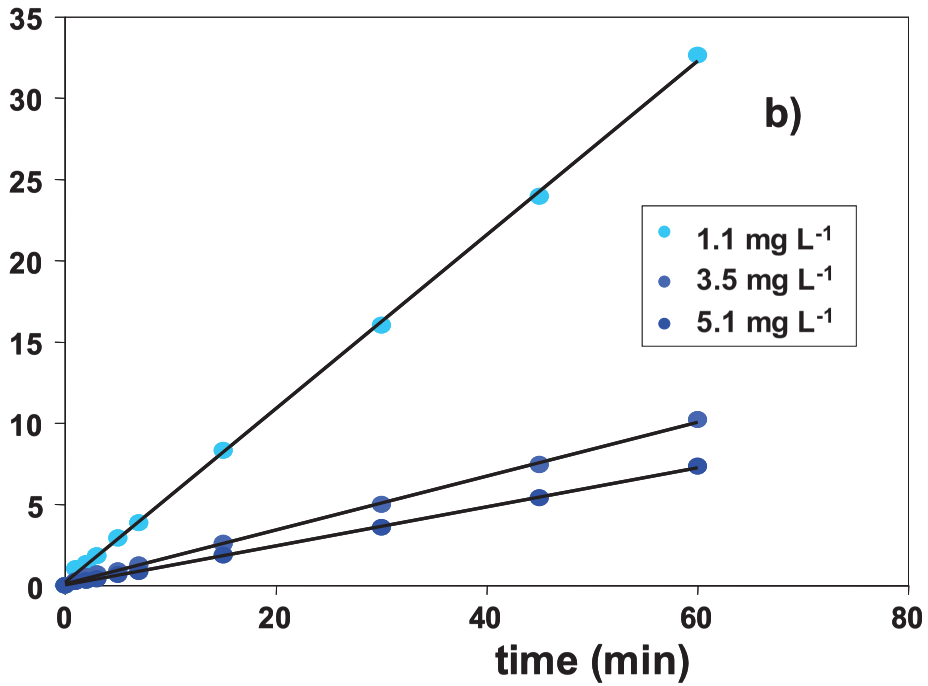

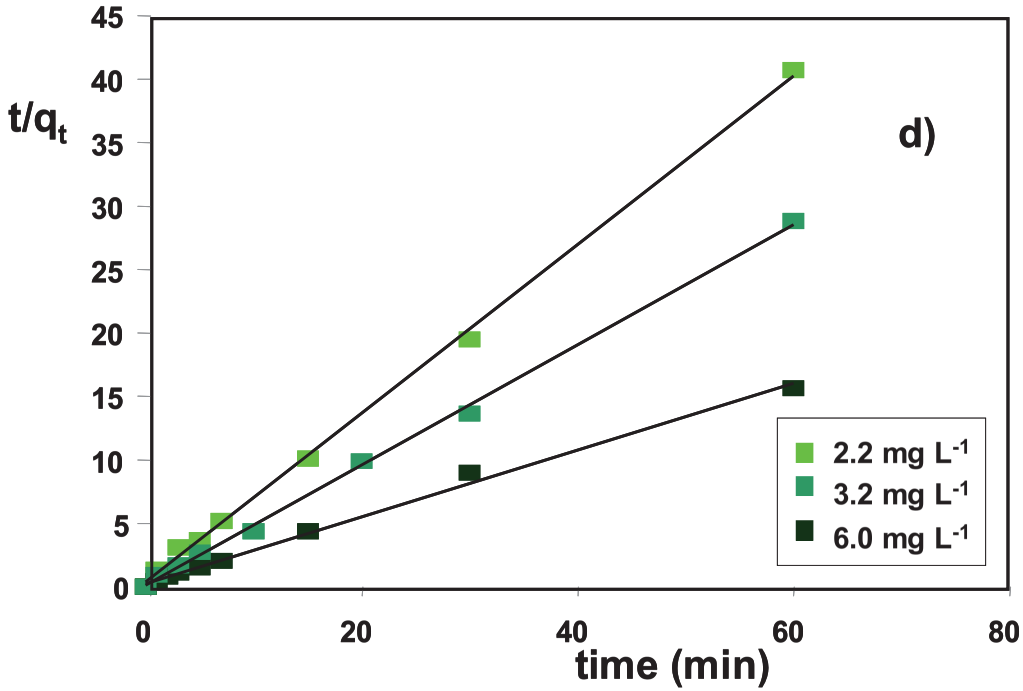

Figure 2

Figure(s)

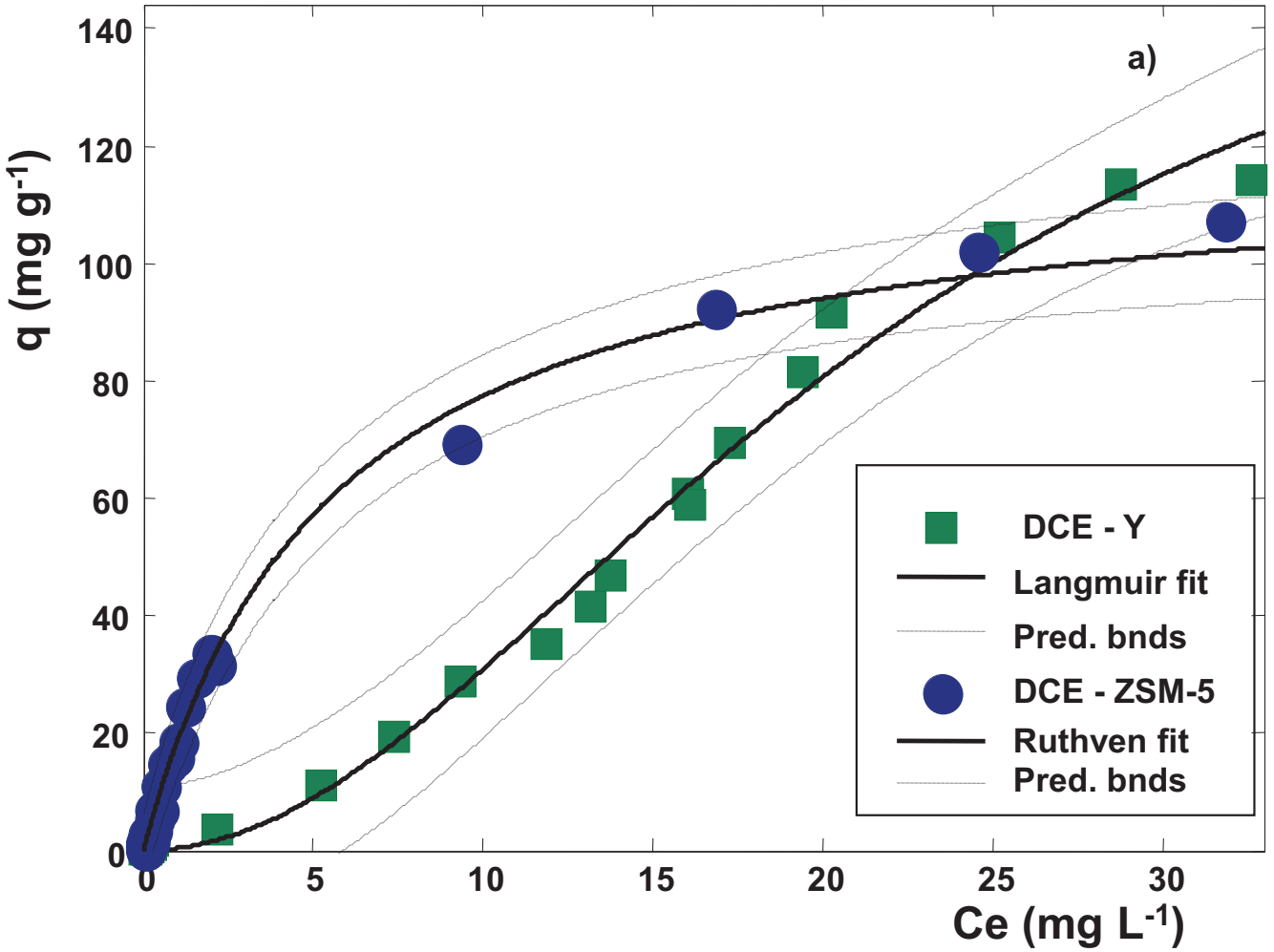

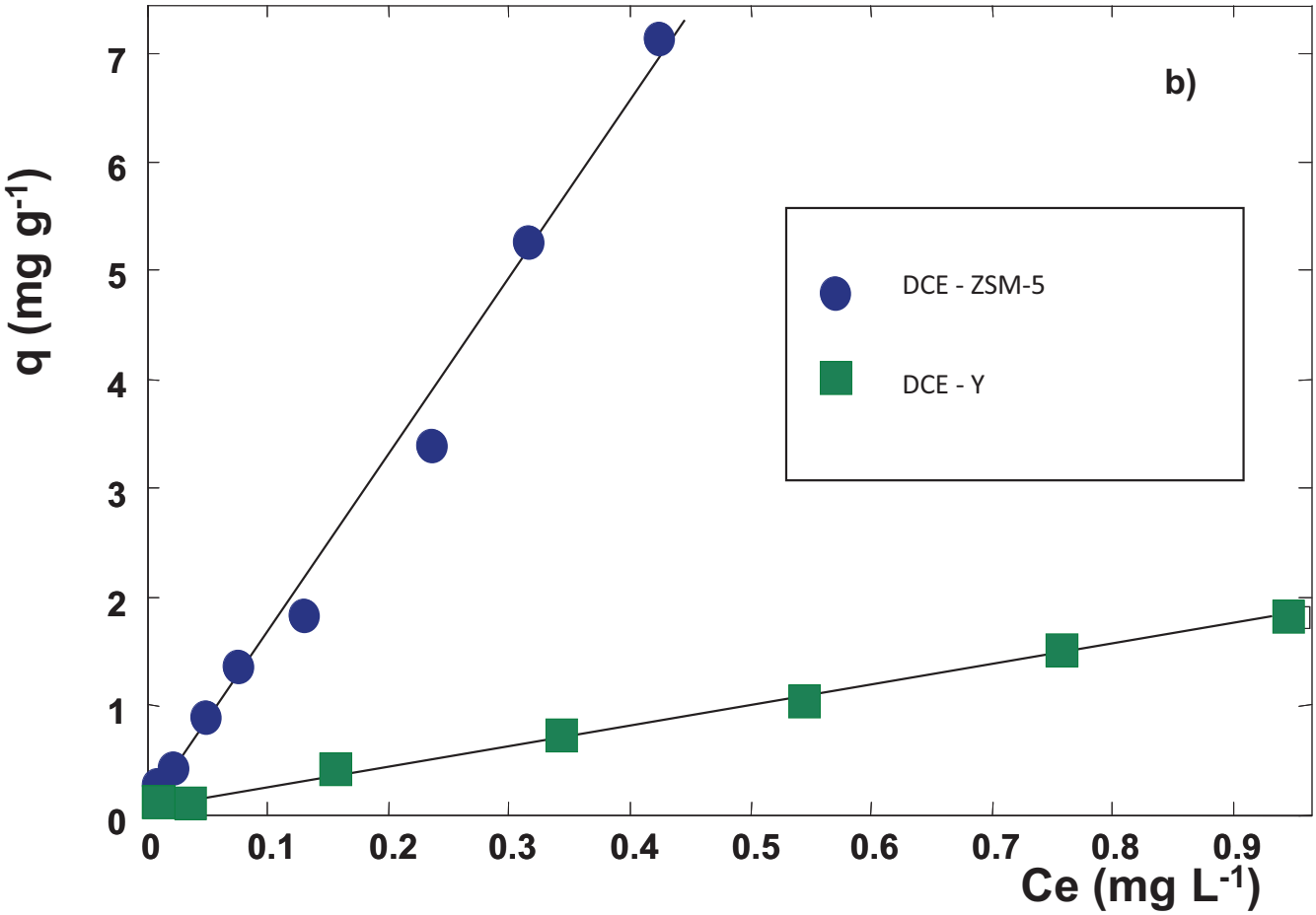

Figure 3

Figure(s)

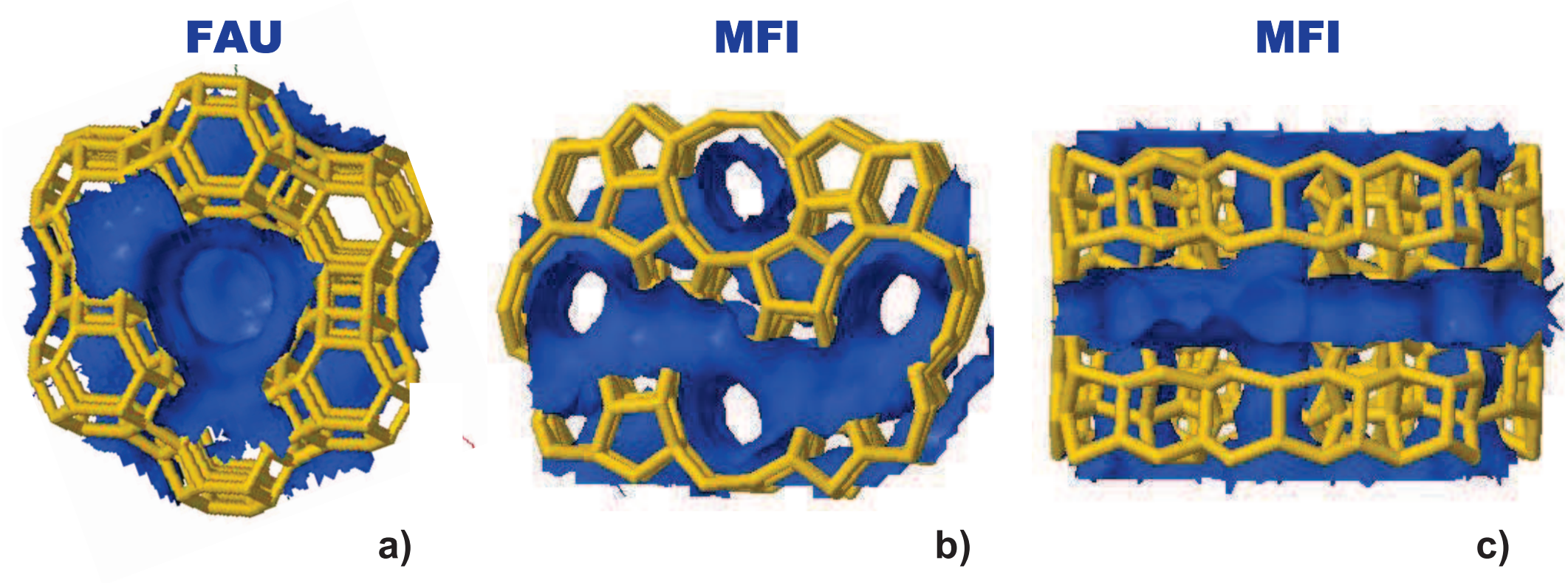

Figure 4

Figure(s)

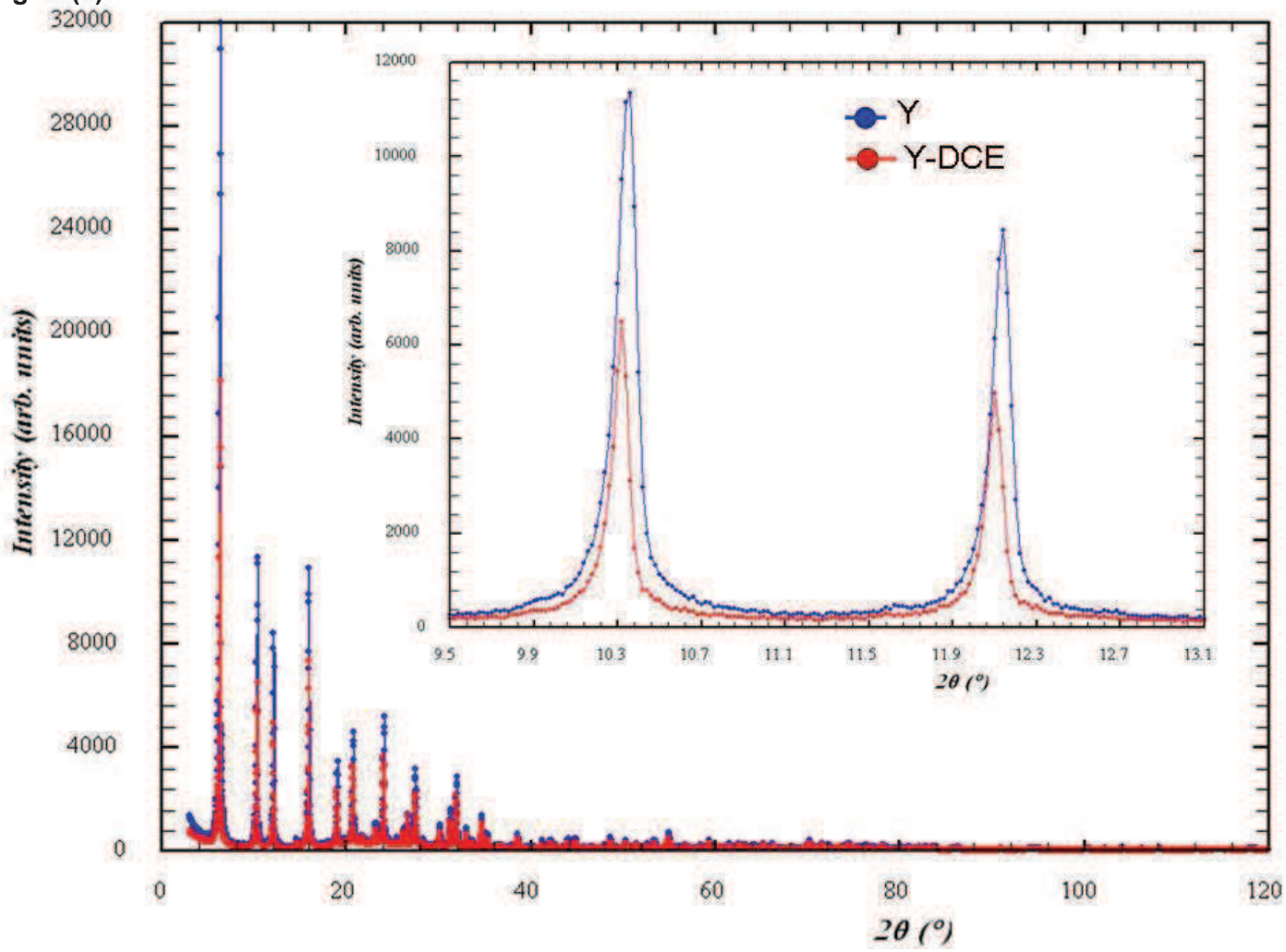

a)

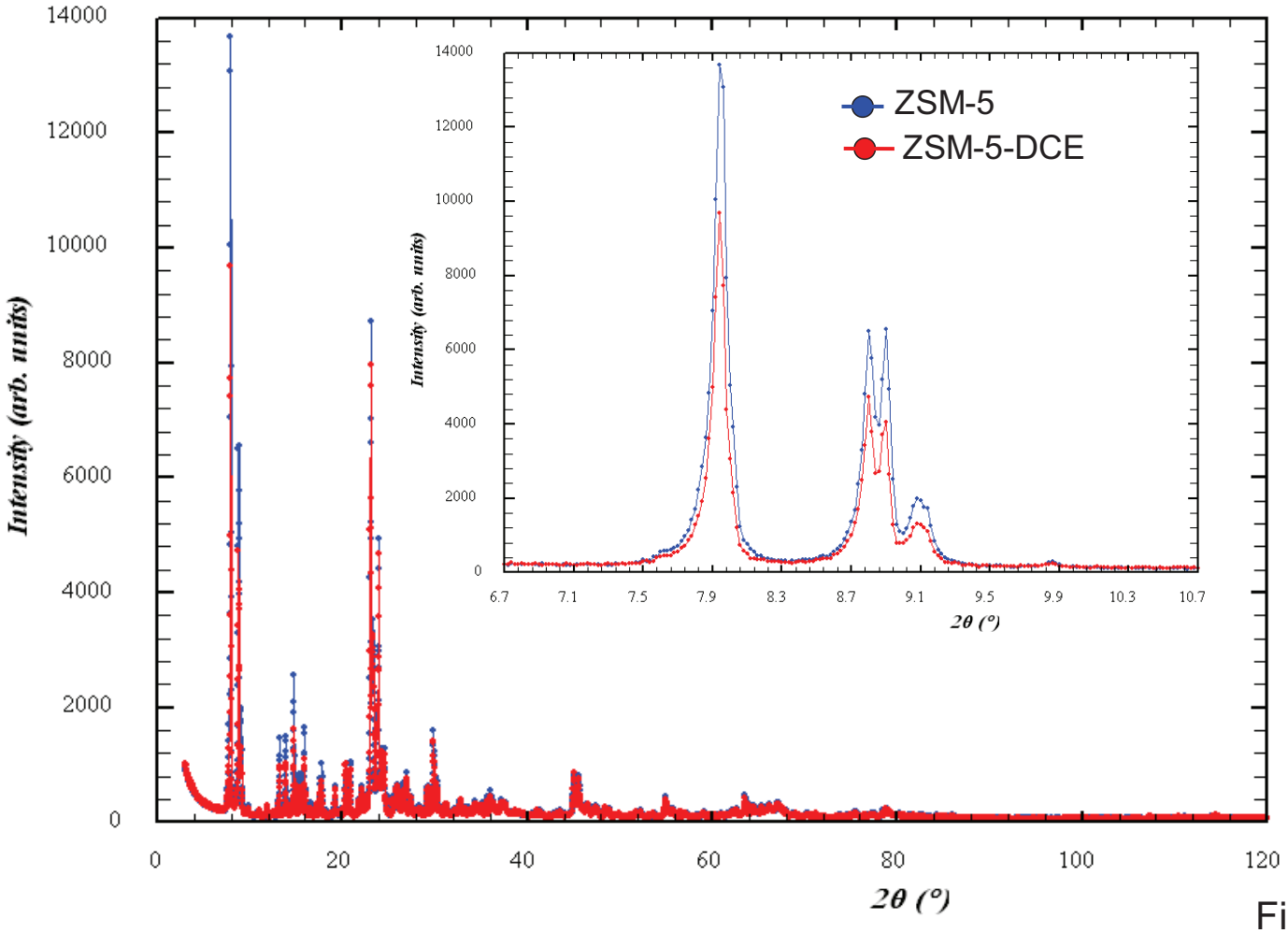

b)

Figure 5

Figure(s)

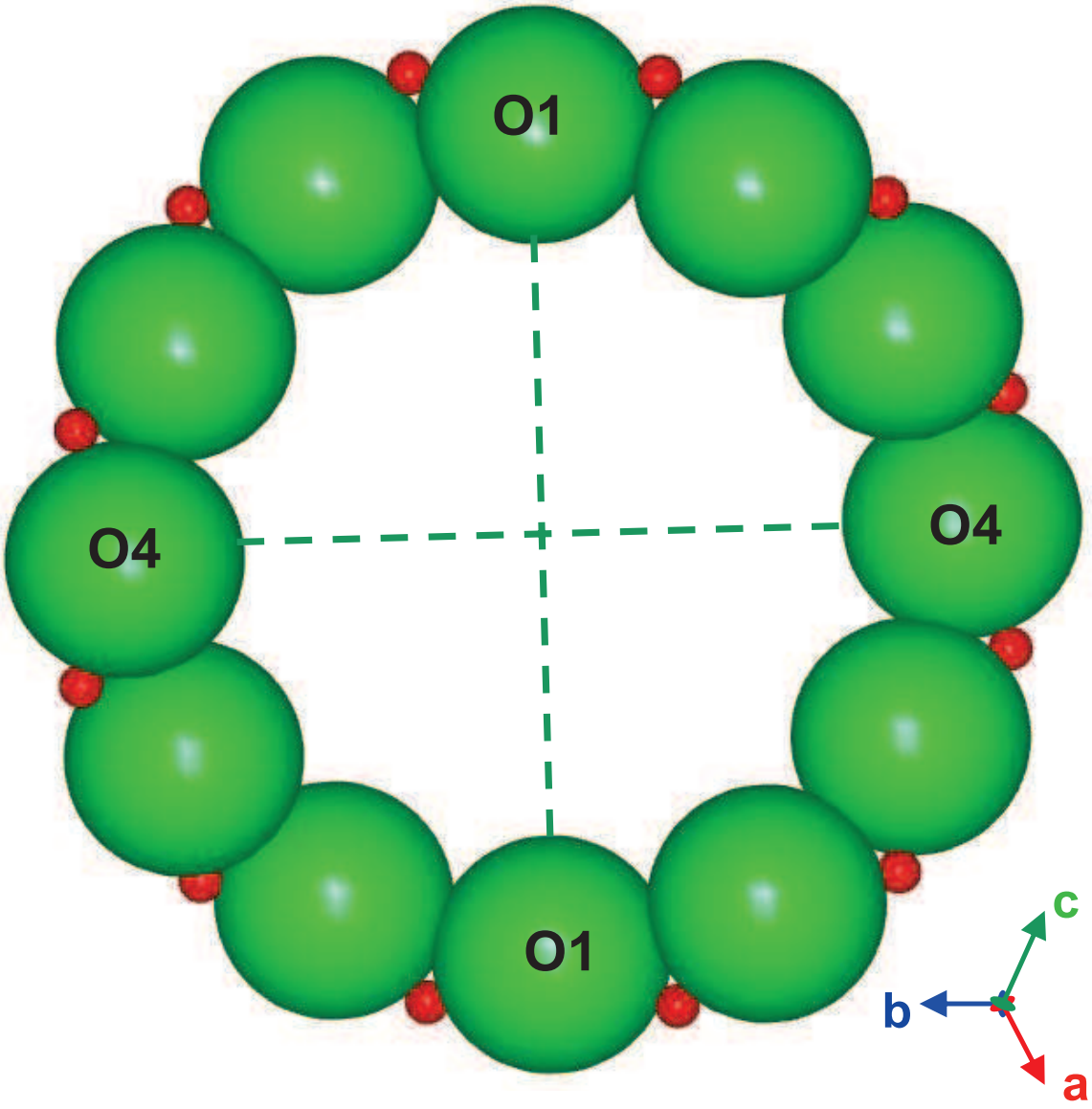

	Y	Y+DCE
O4-O4(Å)	9.81	9.95
O1-O1(Å)	9.70	9.87
CFA	39.07	40.81

Figure 6

Figure(s)

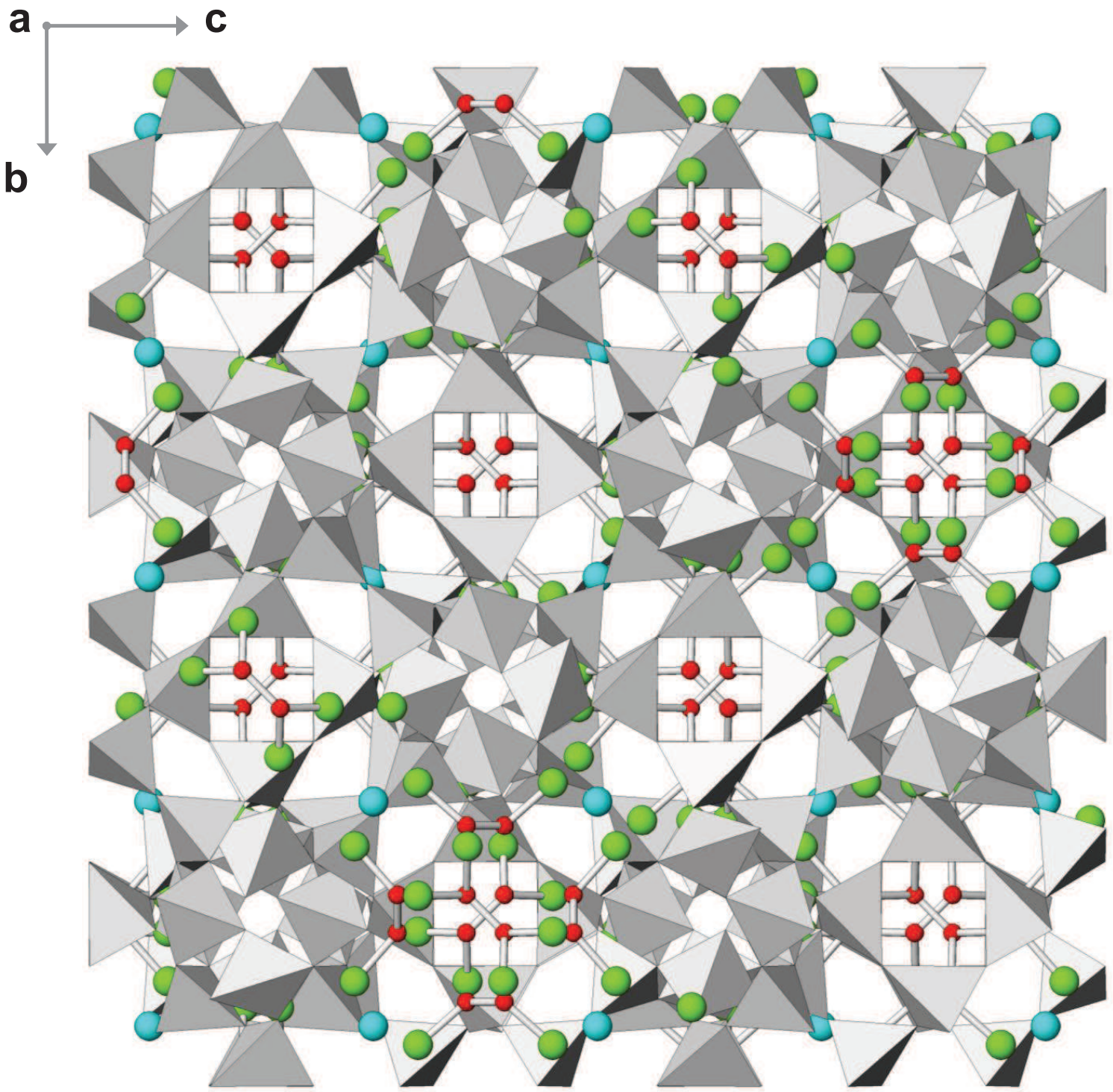

Figure 7

Figure(s)

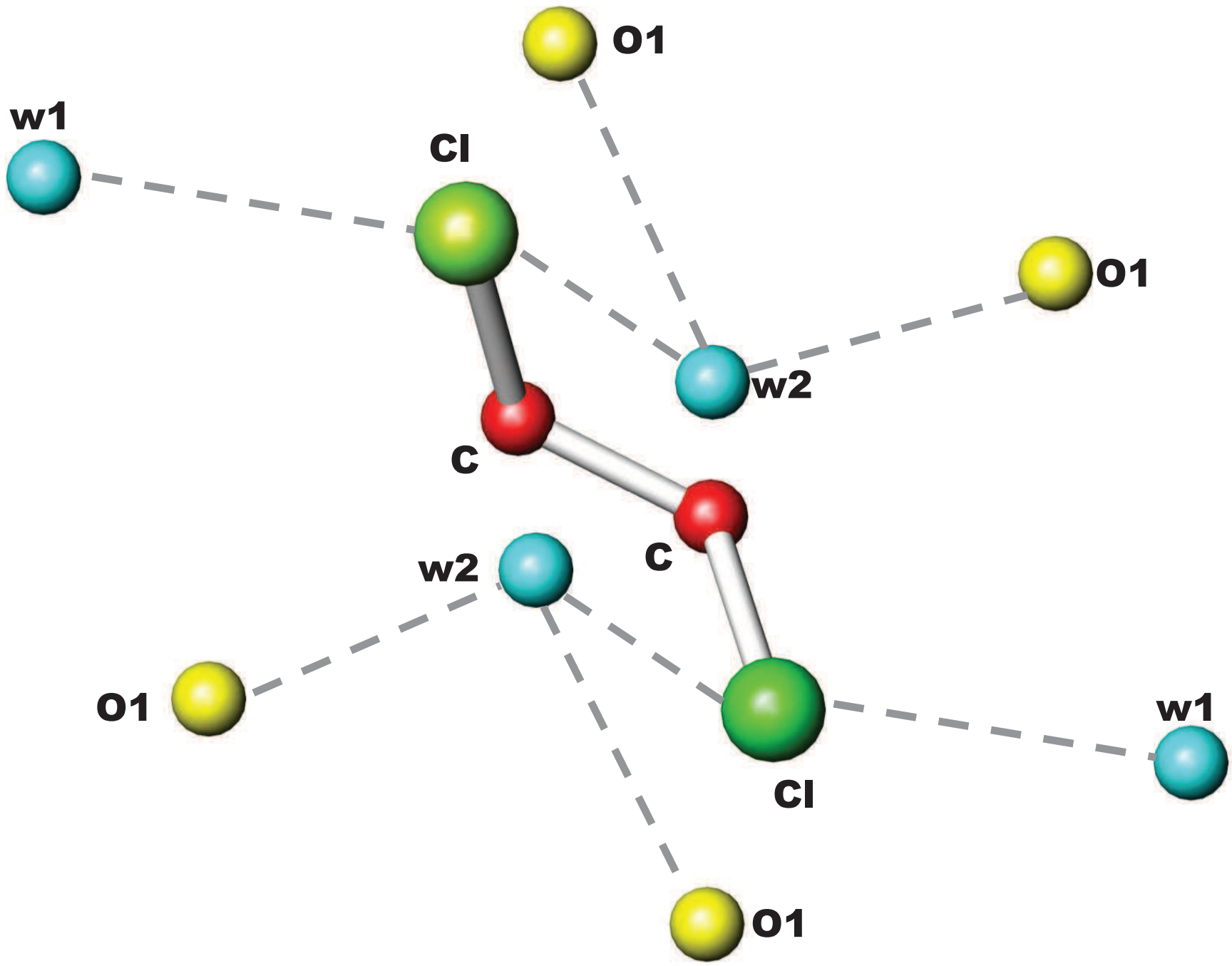

Figure 8

Figure(s)

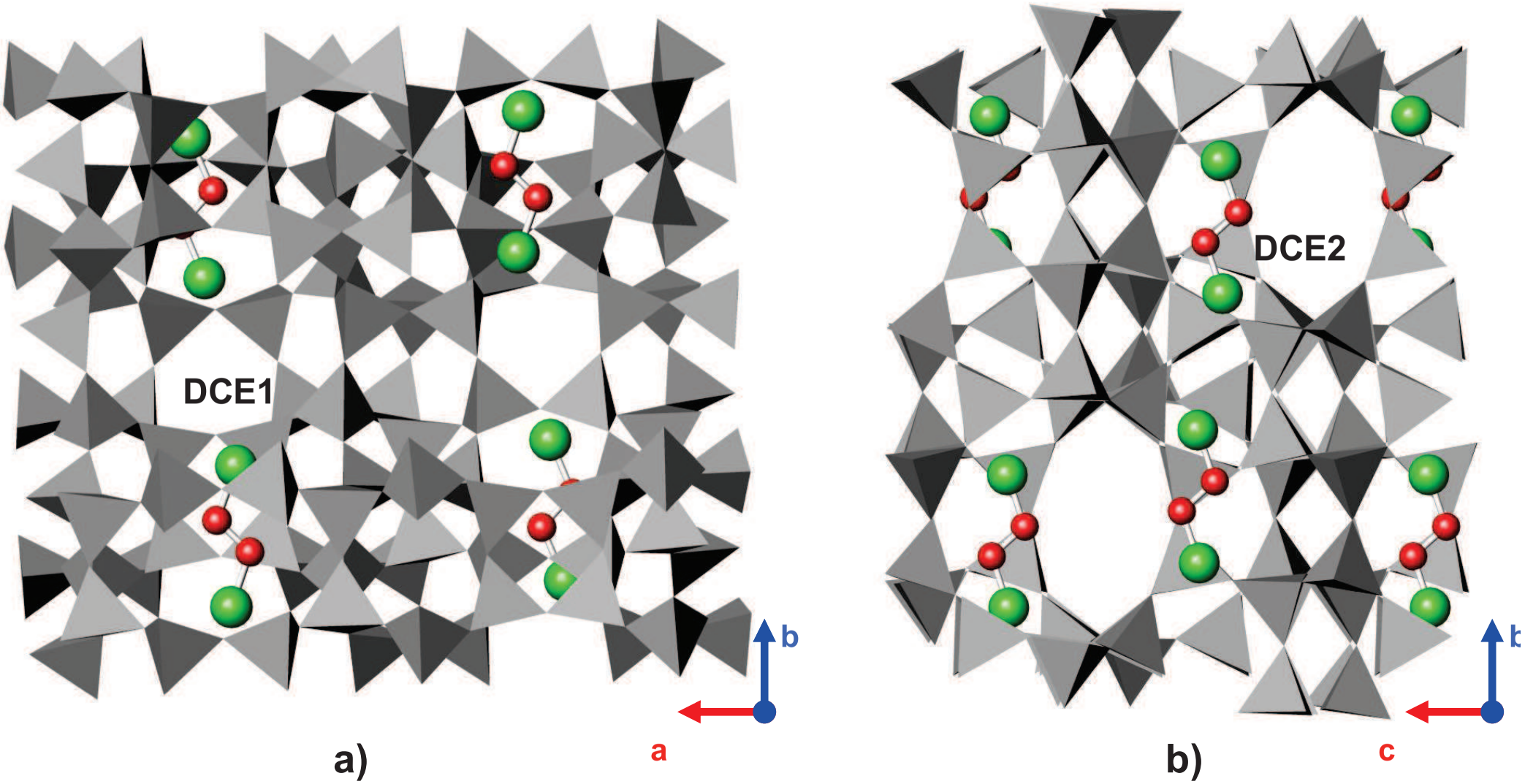

Figure 9

Figure(s)

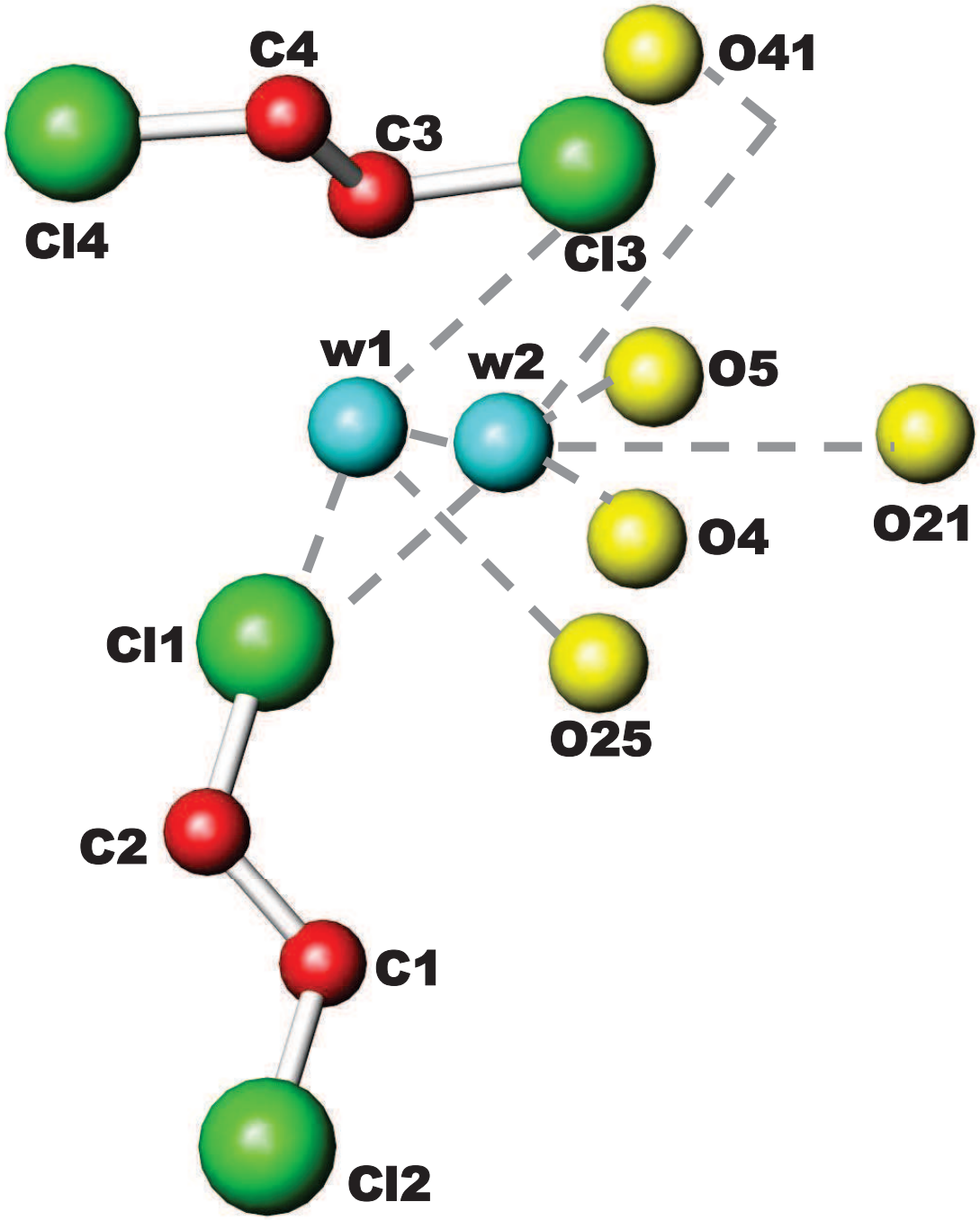

Figure 10

Figure(s)

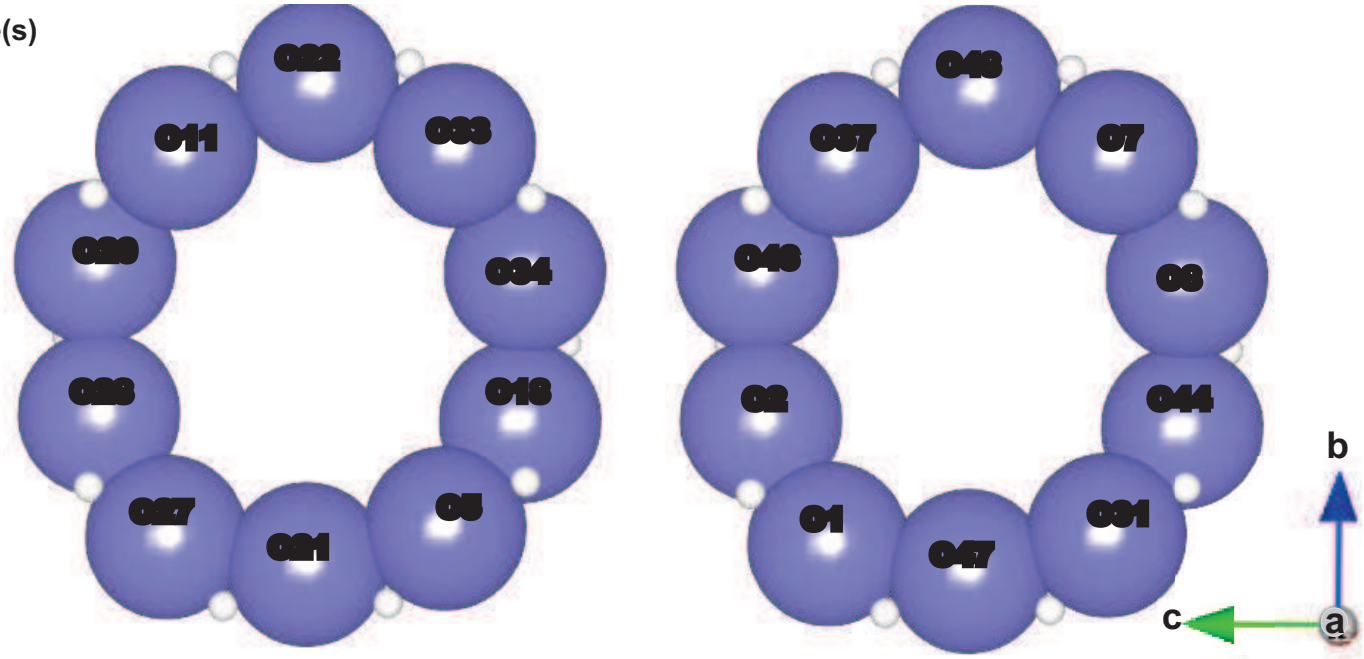

10-ring [100]	ZSM-5	ZSM-5-DCE	10-ring [100]	ZSM-5	ZSM-5-DCE
O22-021	8.04	8.03	**O47-048**	7.93	7.83
O11-O5	8.23	8.11	**O31-O37**	8.20	8.23
O20-O18	8.21	8.18	**O46-O44**	8.19	8.22
O28-O34	8.07	8.09	**O8-O2**	8.08	8.24
O27-O33	8.03	8.07	**O1-O7**	7.98	8.01
l/s	1.025	1.019	**l/s**	1.034	1.052

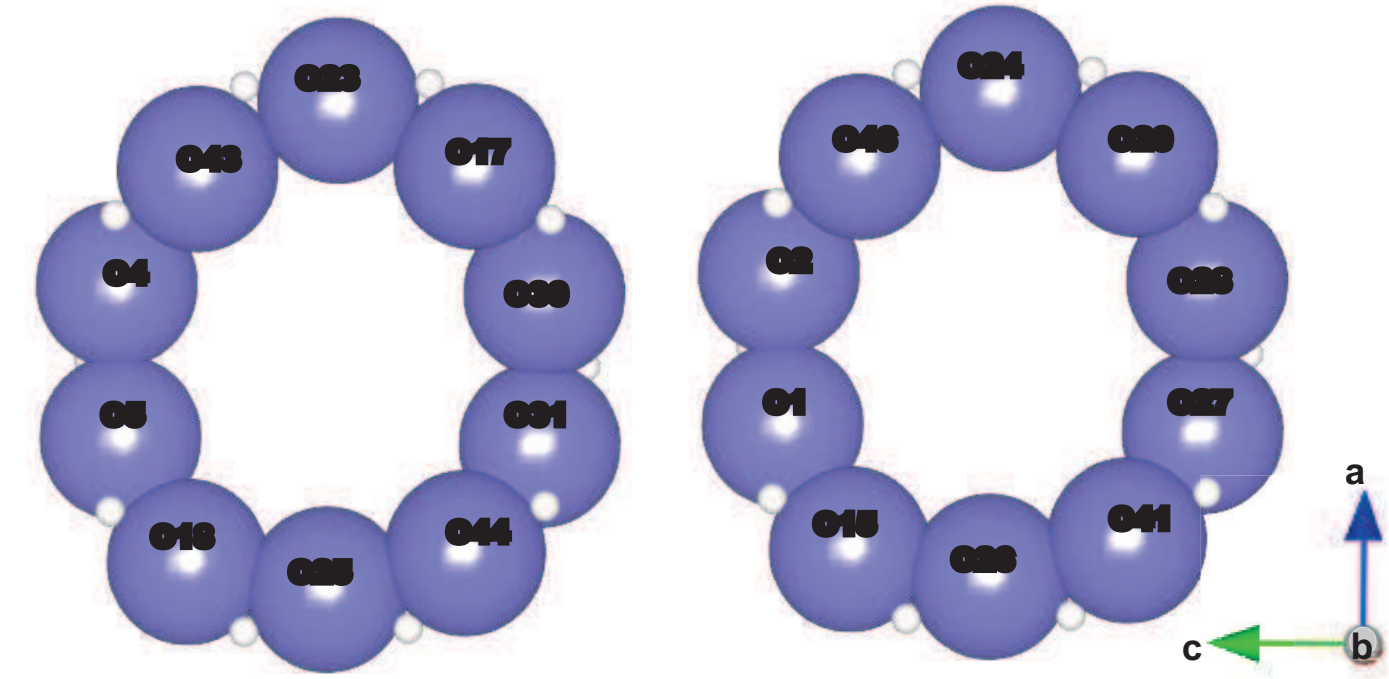

10-ring [010]	ZSM-5	ZSM-5-DCE	10-ring [010]	ZSM-5	ZSM-5-DCE
O23-O25	8.20	8.18	**O24-O26**	7.84	7.93
O43-O44	8.13	8.21	**O46-O41**	8.22	8.40
O4-O31	7.91	7.90	**O2-O27**	7.85	7.94
O5-O30	8.31	8.31	**O1-O28**	7.90	8.10
O18-O17	7.81	7.73	**O15-O20**	7.95	7.94
l/s	1.064	1.075	**l/s**	1.048	1.058

Figure 11

Table(s)

Table 1. Lattice parameters and refinement details for ZSM-5 after DCE adsorption

	Y-DCE	ZSM-5-DCE
Space Group	*F d-3*	*P* $2_1/n$
a (Å)	24.2767(6)	20.1174(6)
b (Å)	24.2767(6)	19.8999(5)
c (Å)	24.2767(6)	13.3892(4)
α(°)	90	90.546(3)
β(°)	90	90
γ(°)	90	90
V ($Å^3$)	14307.6(6)	5359.9(3)
Refined pattern 2θ range (°)	3-110	3-110
R_{wp} (%)	8.65	9.12
R_p (%)	7.60	8.40
R_F^2 (%)	7.42	9.10
N^o of contributing reflections	1658	5601
N_{obs}	5319	14142
N_{var}	65	289
λ = 1.5417(1) Å		

Estimated standard deviations in parentheses refer to the last digit

$R_p = \sum[Y_{io}-Y_{ic}]/\sum Y_{io}$; $R_{wp} = [\sum w_i(Y_{io}-Y_{ic})^2/\sum w_i Y_{io}^2]^{0.5}$; $R_F^2 = \sum|F_o^2-F_c^2|/\sum|F_o^2|$

Table 2: Uptake kinetics of DCE on ZSM-5 and Y. (see Eq. 1)

Organic – Zeolite	C_0 mg L^{-1}	k_2 g mg^{-1} min^{-1}	q_e (kinetics) mg g^{-1}	q_e (equilibrium) mg g^{-1}	$t_{1/2}$[1] min	k'_2 g mg^{n-1} L^{-n} min^{-1}	n
	1.1	**1.33**	**1.9**	**2.3**	**0.40**		
DCE-ZSM-5	**3.5**	**0.32**	**6.2**	**6.3**	**0.51**	**1.45**	**1.14**
	5.1	**0.24**	**8.3**	**9.3**	**0.53**		
	2.2	**0.86**	**1.5**	**1.9**	**0.77**		
DCE-Y	**3.2**	**0.72**	**2.3**	**2.8**	**0.72**	**2.55**	**1.24**
	6	**0.26**	**3.8**	**4.2**	**1.09**		

[1] $t_{1/2}$ is calculated as the reciprocal of the product of k_2 and q_e.

Table 3: Fitting Results of the adsorption data of DCE on ZSM-5 and Y.

Organic - Zeolite	Equation[1]	Parameters				R^2
DCE-ZSM-5	$q = \frac{q_s K_L C_e}{1 + K_L C_e}$	K_L (L mg^{-1}) 0.19 (0.16, 0.21)	q_s (mg g^{-1}) 120 (113, 127)			0.9927
DCE-ZSM-5	$q = \frac{q_s K_L C_e}{1 + K_L C_e} + \frac{q_{s,1} K_{L,1} C_e}{1 + K_{L,1} C_e}$	K_L (L mg^{-1}) 0.23 (0.18, 0.28)	q_s (mg g^{-1}) 82 (73, 91)	$K_{L,2}$ (L mg^{-1}) 0.11 (0.02, 02)	$q_{s,2}$ (mg g^{-1}) 37 (33, 42)	0.9987
DCE-ZSM-5	$q = K C_e$	K (L mg^{-1}) 13 (12, 14)				0.9929
DCE-Y	$\frac{q}{q_s} = \frac{K_r C_e + R(K_r C_e)^2}{1 + K_r C_e + R/2(K_r C_e)^2}$	K_r (L mg^{-1}) 0.014 (0.009, 0.019)	q_s (mg g^{-1}) 175 (136,214)	R 4.3 (2.7,5.0)		0.9911
DCE-Y	$K_{FG} C_e = \frac{\theta}{1-\theta} exp\left(\frac{2\theta W}{RT}\right)$	K_{FG} (L mg^{-1}) 0.0923	q_s (mg g^{-1}) 178	W (kJ mol^{-1}) 5.2		0.9920
DCE-Y	$q = K C_e$	K (L mg^{-1}) 2.0 (1.3, 2.8)				0.9892

[1] q (mg g^{-1}) is the sorbed concentration, C_e (mg L^{-1}) is the concentration in the solution at equilibrium, $K_{L,i}$ (L mg^{-1}) is the Langmuir coefficient (binding constant), and $q_{s,i}$ (mg g^{-1}) the saturation capacity of site i. θ is the ratio q / q_s, R is the parameter accounting for adsorbate-adsorbate interactions in a cage and W the interaction energy (kJ mol^{-1})

Table 4. Selected bond distances of extraframework atoms in Y-DCE and ZSM-5-DCE, respectively.

Y-DCE					
C-C	1.450(2)	**w2-Cl**	2.151(5)	**w1-Cl[x6]**	2.868(3)
C-Cl	1.7493)	**w2-O1**	3.06(9)	**w2-O1**	3.26(4)
ZSM-5-DCE					
C1-C2	1.411(23)	**C3-Cl3**	1.730(24)	**w2-O4**	2.63(4)
C1-Cl2	1.774(23)	**C3-C4**	1.419(24)	**w2-O5**	3.019(32)
C1-Cl1	2.684(22)	**C3-Cl4**	2.626(24)	**w2-O21**	2.58(27)
C2-Cl2	2.666(22)	**Cl3-C4**	2.629(23)	**w2-O41**	2.880 (34)
C2-Cl1	1.769(23)	**C4-Cl4**	1.711(24)	**w2-Cl1**	2.53(7)
Cl3-w1	3.18(3)	**w1-Cl1**	2.24(7)	**w1-O25**	3.32(3)
		w1-w2	2.09(7)	**w1-C13**	3.18(13)

LOCATION OF MTBE AND TOLUENE IN THE CHANNEL SYSTEM OF THE ZEOLITE MORDENITE: ADSORTPION AND HOST-GUEST INTERACTIONS.

Rossella Arletti[1*], Annalisa Martucci[2], Alberto Alberti[2], Luisa Pasti[3], Marianna Nassi[3], Roberto Bagatin[4]

Department of Earth Sciences, University of Torino Via Valperga Caluso 35, I-10125, Torino, Italy

[2] Department of Earth Sciences, University of Ferrara, Via G. Saragat 1 I-44100, Ferrara, Italy

[3] Department of Chemistry, University of Ferrara, Via L. Borsari 26, I-44100 Ferrara, Italy

[4] Research Centre for Non-Conventional Energy - Istituto ENI Donegani, Environmental Technologies, Via Fauser 4, I-28100 Novara, Italy

*rossella.arletti@unito.it; Tel: +390116705122; Fax: +390116705128

ABSTRACT

This paper reports a study of the location of Methyl Tertiary Butyl Ether (MTBE) and toluene molecules adsorbed in the pores of the organophylic zeolite mordenite from an aqueous solution. The presence of these organic molecules in the zeolite channels was revealed by structure refinement performed by Rietveld method. About 3 molecules of MTBE and 3.6 molecules of toluene per unit cell were incorporated into the cavities of mordenite, representing 75% and 80% of the total absorption capacity of this zeolite. In both cases a water molecule was localized inside the side pocket of mordenite. The saturation capacity determined by the adsorption isotherms, obtained by batch experiments, and the weight loss given by thermogravimetric (TG) analyses were in very good agreement with these values. The interatomic distances obtained after the structural refinements suggest MTBE could be connected to the framework through a water molecule, while toluene appears directly bonded to framework oxygen atoms. The rapid and high adsorption of these hydrocarbons into the organophylic mordenite zeolite makes this cheap and environmental friendly material a suitable candidate for the removal of these pollutants from water.

1. Introduction

Hydrocarbons and halogenated compounds are organic pollutants in industrial waste, especially in waste water deriving from oil refineries, petrochemical plants, and even from common petrol stations. The effective removal of these pollutants from waste water is a problem of great importance and interest and despite significant efforts in environmental restoration over the past 30 years, it remains one of the more difficult and expensive environmental problems. Physical

adsorption has proven to be one of the most efficient methods for quickly lowering the concentration of pollutants in waste water [1]. Activated carbons have been the most commonly used adsorbents [2], but they present some disadvantages in that they are relatively expensive, difficult to regenerate, and their performance in removing pollutants is greatly reduced in the presence of natural organic matter, leading to competitive-adsorption effects [3]. Inorganic adsorbents with a high surface area and hydrophobic behavior represent a promising alternative to carbon adsorbents [1,4,5,6,7,8].

Recently, porous materials such as zeolites have been used as sorbents for water treatment, due to their environmentally friendly nature. Zeolites are crystalline aluminosilicates with unique microporosity properties. Their frameworks, built from SiO_4 and AlO_4 tetrahedral units of, present nanometre-sized channels and cages. Their adsorption properties are strongly dependent not only on pore dimensions but also on their chemical properties. The Silica/Alumina Ratio is a fundamental parameter that defines zeolite polarity and influences the hydrophobicity or hydrophilicity of each zeolite. While the thermodynamics and kinetics of gas phase adsorption of organic molecules by zeolites has been widely investigated [9], studies of adsorption of organic molecules from aqueous solutions by zeolites are less numerous [5,6,10,11,12,13,14,15]. Adsorption from aqueous solutions depends not only on the dimension of the pore systems, but also on the competition between the adsorbate and water, strictly linked to the hydrophobicity of the zeolite considered. Databases for correlations between adsorption capacity and pore volume in a given pore size range are limited to very few compounds [11]. Moreover, the knowledge of such parameters may not be sufficient to model and predict adsorption properties. Understanding the science behind adsorption processes helps the operators to design a system that exploits the full capability of adsorbent materials.

The aims of this work are: i) to investigate the adsorptive properties of mordenite (framework type MOR) for the removal of Methyl Tertiary Butyl Ether (MTBE) and toluene (TOL), two organic pollutants often found in ground and surface water; ii) to define the structure of the zeolite after the adsorption treatment of the organic molecules; iii) to comprehend the interaction between the adsorbate and the zeolite framework. A knowledge of the interaction between adsorbent and adsorbate will provide an understanding of the properties of the selected zeolite and be useful for design an adsorbent with high capacity and selectivity. Recent studies [13,15,16] have already highlighted the effectiveness of the zeolite mordenite for the removal of MTBE, but a structural study for the definition of the host-guest interactions is completely lacking. Hung and Lin [16] studied the absorption of MTBE from natural water onto mordenite in comparison with carbonaceous resins. Among the samples tested, one of the resins and mordenite emerged as the most effective adsorbents for MTBE, it being demonstrated that for these two sorbents there was no competition between the organic matter, commonly dispersed in natural water, and the MTBE

molecules. Anderson [13] showed that, after equilibration of a 100μg/L MTBE solution with 5mg of solid phase mordenite powder, the percentage of removal of the pollutant was about 96%. When mordenite is substituted with other zeolites (i.e. ZSM-5 and Y), this percentage falls to 63% and 5% respectively. Unfortunately, the lack of a structural investigation of the MOR powder after adsorption made it impossible to fully explain this high affinity. MTBE molecule dimensions are such that it can fit equally in the channels of both MOR and ZSM-5. The reason for a more efficient removal by MOR must lie in interactions of the molecule with the mordenite framework. Recently, silicalite-1, its polymeric modification and granular activated compound [17] have also been used for MTBE removal. The results, demonstrated high affinity of zeolites for MTBE molecules when compared with other materials.As stated above, while some data on MTBE adsorption in mordenite has been published, to the knowledge of the authors no data are available regarding toluene adsorption by this zeolite. For this reason, in this study the adsorption capacity, the affinity of MOR with MTBE and toluene, and the interaction of the two molecules with the framework are discussed in detail.

2. Experimental

2.1 Materials

As stated in the introduction, two pollutants were chosen for this study: Methyl Tertiary Butyl Ether (MTBE) and toluene. These two molecules are contaminants found in urban rain water, ground water, and surface water. MTBE is an additive whereas toluene is a component of fuel and they are commonly present in waste water deriving from oil refineries and petrochemical plants. MTBE has been found both in drinking and in natural water at different concentrations. Currently, MTBE is listed on EPA's Drinking Water Contaminant Candidate List and drinking water levels have been set at 20 μg L^{-1} for odor and 40 μg L^{-1} for taste (EPA, 2002). In groundwater, levels of contamination over 100 mg L^{-1} are not uncommon due to spills at automobile gasoline service stations. In particular, Methyl Tertiary Butyl Ether is a primary constituent of reformulated gasoline, accounting for 10-15 % of reformulated fuels. Although the health issues associated with exposure to MTBE are still debated, evidence supports its role as a possible human carcinogen [13,18]. MTBE and toluene standard solutions were prepared using purified water from a MilliQ water purification system (Millipore, DA, USA) together with MTBE (HPLC grade, Fisher Scientific, PA, USA) or Toluene (HPLC grade, Sigma Adrich, Steinheim, Germany). Sodium chloride (purity 98%) was obtained from Sigma-Aldrich (Steinheim, Germany). The zeolite chosen as sorbent was a commercial as-synthesised hydrophobic mordenite (referred to below as MOR), with SiO_2/Al_2O_3 equal to 200 and Na_2O content lower than 0.1 wt%, and purchased from HSZ-690HOA Tosoh

Corporation in its protonated forms.

The crystal structure of mordenite was first determined by Meier [19] in 1961. The framework can be described as the assembly of single 6-ring sheets linked by single 4-rings, or, alternatively, from a combination of 5-1 secondary building units (SBUs). A pore system, consisting of 12-membered and 8-membered rings of TO_4 tetrahedra, runs parallel to the [001] direction This channel system is interconnected along [010] through 8-ring side pockets. The topological symmetry of mordenite is orthorhombic *Cmcm* [20], with four symmetrically independent tetrahedral cation sites and ten framework oxygen sites. The real symmetry is reduced to $Cmc2_1$ [21] in the natural phase in order not to constrain one oxygen in an inversion center, and consequently to avoid a straight, unstable T-O-T angle.

2.2 Methods

Batch Experiments

In order to obtain adsorption equilibrium isotherm data for the powder sorbent, aqueous phase adsorption experiments were performed in 25 mL crimp top reaction glass flasks sealed with PTFE septa (Supelco, PA, USA) using a fixed sorbent/liquid ratio (0.1 g sorbent/25 mL aqueous solution) and initial solutions of varied concentrations of MTBE and toluene, respectively. In all experiments, the flasks were agitated on a fixed speed rotator (200 rpm) at room temperature (25±2 ◦C) for a minimum of 24 h to achieve adsorption equilibrium. A 24 h equilibration time was chosen on the basis of kinetics testing conducted as part of this work. In addition, previous work on powdered zeolite showed that 24 h is sufficient time for MTBE to reach equilibrium [8]. Control experiments were performed periodically together with the adsorption experiments, using blank solutions of MTBE and toluene and no adsorbent material, to ensure that losses did not occur during the experiments. Following adsorption, solid–liquid separation was achieved by centrifugation for 10 min. at 10000 rpm, and MTBE or toluene in the aqueous supernatant samples was quantified using gas chromatography (GC) with solid phase micro extraction (SPME) in head space mode. When necessary, dilution was made in order to keep the measurements within the linear range of the standard curves.

2.3 *Gas chromatography*

A solid phase microextraction (SPME) system, supplied by Supelco, PA, USA was used to extract the organic contaminant (MTBE or toluene) from the aqueous phase of each sample using carboxen/polydimethylsiloxane (CAR/PDMS) 85-μm film thickness fibres (Supelco, Bellefonte, PA). At the beginning of each analysis, the SPME fibre was conditioned under helium for half an

hour in the injector unit at 250 ◦C and was systematically cleaned at 250 °C for 20-30 minutes after every extraction The headspace (HS) mode was used for extraction from a sample volume of 10 ml of contaminant solutions. The addition of an inorganic salt is common in order to enhance the activity coefficients of volatile components in aqueous solutions, increasing the concentration in the headspace vapour. In the present work, 2 mL of a sodium chloride solution (300 g L^{-1}) were added to the sample which was placed in 25 mL glass flasks sealed with Teflon screw caps. After equilibration at 40 (±0.5) °C, for 10 min, the SPME was inserted and the samples were maintained under controlled agitation with a magnetic stirrer (300 rpm) for 10 min. Finally, the fibre was inserted into the GC injector for analysis. The desorption time was 1 min. A GC HRGC 5160 MEGA SERIES Instrument (Carlo Erba, Mi, I) equipped with a split/splitless injector, a flame ionization detector (FID) and a fused-silica SE30 capillary column (60m x 0.25 mm I.D:, 0.25 μm film thickness; J&W Scientific, USA) was employed in this work. Helium (99.999%) was used as a carrier gas at a constant head pressure of 50 kPa The detector and injector temperatures were held constant at 250 °C. Helium 99.9 % used as the carrier gas at a constant flow of 1 mL min^{-1}. Hydrogen and air were used to maintain the detector flame at a pressure of 40 and 80 KPa, respectively. The GC oven program was as follows: 35 °C for 1min, ramped to 50 °C at 7.5 °C min^{-1}, held for 2min, ramped to 90 °C at 20◦C min^{-1}, held for 2min, finally ramped to 200 °C at 40°C min^{-1} and held for 10 min. The MTBE (or toluene) on the SPME fibre was thermally desorbed in the GC inlet using the splitless mode at 250 °C for 5 min. The linearity of the method for quantitative analysis was tested by the evaluation of the calibration curves: standard solutions of MTBE and toluene in MilliQ water were analysed at varying concentration levels in the range 0.01 - 10 ppm as single contaminants. Each concentration was analysed twice. The linearity range was evaluated, as well as the method detection limit (LOD) and computed from the calibration line. Good linearity was observed with a correlation coefficient of 0.9952 and 0.9984 for MTBE and toluene respectively. Exhausted MTBE and toluene mordenite samples were prepared by repeating batch adsorption steps on the same zeolite sample, until the concentration of the solution in contact with the zeolites did not change. The concentration of the organics in the aqueous solution was analyzed by HS-SPME-GC and this operation was repeated until the concentration of MTBE or toluene in the solution did not decrease after contact with the zeolite. These exhausted samples will be indicated below as MTBE-MOR and TOL-MOR, respectively.

2.4 X-ray Powder Diffraction analyses

X-Ray Powder Diffraction patterns (XRPD) were collected at room temperature on untreated mordenites, MTBE-MOR, and TOL-MOR. The experiments were carried out on a Bruker D8 Advance diffractometer, with Bragg-Brentano θ-θ geometry, equipped with Sol-X detector using

Cu $K_{\alpha1,\alpha2}$ radiation. The spectra were collected in the 2θ range 3°-115° with a 0.02° step and counting times of 12 s/step. Rietveld profile fitting was performed on all the spectra using the GSAS package[22] , with the EXPGUI [23] interface. The powder patterns of the untreated and two exhausted mordenites are reported in Figure 1. Structural details of untreated mordenite can be found in Martucci et al. [24] or asked to those authors since the mordenite sample studied here was the same as used in [24] . The coordinates used in [24] were taken as starting coordinates for the exhausted MTBE-MOR sample refinement, while those from Alberti et al. [21] were used for the TOL-MOR sample, for the reason reported in RESULTS AND DISCUSSION. The background curve was fitted by a Chebyshew polynomial with an average of 20 coefficients. The pseudo-Voigt profile function proposed by Thomson et al. [25] and peak intensity cut-off were applied. The 2θ-zero shift, the scale factor and unit-cell parameters were allowed to vary for all the histograms. The refined structural parameters for each data histogram were the following: fractional coordinates and isotropic displacement factors for all atoms and occupancy factors for the extraframework atoms. Occupancy factors and isotropic displacement factors were varied in alternate cycles. The isotropic displacement parameters were constrained in the following way: the same value for all tetrahedral cations, a second value for all framework O atoms, and a third value for all the extra-framework sites. Soft restraints were applied to the T–O distances [Si–O = 1.60(2)–1.63(2)] and the weight was gradually decreased after the initial stages of refinement, down to 10. The crystallographic data and refinement details are reported in Table 1. Tables 2 and 3 report the final atomic positions, thermal parameters, and occupancies of MTBE-MOR and TOL-MOR, respectively. The interatomic distances and angles are listed in Tables 4 and 5.

2.4 Thermal analyses

Thermogravimetric (TG) and differential thermal analysis (DTA) measurements of both as-synthesized and exhausted samples were performed in air up to 900°C using an STA 409 PC LUXX® - Netzch at 10°C/min. heating rate. The TG-DTA plots are reported in Figure 2.

RESULTS AND DISCUSSION

Batch experiments

The adsorption data of MTBE and toluene in water on mordenite vs. time is reported in Figure 3. It can be seen that in both cases equilibrium was reached within few minutes. The equilibration time employed in the batch experiments is, however, longer, since it was found that differences in adsorption arise from short time contact [26]. The pollutant (MTBE or TOL) concentrations in contact with the sorbent at the equilibrium are indicated as c_e. Figure 4 shows the MTBE and TOL sorption isotherms at room temperature (25 °C) for mordenite. In Figures 4 a and b *q,* the adsorbed

concentrations i.e. the mass of adsorbed pollutant per gram of sorbent (mg g^{-1}) vs. c_e the equilibrium concentrations (mg L^{-1}) are reported. The adsorbed concentration q is obtained as:

$$q = \frac{(c_o - c_e) * V}{w} \quad (1)$$

where V is the volume of pollutant aqueous solution (L) and w the weight (g) of adsorbent material.

The initial concentrations (c_0) placed in contact with the sorbent included the μg L^{-1} range up to the 0.1 g L^{-1} range. The latter concentrations are seldom found in natural water, however, in adsorption studies a wider concentration range can be useful to better define the adsorption isotherm [27]. The data in the low concentration range showed that the isotherm is linear (see Figure 4b). Only when the concentration increases is a limiting sorption capacity observed, as reported in Figure 4a. At high concentrations the sorbent become saturated, due to the limited space in the sorbent material available to host MTBE molecules. These results were interpreted by Giaya et al. [28] as consistent with the hypothesis of partition of the organic molecules between the water phase and the sorbent, with adsorption favoured by the environment created by the hydrophobic pore surfaces.

A similar trend was also observed for the adsorption of toluene on mordenite (see Figures 4 a and b). The data were fitted using a Langmuir equation:

$$q = \frac{q_S K_L c_e}{1 + K_L c_e} \quad (2)$$

where q_S is the saturation capacity, (mg L^{-1}) and K_L the equilibrium association constant (L mg^{-1}), and a Freundlich model:

$$q = K_F c_e^{1/n} \quad (3)$$

where K_F is a constant indicative of the adsorption capacity of the adsorbent and n is an empirical constant.

In the low concentration range a linear fitting:

$$q = K\ c_e \quad (4)$$

where K is a constant, is employed. At the low concentration eq. 2 converges with eq. 4 with K equal to $K_L q_s$.

The determination coefficients for the two models (i.e. eqs. 3 and 4) are not very different from each other (see Table 6), however, the latter equation was employed since it has often been used for

fitting volatile organic compounds adsorption on zeolites [29]. The fitted saturation capacity of MOR (see Table 6) is higher for toluene than for MTBE. By contrast, in the low concentration range the slope of linear fitting is higher for MTBE than for toluene, indicating a stronger interaction of MTBE with the adsorbent. For the adsorption of MTBE on zeolites it has been proposed that at low MTBE concentrations the dominant factors for favourable sorption are high Silica Alumina Ratio and high framework density (i.e. rather small pores) to disrupt the structure of water and to increase the affinities, while at high MTBE concentrations hydrophobicity and a large pore volume are important to obtain high capacities. Moreover, it has already been observed that the structure of a zeolite and not only the pore dimensions can play an important role in adsorption [24]. Mordenite has an essentially two-dimensional intersecting pore system, constituted by two channel types as previously described in the Materials section, the smaller channel could limit MTBE diffusion. Therefore, conclusions about adsorption should be considered in the light of the structures of this material.

3. Thermogravimetric and structural analysis

1) *MTBE*

The thermogravimetric curves (TG) of untreated material and MTBE-MOR are reported in Figure 2. The TG curve of the untreated material shows a total weight loss of about 7%. The loss shown in the TG curve is due to water molecules weakly bonded to the surface (loss below 100°C) and water molecules or silanols present inside the channel (loss at higher temperatures). According to the TG analyses, the amount of H_2O bonded to the surface of the grains corresponds to about 3% in weight, while the structural H_2O or OH accounting for the remaining weight loss represent about 4%.. TG analysis of MTBE-MOR clearly indicates adsorption, with the TG curve showing a total weight loss at 900°C of about 11-12% compared to 7% for the untreated powder. At low temperature the TG curve of the treated and untreated samples shows a similar behaviour (with a loss around 3% at 100°C). The residual loss (8-9% in weight) which occurs in MTBE-MOR at higher temperatures (above 200°C), is probably related to the presence of molecules adsorbed in the mordenite channels.

In X-Ray powder diffraction pattern, no remarkable differences are evidenced in the peak positions between treated and untreated samples (Figure 1). No violation of the C-centering systematic was observed and the pattern of MTBE-MOR matched satisfactorily with the space group *Cmcm,* which is usually accepted for mordenite. A comparison of the unit cell parameters reported by Martucci et al. [24] with those derived in the present work (Table 1), revealed small differences in the *a* and *b* parameters. The powder diffraction patterns reported in Figure 1 clearly

highlighted that the peak intensities of MOR and MTBE-MOR are markedly different, especially in low angle range. It is well know that in zeolites the intensities of their low-angle diffraction peaks are extremely sensitive to the arrangement and occupancy of extra-framework species. The decrease in the relative intensity of the first peak could be an indication that MTBE molecules entered the zeolite channels and the adsorption process by the MTBE solution induced changes in the MOR structure. The framework model of Martucci et al [24] was used in the initial stage of Rietveld refinement, which converged readily. At this point, the Difference Fourier map of the electronic density, enabled the location of the MTBE molecule inside the 12-ring channel. In addition, a partially occupied water site was detected. The Rietveld refinement of this model, carried out according to the procedure reported in the EXPERIMENTAL SECTION, converged, indicating partial occupancies by both MTBE and water molecules. As a whole, 3 MTBE molecules and 2.5 water molecules per unit cell were found.

The structure of the MTBE-MOR is reported in Figures 5 and 6; the organic molecules are in the 12-membered ring channel, with their symmetry plane on the mirror plane orthogonal to the *a* axis, whereas the water molecule is located inside the side pocket. Two partially occupied MTBE molecules are symmetrically related by the mirror plane at $z/c = 0.25$ leading to two different molecule orientations, with a face of the molecule's tetrahedron (C3-C1-C3 in Tables 2 and 4 and in Figures 5 and 6) lying on the mirror plane. However, from this refinement the carbon atom C2 which should occupy the center of the tetrahedron of MTBE (Table 2 and Figures 5 and 6) was found on the mirror plane at $z/c = 0.25$, i.e. on the tetrahedron face C3-C1-C3. Therefore a new Rietveld refinement was carried out in the space group $Cmc2_1$, a subgroup of *Cmcm.* Such a symmetry loses the mirror plane orthogonal to *c,* and was invoked by some aurhors, for the framework of MOR itself [21,30]. It is notable that, owing to the position of the MTBE molecule, *Cmcm* can not be the real symmetry but only a pseudosymmetric symmetry, with $Cmc2_1$ as the real symmetry. However, after the refinement in this symmetry, the C2 carbon atom was again located at about the center of the C3-C1-C3 face, and the MTBE molecules showed very similar orientation and occupancy, thus justifying the refinement in the topological symmetry *Cmcm*. At this point a Rietveld refinement in the *Cmcm* space group was performed, with the MTBE guest molecule treated as a rigid body. Its conformation was taken from Slovokhotov et al [31]. These rigid body constrains were progressively reduced and, as a result, the C2 carbon once again shifted up to the position found in the previous refinements. This anomalous result was interpreted as a consequence of the disorder in double configuration of MTBE molecules and the short distance between the position of the two possible C2 carbon atoms, very close to the mirror plane and, consequently, to each other. The high temperature displacement found for the atoms of the MTBE molecule (see Table 2) supports this interpretation. The distances of the water molecule from a framework oxygen

(W1-O5 = 3.13 Å) and a carbon atom (W-C1 = 3.17 Å) (see Table 4) suggest that MTBE molecule could be connected to the framework through water. It is worth noting that the amount of extraframework content (MTBE molecules plus water about 9.7 wt.%) found by the structure refinement is in close agreement with the data of TG analyses (8-9 wt.%) and adsorption isotherms. The data reported in Table 7 shows the changes in the mordenite channels after MTBE adsorption. The 12-ring channel hosting the organic molecule widens, in particular along the O10-O10 direction (Table 4), an effect justified by the molecule orientation (see Figure 5). As a consequence of the 12-ring widening, a narrowing and a distortion of the 8-ring channel to accommodate the structural deformations is observed. The small variations noted in the unit cell volume are the consequence of the combined effect of the widening/contraction of the two channels. It is worth noting that the 3 MTBE molecules found by the structure refinement correspond to 75% the adsorption capacity of the Mordenite 12-ring channels .

2)Toluene

The TG curve of TOL-MOR reported in Figure 2, shows that the total weight loss (about 12%) is slightly greater than that for MTBE-MOR. However, the plot show that the two phases behave in a very different way, with the TOL-MOR loss being faster in the early stage of heating compared with the other sample. At about 200° C the MTBE-MOR loss is about 6%, while TOL-MOR lost more than 9% in weight, which is more than ¾ of the total loss. The remaining 3 % was lost very slowly in the subsequent 600 °C, with the reaction almost completed at 800°C.
As noted above for the MTBE-MOR sample, the powder diffraction pattern of TOL-MOR reported in Figure 1, shows variation in the intensities ratio of the peaks at low 2θ angle, probably in relation to the presence of the molecules in the cavities. Even if no new peaks appear in the pattern, the Rietveld refinement suggested a lowering of symmetry. In fact, the R_F^2 factor was significantly lower when the structure was refined in the $Cmc2_1$ space group, instead of the *Cmcm* used in the previous refinements. Consequently, the starting coordinates for TOL-MOR refinement were taken from the work of Alberti et al [21]. The cell parameters obtained after the refinement are reported in Table 1, and it is evedent that only slight variations occurred, accounting for a small but significant volume expansion. The Fourier differences maps allow localization of the hexagonal ring of toluene molecule in the 12-ring channel (see Figure 7). The centre of the hexagonal ring of the organic molecule lies on the screw axis running along *c*, so that two different toluene molecules are shifted along the z axis of *c*/2 (at a distance of 3.7 Å) as a consequence of the presence of the screw axis parallel to [001]. It was not possible to unambiguously localize the methyl group, probably because of disorder in its position. It is notable that the toluene molecule is not perpendicular to *c* axis, as evidenced by the z/c values of the carbon atoms of the toluene molecule. This tilting explains the

loss of the mirror plane orthogonal to [001] and, consequently, the lowering of symmetry from the space group *Cmcm* to the space group $Cmc2_1$, induced by the adsorption of the organic molecules onto the zeolitic pores.

The occupancy factors of the carbon sites (about 0.9 in Table 3) of the hexagonal ring (C1, C2, C3) indicate adsorption of 3.6 toluene molecules per unit cell. This implies that slightly less than two toluene molecules are hosted inside each 12-member channel. Considering the toluene molecule orientation and the *c* parameter of mordenite (about 7.4 Å), no more than two molecules can be hosted in each channel. Consequently, the absorption of toluene in the mordenite zeolite is very near its maximum capacity (3.6 molecules of 4 maximum permitted).

In addition to the organic molecules, a crystallographic site, partially occupied by water molecules (accounting for 3.6 molecules) was located inside the side pocket, very near the water molecule found in MTBE-MOR. Overall, the electron density of the extraframework species corresponds to a total weight of about 12%. This value is in very close agreement with that found from the TG analysis and adsorption isotherm.

The interatomic distances found in the refined structure make it possible to postulate a stronger interaction between toluene and the mordenite framework compared with the MTBE molecule. Even if it was not possible to localize the methyl group, due to its probable statistically disordered position, it can be presumed that its carbon atom should have a distance lower than 3.00 from an oxygen atom of the framework. In fact, the distances of C1 and C2 from the framework oxygen atoms O2 and O10 are 3.10 and 3.21 Å, respectively (see Table 5), and if a methyl group is bonded to one of these carbon atoms the result is a relatively strong interaction of the molecule with the framework. Considering the geometry of the toluene molecule it is reasonable assume that the methyl group is bonded to C1 and oriented towards framework oxygen O2. Similarly to MTBE adsorption, the presence of the toluene molecules induces a widening of the 12-ring channel with a consequent deformation and narrowing of the 8-ring (see Table 7).

4. Conclusions

X-Ray powder diffraction experiments allowed the localization of host molecules and showed a loading of 75% and 80% of the mordenite total capacity for MTBE and toluene respectively. In both the experiments the organic molecules were found to in the 12-membered ring. . The short distance between the carbons of the toluene 6-ring and framework oxygen atoms indicated a possible strong interaction between the molecule and the guest zeolite, whereas a weaker interaction was observed between MTBE molecules and the mordenite framework.

Figure Captions:

Figure 1: XRPD patterns of untreated, MTBE-sorbed and toluene-sorbed mordenite.

Figure 2: Thermogravimetric analyses of untreated, MTBE-sorbed and toluene-sorbed mordenite.

Figure 3: Adsorption kinetics of MTBE and toluene on mordenite

Figure 4: Adsorption isotherm of MTBE and toluene on mordenite: circle symbols: measured equilibrium concentrations; (a) solid line: fitted Langmuir equation; dashed lines: 95% confidence prediction bounds. (b) Solid line: linear fit equation.

Figure 5: Projection of the MTBE sorbed mordenite along the [001] direction

Figure 6: Details of the location of MTBE molecules in the 12- ring channel viewed along [111].

Figure 7: Projection of the toluene sorbed mordenite along the [001] direction

References

[1] W. T. Tzsai, K.J. Hsien, H.C. Hsu, J. Hazard. Mater. 166 (2009) 635-641.
[2] A. Reife, H.S. Freeman, in: A. Reife, H.S. Freeman (Eds), Environmental Chemistry of Dyes and Pigments, Jonh Wiley & Sons, New York, 1996, pp.3-31.
[3] T.C. Shih, M. Wangpaichitr, M. Suffet, Water Res. 37 (2003) 375-385.
[4] S.W. Blocky, Environmental Progress 12 (1993) 223-230.
[5] M. Khalid, G. Joly, A. Renaud, P. Magnoux, Ind. Eng. Chem. Res. 43 (2004) 5275-5280.
[6] H.T. Shu, D. Li, A.A. Scala, Y. H. Ma, Sep. Purif. Technol. 11 (1997) 27–36
[7] S. J. Allen, in: G. McRay (Ed.) Use of adsorbent for the removal of Pollutants form wastewater, CRC Press Boca Raton, FL, 1996, pp 59-97
[8] W.K. Gupta, I, Alli, in: A.T. Hubbard (Ed.) Encyclopedia of Surface and colloid Science, Marcel Dekker, New York, 2002, pp, 136-166
[9] L.V.C.Rees and D. Shen in: H. van Bekkum, E.M. Flaningen, P.A. Jacobs, J.C. Jansen (Eds.) Introduction to zeolite science and practice, Elsevier, 2001.
[10] A. Rossner, S.A. Snyder, D.R.U. Knappe, Water Res. 43 (2009) 3787-3796.
[11] D.R.U. Knappe, A. Rossner, S.A. Snyder, C. Strickland, American Water Works Association Research Foundation, Denver Colorado, 2007.
[12] I. Braschi, S. Blasioli, L. Gigli, C. E. Gessa, A. Alberti, A. Martucci, J. Hazard. Mater. 178 (2010) 218 – 225.
[13] M.A. Anderson, Env. Sci.Technol. 34 (2000) 725-727.
[14] A. Martucci, L. Pasti , M. Nassi, A. Alberti, R. Arletti, R. Bagatin, R. Vignola, R. Sticca, Micropor. Mesopor. Mater. 151 (2012) 358-367.
[15] L.I Abu-Lail, Removal of chloroform and MTBE from water by adsorption onto granular zeolites: equilibrium, kinetic and mathematical modeling study, A Dissertation in Civil & Environmental Engineering, Worcester Polytechnic Institute, Department of Civil & Environmental Engineering, 2010.
[16] H.W. Hung, T.F. Lin, J. Hazard. Mater. B 135 (2006) 210-217.
[17] D. Zadaka-Amir, A.Nasser, S.Nir, Y.G. Mishael, Micropor. . Mesopor. Mater. (2011) doi:10.1016/j.micromeso.2011.10.033
[18] U.S. EPA - Office of Environmental Health Hazard Assessment, Public Health
Goal for methyl tertiary butyl ether (MTBE) in Drinking Water, OEHHA, California (1999) p.136
[19] W.M. Meier, Zeit. Krist. 115(1961) 439-450.
[20] S.M. Csicsery, Zeolites chemistry and Catalysis. ACS Monographs 171, Am. Chem. Soc., Washinton DC, 1976.
[21] A. Alberti, P. Davoli P., G. Vezzalini, Zeit. Krist 175 (1986) 249-256.
[22] A.C. Larson, R.B. Von Dreele, GSAS-General Structure Analysis System. Report LAUR 86–748, Los Alamos National Laboratory, Los Alamos, New Mexico,1996.
[23] B.H. Toby, Journal. Appl. Crystallogr. 34 (2001)210–213.
[24] A. Martucci, L. Pasti, N. Marchetti, A. Cavazzini, F. Dondi, A. Alberti, Micropor. Mesopor. Mater. 148 (2012) 174–183.
[25] P. Thomson, D.E. Cox, J. B. Hastings, J. Appl. Crystallogr. 20 (1987) 79–83.
[26] A. Erdem-Senatalar, J.A. Bergendahl, A. Giaya, R.W. Thompson, R. W., Environ. Eng. Sci. 21 (2004) 722-729.
[27] J.P. Mota, S., Lyubchik, S., Recent Advances in Adsorption Processes for Environmental Protection and Security NATO Science for Peace and Security, Series C: Environmental Security, Springer, The Netherlands, 2008.
[28] A. Giaya, R.W. Thompson, R. Denkewicz Jr., Micropor. Mesopor. Mat. 40 (2000) 205-218.
[29] B.A. De Moor, M-F. Reyniers, O.C. Gobin, J. A. Lercher, G. B. Marin, J. Phys. Chem. C 115 (2011) 1204-1219
[30] P. Simoncic, T. Armbruster, Am. Mineral. 89 (2004) 421-431.

[31] Yu.L. Slovokhotov, T.V. Timofeeva, M.Yu. Antipin, Yu.T. Struchkov, J. Mol. Struct., 112 (1984) 127-140.
[32] Ch. Baerlocher, L.B. McCusker, D.H. Olson. Atlas of Zeolite Framework Types. Sixth revised ed. Elsevier, Amsterdam, 2007.

Table 1: Lattice parameters and Rietveld refinement details before (MOR, data from Martucci et al. [24]), and after MTBE (MTBE-MOR) and toluene (TOL-MOR) adsorption**.**

	MOR [24]	**MTBE- MOR**	**TOL-MOR**
Space group	*Cmcm*	*Cmcm*	$Cmc2_1$
***a*(Å)**	18.069(1)	18.0572(6)	18.0709(9)
***b*(Å)**	20.219(1)	20.2323(6)	20.2372(8)
***c*(Å)**	7.456(3)	7.4572(2)	7.4577(3)
***V*(Å^3)**	2723.9(2)	2724.3(1)	2727.3(2)
R_{wp}		14.05	12.03
R_p		11.05	9.08
R_F^2		9.2	10.04
N° Reflections		2204	2295
N°Obs		5674	5680
N° Variables		87	114

Table 2: MTBE-MOR atomic coordinates, occupancies (F) and displacement parameters (UISO $Å^2$ x100)

	x/a	y/b	z/c	F	Uiso
Si1	0.3054(3)	0.0730(2)	0.0416(7)	1.0	0.0274(9)
Si2	0.3049(3)	0.3113(2)	0.0423(6)	1.0	0.0274(9)
Si3	0.0860(4)	0.3812(4)	0.25	1.0	0.0274(9)
Si4	0.0828(5)	0.2223(4)	0.25	1.0	0.0274(9)
O1	0.1204(5)	0.4084(5)	0.4343(10)	1.0	0.032(2)
O2	0.1226(5)	0.1891(6)	0.4199(12)	1.0	0.032(2)
O3	0.2349(4)	0.1187(4)	0.9949(14)	1.0	0.032(2)
O4	0.0887(8)	0.3017(4)	0.25	1.0	0.032(2)
O5	0.1704(8)	0.1876(11)	0.75	1.0	0.032(2)
O6	0.1702(9)	0.4194(9)	0.75	1.0	0.032(2)
O7	0.2254(7)	0.50	0.50	1.0	0.032(2)
O8	0.25	0.25	0.5	1.0	0.032(2)
O9	0.00	0.4026(11)	0.25	1.0	0.032(2)
O10	0.00	0.1930(11)	0.25	1.0	0.032(2)
C1	0.50	0.393(4)	0.25	0.74(2)	0.38(3)
C2	0.50	0.469(4)	0.25	0.74(2)	0.38(3)
C3	0.422(2)	0.5019(34)	0.25	0.74(2)	0.38(3)
C4	0.00	0.063(5)	0.042(3)	0.39(2)	0.38(3)
O11	0.00	-0.001(4)	0.080(1)	0.39(2)	0.38(3)
W1	0.481(7)	0.2368(25)	0.25)	0.33(1)	0.38(3)

Table 3: TOL-MOR atomic coordinates, occupancies (F) and displacement parameters (UISO $Å^2$ x100).

	x/a	*y/b*	*z/c*	F	Uiso
Si1	0.3076(10)	0.0740(15)	0.04326	1	0.0078(8)
Si1a	0.6991(10)	0.9267(15)	0.9539(16)	1	0.0078(8)
Si2	0.3060(13)	0.3114(13)	0.043(4)	1	0.0078(8)
Si2a	0.6950(13)	0.6889(13)	0.964(4)	1	0.0078(8)
Si3	0.0850(6)	0.3811(5)	0.233(3)	1	0.0078(8)
Si4	0.0849(5)	0.2232(5)	0.244(4)	1	0.0078(8)
O1	0.1226(15)	0.4033(20)	0.420(4)	1	0.0068(1)
O1a	0.8777(16)	0.5877(19)	0.558(5)	1	0.0068(1)
O2	0.1260(14)	0.1861(16)	0.408(4)	1	0.0068(1)
O2a	0.8840(14)	0.8039(19)	0.554(4)	1	0.0068(1)
O3	0.2345(17)	0.1181(15)	0.006(5)	1	0.0068(1)
O3a	0.7707(17)	0.8851(14)	0.020(5)	1	0.0068(1)
O4	0.0895(7)	0.3028(5)	0.260(5)	1	0.0068(1)
O5	0.1675(8)	0.1917(11)	0.754(4)	1	0.0068(1)
O6	0.1621(9)	0.4189(8)	0.7522(17)	1	0.0068(1)
O7	0.2251(8)	0.4986(16)	0.498(6)	1	0.0068(1)
O8	0.2487(23)	0.2524(18)	0.518(6)	1	0.0068(1)
O9	0	0.4115(11)	0.240(9)	1	0.0068(1)
O10	0	0.1945(13)	0.245(10)	1	0.0068(1)
W1	0.5	0.231(1)	0.250(11)	0.90(2)	0.129(2)
C1	0.5413(2)	0.427 (1)	0.096(5)	0.89(1)	0.062(9)
C2	0.5414(2)	0.545 (1)	0.140(4)	0.89(1)	0.062(9)
C3	0.5867(7)	0.484 (1)	0.165(5)	0.89(1)	0.062(9)

Table 4: T-O framework distances (Å) and selected interatomic distances for MTBE-MOR

		Distance
Si1-	**O1**	1.604(4)
	O3	1.611(4)
	O6	1.622(4)
	O7	1.610(4)
Si2-	**O2**	1.595(4)
	O3	1.612(4)
	O5	1.612(3)
	O8	1.619(3)
Si3-	**O1**	1.606(3)
	O1	1.606(3)
	O4	1.609(4)
	O9	1.612(4)
Si4-	**O2**	1.604(3)
	O2	1.604(3)
	O4	1.609(4)
	O10	1.609(4)
C1-	**C2**	1.552(4)
C2-	**C3**	1.552(4)
	O11	1.410(5)
C3-	**C2**	1.552(4)
	O11	2.499(4)
O11-	**C4**	1.552(4)
	C2	1.410(5)
C4-	**O11**	1.552(4)
W1-	**C1**	3.17(2)
	O5	3.13(4)

x2

Angle	Degrees
O1-Si1-O3	114.7(7)
O1-Si1-O6	103.3(6)
O1-Si1-O7	114.0(7)
O3-Si1-O6	111.5(9)
O3-Si1-O7	102.2(5)
O6-Si1-O7	111.4(8)
O2-Si2-O3	105.8(6)
O2-Si2-O5	108.9(6)
O2-Si2-O8	112.8(6)
O3-Si2-O5	106.1(9)
O3-Si2-O8	111.4(5)
O5-Si2-O8	111.6(8)
O1-Si3-O1	117.6(10)
O1-Si3-O4	109.4(5)
O1-Si3-O9	106.3(4)
O1-Si3-O4	109.4(5)
O1-Si3-O9	106.3(4)
O4-Si3-O9	107.4(12)
O2-Si4-O2	104.3(10)
O2-Si4-O4	112.9(7)
O2-Si4-O10	105.2(4)
O2-Si4-O4	112.9(7)
O2-Si4-O10	105.2(4)
O4-Si4-O10	115.3(12)

Table 5

Table 5: T-O framework distances (Å) and selected interatomic distances for TOL-MOR.

	Distance
Si1- O1	1.626(10)
O3	1.620(10)
O6	1.658(10)
O7	1.618(10)
Si1a- O1a	1.615(10)
O3a	1.620(10)
O6	1.653(10)
O7	1.618(10)
Si2- O2	1.589(10)
O3a	1.631(10)
O5	1.645(10)
O8	1.638(10)
Si2a- O2a	1.583(10)
O3	1.629(10)
O5	1.649(10)
O8	1.615(10)
Si3- O1	1.617(10)
O1a	1.600(10)
O4	1.599(9)
O9	1.656(8)
Si4- O2	1.617(10)
O2a	1.618(10)
O4	1.618(9)
O10	1.640(9)
C1- C1	1.493(8)
C3	1.504(7)
O2	3.100(8)
C2- C2	1.497(8)
C3	1.492(7)
O10	3.210(8)
C3- C1	1.504(7)
C2	1.492(8)
O3a	3.441(7)

Angle	Degrees
O1_Si1_O3	112.3(23)
O1_Si1_O6	104.5(17)
O1_Si1_O7	115.0(20)
O5_Si1_O6	112.6(17)
O5_Si1_O7	99.6(21)
O9_Si1_O7	113.2(22)
O1a_Si1a_O3a	116.5(26)
O1a_Si1a_O6	94.1(18)
O1a_Si1a_O7	108.7(20)
O3a_Si1a_O6	123.4(19)
O3a_Si1a_O7	101.1(20)
O6_Si1a_O7	113.1(22)
O2_Si2_O3a	102.0(21)
O2_Si2_O4	112.5(19)
O2_Si2_O9	114.9(28)
O3a_Si2_O4	104.4(20)
O3a_Si2_O9	118.2(23)
O5_Si2_O9	104.6(21)
O2a_Si2a_O3	113.3(22)
O2a_Si2a_O5	97.4(16)
O2a_Si2a_O8	113.3(28)
O3_Si2a_O5	110.1(21)
O3_Si2a_O8	108.8(25)
O5_Si2a_O8	113.6(23)
O1_Si3_O1a	114.8(12)
O1_Si3_O4	98.4(19)
O1_Si3_O9	105.0(22)
O1a_Si3_O4	118.2(18)
O1a_Si3_O9	105.7(21)
O4_Si3_O9	114.3(13)
O2_Si4_ O2a	110.1(12)
O2_Si4_O4	112.5(21)
O2_Si4_O10	105.0(23)
O2a_Si4_O4	112.7(24)
O2a_Si4_O10	102.2(26)
O4_Si4_O10	113.6(13)

Table 6: Fitted Parameters of the Isotherm Models (see eqs. 2-4)

Zeolite - Organic	*Adsorption model*	K_L (L mg^{-1})	q_S (mg g^{-1})	R^2
MOR - MTBE	Langmuir	0.293 (0.262, 0.324)	70.8 (57.0, 84.6)	0.9826
MOR - Tol	Langmuir	0.138 (0.117, 0.160)	150.5 (139.1, 161.9)	0.9964
		K_F (mg g^{-1})(L g^{-1})^n	n	R^2
MOR- MTBE	Freundlich	19.4 (18.1, 20.6)	0.574 (0.552, 0.595)	0.9935
MOR - Tol	Freundlich	21.0 (17.8, 24.2)	0.615 (0.544, 0.686)	0.9763
		K		R^2
MOR - MTBE	Linear	47.6 (44.5, 49.7)		0.9832
MOR - Tol	Linear	17.3 (16.0, 18.6)		0.9881

Table 7 Free diameter (Å) of the 12-ring and 8-ring channels and free area (Å^2) before (MOR, data from Martucci et al. [24]), and after MTBE (MTBE-MOR) and toluene (TOL-MOR) adsorption**.**

([a] sensu Baerlocher et al. [32]). Labels refer to Figure 5.

		Untreated MOR	MTBE-MOR	TOL-MOR
12-ring	O10-O10	5.74	5.95	6.01
	O3-O3	6.91	7.05	6.92
	O2-O2	6.14	6.2	6.25
	O7-O7	7.15	7.22	7.24
	Free Area[a]	33.14	34.31	36.63
8-ring	O7-O7	5.41	5.44	5.43
	O9-O9	3.01	2.72	2.47
	O1-O1	3.20	3.10	3.18

*Figure 1
Click here to download high resolution image

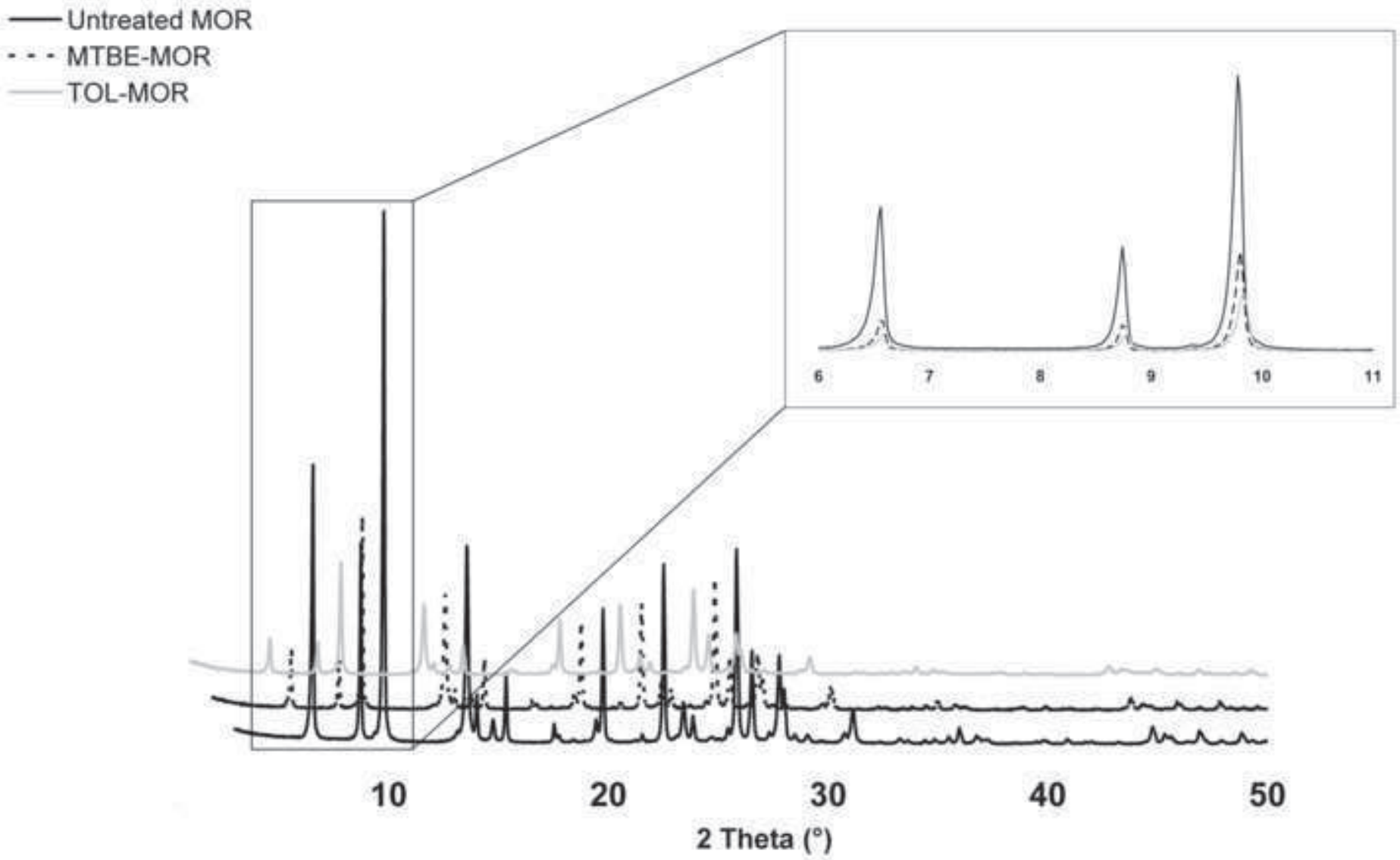

*Figure 2
Click here to download high resolution image

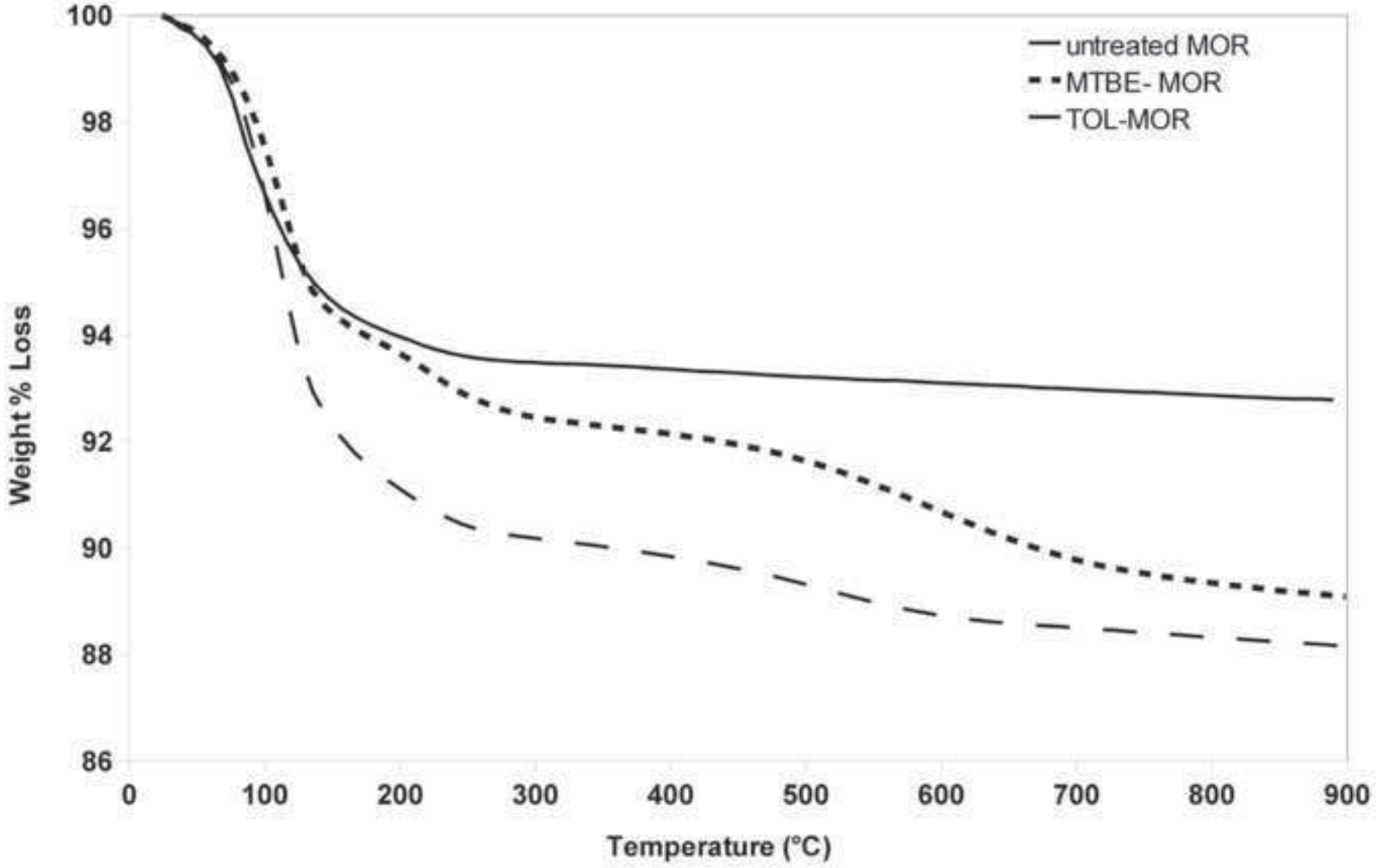

*Figure 3
Click here to download high resolution image

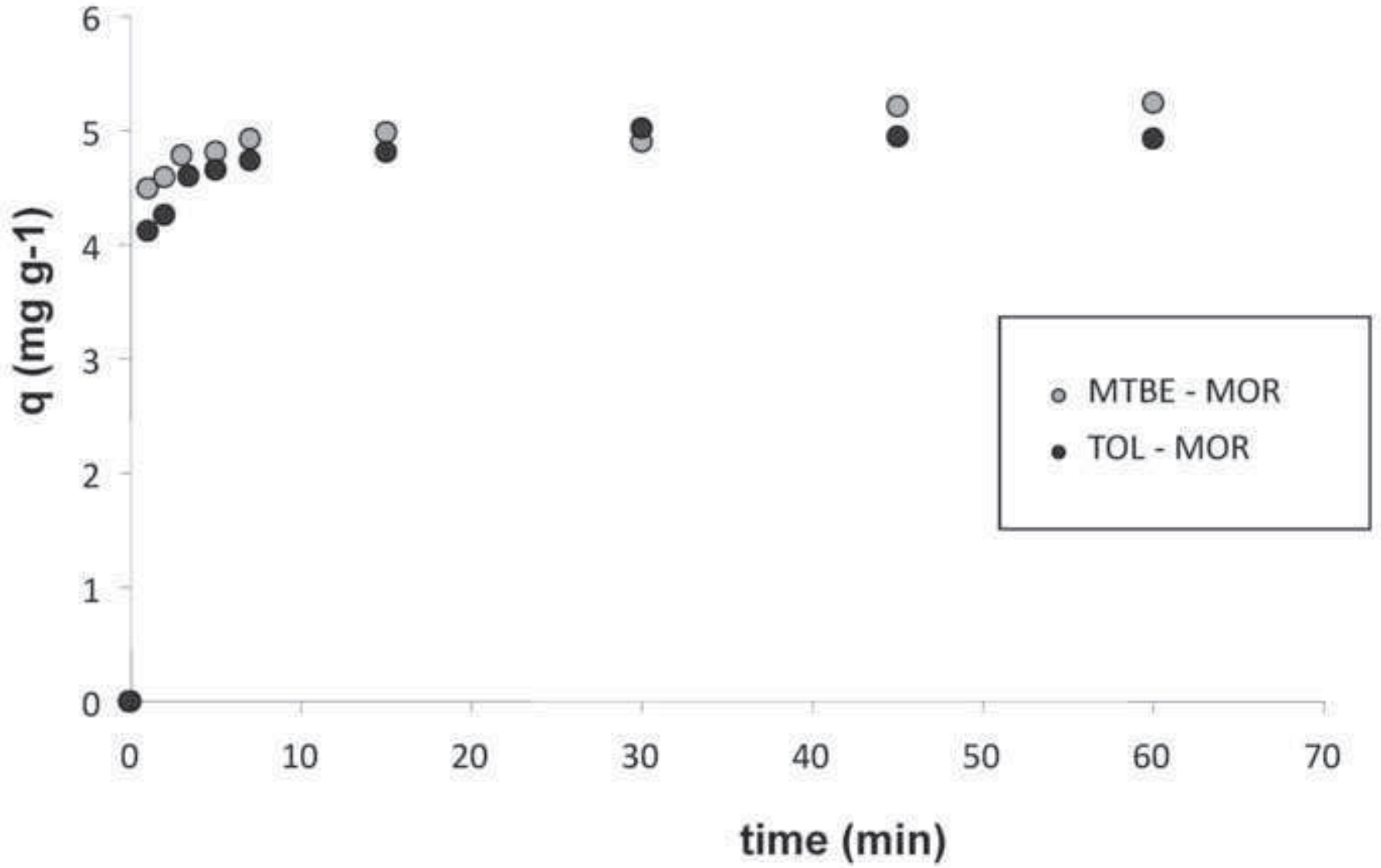

*Figure 4a
Click here to download high resolution image

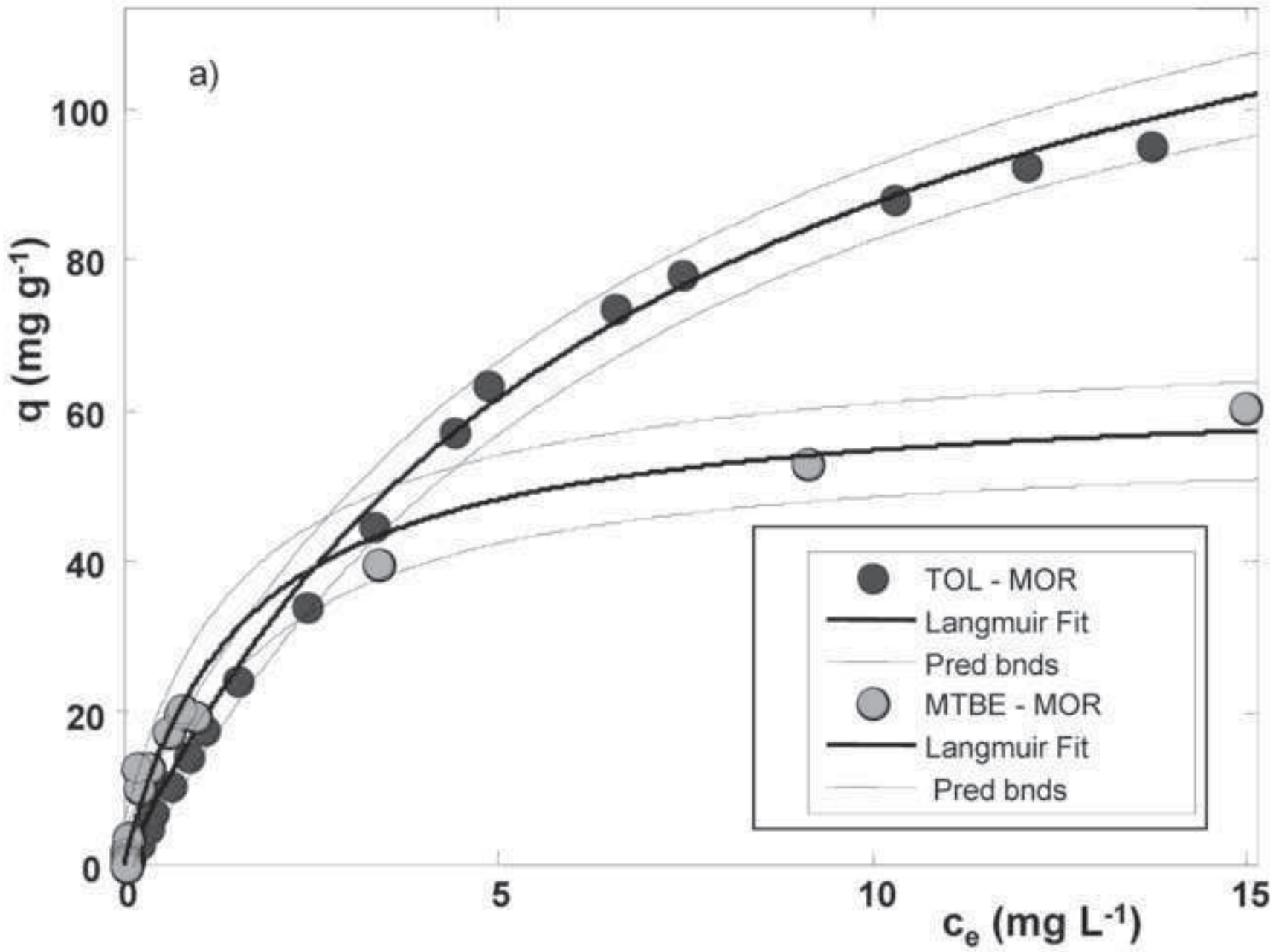

*Figure 4b
Click here to download high resolution image

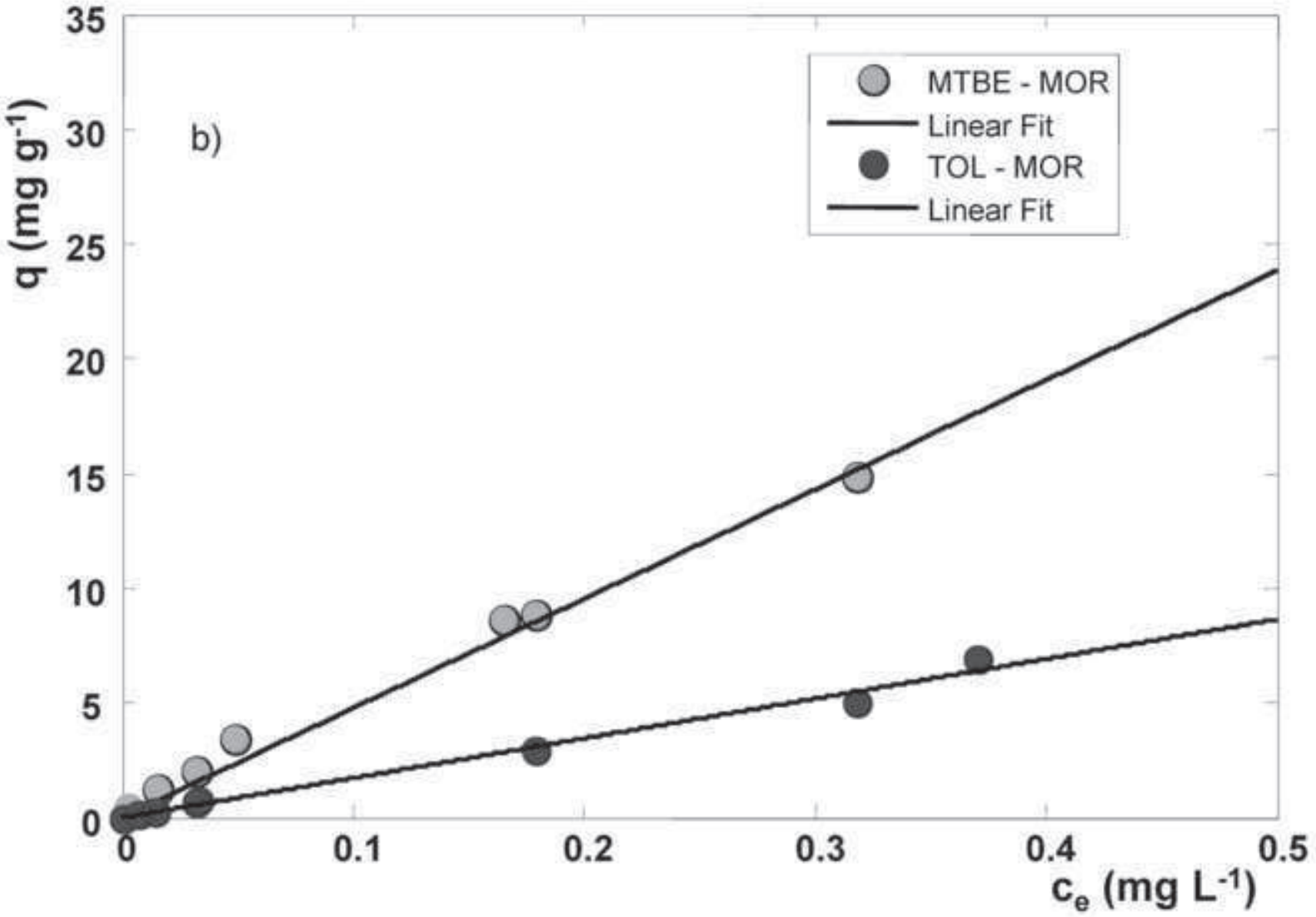

*Figure 5
Click here to download high resolution image

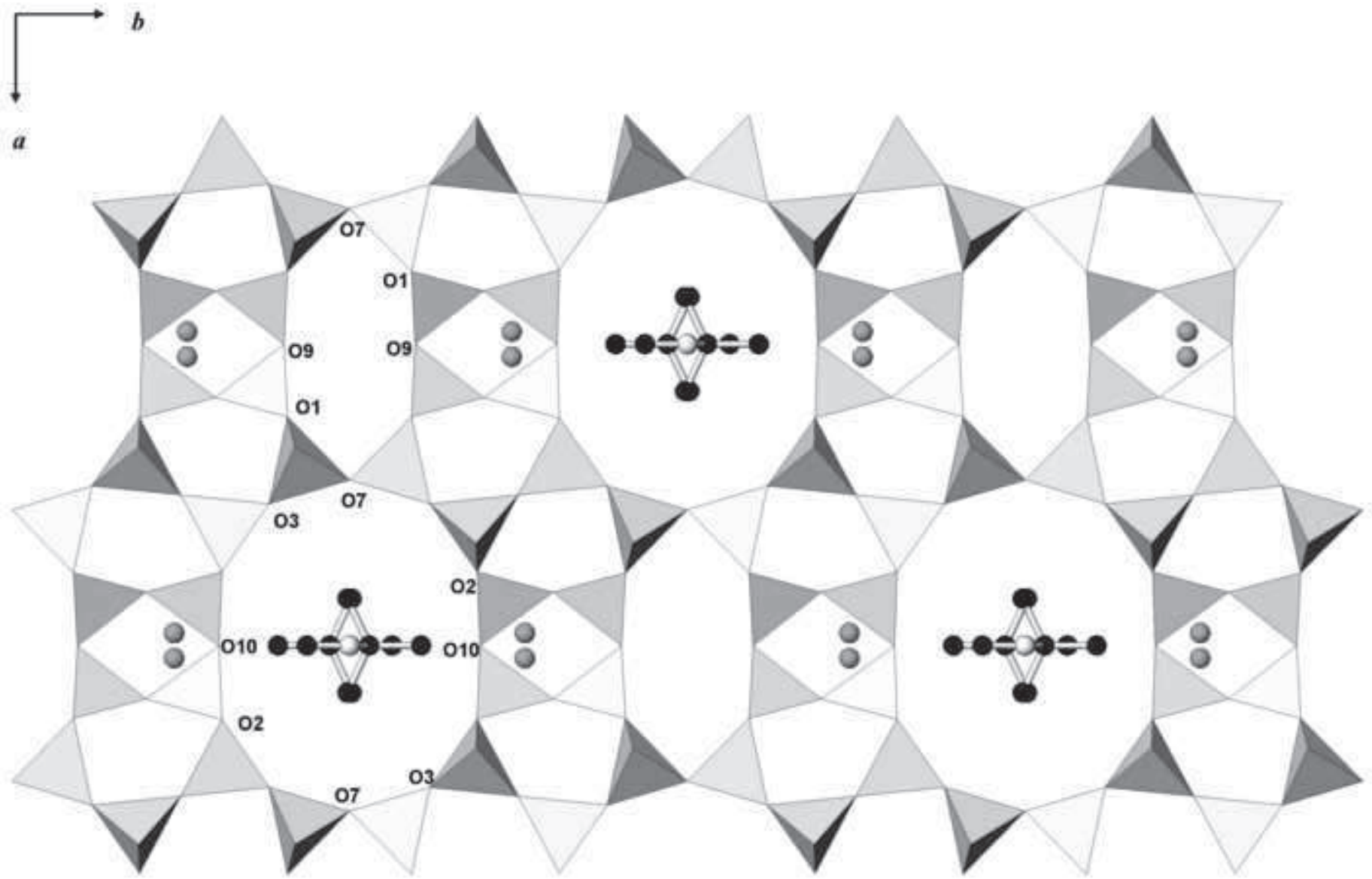

*Figure 6
Click here to download high resolution image

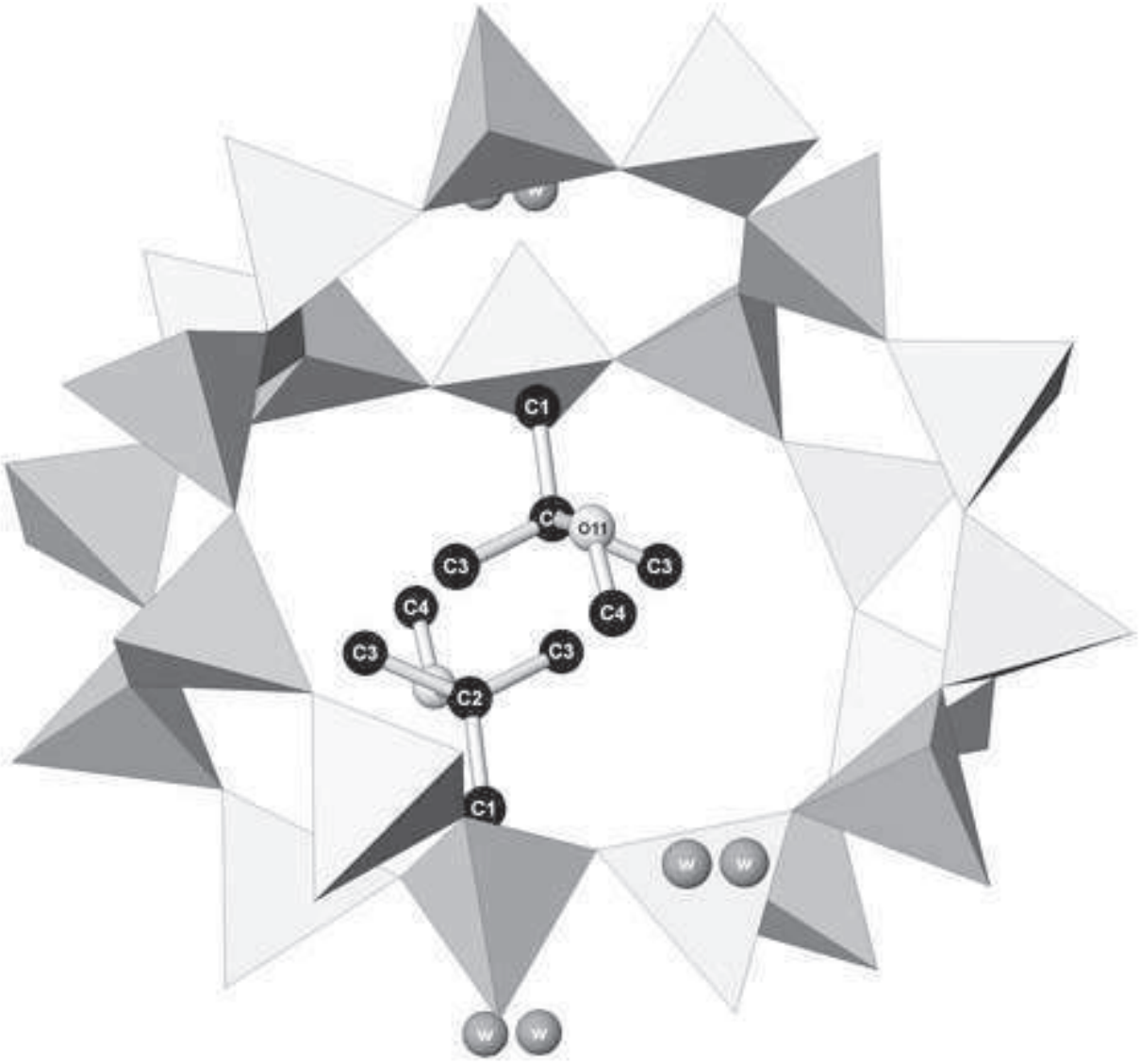

*Figure 7
Click here to download high resolution image

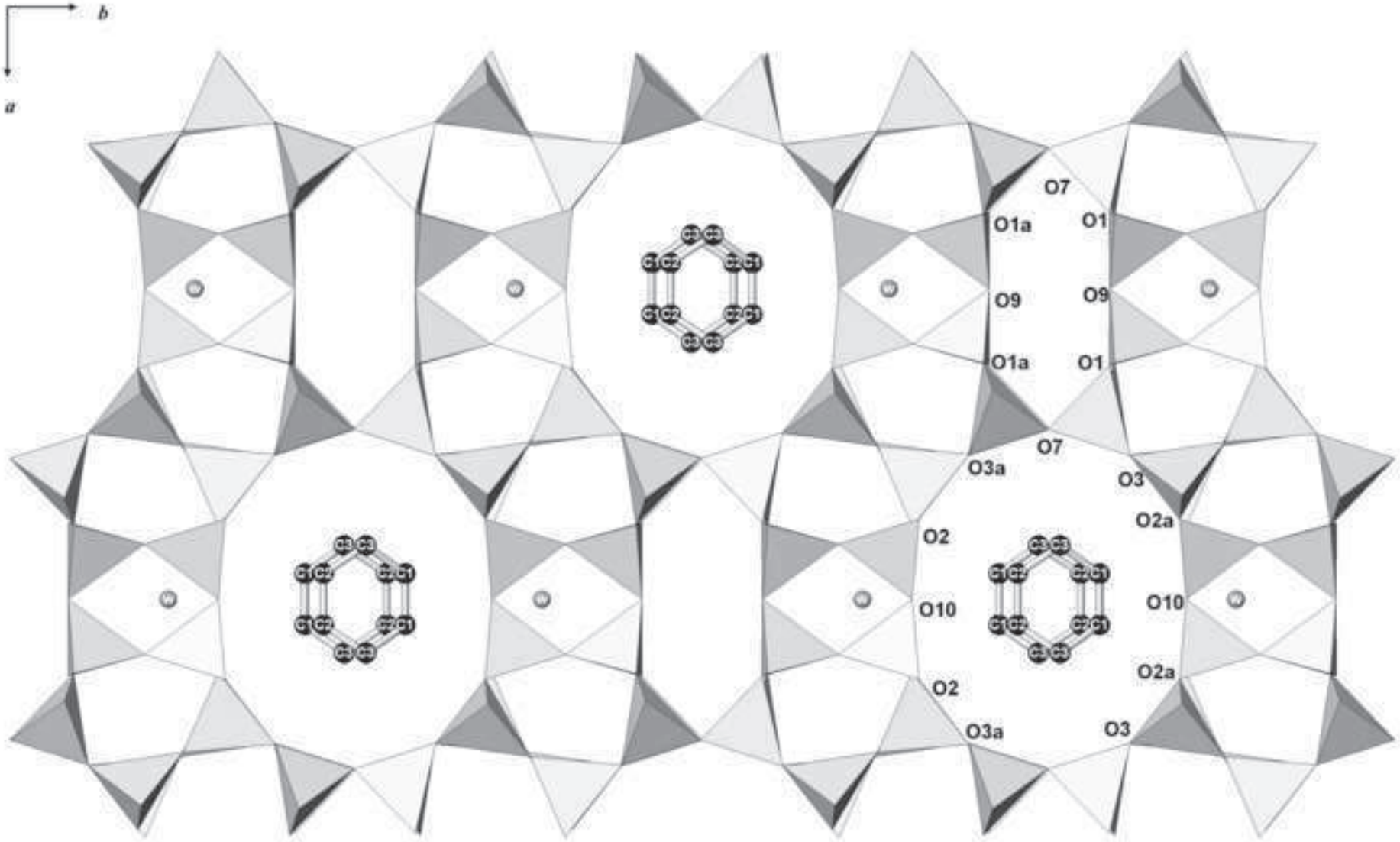

*Graphical Abstract (TOC Figure)
Click here to download high resolution image

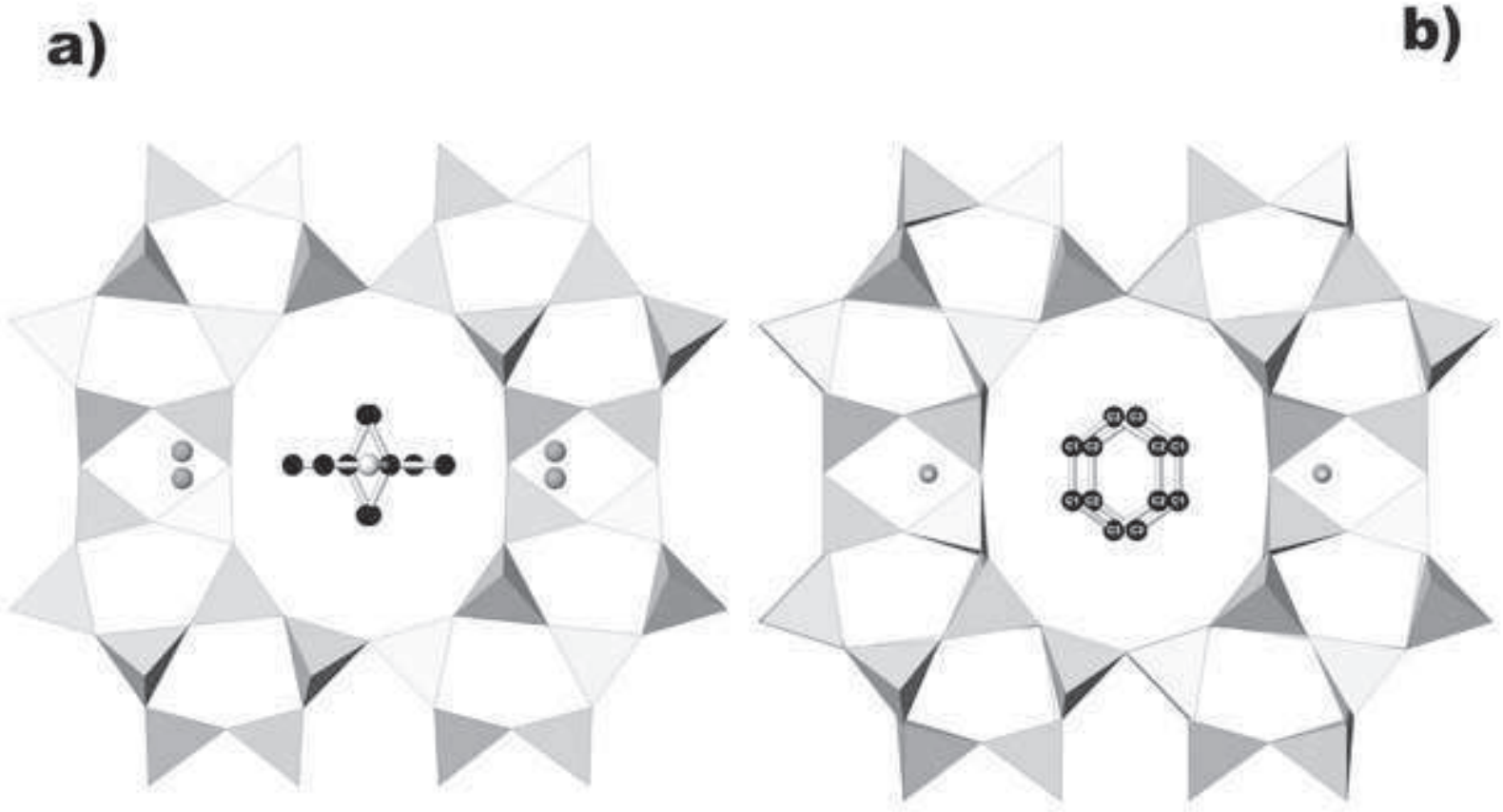

ACKNOWLEDGEMENTS

I would like to give thanks Dr. Luisa Pasti for her precious lessons during my years of PhD and for her time spent to my thesis.

I would like to thank Prof. Francesco Dondi and all group of Analytical Chemistry for their continuous willingness.

I would like to give thanks Dr. Roberto Bagatin for his scientific support and ENI for their financial support on this project.

I would like to thank the group of Earth Science (in particular Prof. Alberto Alberti and Dr. Annalisa Martucci) for their collaboration.

I would like to thank Prof. Francesco Di Renzo and Dr. Anne Galarneau, who gave me the chance to work in their laboratory.

I would like to give thanks to my parents for their affection.

Lots of thanks also to my friends.